



**GRIGORE T. POPA** UNIVERSITY OF  
MEDICINE AND PHARMACY IASI

# **HABILITATION THESIS**

**Innovative approaches in pain research and  
therapy: trace elements and nanotechnologies**

**Bogdan Ionel TAMBA, M.D, PhD.**

**2019**



## Table of contents

<b>Abstract</b> .....	5
<b>Rezumat</b> .....	7
<b>SECTION I - SCIENTIFIC ACHIEVEMENTS</b> .....	9
1.1 Assessing the influence of trace elements on analgesic drugs and pain .....	9
1.1.1 Background and motivation for research .....	9
1.1.2 Material and methods .....	13
1.1.3 Results .....	16
1.1.4 Discussions .....	30
1.1.5 Conclusions .....	38
1.2 Nanotechnology applications in medicine .....	39
1.2.1 Background and motivation for research .....	39
1.2.2 Preparation, characterization and biodistribution studies of novel nanoparticles .....	46
1.2.3 Investigating nanoparticles in the field of pain research .....	73
<b>SECTION II – PAST, PRESENT AND FUTURE</b> .....	101
2.1 Career overview .....	101
2.2 Future projects in the academic and professional field.....	102
2.2.1 Improvements in the academic field.....	102
2.2.2 Additional professional development.....	103
2.3 Perspectives for future research .....	103
2.3.1 Translating basic research to pain management practice .....	106
2.3.2 Advanced drug delivery systems and nanotechnology .....	108
2.3.3 Networks for advanced preclinical and clinical imaging studies .....	111
<b>BIBLIOGRAPHIC REFERENCES</b> .....	113



## Abstract

This thesis aims to objectively analyze the scientific, professional and academic accomplishments from the postdoctoral period. These achievements could not have been possible without the research I performed during my PhD studies, which I completed in 2010 when I defended the doctoral thesis entitled "*Experimental studies regarding the influence on the algesic process and behavior of some trace elements and drug combinations*", under the supervision of Professor Ostin Mungiu, M.D., PhD, University of Medicine and Pharmacy "Grigore T. Popa", and for which I was conferred the title of Doctor of Medical Sciences by Ministry of Education order no: .EC. 4387/06.06.2011.

This document describes the main research directions, along with a plan to further develop my academic, professional and research career, as recommended by CNATDCU and the current legislation.

The first part of my thesis describes my most significant accomplishments from the postdoctoral period. The first chapter is entitled "**The importance of assessing the influence of trace elements on analgesic drugs and pain**" and comprehensively presents the most important research on the influence of some trace elements and drug combinations on the algesic process and on behavior.

Trace elements' pathology is often overlooked in research and current data is at best insufficient and often controversial. This is even more obvious when one takes into consideration the possible relations between trace elements and neural signal transmission or pain modulation. Recent data indicate that there are some intra and extra cellular changes of the trace elements' transport during general or local anesthesia or during presurgery analgesia (as it's the case for zinc and selenium), which is why I believe this field deserves further interest.

The second chapter presents my other research area of interest, which is "**Nanotechnology applications for pain therapy**". Pain alleviation is one of the most important problems related to our health and, since the beginning of humanity, people strived to find effective cures. Minimal invasiveness represents an important requirement and empirical formulations of curative mixtures were developed and perfected through generations as creams, ointments, pastes, powders, liquid extracts of animal or vegetal origins.

Nanotechnology is a multidisciplinary science field that over the last two decades has offered a diverse range of nanoscale tools specially created for therapeutic use in medicine. Thus, the applicability of techniques and methods based on nanotechnology offers implantable drug delivery devices, transdermal and transmucosal delivery systems for different types of drug for cancer, pain, etc. As such, I wish to continue working in this field because I believe that treating pain with nanotechnology may be the future of pain relief.

Section II of the habilitation thesis presents a brief overview of my career so far, followed by a chapter dedicated to future projects in the academic and professional field. This part offers details of what I intend to focus on in the relationship with students and young

trainees, methods of improving the teaching process and suggestions for improved research education. The section concludes with perspectives for future research, a chapter where I detail the main research directions I will focus on, based on previous work and collaboration networks established by myself and my research team.

The references section includes articles and books that support the information from this habilitation thesis.

The scientific results obtained in the 8 years of postdoctoral research are included in over 80 published papers (over 35 of them are articles published in ISI indexed journals) and 8 books and/or book chapters that have generated 178 citations (h-index 9 – ISI Thompson). In this period, I have been member or director of 17 research projects (7 international with multiple partners) totaling over €8 mil that have been focused on clinical pharmacology, drug development, nanomedicine and pain therapy.

My professional and scientific achievements will help me contribute to the education of future generations of students and physicians. By coordinating PhD students, I will be able to both select and train high-quality new university teaching staff worthy of a modern European university and develop scientific research in the field of clinical pharmacology related areas.

## Rezumat

Elaborearea acestei teze de abilitare reprezintă un moment de bilanț pentru a analiza obiectiv realizările științifice, profesionale și academice obținute în perioada postdoctorală. Aceste realizări se bazează pe activitatea din perioada aferentă studiilor doctorale pe care le-am finalizat în anul 2010 odată cu susținerea publică a tezei de doctorat intitulată: "*Studii experimentale privind influența asupra procesului algezie și a comportamentului a unor oligoelemente și asociații medicamentoase*" - Coordonator Științific Prof. Univ. Dr. Ostin Mungiu, Universitatea de Medicină și Farmacie "Grigore T. Popa", Iași și conferirea titlului de Doctor în Științe Medicale, prin Ordinul M.E.C. 4387/06.06.2011.

Lucrarea include principalele direcții de cercetare, alături de un plan de dezvoltare a carierei academice, profesionale și de cercetare, conform recomandărilor CNATDCU și a legislației în vigoare.

În perioada postdoctorală am continuat studiile centrate pe terapia durerii, urmând două direcții prezentate în prima secțiune a tezei de abilitare.

Primul capitol, cu titlul "**Importanța evaluării influenței oligoelementelor asupra medicamentelor analgezice și asupra durerii**" prezintă comprehensiv cele mai importante cercetări privind influența asupra procesului algezie și a comportamentului a unor oligoelemente și asociații medicamentoase. Patologia oligoelementelor constituie un domeniu deschis cercetării deoarece, datele actuale sunt insuficiente și adesea neconcordante. Faptul acesta este și mai evident dacă se are în vedere relația posibilă cu diversele etape ale fenomenului algezie sau pentru o eventuală posibilitate de implicare în analgezie. Evidențierea unor modificări ale transportului intra și extracelular al oligoelementelor pe parcursul anesteziei generale sau locale sau în cadrul analgeziei perioperatorii (cum s-a demonstrat pentru zinc și seleniu), justifică o aprofundare a investigațiilor și la alte elemente din această categorie.

A doua direcție de cercetare denumită "**Aplicații nanotehnologice în terapia durerii**" include rezultatele obținute în ultimii ani în studiile centrate pe managementul durerii prin intermediul nanotehnologiei. Îndepărtarea durerii este una dintre cele mai importante probleme legate de sănătatea noastră și, de la începutul omenirii, se încearcă găsirea unui remediu. Invazivitatea minimă reprezintă o cerință importantă și formulările empirice ale amestecurilor curative au fost dezvoltate și perfecționate de-a lungul generațiilor sub formă de creme, unguente, paste, pulberi, extracte lichide de origine animală sau vegetală.

Nanotehnologia reprezintă un domeniu științific multidisciplinar care în ultimele două decenii a oferit o gamă variată de instrumente nanometrice fabricate special pentru uz terapeutic în medicină. Astfel, aplicabilitatea tehnicilor și metodelor bazate pe nanotehnologie, conferă dispozitive implantabile de livrare a medicamentelor, sisteme transdermale și transmucozale pentru diferite tipuri de medicamente pentru cancer, anestezice etc. Tratarea durerii cu nanotehnologii poate fi viitorul ameliorării durerii.

Cea de-a doua secțiune a tezei de abilitare prezintă un rezumat al carierei mele până în prezent, urmat de un capitol dedicat planurilor mele pentru dezvoltarea academică și profesională ulterioară. Aici, sunt oferite detalii referitoare la obiectivele mele în relația cu

studenții și tinerii medici, metodele prin care intenționez să îmbunătățesc procesul didactic și idei pentru creșterea educației în cercetare. Secțiunea se încheie cu prezentarea direcțiilor de cercetare viitoare bazate pe rezultatele și colaborările laboratorului nostru de cercetare.

Referințele, bibliografia include susținerea informațiilor existente în această teză de abilitate.

Rezultatele științifice obținute în cei 8 ani de cercetare postdoctorală sunt cuantificate în peste 80 lucrări științifice (peste 35 sunt articole publicate în reviste indexate ISI), 8 cărți și/sau capitole de carte, 178 de citări (h-index 9, ISI Thompson), membru sau director în 17 granturi de cercetare (din care 7 internaționale cu multipli parteneri) în valoare de peste 8 milioane de euro; în domeniul farmacologiei clinice, nanomedicinei, dezvoltării medicamentelor și terapia durerii.

Realizările mele profesionale și științifice de până acum reprezintă suportul ce îmi va permite, atât continuarea educării generațiilor următoare de studenți și medici, precum și selectarea și formarea noilor cadre universitare și doctoranzi la o calitate adaptată cerințelor unei universități europene moderne, în paralel cu dezvoltarea cercetării științifice, atât în domeniul farmacologiei clinice, cât și în domeniile conexe.

## SECTION I - SCIENTIFIC ACHIEVEMENTS

### 1.1 ASSESSING THE INFLUENCE OF TRACE ELEMENTS ON ANALGESIC DRUGS AND PAIN

#### 1.1.1 Background and motivation for research

Approximately 20% of Europe's adult population suffers from chronic pain, which has become a condition in itself (van Hecke et al., 2013). Therapeutic options for the treatment of chronic pain include life-style changes and interventions but, mainly, the regular administration of analgesics.

Trace elements represent a group of essential metals or metalloids necessary for life, present in minute amounts. Most of them (Fe, F, Mg, Si, Zn) are involved in various biochemical enzymatic and metabolic processes, and some have been investigated in relation to pain perception and control. Several studies have been performed to assess the potential beneficial role of dietary supplements, but the results have been controversial (Soni et al., 2010).

Analgesic adjuvants are drugs not specifically designed for an analgesic effect but, when used, can enhance the effect of other analgesic drugs or improve pain control. Most popular analgesic adjuvants include antidepressants and anticonvulsants; currently, trace elements are at the bottom of the list, despite being some of the most easily administered and cheapest available options.

Tramadol is a commonly prescribed, atypical, centrally acting, synthetic analgesic. In addition to its effect on m-opioid receptors, tramadol inhibits the reuptake of both serotonin and norepinephrine, an effect that contributes to its analgesic efficacy (Grond and Sablotzki, 2004). Tramadol is commonly indicated in both acute and chronic pain states, ranging from trauma or renal colic to malignant pain (Khandave et al., 2010), and is frequently marketed in combination with acetaminophen, resulting in longer duration of action and enhanced analgesic effect (Dhillon, 2010).

Widely spread, Zinc ( $Zn^{2+}$ ) is a virtually non-toxic trace element. 5-15% of the cerebral  $Zn^{2+}$  is found in the presynaptic vesicles of glutamergic nerve terminations, thus having a possible role in the synaptic transmission (Pan et al. 2011; Ketterman and Li 2008; Kay, 2008, Maserejian et al., 2012). Mayer et al (1989) showed that  $Zn^{2+}$  is released simultaneously with glutamate, exerting the role of a non-competitive NMDA antagonist while Mayer and Vyklicky (1989) showed that  $Zn^{2+}$  does not prevent the NMDA binding site affinity or glycine binding on the NMDA receptor.  $Zn^{2+}$  also inhibits AMPA and intrathecal  $Zn^{2+}$  in mice produces an anti-nociceptive effect, but no change in the thermoalgeic tests (Bresink et al 1996; Larson et al 2000). Animal studies also show that  $Zn^{2+}$  chelators induce hyperalgesia,  $Zn^{2+}$  ions have antinociceptive roles in neuropathic pain and that  $Zn^{2+}$  biological fraction modulation induces analgesia (Larson et al 2000; Liu et al 1999; Rodriguez-Munoz et al, 2011).  $Zn^{2+}$  and copper ( $Cu^{2+}$ ) also reduce pain and inflammation in patients (Lansdowne 1996; Hankanen et al 1991) and Kugelmas (2000) showed the utility of  $Zn^{2+}$  in muscle cramps pain.

Extracellular Zn has been shown to modulate membrane signaling and to influence NMDA receptors, which are known to play a role in pain transmission (Nozaki et al., 2011). Zn also plays an essential role in the downregulation of the neutral endopeptidase that degrades endogenous opioids (Kontargiris et al., 2012). Furthermore, Zn supplementation may relieve pain in patients with burning mouth syndrome (Cho et al., 2010), and dietary Zn intake has shown painrelieving effects (Nozaki et al., 2011).

Magnesium ( $Mg^{2+}$ ), the 4-th most abundant cation in the human body, is required for the presynaptic delivery of acetylcholine and may induce similar effects with  $Ca^{2+}$  channel blockers.  $Mg^{2+}$  is able to block mechanic hyperalgesia in rats (Lee et al 2011) and has an antinociceptive effect in neuropathic pain rat models (Xiao, 1994). Begon et al (2002) proved that intraperitoneal  $Mg^{2+}$  induces a partially or fully reversible effect on mechanical hyperalgesia in diabetic rats and leads to increased levels of  $Mg^{2+}$  in the cerebrospinal fluid and other brain regions. Koning et al. (1998) explain  $Mg^{2+}$ 's effect through its interaction with the NMDA linked Na/Ca channel, although other authors showed an NMDA-independent antinociceptive effect (Nikolaev et al 2012; Poleszak et al 2008).

Magnesium's effects in postoperative analgesia and habitual cephalalgia were assessed with good outcomes (Lee et al 2012; Mauskop et al 1994). However, while Begon (2000) advocates the  $Mg^{2+}$  passage through the blood brain barrier, Takano et al (2002) explains the anti hyperalgesic effect of intrathecal administered  $Mg^{2+}$ , by other mechanisms. Brill et al (2002) later confirms in another clinical study, the effectiveness of i.v.  $Mg^{2+}$  in neuropathic pain. Still the data is at best contradictory, since a previous peripheral neuropathy clinical study by Felsby et al (1995) yielded negative results.

Magnesium (Mg) is the main intracellular divalent cation that influences the response of nerve tissue to stimuli (Biernat et al., 2014). It is involved in several metabolic processes, protein synthesis, and neuromuscular excitability (Laires et al., 2004) and may have a permissive effect on catecholamine's actions (Iannello and Belfiore, 2001). Mg also enhances endothelium-dependent vasodilatation and reduces inflammation. Severe Mg deficiency has been shown to affect oxidative metabolism adversely (Del Gobbo et al., 2013). The systemic administration of perioperative Mg has been shown to reduce postoperative pain and opioid consumption (De Oliveira et al., 2013).

$Cu^{2+}$  is an essential trace element that may too play a part in the signaling pathways of the nervous system. Extracellular ionic  $Cu^{2+}$  is a powerful inhibitor for K channels (Ma et al 2008) and  $Cu^{2+}$  deficit decreases dopamine levels in rat brain (Yu et al 2008).  $Cu^{2+}$ -based preparations alone proved to be as efficient as morphine or exerted an improved analgesic effect when combined with non-steroid anti-inflammatory drugs in rats, possibly through an activation of  $Cu^{2+}$ -dependent opioid receptors (Okuyama et al 1987). Popa et al (2006) showed that  $Cu^{2+}$  acts as a Na channel blocker, but expressed doubts over a possible therapeutic use. Some attempts to make a  $Cu^{2+}$  based acetilsalicylic acid yielded limited results (Li et al 1990). Later, Guilarte and Chen (2007) showed that the  $Cu^{2+}$  is an NMDA inhibitor and Jones et al (2007) presented a possible toxic interaction between  $Cu^{2+}$  and serotonin in neurodegenerative diseases. In 2008, Ma et al proved that  $Cu^{2+}$  is a powerful bradykinin and K channel inhibitor, both having an important role in pain transmission, while Yu et al and Tamba et al argued for a  $Cu^{2+}/Zn^{2+}$  superoxide dismutase role, linked to neuropathic and inflammatory pain mechanisms.

Manganese (Mn) plays an important role in enzyme activation. Both Mn catalase and Mn superoxide dismutase require this trace element, so Mn is involved in detoxification of superoxide free radicals and reducing oxidative stress (Martinez-Finley et al., 2013). Exposure to high concentrations of Mn has been shown to induce neurological anomalies such as behavioral changes, movement disorders, and muscle spasms (Kondakis et al., 1989). Mechanisms involved include:

- 1) Mn's preferential uptake by the brain (Martinez-Finley et al., 2013), where it increases the rate of oxidative phosphorylation;
- 2) Mn's influence on the dopaminergic system (Bird et al., 1984); and
- 3) an increase in reactive oxygen species in the presence of high levels of Mn (Zwingmann et al., 2003).

Heavy metal trace elements (HMTE) represent a group of metals or metalloids present in minute amounts in humans and include Cobalt (Co), Nickel (Ni) and Molybdenum (Mo), which are considered essential for human health (Gromiec et al., 2013).

The rationale of our study is based on several critical statistical data:

- over 50.000 dietary or food supplements are on the market today with many containing Co, Ni and Mo;
- 40% of the US general population (Kawamoto et al., 2013) and more than 65% of chronically ill patients take nutritional supplements (Eisenberg et al., 2011; Van Rompay et al., 2008);
- Pain, and especially chronic pain, affects more than 1.5 billion people worldwide;
- The inclusion of so called pain food supplements has become a common therapeutic approach.

For years, Cobalt, Nickel or Molybdenum were mostly associated with toxic effects and scarcely investigated for other physiological roles, especially in pain generation, transmission or modulation.

Cobalt (Co) is a constituent of cobalamin, and this was considered its only role. Dietary intake varies between 5 - 50µg/day. Co is a potent inducer of oxidative stress leading to toxicity, carcinogenicity, DNA damage and sister-chromatid exchange (Jomova and Valko, 2011). Co shows cytotoxic effects on various cell types including neurons (Wang et al., 2006), can induce apoptosis and necrosis (Huk et al., 2004) but also damage mitochondria (Battaglia et al., 2009). Co cations can also block Ca-mediated neural transmission, following central administration. No direct investigation has been performed so far regarding its role in pain following peripheral administration.

Nickel (Ni) plays an important role in animals (Schaumlöffel, 2012) while low levels are reducing growth and severely interfere lipid metabolic pathways in rats (Stangl and Kirchgessner, 1996). Dietary intake can reach 1 mg/day (Wong et al., 2012). Ni role in nociception has been little investigated. Ni is a non-selective Ca channels blocker, inhibiting the delivery of pain mediators (Barritt, 1999; Prado, 2001). Ni may induce direct contact dermatitis. Pain and itching sensory neurons are part of the DRG and trigeminal system and Ni effect in itching induction can be amplified by tissue acidosis (Luebbert et al., 2010). Chronic exposure to Ni can lead to impaired olfaction and anosmia (Jia et al., 2010), neurotoxicity, headaches, lethargy and ataxia. Ni exposure damages the mitochondrial function and impairs cell viability, inhibits the cell proliferation, blocks neuronal Ca channels,

including voltage-dependent T-type and R-type (Kang et al., 2006; 2007), ASIC's (Staruschenko et al., 2007) as well as GABA-activated channels (Fisher and Macdonald, 1998).

Molibdenum (Mo), part of several redox enzymes, is involved in the control mechanisms of purines and fats metabolism. Dietary intake ranges from 0.16–0.2 mg/day (Holzinger, 1998). Data on Mo and pain is also very limited. A single pilot clinical study (Moss, 1995) showed a significant pain relieve in the Mo treated group.

These data intrigued and challenged me to try to investigate together with my colleagues if there are any connections between these trace elements and pain reception, transmission and modulation. We believe that, given the enormous quantities of food supplements consumed in the world (including HMTE), with more than 1 billion people with pain worldwide, the scarcity of scientific information of the matter, and the lack of any guidelines or regulations for the healthcare provider or the public for that matter, it is highly important and urgent for both the scientific community as well as the general public to investigate, understand and take eventual measures regarding the trace elements in food supplements in patients with pain.

Modern pain treatments are frequently associated with dietary supplements containing trace elements in patients suffering from chronic algesia. The effect of trace elements on pain remains a largely overlooked and under investigated subject, especially for in-vivo settings. My long term goal is to evaluate the in-vivo effects on nociception and how to ultimately change the patient's life via improved pain therapies. Below are some of the publications that reflect my interest and constant work in the field.

**Tamba BI**, Jaba IM, Mungiu OC. Experimental data regarding the acute effect on nociception of low doses of systemically administered manganese. *Medimond International Proceedings 2007*; 59-65 (E).

**Tamba BI**, Constantin-Leon MM, Petreuş T. Common trace elements alleviate pain in an experimental mouse model. *Journal of Neuroscience Research 2013*; 91(4):554-561.

**Tamba BI**, Alexa Stratulat T. Trace Elements Alleviate Pain in Mice and Humans. In: Watson RR, Zibadi S. *Nutritional Modulators of Pain in the Aging Population*. First edition. London: Academic Press, Elsevier; 2017. pp 199-216.

Alexa T, Mârza A, Voloseniuc T, **Tamba BI**. Enhanced analgesic effects of tramadol and common trace element co-administration in mice. *Journal of Neuroscience Research 2015*; 93(10):1534-1541.

**Tamba BI**, Jaba IM, Bild V et al. The antinociceptive effect of systemically administered Cadmium on acute pain models. *Therapeutics Pharmacology and Clinical Toxicology 2008*; 12(4):483-486.

**Tamba BI**, Jaba IM, Ionescu D et al. Systemically administered - Cobalt pharmacological data regarding an antinociceptive action. *Therapeutics, Pharmacology and Clinical Toxicology* 2009; 13(1):73-76.

**Tamba BI**, Petreuş T, Constantin-Leon MM et al. Heavy metal trace elements induced antinociception in an experimental mouse model. *Revista De Chimie* 2015; 66(7):976-982.

In the following sections I will present some of the results obtained in three research projects aimed at assessing the relationship between trace elements/trace heavy metals and pain perception. Study 1 is centered on the effect of common trace elements on pain, study 2 investigated the effect of adding trace elements to Tramadol on the drug's efficacy and study 3 focused on heavy metals and nociception.

### 1.1.2 Material and methods

#### *Animals*

All animal experimental procedures employed in the studies were strictly in accordance with the *European Community guidelines regarding ethics and approved by UMF animal care and use committee*. The animal facility of the Central Drug Testing Laboratory "Grigore T. Popa" University of Medicine and Pharmacy, Iasi, supplied adult male Swiss mice with an average weight of  $35 \text{ g} \pm 2 \text{ g}$ . The animals were housed in a temperature-controlled room ( $21 \pm 2^\circ\text{C}$ ) with a 12 hours/12 hours light/dark cycle, 4 mice per cage, and allowed to acclimate for at least 24 hours before use, with free access to food and water (Nolen 2011; Zimmermann 1983).

#### *Nociception studies*

The antinociceptive effect of the tested substances was evaluated by hot plate test (HP test) and tail flick test (TF test), behavioral tests that quantify the thermal nociception.

*The Tail Flick Test (TF)* (D'Amour and Smith, 1941) assesses spinal response to pain by measuring the tail flick reflex latency following exposure to a heat stimulus. The Tail-Flick unit (37360, UgoBasile, Italy) focuses a heat source on the distal portion of the mouse's tail (4-5 cm from the tip). The tail-flick latency represents the reaction time necessary for the mouse to remove its tail from the heat source. Animals displaying baseline latencies of more than 7.5 s were excluded from the study. The test was performed at 15', 30', 45', 1 hour respectively, after the administration of substances or saline (control). A maximum TF latency of 15 sec was permitted to minimize tissue damage to the mouse's tail.

The HP test was performed on mice using an Ugo Basile HP device. Temperature was set at  $54 \pm 0.5^\circ\text{C}$ . A chronometer measured the latency observed from the time when the mouse was placed on the heated surface

*The Hot-Plate Test (HP)* (adapted after Woolfe and MacDonald, 1944) assesses both spinal and supra-spinal pathways. The mice were placed in an open Plexiglas tube on the Hot-Plate apparatus (UgoBasile, model-DS 37, Italy) set at a temperature of  $55 \pm 0.1^\circ\text{C}$ ; the response latency was defined as the time between placing the animal on the plate and the occurrence of the first overt behavioral sign of nociception such as (i) the mouse licking a hind paw, (ii) vocalization, or (iii) an escape response. Analgesic measurements were

performed at baseline and 15', 30', 45', 1 hour after administration the drug or 0.9 % saline (control group). A cut-off time of 30 seconds was considered for the HP test. Treatments that produced a significant increase in the nociceptive thresholds were considered to be antinociceptive (Mungiu et al 2002). Animals displaying baseline latencies of more than 15 s were excluded from the study.

The antinociceptive effect on visceral pain of the tested substances was also evaluated by means of *the acetic acid-induced writhing test*. The abdominal stretch, or writhing assay, was performed by injecting 0.1 ml of 1.0 % acetic acid intraperitoneal, in manually restrained mice. Immediately after injection, animals were placed in a large glass cylinder. The number of abdominal stretches occurring in successive 5 minutes time intervals was counted beginning 5 minutes after acetic acid, for a 30 minutes period after intraperitoneal injection of diluted acetic acid. The tested substances were administered 5 minutes prior to acetic acid intraperitoneal injection. Values are reported as the mean ( $\pm$  S.E.M.) for each treatment with groups composed of eight mice. Treatments that produced a significant decrease in the number of abdominal stretches were considered to be antinociceptive. The mice were kept under observation for a period of 72 hours and then sacrificed.

*Unprompted behaviour required Activity Test Cage evaluation* - This assay records spontaneous coordinate activity and its variations in mice. All weight measurements and assay procedures were performed between 9.00 - 11.00 AM. An Ugo Basile Activity Cage System was used to record horizontal and vertical activity, as the total count for beam interruptions for a 2 minutes observation time. Evaluated products were administered 15 min prior this test.

Spontaneous behaviour test was performed in blind (the experimenter was not aware of the treatment received by the animals). The activity cage test was a complementary evaluation, which sought to investigate if, there are, any spontaneous behavioral changes in the test animals for a better interpretation of the pain evaluation tests. The conclusion on the sedative or anxiolytic effects was based on well-established literature data using the activity cage and spontaneous behavior testing.

### *Statistics*

SPSS 16.0 for windows from IBM SPSS Data Collection or Graph Pad Prism 5 softwares were used. Data were expressed as the mean  $\pm$  standard deviation for each measurement time. Differences between treatment groups were analyzed using ANOVA one-way method for comparison at each time point, followed by Bonferroni post-hoc tests. The p values less than 0.05 were used to indicate a significant difference for all tests.

Pain inhibition to various stimuli (Yin et al., 2003) was also calculated according to formula:

$$\% \text{ Inhibition} = [(T_x - T_0) / (T_m - T_0)] \times 100$$

where  $T_0$  represents the latency prior drug administration (onset),  $T_x$  represents the latency for different consecutive time intervals and  $T_m$  is the cut-off time (maximum time allowed) to prevent tissue lesions in mice tail.  $T_m$  is the maximum time allowed (cut-off time) to avoid any possible lesions to the test animal.

*Drugs & Study design*

**Study 1.** All used reagents were purchased from Sigma Aldrich Chemie (GmbH, USA) and included  $Zn^{2+}$  sulphate,  $Zn^{2+}$  citrate,  $Mg^{2+}$  chloride,  $Cu^{2+}$  chloride,  $Cu^{2+}$  sulphate. To eliminate possible interference due to the sulphate group when tested, another salt of the same trace element was also investigated. Different groups of 8 mice were intraperitoneally injected with one of the following formulations: 0.9% saline for the control group (0.3 ml),  $Zn^{2+}$  sulphate (0.5 and 2.0 mg/kg respectively),  $Zn^{2+}$  citrate (0.125 and 0.5 mg/kg respectively),  $Mg^{2+}$  chloride (37.5, 75 and 150 mg/kg respectively),  $Cu^{2+}$  chloride (0.5, 1.0, 2.0 mg/kg respectively) and  $Cu^{2+}$  sulphate (0.5 and 1.0 mg/kg respectively), all salts solved in 0.3 ml saline/mouse.

**Study 2.** The drugs used in these experiments were: Tramadol (KRKA Slovenia), Magnesium Chloride ( $MgCl_2$ ) (Sigma-Aldrich ChimieGmbH, Steinheim, Germany), Manganese Chloride ( $MnCl_2$ ) (Sigma-Aldrich ChimieGmbH, Steinheim, Germany) and Zinc Chloride ( $ZnCl_2$ ) (Sigma-Aldrich ChimieGmbH, Steinheim, Germany); all drugs were freshly diluted in normal saline and administered via the intraperitoneal (i.p.) route.

For each trace element, different doses were tested; they were chosen according to previous dose-dependent studies performed in our laboratory (Tamba et al. 2013). All substances were administered via the i.p. route. Different groups of mice were injected with one of the following formulations: 0.9% saline for the negative control group (0.3 ml), Tramadol 50 mg/kg b.w. for the positive control group, Tramadol 50 mg/kg b.w. +  $ZnCl_2$  (2.4, 1.2 or 0.6 mg/kg b.w.) for the Zn group, Tramadol 50 mg/kg b.w. +  $MgCl_2$  (150, 75 or 37.5 mg/kg b.w.) for the Mg group and Tramadol 50 mg/kg b.w. +  $MnCl_2$  (14.4, 7.2 or 3.6 mg/kg b.w.) for the Mn group.

All mice were assessed by means of the HP and TF tests before substance administration (baseline) and 15, 30, 45 and 60 minutes after administration. Response latencies were automatically recorded.

**Study 3.** Various groups of 8 mice each were selected and specific formulations were injected intraperitoneally. Control groups received 0.1 mL of 0.9% saline while test groups received Co chloride (doses of 3.75 and 7.5 mg/kg b.w. respectively), Ni chloride (doses of 0.5 and 2 mg/kg b.w. respectively) and Na-molybdate (doses of 25 and 50 mg/kg b.w. respectively). All reagents had analytical purity, being purchased from Sigma Aldrich Chemie (GmbH USA). All calculations were made on the chemicals used (not metal component alone).

The doses administered were calculated as fractions of known, published intraperitoneal IP LD50 in mice. We did not use ppm data, as standard toxicity tests and data use LD50 and not ppm.

Our experimental models used doses 5 to 96 times less than known LD50's and did not induce any significant toxic effect. The used doses were:

- 1/24 and 1/12 for Cobalt chloride of LD50. (LD50 90mg/kg b.w.);
- 1/96 and 1/24 for Nickel Chloride (LD50 48 mg/kg b.w.);
- And 1/10 and 1/5 for Sodium Molybdate (LD50 257 mg/kg b.w.).

The pH of the solutions was slightly acid but still at physiological levels. The solvent of the chemical compound was saline (pH 5.5) (Reddi, 2—7), which is also physiological for IP administration and had no effects in control animals. The trace elements however, did not

influence significantly the pH of the injected solutions. Thus, there was no need to use a buffer to attenuate for possible acidity, if any.

### 1.1.3 Results

#### The effect of Zn, Mg and Cu salts on experimental pain

Measurements performed during the TF test show that  $Zn^{2+}$  sulphate induces an increase in TF latency at 15 and 30 minutes from intraperitoneal injection, which indicated a significant antinociceptive effect. TF latency increase and therefore the analgesic effect also seemed to be dose dependent at 15 minutes. For the 0.5 mg/kg  $Zn^{2+}$  sulphate dose, the TF latency is significantly increased at 15 and 30 minutes, with a peak at 30 minutes ( $7.29 \pm 0.23$  sec). In the 45th and 60th minute respectively following the administration, TF latency lowered under the control values, but with no statistical significance. For a 2 mg/kg  $Zn^{2+}$  sulphate dose, TF latency showed the same profile. (Fig. 1A, B, C).

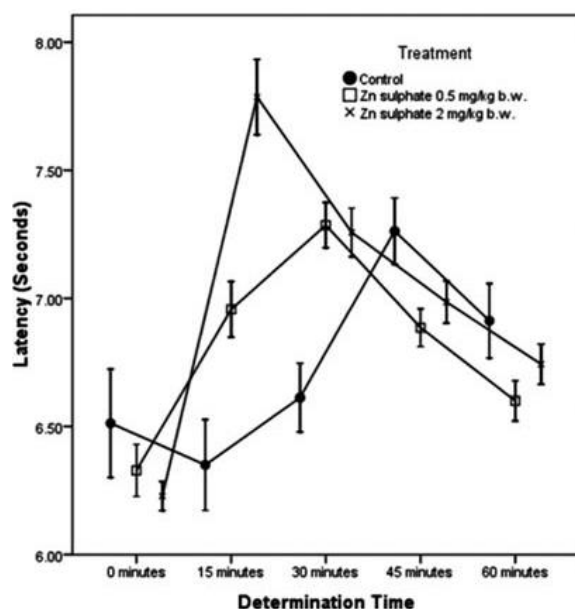


**Fig. 1.A.** Latencies for TF test, after intraperitoneal administration of  $Zn^{2+}$  sulfate in different concentrations (0.5, 2.0 mg/kg)

Pain inhibition calculations showed that  $Zn^{2+}$  sulphate induces a dose-dependent analgesic effect, lowering the TF pain by up to 17.78%. A dose of 0.5 mg/kg reduced the TF pain by 11.03% at 30 minutes while the 2.0 mg/kg dose induces a maximal inhibition of 17.78% at 15 minutes. The maximum dose effect is recorded at 15 minutes after administration. (Table I).

The HP test (HP) following intraperitoneal administration of  $Zn^{2+}$  sulphate showed increased and dose dependent latencies at 15, 30, 45 and 60 minutes (fig. I. 1A, B, C). Statistically significant effects were recorded at 15 and 30 minutes for a 0.5 mg/kg dose, with a peak at 30 minutes ( $12.87 \pm 0.32$  sec); at 45 and 60 minutes, the latency was increased but with no statistical significance. The same effect was recorded for all intervals for a 2.0 mg/kg dose, with a peak at 15 minutes ( $13.91 \pm 0.62$  sec).

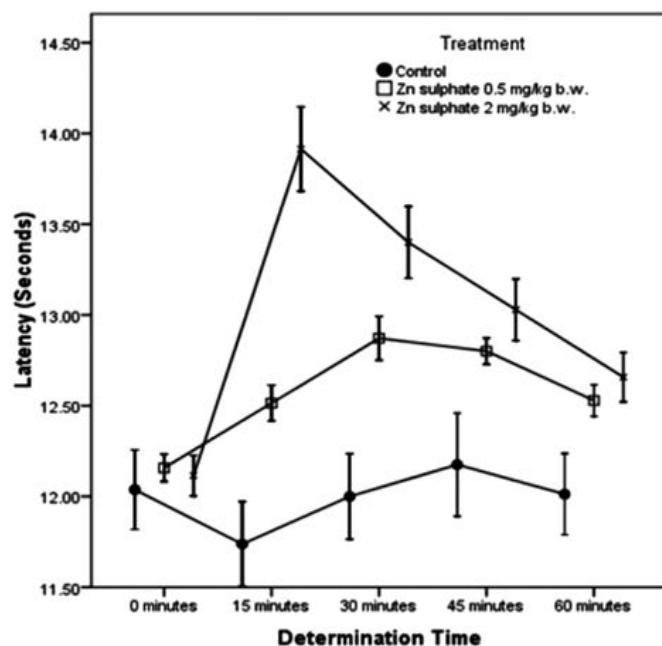


**Fig. 1B.** Latencies for HP test, after intraperitoneal injection of  $Zn^{2+}$  sulfate in different concentrations (0.5, 2.0 mg/kg).

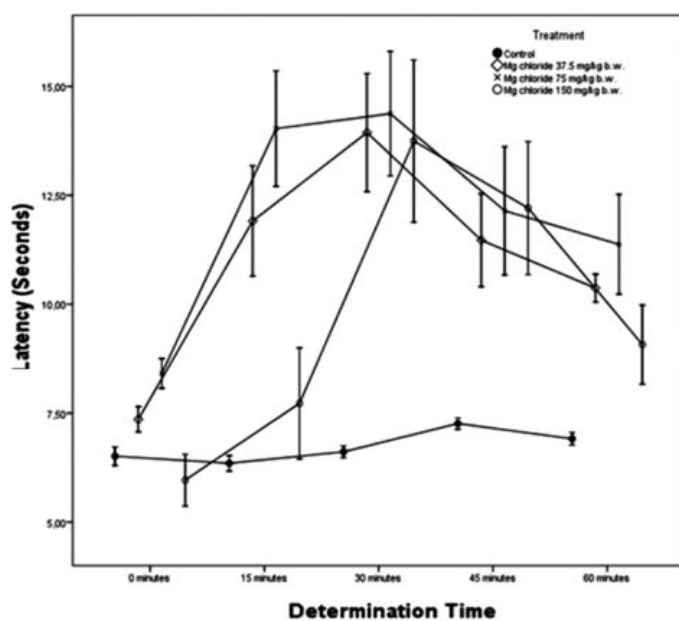


**Fig. 1C.** Latencies for TF test, after intraperitoneal injection of  $Mg^{2+}$  chloride at different concentrations (37.5, 75, 150 mg/kg).

Acetic acid-induced writhing test results show that  $Zn^{2+}$  sulphate induced a statistically significant nociceptive effect, illustrated by the decrease of the total number of writhings at 10, 20 and 30 minutes for the 0.5 mg/kg dose and at 5, 10, 15, 20 and 25 minutes for the 2.0 mg/kg dose; the maximum inhibition for visceral pain was recorded at 10-15 minutes from  $Zn^{2+}$  sulphate administration. Our results showed that pain inhibition was more significant at the 2.0 mg/kg dose (25.71% at 10 minutes) than at the 0.5 mg/kg dose (17% at 10 minutes). (table II).

The activity cage test after the administration a dose of 1.0 mg/kg showed no significant changes during evaluation of the spontaneous behavior (Fig. 3 A,B). Similar data on all test evaluations were obtained for the  $Zn^{2+}$  citrate doses of 0.125 and 0.5 mg/kg respectively.

**Table I.** Average pain inhibition values for tested substances in TF and HP assays after administration of Zn<sup>2+</sup> Sulfate 0.5 and 2.0 mg/kg; Mg<sup>2+</sup> Chloride 37.5 and 150 mg/kg; and Cu<sup>2+</sup> Chloride 0.5, 1.0, and 2.0 mg/kg

Drug	0 min	15 min	30 min	45 min	60 min
Zn <sup>2+</sup> sulfate, 0.5, TF	0.00	7.26	11.03	6.40	3.11
Zn <sup>2+</sup> sulfate, 0.5, HP	0.00	2.00	4.01	3.60	2.08
Zn <sup>2+</sup> sulfate, 2.0, TF	0.00	17.79	11.74	8.63	5.85
Zn <sup>2+</sup> sulfate, 2.0, HP	0.00	10.08	7.20	5.11	3.03
Mg <sup>2+</sup> chloride, 37.5, TF	0.00	49.79	65.57	50.12	38.26
Mg <sup>2+</sup> chloride, 37.5, HP	0.00	23.18	31.88	24.88	5.75
Mg <sup>2+</sup> chloride, 75, TF	0.00	57.31	58.15	34.79	34.18
Mg <sup>2+</sup> chloride, 75, HP	0.00	29.60	20.41	16.88	17.20
Mg <sup>2+</sup> chloride, 150, TF	0.00	17.67	72.68	71.39	45.40
Mg <sup>2+</sup> chloride, 150, HP	0.00	30.24	20.54	23.13	13.74
Cu <sup>2+</sup> chloride, 0.5, TF	0.00	4.96	1.90	-0.81	-2.57
Cu <sup>2+</sup> chloride, 0.5, HP	0.00	3.17	1.97	-0.01	-1.84
Cu <sup>2+</sup> chloride, 1.0, TF	0.00	9.58	6.88	4.49	1.81
Cu <sup>2+</sup> chloride, 1.0, HP	0.00	8.59	6.80	5.10	2.92
Cu <sup>2+</sup> chloride, 2.0, TF	0.00	18.97	28.60	23.62	18.00
Cu <sup>2+</sup> chloride, 2.0, HP	0.00	15.52	23.73	19.59	13.44

Measurements performed during the TF test show that Mg<sup>2+</sup> chloride induced a significant TF latency at 15 and 30 minutes after intraperitoneal administration, indicating a significant antinociceptive effect. In the 45th and 60th minute respectively, TF latency values lower under control values, with no statistical significance. TF latency seems to be dose dependent: for a 37.5 and 75 mg/kg Mg<sup>2+</sup> chloride dose, TF latency is significantly increased for all intervals, recording a peak at 30 minutes, (at  $13.94 \pm 4.29$  sec). Increasing the dose at 150 mg/kg changed only the evolution of the anti-nociceptive effect but not its intensity. Following TF latencies conversion to a percent of the maximum possible effect, Mg<sup>2+</sup> chloride induces a dose-dependent analgesic effect by lowering the TF pain by 72.68% (Table I).

**Table II.** Average Pain Inhibition Values for Tested Substances in the Writhing Test After Administration of Zn<sup>2+</sup> Sulfate 0.5 and 2.0 mg/kg; Mg<sup>2+</sup> Chloride 150 mg/kg; and Cu<sup>2+</sup> Chloride 0.5, 1.0, and 2.0 mg/kg

Drug	5 min	10 min	15 min	20 min	25 min	30 min
Zn sulfate 0.5 mg/b.w.	13.61	17.01	7.52	16.30	4.15	14.29
Zn sulfate 2 mg/b.w.	18.27	25.71	20.52	25.02	17.33	0.00
Mg chloride 150 mg/b.w.	86.03	83.75	84.71	89.54	86.82	85.71
Cu chloride 0.5 mg/b.w.	21.37	26.29	30.45	35.48	43.69	48.21
Cu chloride 1 mg/b.w.	22.92	40.80	39.62	41.58	43.69	46.43
Cu chloride 2 mg/b.w.	22.40	40.80	38.10	57.28	54.47	42.86

The HP test (HP) following intraperitoneal administration of Mg<sup>2+</sup> chloride showed anti-nociceptive effect for all doses and all recorded intervals, but only some doses/intervals were statistically significant. The response intensity is not dose dependent. Significant latencies were recorded for the low dose (37.5 mg/kg) at 15 and 30 minutes (that includes a peak of  $15.75 \pm 5.32$ ); for medium and high doses, the effect was faster and the peak latency

recorded at 15 minutes was of  $14.16 \pm 6.50$  for 75mg/kg dose and  $15.03 \pm 5.46$  for 150 mg/kg dose (Fig. 2A, B, C).

HP latencies conversion to a percent of the maximum possible effect showed that  $Mg^{2+}$  chloride induces an antinociceptive effect, lowering the pain by 31.89%. The maximum dose-dependent effect is recorded at 15 minutes after administration of the low dose and at only 15 minutes for the medium and higher doses (Table I).

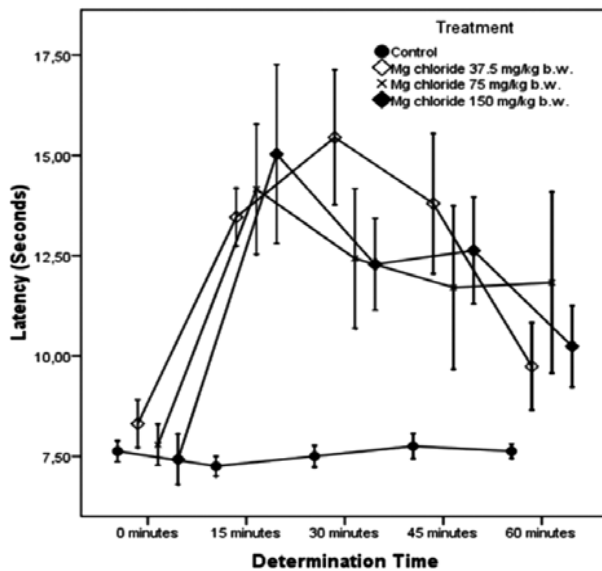


**Fig. 2A.** Latencies for HP test, after intraperitoneal injection of  $Mg^{2+}$  chloride at different concentrations (37.5, 75, 150 mg/kg)

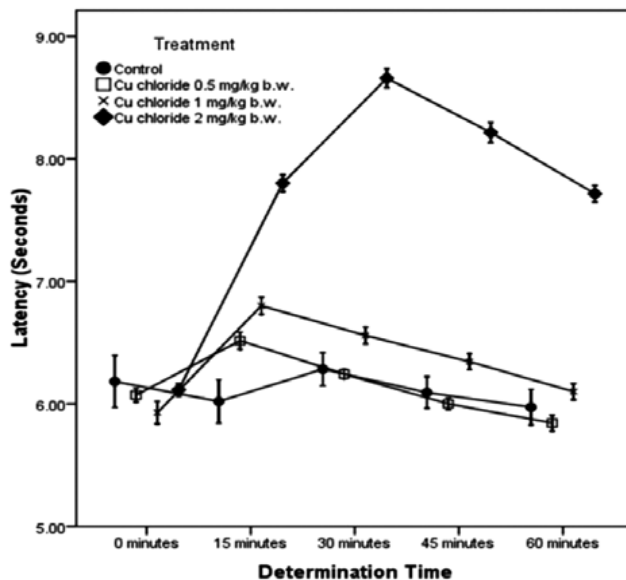


**Fig. 2B.** Latencies for TF test, after intraperitoneal injection of  $Cu^{2+}$  chloride at different concentrations (0.5, 1.0, 2.0 mg/kg)

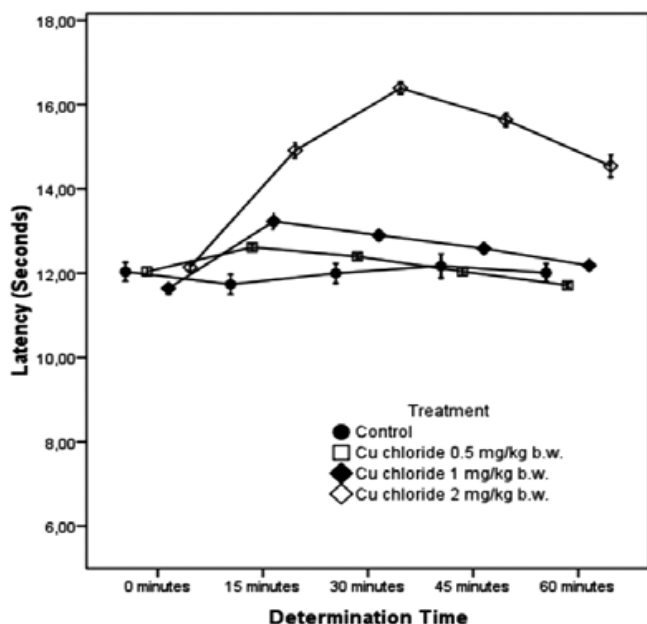


**Fig. 2C.** Latencies for HP test, after intraperitoneal administration of Cu<sup>2+</sup> chloride at different concentrations (0.5, 1.0, 2.0 mg/kg)

Acetic acid-induced writhing test results showed that Mg<sup>2+</sup> chloride induces a statistically significant nociceptive effect, by decreasing the total number of writhings at 15-20 minutes for the 150 mg/kg dose (Table II). The activity cage test with a dose of 150 mg/kg showed significant changes during evaluation of the spontaneous behavior, recording an important sedation effect together with an anxiolytic action (Fig. 3A, B).

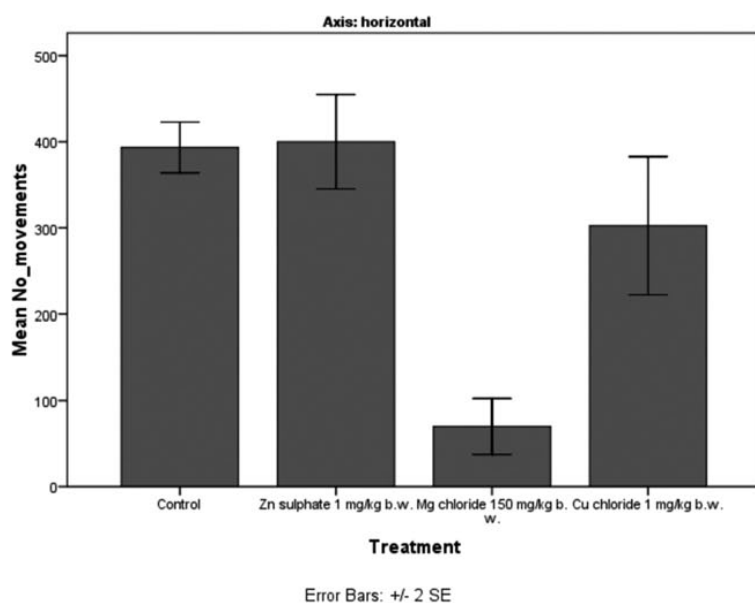


**Fig. 3A.** Number of spontaneous movements per time interval in activity cage test, on horizontal axis after administration of 0.9% saline for the control group, Zn<sup>2+</sup> sulfate 1 mg/kg, Mg<sup>2+</sup> chloride 150 mg/kg, and Cu<sup>2+</sup> chloride 1.0 mg/kg.

Measurements performed during the TF test showed that Cu<sup>2+</sup> chloride induced a significant TF latency at 15, 30, 45 and 60 minutes after intraperitoneal administration, indicating a significant antinociceptive effect. TF latency seems to be significantly dose dependent only at 15 minutes for 0.5 mg/kg and 1 mg/kg Cu<sup>2+</sup> chloride dose. The most important analgesic effect was recorded for the 2 mg/kg Cu<sup>2+</sup> chloride dose, with a maximum effect at 30 minutes and a mean TF latency of 8.66 ± 0.21 (fig. I.2). Following TF latencies conversion to a percent of the maximum possible effect, Cu<sup>2+</sup> chloride induces a dose-

dependent analgesic effect by lowering the TF pain by 28.60% (2 mg/kg dose, at 30 minutes). (Table I).

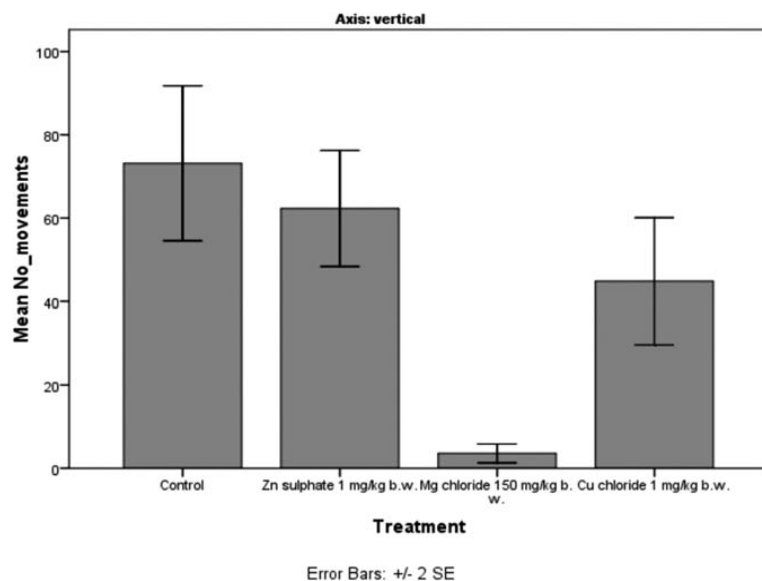


**Fig. 3B.** Number of spontaneous movements per time interval in activity cage test, on vertical axis after administration of 0.9% saline for the control group, Zn<sup>2+</sup> sulfate 1 mg/kg, Mg<sup>2+</sup> chloride 150 mg/kg, and Cu<sup>2+</sup> chloride 1.0 mg/kg.

The HP test (HP) following intraperitoneal administration of Cu<sup>2+</sup> chloride showed anti-nociceptive effects for all doses and all recorded intervals, but only some doses/intervals were statistically significant. The response intensity is dose dependent. Significant latencies were recorded for the low dose (0.5 mg/kg) at 15 minutes (that includes a peak of  $12.61 \pm 0.19$ ); at 30 minutes, the latency values lowered under control values. For medium dose (1 mg/kg), significant latencies were recorded at 15 minutes (with a peak of  $13.23 \pm 0.51$ ) and at 30 minutes. The higher dose (2 mg/kg) induced a maximum intensity effect at 30 minutes (with a peak of  $16.39 \pm 0.38$ ) (fig. I.2). HP latencies conversion to a percent of the maximum possible effect showed that Cu<sup>2+</sup> chloride induces an antinociceptive effect, lowering the pain by 23.73% (table I).

Acetic acid-induced writhing test results showed that Cu<sup>2+</sup> chloride induced a statistically significant nociceptive effect, by decreasing the total number of writhings at 20-25 minutes for the 2 mg/kg dose (Table II). Activity cage test with a dose of 1 mg/kg Cu<sup>2+</sup> chloride shows slightly anxiolytic action (fig. I.3). Similar data on all test evaluations were obtained for the Cu<sup>2+</sup> sulphate doses of 0.5 and 1.0 mg/kg respectively.

### The effect of common trace elements and tramadol co-administration in mice

#### *Influence of Zn-Tramadol administration on acute nociception*

In the TF test (n=6 mice/each group), Zn significantly enhanced Tramadol's analgesic effect 30 minutes after i.p. administration, with  $p < 0.05$  (Turkey post-hoc analysis) for all three doses when compared with Tramadol alone. ANOVA repeated measures revealed a statistically significant substance effect in time ( $F(12, 60) = 1.935, P = 0.0476$ ). In the large and medium doses (2.4 and 1.2 mg/kg b.w.), this effect was transitory, and although the latency response was longer in the Zn group, it no longer reached significance at 45 and 60 minutes. Tramadol group average was  $15.18 \pm 1.93$  sec at 45 minutes and  $13 \pm 2.17$  sec at 60 minutes, whereas in the Zn group, the averages were  $17.57 \pm 2.04$  sec at 45 minutes and

16.20±1.73 sec at 60 minutes for the 2.4 mg/kg b.w. dose and 19.73±1.36 sec at 45 minutes and 19.15±1.28 sec at 60 minutes for the 1.2 mg/kg b.w. dose.

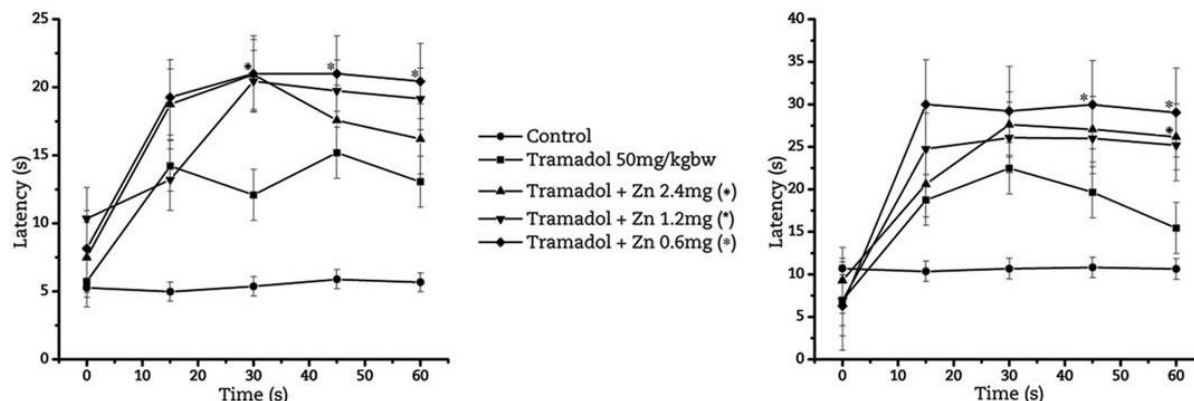


**Fig. 4.** Average latency values for Zinc (Zn) and Tramadol co-administration; \*=p<0.05 when compared to Tramadol alone

By contrast, the smallest dose (0.6 mg/kg b.w.) induced a long-lasting effect, with significant differences in latency at 30, 45 and 60 minutes when compared with Tramadol alone and average latencies of 21 s at 30 and 45 minutes and 20.43±0.42 sec at 60 minutes (Fig. 4).

When compared with saline, all groups treated with Zn-Tramadol combination or Tramadol alone had a statistically significant analgesic effect on the TF test that started after 15 minutes and persisted until the end of the experiment. All three doses induced an average pain inhibition of over 50% (76.95% for the 0.6 mg/kg b.w. dose, 58.54% for the 1.2 mg/kg b.w. dose and 63.08% for the 2.4 mg/kg b.w. dose); Tramadol's average pain inhibition in the TF test was 36.9% (Table III).

**Table III.** Average pain inhibition values for tested substances in the TF test after administration of trace metals

Drug	0 min	15 min (%)	30 min (%)	45 min (%)	60 min (%)
<i>Tramadol</i>	0.00	50.79	39.01	48.04	46.66
<i>Tramadol+ZnCl<sub>2</sub></i> 2.4 mg/kg b.w.	0.00	83.86	99.52	70.82	61.20
<i>Tramadol+ZnCl<sub>2</sub></i> 1.2 mg/kg b.w.	0.00	27.47	99.52	86.18	83.53
<i>Tramadol+ZnCl<sub>2</sub></i> 0.6 mg/kg b.w.	0.00	89.37	100.00	100.00	95.53
<i>Tramadol+MgCl<sub>2</sub></i> 150 mg/kg b.w.	0.00	56.95	58.89	89.60	60.55
<i>Tramadol+MgCl<sub>2</sub></i> 75 mg/kg b.w.	0.00	77.12	100.00	91.67	68.55
<i>Tramadol+MgCl<sub>2</sub></i> 37.5 mg/kg b.w.	0.00	70.48	83.33	75.56	77.94
<i>Tramadol+MnCl<sub>2</sub></i> 14.4 mg/kg b.w.	0.00	78.27	80.93	100.00	89.08
<i>Tramadol+MnCl<sub>2</sub></i> 7.2 mg/kg b.w.	0.00	100.00	100.00	100.00	100.00
<i>Tramadol+MnCl<sub>2</sub></i> 3.6 mg/kg b.w.	0.00	82.70	93.39	64.96	99.80
<i>Saline</i>	0.00	-2.01	0.71	7.30	3.77

For the HP test (n=6 mice/each group), adding Zn had a similar effect on Tramadol's analgesic effect, only its onset was at 60 minutes for the 2.4 and 1.2 mg/kg b.w. doses, with an average of  $15.52 \pm 2.83$  sec in the Tramadol group versus  $26.17 \pm 2.34$  sec in the Zn 2.4 mg/kg b.w. group and  $25.18 \pm 2.58$  sec in the Zn 1.2 mg/kg b.w. group ( $p < 0.05$  - Turkey post-hoc test). ANOVA repeated measures revealed a statistically significant substance effect in time ( $F(12, 60) = 2.617$ ,  $P = 0.0071$ ). In the 0.6 mg/kg b.w. group, the onset was earlier and persisted until the end of the experiment, with an average latency response of  $29.95 \pm 1.88$  sec at 45 minutes and  $29.02 \pm 1.33$  sec at 60 minutes, statistically different from the averages of the Tramadol group ( $19.67 \pm 3.02$  s at 45 minutes and  $15.52 \pm 2.83$  sec at 60 minutes) (Fig. 4). When compared with saline, all groups treated with Zn-Tramadol combination had a statistically significant analgesic effect on the HP test that started after 15 minutes and persisted until the end of the experiment. The Tramadol group induced a significant analgesic effect on the HP test that lasted until 45 minutes.

All three doses induced an average pain inhibition of over 60% (78.41% for the 0.6 mg/kg b.w. dose, 64.88% for the 1.2 mg/kg b.w. dose and 62.40% for the 2.4 mg/kg b.w. dose); Tramadol's average pain inhibition in the HP test was 41.74% (Table IV).

No statistically significant differences were noted between the groups at baseline assessment of TF and HP.

***Influence of Mg-Tramadol administration on acute nociception*** - The TF test (n=6 mice/each group) revealed that adding Mg did not produce a statistically significant enhancement of Tramadol's analgesic effect for the 150 mg/kg b.w. dose.

**Table IV.** Average pain inhibition values for tested substances assessed by the HP test after administration of trace metals

Drug	0 min	15 min (%)	30 min (%)	45 min (%)	60 min (%)
Tramadol	0.00	50.37	66.54	54.94	36.85
Tramadol+ZnCl <sub>2</sub> 2.4 mg/kg b.w.	0.00	54.03	89.30	86.18	82.48
Tramadol+ZnCl <sub>2</sub> 1.2 mg/kg b.w.	0.00	77.22	83.63	83.43	80.11
Tramadol+ZnCl <sub>2</sub> 0.6 mg/kg b.w.	0.00	100.00	96.74	99.81	95.51
Tramadol+MgCl <sub>2</sub> 150 mg/kg b.w.	0.00	29.70	41.52	49.04	33.90
Tramadol+MgCl <sub>2</sub> 75 mg/kg b.w.	0.00	83.75	90.69	94.90	99.29
Tramadol+MgCl <sub>2</sub> 37.5 mg/kg b.w.	0.00	89.57	89.96	88.64	75.81
Tramadol+MnCl <sub>2</sub> 14.4 mg/kg b.w.	0.00	72.68	86.65	86.57	78.90
Tramadol+MnCl <sub>2</sub> 7.2 mg/kg b.w.	0.00	82.30	84.56	96.22	90.38
Tramadol+MnCl <sub>2</sub> 3.6 mg/kg b.w.	0.00	89.57	89.96	88.64	75.81
Saline	0.00	-1.66	-0.31	0.55	-0.28

However, the average latency response was longer throughout the experiment in the Mg group. Both the intermediate and the small Mg dose induced significant changes after 30 minutes (with an average of  $12.08 \pm 1.87$  sec in the Tramadol group vs. 21.00 sec in both the

75 mg/kg b.w. and 37.5 mg/kg b.w. Mg-Tramadol groups,  $p < 0.05$  - Turkey post-hoc test); the 37.5 mg/kg b.w. Mg group had a more persistent increase in latency response, with statistically significant longer times that were also present 60 minutes after the i.p. administration ( $13.00 \pm 2.17$  sec in the Tramadol group vs.  $20.23 \pm 1.89$  sec in the Mg group) (Fig. 5). ANOVA repeated measures revealed a statistically significant substance effect in time ( $F(16, 80) = 2.766, P = 0.0014$ ).

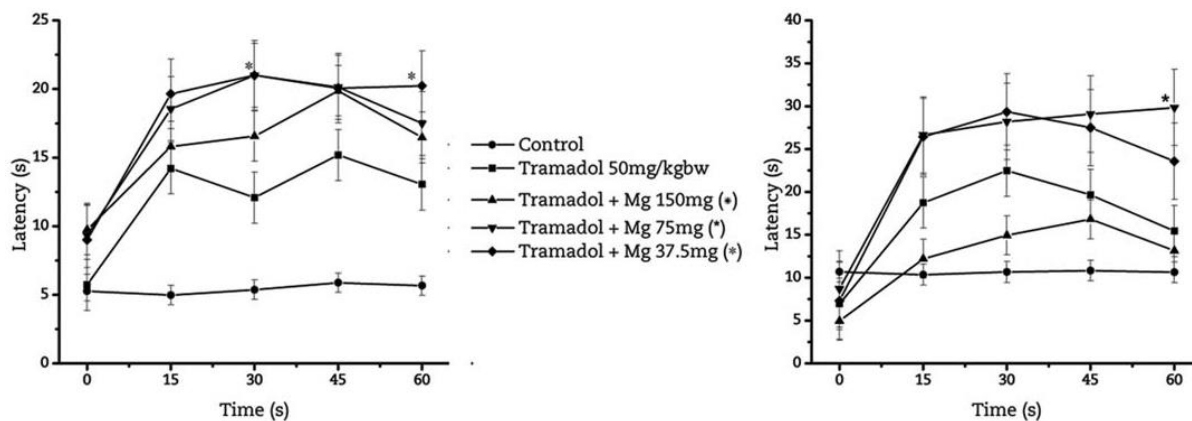


**Fig. 5.** Average latency values for Mg and tramadol coadministration. \* $P < 0.05$  compared with tramadol alone

When compared with saline, all groups treated with Mg-Tramadol combination or Tramadol alone had a statistically significant analgesic effect on the TF test that started after 15 minutes and persisted until the end of the experiment.

All three doses induced an average pain inhibition of over 50% (61.46% for the 37.5 mg/kg b.w. dose, 67.47% for the 75 mg/kg b.w. dose and 53.20% for the 150 mg/kg b.w. dose); Tramadol's average pain inhibition in the TF test was below 40% (Table III).

In the HP test ( $n=6$  mice/each group), the 150 mg/kg b.w. Mg dose did not induce significant modifications throughout the experiment. The 75 mg/kg b.w. dose significantly enhanced Tramadol's analgesic effect after 60 minutes, with an average latency response of  $15.52 \pm 2.83$  sec in the Tramadol group vs.  $29.83 \pm 2.63$  sec in the Mg group ( $p < 0.05$  - Turkey post-hoc test). The average latency response time was longer in the 37.5 mg/kg b.w. Mg group when compared with Tramadol, although it did not reach statistical significance (Fig. 5). ANOVA repeated measures revealed a statistically significant substance effect in time ( $F(16, 80) = 5.902, P < 0.0001$ ). When compared with saline, the 150 mg/kg b.w. Mg group did not induce significant changes; Tramadol group induced significant changes at 15, 30 and 45 minutes, but averages had a tendency to decrease in the Tramadol group at 60 minutes. The small and intermediate Mg dose induced a statistically significant analgesic effect on the HP test that started after 15 minutes and persisted until the end of the experiment.

The intermediate and the small Mg doses induced an average pain inhibition of over 60% (68.80% for the 37.5 mg/kg b.w. dose and 73.73% for the 75 mg/kg b.w. dose); the 150 mg/kg b.w. induced a 33.90% average pain inhibition, smaller than the average of Tramadol (41.74%); this difference, however, was not statistically significant (Table IV).

No statistically significant differences were noted between the groups at baseline assessment of TF and HP.

### ***Influence of Mn-Tramadol administration on acute nociception***

In the TF test (n=6 mice/each group), the intermediate dose induced the most persistent effect, with statistically significant differences (from the Tramadol alone group) in latency response time that started after 15 minutes and persisted until the end of the experiment (average values of 21 seconds in the Mn-Tramadol group at 15, 30, 45 and 60 minutes, respectively vs.  $14.22 \pm 1.94$  sec,  $12.08 \pm 1.87$  sec,  $15.18 \pm 1.93$  sec and  $13.00 \pm 2.17$  sec in the Tramadol group at the same times,  $p < 0.05$  - Turkey post-hoc test). Both the high and small dose of Mn increased Tramadol's analgesic effect, only in high dose the effect was statistically significant after 30 minutes and in the small dose group the effect was significant until 45 minutes (Fig. 6). ANOVA repeated measures revealed a statistically significant substance effect in time ( $F(16, 80) = 4.967$ ,  $P < 0.0001$ ).

When compared with saline, all groups treated with Mn-Tramadol combination or Tramadol alone had a statistically significant analgesic effect on the TF test that started after 15 minutes and persisted until the end of the experiment ( $p < 0.05$  - Turkey post-hoc test). All three doses induced an average pain inhibition of over 60% (68.17% for the 3.6 mg/kg b.w. dose, 80.00% for the 7.2 mg/kg b.w. dose and 69.65% for the 14.4 mg/kg b.w. dose); Tramadol's average pain inhibition in the TF test was below 40% (Table I).

In the HP test (n=6 mice/each group), neither the high, nor the small Mn dose induced a statistically significant analgesic effect when compared with Tramadol alone. The intermediate dose (7.2 mg/kg b.w.) enhanced Tramadol's effect 45 minutes after administration, with an average response latency of  $29.10 \pm 1.45$  sec vs.  $19.67 \pm 3.02$  sec in the Tramadol alone group. This effect persisted until the end of the experiment, with  $27.85 \pm 2.46$  sec in the Mn-Tramadol group vs.  $15.52 \pm 2.83$  sec in the Tramadol alone group at 60 minutes (Fig. 3). ANOVA repeated measures revealed a statistically significant substance effect in time ( $F(16, 80) = 6.630$ ,  $P < 0.0001$ ). When compared with saline, all Mn doses induced a statistically significant effect on the HP test that started after 15 minutes and persisted until the end of the experiment.

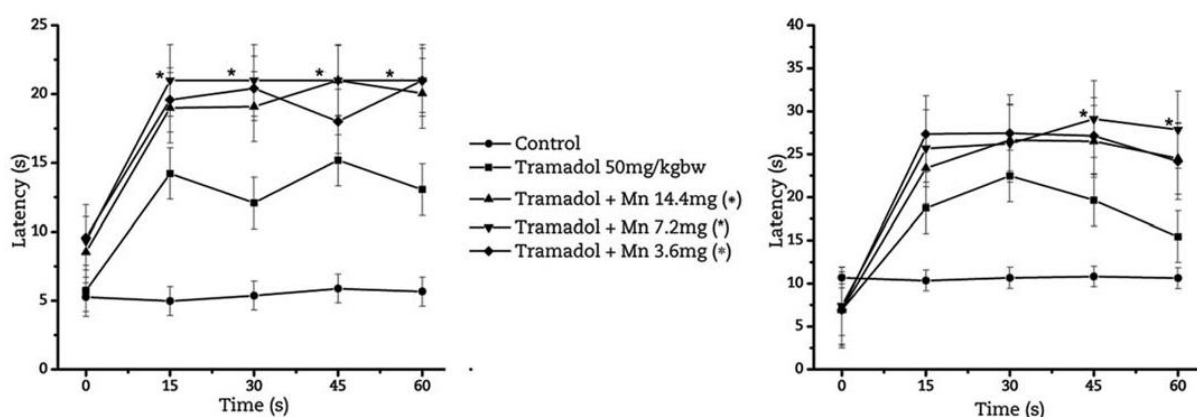


**Fig. 6.** Average latency values for Mn and tramadol coadministration. \* $P < 0.05$  compared with tramadol alone

All Mn doses induced an average pain inhibition of over 60% (68.80% for the 3.6 mg/kg b.w. dose, 70.69% for the 7.2 mg/kg b.w. dose and 64.96% for the 14.4 mg/kg b.w. dose); the average pain inhibition of Tramadol was 41.74% (Table IV).

No statistically significant differences were noted between the groups at baseline (T=0) assessment of TF and HP.

### The effect of heavy metal trace elements in experimental pain models

Results obtained following TF test showed that Co chloride can extend TF latency at 15, 30, 45 and 60 min from intraperitoneal administration, thus indicating a significant antinociceptive effect. This effect seems to be dose-dependent as TF latency increases. At a dose of 3.75 mg/kg Co chloride, the TF latency is slightly increased at 15 and 30 min, with no statistical significance; later, at 45 and 60 min TF lowered significantly beneath control values. At a dose of 7.5 mg/kg Co chloride, the TF latency recorded a similar profile, while reaching statistical difference at 15, 30 and 45 min (Fig. 7). Calculations performed to evaluate pain inhibition showed that Co chloride is inducing a dose-dependent antinociceptive effect while TF pain is reduced up to 30.87%. At 15 minutes, TF pain reduction by 30.87% was onset by a dose of 3.75 mg/kg while the 7.5 mg/kg dose induced the maximal inhibition of 24.31% at 15 min (Table V).

**Table V.** Average pain inhibition values for tested substances in tf and hp assays following administration Co chloride 3.75 and 7.5 mg/ kg, Ni chloride 0.5 and 2.0 mg/kg, sodium

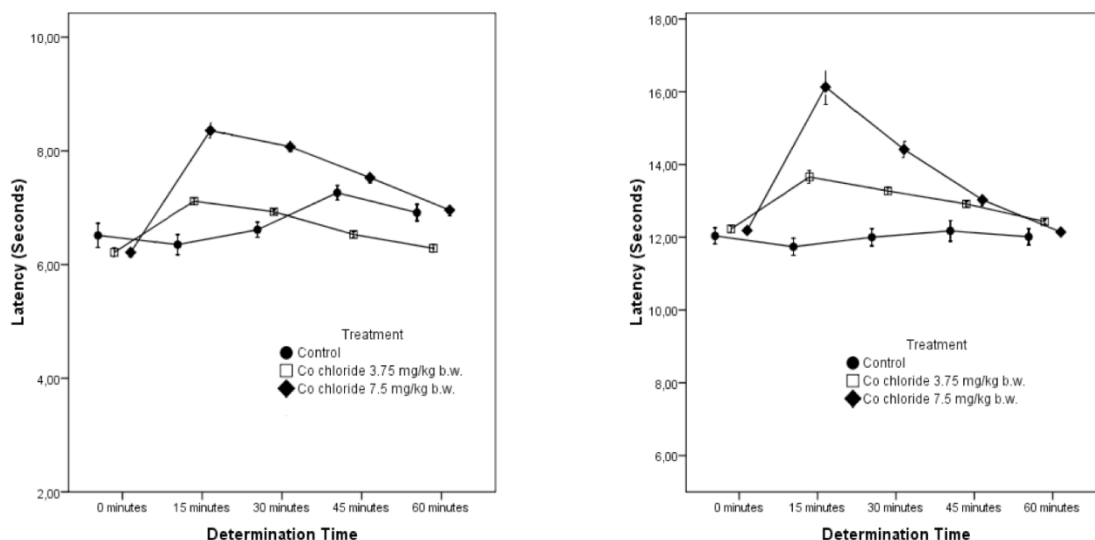
#### Molybdate 25 and 50 mg/kg

Drug-test/time interval	0'	15'	30'	45'	60'
Co chloride 3.75 TF	0	10.22	8.10	3.55	0.79
Co chloride 7.5 TF	0	24.31	21.12	14.96	8.41
Co chloride 3.75 HP	0	8.03	5.86	3.85	1.12
Co chloride 7.5 HP	0	22.13	12.52	4.74	-0.25
Ni chloride 0.5 TF	0	9.70	6.94	4.36	0.13
Ni chloride 2 TF	0	13.41	20.42	13.40	9.57
Ni chloride 0.5 HP	0	3.37	1.68	0.48	-0.73
Ni chloride 2 HP	0	11.32	19.01	11.70	6.91
Sodium Molybdate 25 TF	0	8.79	6.87	3.18	-0.50
Sodium Molybdate 50 TF	0	12.42	10.31	6.59	1.58
Sodium Molybdate 25 HP	0	4.08	3.04	1.68	-0.25
Sodium Molybdate 50 HP	0	9.22	7.95	3.97	1.03

The intraperitoneal administration of Co chloride was evaluated by HP test and increased dose dependent latencies were observed at 12, 30, 45 and 60 min (Fig. 7). Doses of 3.75 mg/kg and 7.5 mg/kg induced statistically significant effects at 15 and 30 min. Peak values were measured at 15 min for the 3.75 mg/kg dose ( $13.66 \pm 0.46$  sec) and the 7.5 mg/kg dose ( $16.13 \pm 1.27$  s).

Maximum possible effect deduced by HP latencies conversion into percent values showed an antinociceptive effect for Co chloride while pain is diminished by 22.46%.

In HP test, pain was reduced by 8.03% for a dose of 3.75 mg/kg at 15 min while the maximal inhibition of 22.13% at 15 min was induced by the dose of 7.5 mg/kg.



a)

b)

**Fig. 7.** a. Latencies for TF test, after intraperitoneal administration of Co chloride in different doses (3.75 and 7.5 mg/kg respectively), b. Latencies for HP test, following Co chloride intraperitoneal injection in different doses (3.75 and 7.5 mg/kg respectively)

Co chloride is inducing a statistically significant pain reduction illustrated by writing test results, on all recorded time intervals for all tested doses. Visceral pain undergone maximal inhibition always records for the 7.5 mg/kg doses (100%). Pain inhibition in our study was more important for the 7.5 (100% continuously) than for the 3.75 mg/kg dosage (67.86% at 30 min) (Table VI).

**Table VI.** Average pain inhibition values for tested substances in wt following administration of Co chloride 3.75 and 7.5 mg/kg, Ni chloride 0.5 and 2.0 mg/kg, Sodium molybdate 25 and 50 mg/kg.

Drug/time interval	5'	10'	15'	20'	25'	30'
Co chloride 3.75	42.06	45.45	36.57	47.69	40.09	67.86
Co chloride 7.5	100.00	100.00	100.00	100.00	100.00	100.00
Ni chloride 0.5	20.33	17.01	-0.12	7.58	2.95	7.14
Ni chloride 2	67.41	64.60	34.27	16.30	-3.04	-37.50
Sodium Molybdate 25	21.37	20.49	18.99	25.89	23.32	44.64
Sodium Molybdate 50	36.37	41.96	41.92	40.71	35.30	62.50

Spontaneous behaviour changes were significant for the 3.75 mg/kg Co chloride dose, following evaluation by activity cage test. A mild sedative and anxiolytic effect was recorded.

Measurements performed for Ni chloride intraperitoneal administration (TF test) showed a significant latency at 15, 30, 45 and 60 min and indicated a significant antinociceptive effect. TF latencies were dose-dependent for the 0.5 mg/kg and 2 mg/kg doses at 15 and 30 min and the maximal effect recorded at 30 min led to a mean TF latency of  $7.87 \pm 0.15$  s (Fig. 8). Conversion of TF latencies into a percent of maximum possible effect led to the observation that Ni chloride analgesic effect is dosedependent and is expressed by TF pain decrease up to 20.41% (2 mg/kg dose, at 30 min) (Table V).

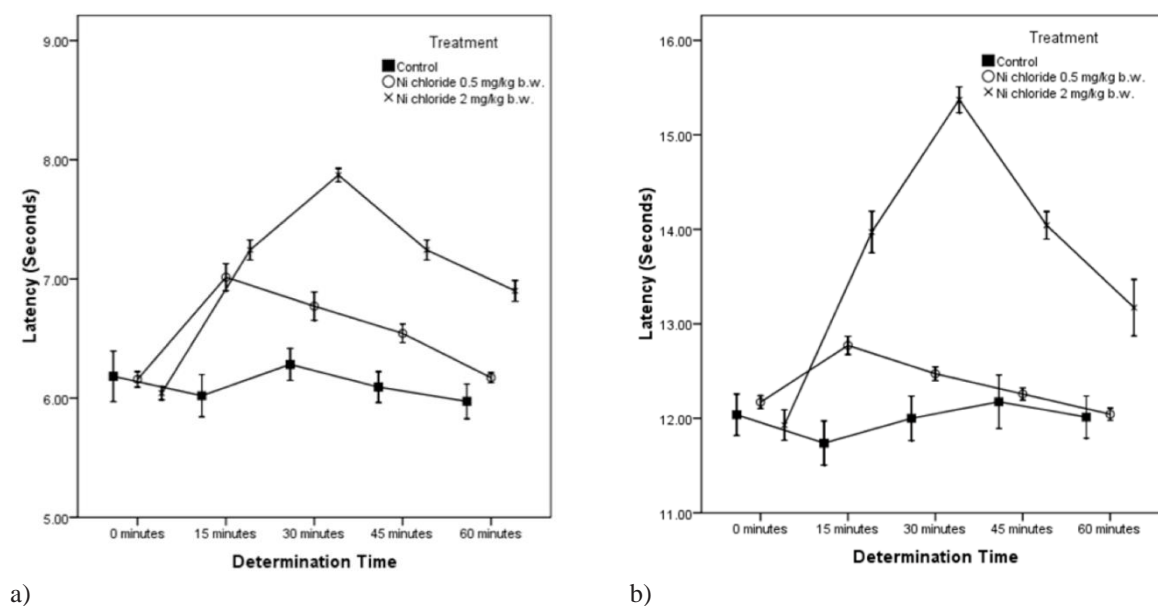


**Fig. 8.** a. Latencies for TF test, following Ni chloride intraperitoneal injection at different doses (0.5 and 2 mg/kg respectively). b. Latencies for HP test, following Ni chloride intraperitoneal injection at different doses (0.5 and 2 mg/kg respectively)

For the same salt, administered also intraperitoneally, HP test emphasized antinociceptive effects for all recorded time intervals and all doses while only some of the results are statistically significant. A dose-dependent effect was reflected by the response intensity. Even low doses (0.5 mg/kg) induced significant latencies at 15 min (that includes a peak of  $12.77 \pm 0.26$ ). Maximal intensity effect at 30 min was obtained by a higher dose of 2 mg/kg (peak at  $15.37 \pm 0.36$ ) (Fig. 8). While converting HP latencies in percent of the maximal possible effect, Ni chloride was observed to induce a dose-dependent, antinociceptive effect, reducing the pain up to 19.01% (Table V).

Spontaneous behaviour changes were significant for the 0.5 mg/kg Ni chloride dose, following evaluation by activity cage test at 0 - 15 min and for the 2 mg/kg dose at 0 - 25 min (Table VI). No significant changes in the number of horizontal or vertical movements were recorded for a dose of 1 mg/kg Ni chloride.

Evaluation regarding sodium Molybdate effects following intraperitoneal injection by TF test showed an increase in TF latency at 15, 30 and 45 min, thus indicating a significant antinociceptive effect. TF latency increase expressing analgesic effect seems to be dose-dependent. A significant TF latency is observed at 15 min for a dose of 25 mg/kg sodium Molybdate. For a higher dose of 50 mg/kg, the latency profile is reproducible but with statistical significance at 15, 30 and 45 min (Fig. 9). A dose-dependent analgesic effect is induced by sodium Molybdate, and TF pain is lowered up to 13.40%, following pain inhibition calculations. TF pain was reduced by 8.79% at 15 minutes for a dose of 25 mg/kg while the dose of 50 mg/kg is inducing a maximal inhibition of 12.42% at 15 min (Table V).

Sodium Molybdate intraperitoneal administration effect was evaluated also by HP test. Observed latencies were increased and dose-dependent at 15, 30, 45 and 60 min (Fig. 9). Only at 15 and 30 min, recorded effects were statistically significant for all tested doses. Peak values were measured at 15 min for all doses ( $12.87 \pm 0.14$  s for the 25 mg/kg;  $13.69 \pm 0.32$  s for the 50 mg/kg). Conversion of HP latencies into percent of maximum possible effect led to

the observation that sodium Molybdate reduced the pain by 9.22% and induced an antinociceptive effect. HP pain was reduced by 4.07% at 15 minutes for a dose of 25 mg/kg while maximal inhibition of 9.22% was reached at 15 min for a dose of 50 mg/kg (Table V).

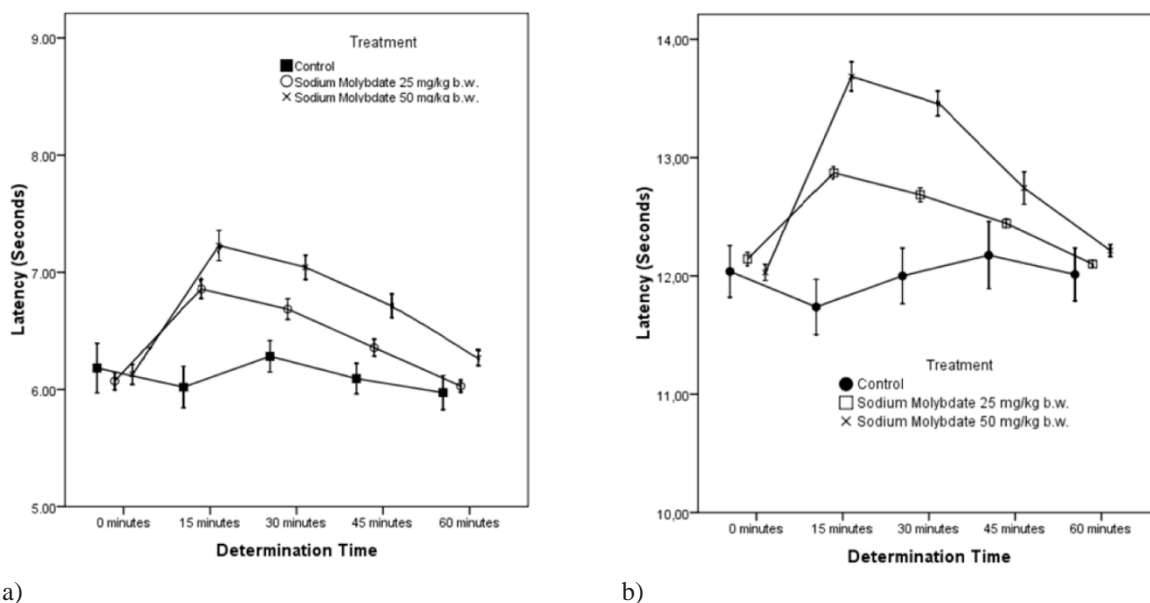


**Fig. 9.** a. Latencies for TF test, following sodium Molybdate intraperitoneal injection at different doses (25 and 50 mg/kg respectively). b. Latencies for HP test following sodium Molybdate intraperitoneal injection at different doses (25 and 50 mg/kg respectively)

Spontaneous behaviour changes were significant for all doses and recorded time intervals and were expressed by the decrease of the total number of writhings. Maximum inhibition regarding visceral pain was observed at 30 min for all doses. Present results showed maximum pain inhibition as more significant for a dose of 50 mg/kg dose (62.50%) than for a dose of 25 mg/kg (44.64%) (Table VI). A mild sedative effect is suggested by significant changes in horizontal axis movements for a dose of 50 mg/kg in the cage activity test (Fig. 10).

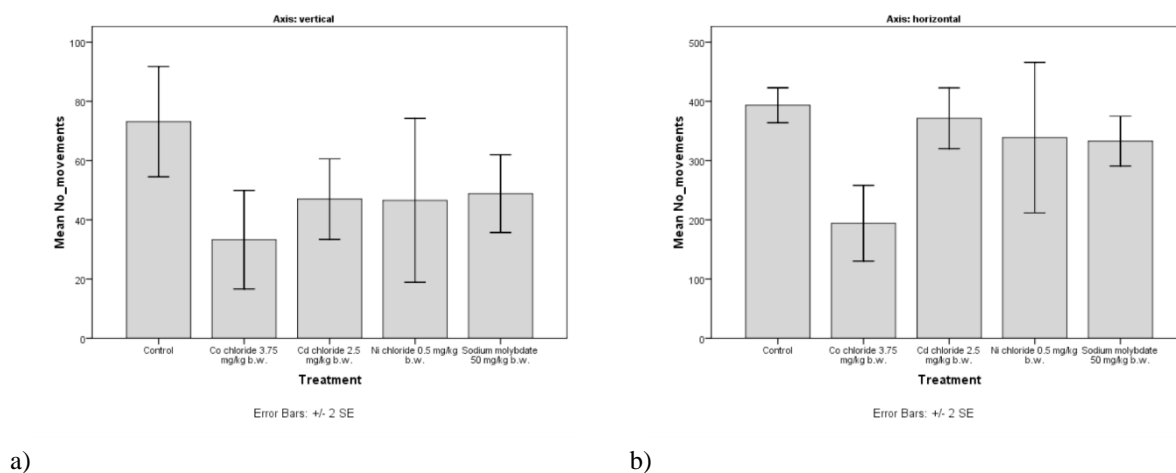


**Fig. 10.** a. Number of spontaneous movements per time interval in activity cage test, on horizontal ax, following administration of 0.9% saline for the control group, Co chloride 3.75 mg/kg, Ni chloride 0.5 mg/kg and sodium Molybdate 50 mg/kg. b. Number of spontaneous movements per time interval in activity cage test, on vertical ax, following administration of 0.9% saline for the control group, Co chloride 3.75 mg/kg, Ni chloride 0.5 mg/kg and sodium Molybdate 50 mg/kg.

#### 1.1.4 Discussions

##### **Zn, Mg and Cu decrease pain intensity in mice**

The anti-nociceptive effect of zinc in our evaluation processes was moderate and we observed an inhibition of 4-17% in thermoalgesic tests and 17-25% in chemoalgesic tests. Our results showed no significant differences between the two  $Zn^{2+}$  salts used.  $Zn^{2+}$  sulphate, when explored by activity cage test, did not show any significant behavioural changes, while  $Zn^{2+}$  citrate had some positive results.

We have also shown that magnesium salts induced various degrees of anti-nociceptive action for all performed tests. In comparison to the HP test, which showed no dose-dependent effect (pain inhibition – 30%), the TF test showed a pain inhibition of 58-72% at 30 minutes. The most suggestive values appear at writhing test, where the anti-nociceptive effect reaches 85%. Behavioral effects evaluated by activity cage test denote both a sedative and anxiolytic action. Our results are consistent with previous studies (Begon et al 2002, Srebro et al 2018) though administration ways are different. Positive effects on the behavioral parameters allege for a  $Mg^{2+}$  chloride passage through the blood brain barrier (BBB). There is a documented correlation between the anti-nociceptive and central nervous system depressing actions (Fawcett et al 1999; Durlach, et al 2000). From our results, we may conclude that  $Mg^{2+}$  chloride exerts an anti-nociceptive action in a dose of 150 mg/kg, with low results for TF test but with important effect in HP test (inhibition values of 30% at 15 minutes, 56% at 30 minutes and 22% at 60 minutes).

Our results regarding copper salts show potential anti-nociceptive effects during thermoalgesic tests and especially during chemoalgesic tests. It is difficult to explain the analgesic effect while copper ion is involved in many molecular mechanisms of pain relief. Some researches (Yu et al 2008) showed that  $Cu^{2+}$  sulphate administration induces dopaminergic neurons lesion with antioxidant defense inhibition and apoptosis induction.

$Zn^{2+}$  ion (in both used salts) showed moderate anti-nociceptive effects (4-25%), more evident on chemoalgesic test. Significant behavioral changes were recorded also following administration of  $Zn^{2+}$  sulphate and citrate. Magnesium (as chloride) induced an anti-nociceptive effect in analgesic tests (30-85%) with highest values in writhing tests. It also induced sedative and anxiolytic actions. Copper chloride induced an anti-nociceptive dose dependent effect (5% at minimal dose, 9.58% at medium dose and 28% at maximal dose) in TF test and of 3.17 – 23.7% at HP test. Behavioral tests showed that  $Cu^{2+}$  chloride exerts an anxiolytic effect.

##### ***The effect of Zinc on experimental pain***

Our research showed the  $Zn^{2+}$  effect in the periphery, where pain is transmitted by the A delta and C fibers. We hypothesize that, in our experimental conditions,  $Zn^{2+}$  influences glutamatergic receptors both at the peripheric and spinal levels (thus explaining why in most our experiments analgesia occurs after a latency of 10-15 minutes, time required to cross the blood-brain barrier and reach the synaptic space). How and where does  $Zn^{2+}$  act in the synaptic space is not precisely known but several authors have provided additional info, though sometimes it is contradictory (Luo et al 2018). Takeda et al (2003) argue that zinc increases the presynaptic release of glutamate or GABA, with Smart et al (2004) confirming these claims but advancing the hypothesis (not confirmed yet) that zinc may act as a direct

neurotransmitter too, by postsynaptic signaling pathways' modulation Li and Clark (2000) presented further data showing a reduction of inflammatory pain (formalin model) due to inhibition by zinc (zinc-protoporphyrin intrathecal) of hemoxigenase at spinal level, but with no effect on the peripheric thermal testing or hemoxigenase levels reported. Another possible mechanism of action for zinc ions is the interference with the potassium channels, Prost et al (2004) showing that zinc ion has the ability to open the K-ATP channel in pancreatic cells, acting on both sides of the membrane.

Zinc also interferes with the nicotinic receptor ion channel, modulating the nicotinic receptor function (Hsiao et al 2008). On the other hand, in a recent study Talya et al (2009) showed that  $Zn^{2+}$  acts as an allosteric modulator of the alpha-beta portion of the heteropentameric (alpha 4-beta 2) of the nicotinic receptor. Of great importance to our study is that Talya et al (2009) argue the modulator role of  $Zn^{2+}$  ions can both stimulate (alpha-alpha interface) and inhibit (beta-alpha interface) nicotinic receptor alpha 4-beta 2 depending on the concentration of zinc used (Taly et al 2009). This fact could, in our view, explain the sometimes similar and sometimes different results obtained by other authors regarding the involvement of zinc in pain, vs the data presented by us (Hsiao et al 2008; Taly et al 2009). In fact, many authors consider the nicotinic receptor as useful targets for therapeutic agents in pain management (Meyer 2006; Rowley et al 2008). These hypotheses will need however further exploration.

The  $Zn^{2+}$  sulfate dose used by us did not show significant changes in spontaneous behavior when assessed by the activity cage test. Literature review provided comparative data (Nozaki et al 2011; Matsunami et al 2011), except Krocza et al (2001) who reports an "anti-depressant-like" effect in forced swim test in rats without providing a dose that produced this effect or the zinc salt used.

### ***The influence of Magnesium on pain perception***

Our view is that one could explain the analgesic effect by a peripheric mechanism but the central behaviour inhibitory actions of our tests lead to the conclusion that the  $Mg^{2+}$  does cross the BBB. Hasanein et al (2006) confirms previous results regarding the anti hyperalgesic effect of i.p administered  $Mg^{2+}$  for mechanoalgeic tests in rats with diabetic neuropathy. However, the author proposes another mechanism for this effect: the normalization of glycemia rather than the interference with the Na/Ca channel of the NMDA receptor or the lowering action on pro nociceptive free radicals. As for the relation between the anti nociceptive effect and the CNS depressant activity, several authors have investigated it and confirmed it (Fawcett et al 1999; Durlach et al 2000).

Our current study showed a reduction in both horizontal and vertical mobility after the administration of  $Mg^{2+}$  chloride, in agreement with recent data obtained by Bindar et al (2010).

### ***Administering Copper salts has analgesic effects in murine pain models***

Our results show a potential analgesic effect of  $Cu^{2+}$  salts in both the thermoalgeic and the chemoalgeic tests. Although different from our experimental conditions, literature data is consistent with our results (Cazanga et al 2018). However, it seems difficult to clearly explain how  $Cu^{2+}$  ions induce analgesia. As with other bivalent trace elements,  $Cu^{2+}$  too is transported to specific molecules ( $Cu^{2+}$  (+)-ATPase) using guidance proteins (chaperone)

(Gonzales-Guerrero, Argüello 2008).  $\text{Cu}^{2+}$  from the central nervous system cells is coupled in the enzymatic systems involved in the synthesis of catecholamines, opioid peptides and of neuropeptides (Kim et al 2008). The possible role of  $\text{Cu}^{2+}$  in analgesia was presented by Jacka et al (1983) on an inflammatory arthritis model in rats, which tested the antinociceptive effects of salicylate after  $\text{Cu}^{2+}$  pretreatment (mechanical pain tests). The data presented by us and the literature data converge on the  $\text{Cu}^{2+}$  certain involvement in analgesia, but unfortunately, due to various cellular and molecular actions, and not always beneficial, high selectivity pain drugs based on  $\text{Cu}^{2+}$  do not exist yet. In fact, it may never get to that, as research by Yu et al (2008) has shown that  $\text{Cu}^{2+}$  sulphate administration (striatal nuclei injections in rats) damages the dopaminergic neurons, causing apoptosis.

### **Common trace elements enhance the analgesic effects of tramadol when co-administrated in mice**

The results of our study suggest that all three trace elements (Zn, Mg and Mn) enhance Tramadol's analgesic effect. Co-administration induced a statistically significant latency increase in both TF and HP tests when compared to the Tramadol-alone group. This result may be a consequence of modifications in the absorption and release rate of Tramadol. A recent study tested the interaction between Diclofenac and trace elements in an in vitro model of the gastro-intestinal tract; the results indicated that both Zn and Mg increased the drug's release rate, influencing the pharmaceutical availability in gastro resistant tablets (Biernat et al. 2014).

In our study, drugs were delivered via the i.p. route, which is somewhat similar to oral administration, due to the absorption in the mesenteric vessels and hepatic metabolization (Turner et al. 2011). It is thus possible that the absorption process of Tramadol is influenced by trace elements. A 2013 study indicated that some trace elements (such as Zn and Mg) may have an analgesic effect of their own in several animal models of pain and nociception (Tamba et al. 2013), while another previous paper showed that Mn chloride administration in mice is associated with thermal analgesia (Tartau L et al. 2006). Taking the two hypotheses together (enhancement of absorption and analgesic effect of trace elements on their own but with different mechanisms), a synergic effect between Tramadol and trace elements is a likely explanation.

Another possibility is an additive effect between Tramadol and these trace elements, considering that the main effect of tramadol is on  $\mu$ -opioid receptors, and there are papers exploring all three trace elements involvement in the modulation of these receptors. However, published data in the field is rather scarce. To our knowledge, this is the first study assessing the influence of trace elements (found in most dietary supplements) on analgesic drugs and pain.

#### ***The effect of a Zinc-Tramadol combination on pain***

All doses of Zn enhanced Tramadol's effect in both TF and HP tests - adding Zn to Tramadol increased pain inhibition by almost 20% when compared with the Tramadol alone group. The most effective dose seems to be the smallest one - 0.6 mg/kg b.w.; the onset of its effect was at 30 minutes in the TF test and 45 minutes in the HP test. This suggests that Zn enhances Tramadol's effect at both spinal and supra-spinal level; the 15 minutes difference

between onset of effect in the HP and TF tests may be explained as the time necessary for Zn to cross the blood-brain barrier (BBB), thus indicating that the added effect is a consequence of Zn's own analgesic action and not its effect on Tramadol metabolization.

Our data falls in line with previously published studies that have investigated the effect of Zn on pain. A study performed in mice indicated that NMDA receptors are highly sensitive to Zinc and that Zn regulation is an essential part in pain transmission and chronic pain development (Nozaki et al. 2011b). Previous research on the analgesic effect of Zn alone indicated that it acts both centrally and in the periphery (Tamba et al. 2013), thus suggesting that Zn enhances Tramadol's analgesic effect by a synergic mechanism.

In the spinal cord, zinc homeostasis has been shown to influence spinal cord recovery (Wang et al. 2011) and zinc dietary supplementation may regulate the expression of Zinc Transporter 1 in the dorsal horn of rats after spinal cord injury (Su et al. 2012). In the brain, it acts as a neuromodulator of glutamergic transmission, antagonizes NMDA receptors (Ilouz et al. 2002) and some authors suggested it may modulate  $\gamma$ -aminobutyric acid receptors (GABARs), glycine and adenosine triphosphate (ATP) receptors (Hsiao et al. 2008; Smart et al. 2004). Other authors have suggested that Zn may influence pain through the nicotinic receptor ion channel (Hsiao et al. 2008) and that this influence can be either excitatory or inhibitory (Taly et al. 2009). Its deficiency is associated with inflammatory processes (Marcellini et al. 2006), and inflammation plays an important part in most pain processes.

Another possible explanation for Zn's influence on Tramadol's analgesic abilities is its antidepressive effect. Current hypotheses for depression include anomalies in neurotransmission and Zn has shown antidepressant-like activity in animal models (Siwek et al. 2010) and has been shown to enhance traditional antidepressants' effect in animal models (Cunha et al. 2008) as well as in humans (Siwek et al. 2009). It is thus possible that a similar mechanism is involved in enhancing the effect of analgesics or that by improving depression/mood, animals have a higher threshold for pain.

In our study, the smallest dose of Zn induced the strongest antinociceptive effect. This can be explained by Zn's neurotoxic effects at high doses. As most neuromodulators, its effect can be either excitatory or inhibitory and most likely this depends on Zn's concentration (Nozaki et al. 2011b). As the dose increases, the amplitude of Zn's effect decreases and probably higher doses may even lead to hyperalgesia. The 0.6 mg/kg b.w. dose is higher than the recommended daily dose (6.4 mg/d or 5.7 mg/d in males, respectively females) (Lowe et al. 2013), but it is still in the same range (equivalent of 42 mg for a 70-kg person), while the intermediate and the high dose far exceed the daily recommended dose.

### ***Magnesium and Tramadol co-administration have an enhanced analgesic effect***

The small and medium Mg dose enhanced Tramadol's effect in both TF and HP tests, with an average increase of over 20% in pain inhibition when compared with Tramadol alone. Although the smallest dose (37.5 mg/kg b.w.) induced the most important increase in response latency in both tests, in the HP test this did not reach statistical significance. The intermediate dose (75 mg/kg b.w.) induced a significant change after 60 minutes in the HP test. Both doses induced significant changes after 30 minutes in the TF test. The large Mg dose induced no statistically significant enhancement of Tramadol's analgesic effect as assessed by TF and HP. Even more, in the HP test, this dose decreased Tramadol's average pain inhibition by approximately 8%. This suggests that Mg enhances Tramadol's effect

especially due to a spinal mechanism; the latency between onset of effects in the TF and HP test can be a result of Mg's crossing of the BBB.

The relationship between Mg and pain is a subject of great recent interest, with several studies that indicate a potential role for Mg as a co-analgesic. A 2013 meta-analysis of randomized controlled trials, that included over 1000 human participants, revealed that perioperative magnesium administration reduces both pain and opioid consumption (De Oliveira et al. 2013). One other study found that adding MgSO<sub>4</sub> to sufentanyl in the patient-controlled intravenous analgesia system enhanced analgesia in patients undergoing orthopedic surgery (Sedighinejad et al. 2014). Systemic administration of Mg has been found to prolong anesthesia and duration of analgesia (Shukla et al. 2011) and MgSO<sub>4</sub> concurrent administration decreased the rocuronium dose required for anesthesia (Kim et al. 2012). One study indicated that adding Mg to metamizol administration significantly decreased pain scores after tonsillectomy, thus indicating that Mg acts as a co-analgesic for metamizol (Tugrul et al. 2014).

A systematic review that underlined Mg's analgesic effect also indicated that it is most likely a consequence of an opioid-independent mechanism (Murphy et al. 2013), thus indicating that Mg's effect is most likely synergic with Tramadol's. Other potential effects of Mg that may influence pain and pain transmission include:

- a. Ca channel inhibition (Dacey 2001)
- b. effect on both pre- and post-synaptic neuromuscular transmission (Dubé & Granry 2003), by decreasing the effects of acetyl-choline on muscle receptors and increasing the threshold of axonal excitation and c. antagonism of the NMDA receptor.

In the current study, adding large-dose Mg to Tramadol did not influence significantly Tramadol's analgesic effect - the Tramadol alone and Tramadol + 150 mg Mg groups induced similar latency values. This is in accordance to our previous paper (Tamba et al. 2013) where we showed that the smaller 37.5 followed by the 75 mg/kg b.w. doses had the best analgesic effects while the 150-mg dose had a more moderate, and less significant antinociceptive action. This could be explained by the fact that our dose was 30 times higher than the average recommended daily dose (we administered 150 mg/kg b.w. and the daily recommended Mg requirement is 250 to 350 mg) (Dubé & Granry 2003) and that a possible CNS depressant activity at this dose could alter tramadol's effect.

### ***Manganese increases Tramadol's efficacy***

Adding Mn to Tramadol lead to an increase in response latency in TF test, regardless of the Mn dose administered, although the most effective dose seems to be the intermediate one (7.2 mg/kg b.w.). Average pain inhibition was increased by more than 20% in all doses when compared with Tramadol. However, in the HP test, Mn proved less effective and only the intermediate dose significantly enhanced Tramadol's effect after 45 minutes (although the other doses also had average pain inhibition values larger than Tramadol's this did not reach statistical significance); these results suggest that, besides its central well-known site of action, Mn also acts at the spinal level. This hypothesis is supported by the fact that Mn supplementation enhanced Tramadol's analgesic effect especially in the TF test, which assesses spinal pathways and less so in the HP test that evaluates both spinal and supra-spinal pain transmission.

There are few studies that explore the effects of acute Mn administration. However, chronic Mn exposure has been extensively studied due to its neurotoxicity, probably secondary to mitochondrial dysfunction and energy imbalance (Zwingmann et al. 2003b); consequences of chronic exposure are expressed especially in astrocytes and consist in neurodegeneration and neuroinflammation (Hazell 2002), located especially in the supra-spinal structures.

Some studies have indicated that Mn or other Mn-containing substances may have analgesic effects. A study performed on patients with degenerative joint disease who received a combination of several supplements that included manganese ascorbate, indicated that knee osteoarthritis symptoms were relieved after this treatment (Leffler et al. 1999). However, the relationship between acute Mn administration and pain is unknown. One possible explanation of the analgesic effect of Mn could be its effect on Ca channels. A 2006 *in vitro* study indicated that sub-acute exposure to Mn inhibited Ca signaling (Tjalkens et al. 2006) in astrocytes due to its indirect effect on transient receptor potential (TRP) channel TRPC3. Both astrocytes and TRPC3 are also found in the spinal cord (Miyano et al. 2010) and are probably as sensitive to Mn as those in the brain. In the spinal cord, high levels of Mn have been shown to block synapses by interfering with nerve conduction along nerve fiber tracts (Bagust & Kerkut 1980) and in the superior cervical ganglion manganese ions induced a blockage of synaptic transmission. Furthermore, a paper by Gunter et al. hypothesized that Mn cannot only inhibit Ca transporters, but can also substitute for Ca in some transport processes (Gunter et al. 2006). Due to the fact that Mn affects *supra-spinal* Ca channels, we hypothesize that its analgesic effects could be a consequence of Mn's effect on *spinal* Ca channels - a reduction in Ca pre-synaptic influx may induce an apparent antinociceptive effect (Surprenant et al. 1990).

## **Heavy metal trace elements induce antinociception in mice**

### ***The effect of Cobalt on experimental pain***

Our results both confirm and add to previous studies, showing for the first time the presence of a dose-dependent *in vivo* antinociceptive effect of Co chloride. Antinociceptive activity during thermoalgesic tests shows an inhibition degree of 27-31% in TF and 18-40% in HP.

Antinociceptive effect for Co chloride during WT is more present, ranging between 36 to 100%. The lower dose of Co chloride we used represents 1/24 of LD50, thus limiting the potential toxic effects from interfering with our study.

Spontaneous behaviour tests indicate both sedation and an anxiolytic effect in our experimental construct, inferring a possible toxic CNS effect (Knyazev et al., 2012; Karson et al., 2013; Barbee et al., 2014; Nieto-Fernandez et al., 2006). However, the difference between the 100% nociceptive protection in visceral pain WT and the 31% effect in TF at the same time intervals and dose, dismisses as only possible explanation for our results the CNS depressant effect observed.

Co, Ni or Mn ions perfused in a Ca-deficient environment block synaptic transmission (Yin et al., 2003; Knyazev et al., 2012; Karson et al., 2013; Barbee et al., 2014; Nieto-Fernandez et al., 2006; Angstadt and Friesen, 1991) and microinjections of Co chloride in dorsal rat mesencephalon or the periapeductal gray, an area involved in visceral nociception, induce antinociceptive effects in rats (Hamann et al., 1992; Cavun et al., 2004). Co chloride

also inhibits synaptic transmission at periapuductal grey level (Keay et al., 1997), and may act as a presynaptic blocker involved in nociception (Allen and Pronych, 1997). However, it appears that the mechanisms and involvement of this HTME in nociception is far more complex. Engelman et al. (1999) used Co chloride to identify Ca permissive AMPA receptors in the dorsal horn of lamina I and lateral area of lamina II. In lamina I, Co-positive NK1 receptors for P-substance are also present, concluding that they might play a role in nociception. Tong and MacDermott (Tong and Macdermott, 2006) observed that AMPA receptors contribute to the dorsal horn synaptic transmission and are involved in pain signaling pathways, making a Ca channel block through Co replacement a possible explanation for the antinociceptive effect observed in our experiments. Like other metal trace elements (Zn, Ni, Cd, Mn), Co uses specific intracellular transporters (Komeda et al., 1997), becoming cofactor for enzymes involved in the synthesis of neuropeptide and neuromediators but also in the superoxide metabolism. A functional connection between ACDP4 transporter and the ionic chaperonin COX11 suggests specific intracellular sites for these metallic ions (Guo et al., 2005). Valinoid and capsaicinsensitive thermoreceptors were also thoroughly investigated using Co's ability to use calcium channels (Nicholas et al., 1999; Rosa et al., 2008) investigated the inductive role of cobalt-protoporphyrin on hem-oxygenase-1, known as a modulator for inflammatory pain, which might present novel pharmacological targets for analgesic drug development.

The data available shows a complex role in pain for Co at various CNS levels, observations in agreement with our previous results (Tamba et al., 2008; Voiley, 2004). Furthermore, previous works lack in-vivo behaviour experimental data regarding Co and thus our results might represent a starting point for the presented subject.

### ***The effect of Nickel on experimental pain***

Acid-sensing ionic channels, present in central and peripheral neurons, with a specific role in nociception, neural hyperexcitability and hyperalgesia, can be inhibited in a dose-dependent manner by Ni ions (Chen et al., 2002; Nelson et al., 2007). Nelson et al. (2007) insists on the Ni role on Ca channels according to their Zn affinity.

Our results show that Ni ion plays a moderate but significant and dose-dependent antinociceptive action in thermoalgesic tests, ranged from 9.7 to 20% between 15- 30 min and effect persistence over 60 min for 2 mg/kg in HP test. WT show peculiar results – an initial short but significant antinociceptive action, followed by a hyperalgesic trend in the second part of the test. This biphasic aspect made us consider two different mechanisms; one mechanism involving a fast response while the second mechanism being delayed until the trace element arrives to some specific structures (channels, enzymes) whose impaired activity leads to the observed hyperalgesia. No significant changes during spontaneous behavior AC were observed. Poor literature data regarding Ni role in nociception allows us just few considerations regarding the mechanism and action place for this rare element in nociception. Prado (2001) studying  $\text{Ca}^{2+}$  involvement in pain and antinociception, reported Ni and other cations ( $\text{Ce}^{3+}$ ,  $\text{La}^{3+}$ ,  $\text{Cd}^{2+}$ ,  $\text{Co}^{3+}$ ,  $\text{Mg}^{2+}$ ,  $\text{Mn}^{2+}$ ) as unselective blockers for the  $\text{Ca}^{2+}$  channel pore. It is also well-known that  $\text{Ca}^{2+}$  is required to induce nociceptive mediator delivery. N and P/Q  $\text{Ca}^{2+}$  channels involved in nociception are found in dendrites and neuronal bodies.

Some channel subtypes are also found in postsynaptic membranes of the glutamatergic neurons, involved in pain transmission. A more thorough study by Nelson et al. (2007)

describes Ni roles on  $\text{Ca}^{2+}$  channels and their affinity for  $\text{Zn}^{2+}$  ions, showing that after a peripheral lesion, the nociceptive receptors become hyperexcitable. These receptors are also located in dorsal ganglia where neurons exhibit an increased number of T-type calcium channels.

Ni ion was also proved to discriminate between various Ttype  $\text{Ca}^{2+}$  channels, its affinity for  $\text{Ca}^{2+}$  3.2 channel being 20 times higher compared to other isoforms. The antinociceptive effect of Ni could be similar to Zn, although this has a non-specific affinity for these channels.

Intrathecal injections of Zn induce antinociceptive effects in mice, while Zn chelating agents lead to hyperalgesia (Kitamura et al., 2006). Though current data may explain Ni antinociceptive action by Ca channels interference in peripheral nerve ends, the hyperalgesic effect observed in the second phase of the writhing test to acetic acid remains to be further investigated.

### ***The effect of Molybdenum on experimental pain***

Mo showed significant antinociceptive effects in all our tests which are dose - independent and appear in a time range of 15- 30 min from administration. The antinociceptive levels in the thermoalgesic tests were too limited to have clinical significance (inhibition values ranging between 8-13% for TF and 4-9% for HP). WT however, showed an antinociceptive activity of 33% at 15 minutes and 68% at 30 min, effect that is associated with a slight sedation (in AC). Current literature lacks data on *in vivo* experimental data regarding Mo action on nociception.

Toxicity studies in animals did not reveal any significant CNS effects nor motor dysfunctions. One pilot study presented 14 patients undergoing pain symptoms that received 500 $\mu\text{g}$  Mo in oral administration for 4 weeks and compared them to a placebo group. Significant pain relieve was recorded in Mo-treated group, together with general status improvement. Mo induced a growth latency of 50- 78%, with visible cortico-dystrophies in a 6 weeks toxicity tests with oral doses of 0.2 mg, 7.5mg or 30 mg/kg/day in rats with similar studies investigating Mo toxic effects on weight and hair color. We found no study regarding nociception or possible action mechanisms at cellular and subcellular level in pain. Mo is included in some Molyhydroxylases family, enzymes involved in metabolism of some drugs in humans. These enzyme functions are not fully understood (Kitamura et al., 2006) but their effect on free radicals is generally accepted. Recent data seem to open a path toward more complex investigations, as chimeric animals (rats with human hepatic cells) were obtained to study various drug effects on Mo-enzymes in the cell (Kitamura et al., 2006) and a potential interference of Mo with pro or antinociceptive molecules. Literature data show only a strong inhibiting effect of methadone on Mo-hydroxylases (Robertson and Gamage, 1994).

### ***Spontaneous behavior test discussion***

The spontaneous behaviour test was negative for nickel chloride, thus validating and eliminating any toxicity related contamination of the interpreted results.

The test did show significant changes for Co and Mo. As explained above, while these changes may infer a possible toxic CNS effect or contamination of the anti-nociception studies, we maintain the conclusion (backed by the literature data too) that the difference between the 100% nociceptive protection in visceral pain WT and the 31% effect in TF at the

same time intervals and dose, dismisses as only possible explanation for our results the CNS depressant effect observed. Had the anti-nociception effects been due only to the toxic or depressant CNS effect of the HMTE, the pain responses would have been similarly decreased in all pain tests performed. But this was not the case as clearly presented.

### ***Limitations***

Due to conflicting and limited *in-vitro* information about these HMTE's influence on pain, and the scarcity of previous *in-vivo* studies, the authors acknowledge the difficulty in choosing the test doses. The doses administered were calculated as fractions of known, published intraperitoneal IP LD50 in mice, and only balanced with the doses for *various in-vitro* studies as well as dietary supplements doses and recommendations. While considering potential toxic effects, the authors also had to look for doses in acute tests that were believed to generate a response on nociception, by extrapolating the literature *in vitro* doses rather than using the daily food intake. Thus, the doses used, and the fraction of LD50 they represent, are clearly within the limits for obtaining a therapeutic response in living organisms but without significant suspicion of toxicity. The way of administration was chosen IP because it provides the standard approach for an acute *in-vivo* test, with much better accuracy, dosing and control than oral administrations. Another critical point in our decision to use IP administration was the ethical committee of our institution that asked for previous existing data on these HMTE and pain.

Due to the scarcity of previous *in-vivo* studies and the difficulty in ethically justifying an oral long-term test with no previous literature data, we started our research from the beginning with the acute IP tests. Our experimental models used doses 10-20 times higher than dietary intakes, but still were a fraction of LD50's and did not induce significant toxicity, while clearly proving the effects that HMTE's produce on nociception.

### **1.1.5 Conclusions**

- Following intraperitoneal injection, Zn, Mg and Cu induced various degrees of anti-nociceptive effects, demonstrated by thermoalgesic and chemoalgesic tests.
- Associating trace elements such as Zn, Mg and Mn to the standard administration of Tramadol induced a more pronounced antinociception as shown by increased response latencies in the TF and HP test.
- Co has a moderate anti-nociceptive activity in thermoalgesic tests and superior values in chemoalgesic tests at higher doses, with some anxiolytic and sedative effects also recorded.
- Mo shows a variable antinociceptive activity in low doses, with a significant improvement for visceral pain. Behaviour tests showed that Mo can play a slightly sedative role.
- Ni chloride induces a moderate antinociceptive action and shows a biphasic effect in WT.

## 1.2 NANOTECHNOLOGY APPLICATIONS IN MEDICINE

Pain removal is one of the most important problems related to our health and, since the beginning of humanity people strived to find a cure. Minimal invasiveness represents an important requirement and empirical formulations of curative mixtures were developed and perfected through generations as creams, ointments, pastes, powders, liquid extracts of animal or vegetal origins.

Many different approaches using various nano-formulated biomaterials have been proposed and investigated, materials like liposomes, nano-particles, nanofibres hydrogel. Nanotechnology is a multidisciplinary science field involving the design and engineering of physical objects less than 500 nanometres in size. Over the last two decades, nanotechnology has offered a diverse range of nanoscale tools specially fabricated for therapeutic use in medicine. Nanotechnology has been demonstrated to have the potential to enhance drug delivery and reduce side effects of these analgesic drugs. Recently, application of novel nanotechnology-based techniques and methods, such as implantable drug delivery devices, and transdermal and transmucosal delivery systems for delivery of different types of drug for cancer, anaesthetics, etc. Treating pain with nanotechnology may be the future of pain relief.

There have been two main directions for my research in nanotechnologies:

- Investigate the in-vitro and in-vivo characteristics of innovative nanoparticles
- Evaluate the potential analgesic applications of developed nanoparticles

### 1.2.1 Background and motivation for research

In the last period, the growing interest in molecular therapy is due to the possibilities offered by nanoparticles (NPs) as new tools for the delivery of therapeutic and target-specific drugs (Morales- Avila et al., 2012). Nanoparticles can be used as novel contrast agents for imaging studies, as layers for drug delivery or as a method for ensuring optimal physical characteristics of certain polymers. Additionally, using a certain material in its nanoparticulate form can significantly change its properties, as observed in *in vitro* and *in vivo* studies.

In the field of **using nanoparticles for diagnosis**, multifunctional radiolabelled nanoparticles provide an ideal platform to combine different approaches such as drug delivery with functional imaging techniques that are used to target the site of the disease via both specific and non-specific mechanisms (Hong et al., 2009). Thus, novel strategies were explored for the radiolabelling of NPs in order to investigate the *in vivo* biodistribution in dependence with their architecture, size and structure (Md et al., 2013). In order to investigate the *in vivo* characteristics of NPs it has to be considered how they are interacting with tissues and cells, and especially which time frame allows a suitable visualization of certain effects and functions (Loudos et al., 2011). The necessity of creating radiolabelled nanocarriers is noticeable in all biomedical fields worldwide. Research in the field is anticipated to lead to advances in understanding biological processes at the molecular level in addition to progress in the development of diagnostic tools and innovative therapies (Peer et al., 2007). Traditional radioisotope agents have certain disadvantages (instability, lack of specificity, low biodistribution, etc.) that must be improved by using new multifunctional radiolabelled structures (Garg et al., 2008; Newman et al., 2003).

Nanoparticles provide a large surface area and different types of functional groups available for bioactive agents or ligand attachment. Diverse nanomaterials with unique properties can be found in various biomedical applications, including *in vitro* or *in vivo* imaging, separation and purification of cells or biomolecules, and delivery of therapeutic agents. In the last two decades, **silica-based nanoparticles** (SNPs) have gained increasing interest for medical applications because of their biocompatibility, versatility, stability, monodispersity, large surface area, high drug loading efficiency, and potential for hybridization with other materials (Argyo et al., 2014).

The surface of SNPs is usually negatively charged due to the presence of the hydroxyl group; therefore, it is convenient to modify the SNPs' surface through the silane chemistry. In order to control the physico-chemical, toxicological and pharmacological properties, various reactive functional groups like amine, carboxyl, phosphate or polyethylene glycol could be easily conjugated to hydroxyl SNPs. Alternatively, the surface chemistry of the SNPs can be fine-tuned for a specific biological application, optimizing the dispersion stability and/or cellular uptake, the covalent attachment of imaging agents and targeting ligands the rational control of drug release rate (Mamaeva et al., 2013).

Numerous studies pointed toward the excellent potential of SNPs as biomarkers, calibration standards in confocal fluorescence microscopy, drug delivery and targeting systems (tumor imaging and therapy *in vitro* and *in vivo*) in biomedical science (Legrand et al., 2008; Lu et al., 2007; Slowing et al., 2007). Imaging agents such as fluorescein isothiocyanate, methylene blue, quantum dots, gadolinium chelates, tetramethylrhodamine or their targeting ligands, such as aptamers, antibodies, peptides, and folic acid, can be easily doped into or modified on the surface (Wu et al., 2014). Despite the growing body of papers related to the use of SNPs as therapeutic and imaging tool, today's challenge remains the biodistribution of silica nanostructures for *in vivo* diagnostic and therapeutic applications.

Another important use for nanoparticles is **formulating complex drug delivery systems** when combined with polysaccharides (Guar gum). **Guar gum** (GG) is a non-ionic natural polysaccharide sourced from the seeds of *Cyamopsis tetragonolobus* (Leguminosae family) and consists of linear chains of (1, 4)- $\beta$ -D-mannopyranosyl units with  $\alpha$ -D-galactopyranosyl units attached via (1, 6) linkages. Because of its ability to produce highly viscous aqueous solutions at lower concentrations, guar gum is used in many applications in industries such as, textile, petroleum, paper, food, explosives and pharmaceuticals (Patel et al., 2014) - it is biocompatible, biodegradable, non-toxic, low-cost and amenable to chemical modifications, properties that make it an ideal material for developing innovative drug delivery formulations (Prabaharan, 2011). However, native guar gum also has shortcomings such as its uncontrolled rates of hydration, high swelling, thickening effect, instability upon storage, high susceptibility to microbial attack and the difficulty to control viscosity due to relative fast biodegradation (Yadav et al., 2008).

Various strategies were developed in order to overcome these issues, offering the opportunity to tailor the physical and chemical properties of guar gum thus yielding materials that may find a wide range of applications. Many approaches dependent on chemical modification of guar gum were aimed at meeting the requirements of special applications (Rana et al., 2011) and included derivatization reactions such as methylation (Risica et al., 2005), sulfation (Wang et al., 2013), hydroxyalkylation (He et al., 2008; Kono et al., 2015),

carboxymethylation (Dodi et al., 2011; Gong et al., 2012), or phosphorylation (Niu et al., 2013). Carboxymethylation in particular has been found to improve water solubility while increasing the solution viscosity, to lower biodegradability and hence increase the shelf life compared to that of the native polysaccharide (Narasimha et al., 2004).

Carboxymethyl guar gum was formulated as microparticles tailored for drug delivery applications (Parveen et al., 2012) and the studies indicated that these drug microcarriers were able to avoid rapid clearance by phagocytes and thus had an extended circulation into the blood stream (Balan and Verestiuc, 2014; Kumari et al., 2010). Microencapsulation of sensitive macromolecules such as, proteins into derivatized carboxymethyl guar gum was also achieved by using multivalent metal ions solutions ( $\text{Ca}^{2+}$  and  $\text{Ba}^{2+}$ ) as cross-linkers (Thimma and Tammishetti, 2001). The maximum retention of bovine serum albumin (BSA) in the beads was only about 50% under the studied conditions, which could be due to the lower rates of cross-linking. Microspheres of carboxymethyl guar gum loaded with abacavir sulfate were formulated using water-in-oil (w/o) emulsions and glutaraldehyde (GA) as crosslinker; it was found that the beads extended the *in vitro* release time in both acidic and alkaline pH conditions when compared with unmodified GG (Sullad et al., 2011). Carboxymethyl guar gum was also combined with gelatine to obtain semi-interpenetrating polymer networks (semi-IPN) in the form of microspheres that were prepared by emulsion cross-linking method using GA and loaded with theophylline (an antasthmatic drug) (Phadke et al., 2014); the results suggested a potential toxicity of the microspheres due to the presence of GA and demonstrated an encapsulation efficiency ranging from 56 to 74 %, which was found to be affected by the amounts of CMGG and cross-linking agent. Congo Red, a hydrophobic dye commonly used for diagnosis and potentially useful as a therapeutic agent, was encapsulated recently into alginate-carboxymethyl guar gum hydrogel microspheres prepared by the extrusion of the biopolymer mixture in the presence of calcium chloride (Bosio et al., 2014). The hydrogel microsphere structure was considered to play a key role in the controlled release of the model drug. Spherical carboxymethyl guar gum nanoparticles in the size range of 12–30 nm was successfully prepared via nanoprecipitation and sonication methods (Gupta and Verma, 2014); it was found that the stability of CMGG nanoparticle suspensions was dependent on the nature of the solvent and on the sonication time, parameters that can be optimized further to tailor CMGG nanoformulations for a wide range of applications. Although nanoprecipitation and sonication are eco-friendly and cost-effective methods to produce nanosized carboxymethyl guar gum nanoparticles, the main disadvantage is the poor stability, property necessary to get a proper drug delivery system with optimal control release.

However, the nanoparticles need to be stabilized against dissolution at different pH by cross-linking, a process in which the free functional groups are partially consumed. Cross-linking of carboxymethyl guar gum functional groups may also reduce the high swelling characteristics of this material and provide better control of drug release from various dosage forms such as microspheres, particles or beads. STMP is a non-toxic cyclic triphosphate often used for the preparation of cross-linked hydrogels and microspheres for pharmaceutical applications (Dulong et al., 2004; Gliko-Kabir et al., 2000; Mocanu et al., 2004). However, to the best of our knowledge, the preparation of carboxymethylated guar gum nanoparticles by ionic gelation with STMP had not been reported in the literature.

Using an innovative approach for **enhancing the analgesic effect of well-known drugs** has been reported as another role for the study of nanoparticles. As such, our research has focused on thus improving **ketoprofen and morphiceptin** efficacy and testing the resulting compounds *in vivo* and *in vitro*.

**Ketoprofen** (Ket), 2-(3-benzoylphenyl)-propionic acid, is an analgesic, antipyretic and a non-steroidal anti-inflammatory drug (NSAID) used for the treatment of rheumatoid arthritis, osteoarthritis and other chronic musculoskeletal conditions (Heyneman et al., 2006; Marie, 1998; Vueba et al., 2006). Conventional dosage forms of this drug, administered orally, three or four doses per day, have side effects such as peptic ulceration or bleeding and anorexia, and some additional side effects (Kantor, 1986; Marie, 1996; Savage et al., 1993) that limit the use of Ket. These disadvantages added to the very short half-life, render Ket as a very good candidate to produce controlled release formulations. Controlled release of the drug is expected to significantly mitigate these harmful systemic effects. Synthetic and natural polymeric or inorganic supports are currently used for designing controlled release drug systems (Babazadeh, 2006; Bonina, 2001; Costantino, 2008; Frunza et al., 2009; Ko et al., 2002; Liu et al., 2008). Among these, the layered double hydroxides (LDHs) are attractive materials for the preparation of controlled release formulations. The general formula of LDHs can be expressed as  $[M_{(1-x)}^{II} M_x^{III}(OH)_2]^{x+} A_{x/z}^{z-} nH_2O$ , where  $M^{II}$  and  $M^{III}$  are divalent and trivalent cations, and  $A^{z-}$  is a group such as  $NO_3^-$ ,  $Cl^-$ ,  $OH^-$ ,  $CO_3^{2-}$ , etc. that can be exchanged with organic anions. The  $x$  value, i.e., the charge density, is equal to the molar ratio  $M^{3+}/(M^{2+} + M^{3+})$ .

The large variety of anions that can be incorporated in the layered double hydroxides and their high anionic exchange capacity of these materials allow their use as matrices for tailoring specific organic–inorganic hybrid nanostructures with new potential applications such as: designing new pharmaceuticals and new biocompatible materials. They are used as inorganic supports in the preparation of new pharmaceutical compositions by intercalation of non-steroidal anti-inflammatory drugs such as ibuprofen, diclofenac, indometacin, fenbufen, salicylic acid (del Arco et al., 2004; del Arco et al., 2009; Frunza et al., 2007, 2008; Li et al., 2007; Sillion et al., 2008).

Previous *in vivo* pharmacological studies on rodents show that pharmaceuticals prepared by drug intercalation in the LDH show a synergic effect. On one hand, the presence of the layered double hydroxides ensures a buffered environment and on the other hand it reduces the ulcerating side effects of the intercalated drug (del Arco et al., 2004; del Hoyo, 2007; Tarnawski et al., 2010).

Besides these properties, LDHs were used because of their capability to prevent taurocholate induced gastric injury in rat that was earlier demonstrated and reported in the literature and this is another reason for choosing them as hosts in the present study (Yu et al., 2003).

**Morphiceptin** (MF) is an opioid tetrapeptide and a potent and highly selective  $\mu$ -opioid receptor agonist. Several studies pointed out that opioid peptides within the same family inhibit pain without inducing some of the side effects specific to classical opioid analgesics as morphine. Atypical opioid peptides such as endomorphins and morphiceptin are less likely to induce respiratory depression and cardiovascular effects at effective antinociceptive doses, two of the most menacing side effects of the opioid analgesics.

However, morphiceptin, similar with other opioid peptides, cannot be delivered into the central nervous system (CNS) in sufficient amount to elicit analgesia when administered systemically, because its targeted delivery is severely restricted by the diffusion limiting blood–brain barrier (BBB). Under normal conditions the BBB, formed by tight endothelial cell junctions of brain capillary, acts as a barrier to toxic agents and safeguards the integrity of the brain, but the same mechanisms that protect the brain from foreign substances also restrict the entry of many potentially therapeutic agents. It is widely accepted that only the compounds which are unionized at physiological pH, lipophilic, and of low molecular mass can cross the BBB by diffusion mechanisms, and other compounds such as amino acids, neuropeptides, and hexoses need specific carrier proteins to pass into the brain. Thus, the BBB prevents the administration of many therapeutic compounds, including antibiotics, antineoplastic agents and CNS active drugs, to the central nervous system, even if in certain pathological situations the BBB is partly disrupted.

In this context, the difficulty encountered by morphiceptin in readily penetrating the BBB (to gain access to the brain and spinal cord to exercise its analgesic activity), as well as its biological instability, make difficult its development for clinical use (Liu et al., 2006; Sommerfeld et al., 1997).

Several invasive (disruption of the BBB, direct drug delivery, intracerebral implantation of controlled release systems) and non-invasive (of chemical or biological nature) strategies were developed to circumvent the BBB and deliver drugs into the brain. Unfortunately, invasive techniques are associated with increased risk of infection and high neurosurgical cost, and most of chemical and biological techniques are too expensive and the efficacy of such technologies is not remarkable (Garcia-Garcia et al., 2005; Abbott and Romero, 1996).

However, with the advances in nanotechnology, colloidal carriers (micelles, emulsions, liposomes and nanoparticles – nanospheres and nanocapsules) became a research subject of increasing interest. Their potential as non-invasive routes for the brain delivery of drugs consists mainly in the possibility to target specific brain tissues thanks to carrier surface linked ligands (Garcia-Garcia et al., 2005; Silva, 2007).

Other clinical advantages offered by colloidal carriers include decreased drug dose, reduced drug side effects, increased drug viability and thus improved patient quality of life. In this context, one of the most attractive and innovative alternatives to transport and deliver entrapped or adsorbed drugs into CNS consists in the use of nanoparticulate carriers. They can easily enter brain capillaries before reaching the surface of brain microvascular endothelial cells, when the surface of these colloids is modified in a proper way. The prolonged blood circulation of the surface-modified colloidal particles enhances exposure of the BBB, which favors the interaction and penetration into brain endothelial cells. Consequently, for more than a decade, surfactant coated nanoparticles have been reported to successfully transport drugs across the BBB and recently the method was applied for some opioid peptides, too (Vauthier et al., 2003; Verdun et al., 1986; Ringe et al., 2004; Couvreur et al., 1979).

As an example, polysorbate 80 (PS 80) coated poly (alkyl cyanoacrylate) nanoparticles have been proved to successfully transport several compounds – including dalargin (Bertholon et al., 2006) hexapeptide, kytorphin dipeptide, loperamide (Alyautdin et al., 1997), tubocurarine (Alyautdin et al., 1998), doxorubicin (Gulyaev et al., 1999), and the NMDA

receptor (Friese et al., 2000)– across the BBB. The surface coating of nanoparticles is an indispensable property for brain targeting effect, the protein adsorption pattern depending on the surface properties of the particles and on the chemistry of the surface-modifying agent (Petri et al., 2007). Few surfactants have been tested and the efficiency of PS 80 as surface coating reagent in facilitating brain delivery of nanoparticles against similar systems involving different surfactants – such as polysorbate 20, 40, 60, poloxamer, poloxamine, Cremopor EZ and RH-40 – was proved (Kreuter et al., 1997).

Last, but not least, research has been also focused on the potential toxicity of some metal nanoparticles – elements that are harmless in their usual state due to their large size, but significantly change properties when reduced to nanoparticles. In our laboratory, we have focused on silver and the **effect of local administration of silver nanoparticles on pain and inflammation**.

Silver has been used for medical purposes since ancient times - Hippocrates believed silver powder had beneficial healing and anti-disease properties (Barillo and Marx, 2014). Aqueous solutions that contained colloidal silver for oral administrations appeared in the early part of the 20th century (Nowack et al., 2011). These solutions, marketed as health maintainers or immunoboosters (Chen and Schluesener, 2008) were quite popular in the 90's. In the 00's, silver nanoparticle suspensions (particles with one or more dimensions on the order of 100 nm or less) (Hadrup and Lam, 2014) entered the market with similar medical recommendations. Silver suspensions have been investigated as treatment of various infections, emphysema, bronchitis (Damiani et al., 2011), chronic rhinosinusitis (Goggin et al., 2014) psoriasis, atopic dermatitis (Abeck and Plotz, 2008) or cystic fibrosis (Baral et al., 2008). They have also been used as anti-inflammatory agents in cystitis, prostatitis, colitis, gastritis, tonsillitis, appendicitis and sinusitis (Barillo and Marx, 2014).

It is common belief that silver is relatively non-toxic to humans. Most studies report only that prolonged exposure to silver may lead to a condition called argyria (irreversible pigmentation of the skin and/or eyes), but the level of exposure required is very high and this disease is quite rare nowadays (Van de Voorde, et al., 2005). Occupational exposure studies consider working with metallic silver as a minimal health risk (Drake, 2005).

However, silver is not an essential element and has no known function in the organism. In 1999, FDA issued a statement to address the widespread use of oral silver suspensions in which it highlighted the absence of scientific evidences to support their use. As such, the product was considered misbranded under the law without appropriate FDA approval as a new drug. Despite FDA's warning, this metal remained available and is nowadays accessible both in brick and mortar stores and in the online market as a homeopathic remedy or a dietary supplement (Griffith et al., 2005). The market-available silver suspensions mostly come from unknown or unreliable sources and there is no actual control of the product's quality. Some on-line shops also sell generators that produce colloidal silver at home, another important factor that contributes to the lack of control for this product. In the current setting, it is quite difficult to assess the amount of silver one individual consumes and the risk of chronic treatment with silver suspensions. It is estimated that of all nanomaterials in the medical and healthcare sector, nanosilver has the highest degree of commercialization (Chen and Schluesener, 2008), with approximately 320 t of nanosilver produced worldwide per year (Nowack et al., 2011). Together with the uncontrolled on-line

market for oral silver suspensions, this metal is also used in the manufacturing of silver-embedded medical equipments (Sussman et al., 2015) (surgical tools, catheters, bandages, needles and stethoscopes) and in implantology (Devasconcellos et al., 2012).

In 2005, the *in vitro* toxicity of several nanoparticles was assessed (Braydich-Stolle et al., 2005) and the authors concluded that silver has the highest concentration-dependent toxicity. In 2014, a Scientific Committee employed by the European Commission issued a document regarding nanosilver and its safety (Scenihr, 2014). The experts concluded that nanosilver's toxic effects are still unknown because too little information is available.

After implant surgery, the post-operative period is characterized by a prolonged systemic and localized inflammatory response (Motaghedi et al., 2014). Consequently, silver particles have prolonged interaction with both normal and inflammatory tissue after implant surgery takes place. Some studies suggest silver particles promote inflammation in normal tissue (Carlson et al., 2008), but the effect of the metal on a pre-existing inflammatory environment is unknown.

One of the main characteristics of inflammation is that pain can result after exposure to normally innocuous stimuli (Kidd and Urban, 2001) or even in the absence of any external trigger. The extent of post-surgery inflammation influences the severity of pain (Jules-Elysee et al., 2012). This is a consequence of inflammatory mediators' release from inflammatory or damaged cells and from the activation of the arachidonic acid pathway (Williangale et al., 1997). These mediators will in turn activate nociceptors by either direct or indirect pathways and modulate primary afferent neurons generating peripheral sensitization (Jepma et al., 2014). As such, inflammatory pain is a distinct type of pain that may be influenced by triggers that have no effect on normal tissue. Clinically, this is expressed as hyperalgesia or allodynia.

In the past fifteen years, my research team and I have worked constantly in the field of nanotechnology and advanced drug delivery, striving to create better analgesic systems and innovative diagnostic tools for chronic conditions. The two main areas of nanoparticle research we have focused on are:

1. preparation of novel particles such as silica nanoparticles or carboxymethyl guar gum nanoparticles and assessing their safety and efficacy
2. investigating nanoparticles in the field of pain research either as pro- or analgesics

Below, some of the most important publications that have stemmed from our research are listed:

**Tamba BI**, Dondas M, Leon MM et al. Silica nanoparticles: Preparation, characterization and *in vitro/in vivo* biodistribution studies. *European Journal Of Pharmaceutical Sciences* 2015; 71: 46-55.

Dodi D, Pala A, Barbu E, Peptanariu D, Hritcu D, Popa MI, **Tamba BI**. Carboxymethyl guar gum nanoparticles for drug delivery applications: Preparation and preliminary *in-vitro* investigations. *Materials Science and Engineering: C* 2016; 63(1):628-636.

Silion M, Hritcu L, Jaba IM, **Tamba BI** et al. In vitro and in vivo behavior of ketoprofen intercalated into layered double hydroxides. Journal of materials Science Materials In Medicine 2010; 21(11):3009-3018.

David G, Jaba IM, **Tamba BI** et al. Antinociceptive effect of morphiceptin loaded poly(butylcyanoacrylate) nanoparticles. Revue Roumaine De Chimie 2010; 55(11):923-930.

Jaba IM, **Tamba BI**, Albu E et al. Exogenous atypical opioid peptides inhibit hyperalgesia associated with Carrageenan peripheral inflammation. Therapeutics, Pharmacology & Clinical Toxicology 2011; 15(4):285-288.

Alexa AI, Alexa Stratulat T, Leon Constantin MM, Alexa ID, **Tamba BI**. Local silver nanoparticles administration promotes inflammation and hyperalgesia in rats. Revista de Chimie 2017; 68(3):490-495.

### 1.2.2 Preparation, characterization and biodistribution studies of novel nanoparticles

**Study 1 - Silica nanoparticles: Preparation, characterization and in vitro/in vivo biodistribution studies.** This study focuses on the biodistribution of silica nanoparticles (SNPs) (fluorescent with Cy5.5 dye and radiolabelled with  $^{99m}\text{Tc}$ , respectively) in rodents, in order to determine possible uses in therapeutic and/or diagnostic schemes. Due to the increasing health concerns regarding the use of nanoparticles in medical applications, and more specifically on amorphous silica nanoparticles, we also performed an acute toxicology screening of SNPs used in this study in order to evaluate their safety.

**Study 2 - Carboxymethyl guar gum nanoparticles for drug delivery applications: Preparation and preliminary in-vitro investigations.** The aim of this work was to investigate the possibility to formulate cost-effectively carboxymethyl guar gum nanoparticles for biomedical applications such as drug delivery using trisodium trimetaphosphate (STMP) as cross-linker.

#### 1.2.2.1 *Materials and methods*

##### *Animals*

Animal care was in accordance with the Guide for the Care and Use of Laboratory Animals published by NIH and with the Policies on the Use of Animals and Humans in Research published by the Society for Neuroscience. The International Association for the Study of Pain (IASP) guidelines for the investigation of pain in animals were followed. The design of the experiments was approved by the University of Medicine and Pharmacy Gr. T. Popa ethics committee. All animals were euthanized at the end of the experiment in accordance with the AVMA Euthanasia.

For these studies, the following animals were used:

- Adult male Swiss mice with an average weight of  $20 \pm 2$  g (study 1,2)
- Male guinea pigs with an average weight of  $600 \pm 50$  g. (study 2)

The animals were housed individually at  $21 \pm 2^\circ\text{C}$  under a 12-hours light/ dark cycle with ad libitum access to food and water. About 24 hours prior to the beginning of the experiment, each animal was accommodated for 15 minutes to the testing room. In the Ketoprofen study, conducted on Swiss mice, access to food was stopped 16 hours before receiving the drug sample.

#### *Analgesic in vivo tests*

##### *Hot Plate test*

For the hot-plate latency test, a rectangular metal surface was heated to a temperature of  $55 \pm 0.5^\circ\text{C}$ . The antinociceptive response was monitored from the time the mouse was placed on the heated surface until the first overt behavioral sign of nociception (paw withdrawal latency) occurred, such as (i) the mouse licking a hind paw, (ii) the mouse shaking a hind paw, (iii) an escape response. Upon the occurrence of any of these signs, the timer was stopped by a foot-operated pedal and the mouse was immediately removed from the plate. Maximum latency (cut-off time) was set at 60 s to prevent tissue damage to the back paws.

##### *Statistical analysis*

Statistical analysis and graphic design was performed with the aid of GraphPad 3.0 software (GraphPad Software, La Jolla, CA). Descriptive statistics and analysis of variance (Mixed ANOVA with Tukey post-hoc test) were performed. Differences between treatment groups were analyzed using ANOVA one-way method for comparison at each time point, followed by Bonferroni post-hoc tests. The experiments were replicated three independent times and the data are presented as  $\pm\text{SD}$  (standard deviation). Differences were considered statistically significant when p-value was less than 0.05.

## **Silica nanoparticles: Preparation, characterization and in vitro/in vivo biodistribution studies**

### *Synthesis of SNPs*

For this part of our study TEOS (tetraethyl orthosilicate), APTES (3-aminopropyltriethoxysilane), aqueous ammonia solution ( $\text{NH}_3$ , 28–30%), Cy5.5 reactive dye and ethanol (>99.9%) from Sigma Aldrich were used. All solutions were prepared with ultrapure water.

Four types of silica nanoparticles derivatives were synthesized and used for in vitro/in vivo evaluation, as follows:

- *batch AA1*: bare SNPs were produced by hydrolysis and condensation of TEOS in ethanol in the presence of ammonia as a catalyst using a modified version of the method described by Stober et al. (1968). Briefly, a solution consisting of ammonia (25%) and water in 100 mL of ethanol was prepared. 0.28 M TEOS solution (in ethanol) was added at room temperature under vigorous stirring for 24 h. Finally, the colloidal solution was separated by centrifugation at 6000 rpm for 5 min and then washed with ethanol and ultrapure water for several times to remove the unreacted species.
- *batch AA2*: the surface amine functionalization involved a standard procedure to synthesize the  $\text{NH}_2$ -SNPs. First, ethanol, ultrapure water and TEOS (0.28 M) mixtures were prepared, followed by addition of 0.14 M APTES in ethanol. The hydrolysis and co-condensation of TEOS and APTES was initiated by the addition of 1 mL of

ammonia solution (25%) to the reaction mixture and stirred for 24 h at room temperature, resulting in the formation of the core-shell-NH<sub>2</sub>-SNPs. Samples were then centrifuged (6000 rpm for 10 min) and washed with ethanol and ultrapure water.

- *batch AA3*: the terminal amine groups from batch AA2 were used for the conjugation of Cy5.5, a near infrared (NIR) optical probe, using a mixture of Cy5.5 dye (commercially available with an N-hydroxysuccinimide ester group for binding to amine groups), ethanol and buffer solution (1 mg; 0.14 M) added under continuous stirring at room temperature for 6 h.
- *batch <sup>99m</sup>Tc-SNPs*: amine surface-modified SNPs (batch AA2) were used for coupling <sup>99m</sup>Tc on the nanoparticle's surface as a radiotracer to study the biodistribution of the so-produced SNPs. Briefly, SNPs were suspended in ultrapure water (5 mg/mL) and dispersed by sonication for 15–20 min. An aqueous solution of NaBH<sub>4</sub> (reducing agent) was added under continuous stirring and homogenized for 1 h. Then, to the above mixture <sup>99m</sup>TcO<sub>4</sub> Na solution was added quickly under vigorous stirring and left for another 30 min. The obtained product was separated by centrifugation and washed with ultrapure water to remove the uncoupled <sup>99m</sup>Tc radionuclide.

<sup>99m</sup>TcO<sub>4</sub> Na (sodium pertechnetate) was chosen for labelling because it is the most commonly used emitting radioisotope in nuclear medicine having a convenient half-life of approximately 6 h, appropriate energy (140 keV) for imaging on a standard gamma camera and less attenuation by soft tissue. A 12.5 GBq Drytec Technetium Generator was used for the production of <sup>99m</sup>TcO<sub>4</sub> Na supplied by GE Healthcare.

### ***Characterization of the SNPs***

SEM experiments were carried out at an accelerating voltage of 20 kV on a field emission scanning electron microscope (FE-SEM, Zeiss, SUPRA VP 40). Samples suspended in ultrapure water (1mg/mL) were deposited on freshly cleaved mica surface, dried and gold/palladium coated. Determinations of nanoparticles size, zeta potential and polydispersity index were performed using a Zetasizer (Zetasizer Nano ZS, Malvern Instruments). The samples were dispersed in ultrapure water and measured at a scattering angle of 90° and 25 °C. Qualitative chemical composition assessment of the nanoparticles was performed by FTIR analysis (Bomem MB 104 spectrometer). The material was finely grounded and dispersed into KBr powder-pressed pellets using a ratio of approximately 1mg sample/200 mg KBr. IR absorbance data were obtained over a range of wavenumbers from 4000 to 400 cm<sup>-1</sup>.

### ***General toxicity screening***

For acute systemic toxicity screening, three groups of mice (10 mice per dose) received intraperitoneal 0.1 mL SNPs buffer solution (batch AA3) in a single dose (25, 50 and 100 mg/kg body weight (bw)) and kept under observation for 5 days after administration. For all experiments, nanoparticles were ultrasonicated for 30 minutes directly prior to use. The maximum possible dose (20 mg SNPs per 1 mL PBS) administered was defined by preliminary experimental results – maximum tolerated dose (MTD) (Kong et al., 2011). The animals were carefully observed for obvious signs of toxicity, such as convulsions or body weight effects. All mice were necropsied to detect macroscopic evidence of organ and tissue damage or dysfunction.

### ***Microscopy biodistribution studies***

Fluorescent silica nanoparticles (batch AA3) (7.5 mg/1 mL PBS) were administered via two routes in 2 groups of 6 mice: intravenously (0.1 mL /mouse) and orally (0.2 mL/mouse). The control group (6 animals) received a similar volume of PBS. At specific times after intravenous (30 min and 2 hours) or oral administration (1, 2, 24, 48 and 72 hours) of the labelled nanoparticles (batch AA3) the mice were deeply anesthetized with xylazine and transcardially perfused with 15 mL 0.9% saline solution, followed by fresh 4% paraformaldehyde (PFA) in 75 mL 0.1 M PBS. Key organs (brain, heart, liver, lung, kidneys, spleen, testis and bladder) were extracted and postfixed overnight in 4% PFA, followed by cryoprotection in 30% sucrose in PBS for 72 hours. Sections of the above-mentioned organs were cut using a freezing microtome (CM 1850 Leica Microsystems, Germany), were collected, mounted on slides and examined in a Leica Confocal Laser Scanning Microscope (TCS SPE DM 5500Q), using a laser diode (635 nm line), taking account that the Cy5.5 fluorochrome is optimally excited near 675 nm and fluoresces near 694 nm.

#### *Scintigraphy biodistribution studies*

<sup>99m</sup>Tc radiolabelled NPs were used in order to study the biodistribution (batch <sup>99m</sup>Tc-SNPs). Five groups of 4 male guinea pigs were injected with 37 MBq/kg bw of <sup>99m</sup>Tc-coupled amino SNPs. Jugular vein was exposed and cannulated for infusion of radiotracer. A control group of 4 male guinea pigs received 37 MBq/kg bw of <sup>99m</sup>TcO<sub>4</sub><sup>-</sup>Na, in the same conditions. The guinea pigs were placed under a dual-head gamma camera (SPECT Siemens Gamma camera with LEAP (Low Energy All Purpose) collimators). The body distribution profile was recorded in dynamic mode till 5 minutes post injection and in static mode every 15 minutes for 2 hours, then every 30 minutes for a total of 6 hours. The animals were sacrificed after 6 hours and different organs were extracted and immediately gamma counted.

### **Carboxymethyl guar gum nanoparticles for drug delivery applications: Preparation and preliminary in-vitro investigations**

#### *Materials*

Guar gum (Mw 220 kDa), trisodium trimetaphosphate Na<sub>3</sub>P<sub>3</sub>O<sub>9</sub> (STMP), Rhodamine B (RhB) and sodium hydroxide (NaOH) were purchased from Sigma-Aldrich, Germany. Chloroacetic acid (CAA) was obtained from Merck, Germany. Ethanol and acetone were procured from the Chemical Company (Iasi, Romania). Analytical grade chemicals were used as received without further purification. All solutions were prepared with ultrapure water (18.2 MΩ•cm).

#### *Guar gum purification*

Commercial guar gum was purified as described in the literature (Cunha et al., 2007) with some modifications. Briefly, commercial guar gum (5 g) was extracted with ethanol (Soxhlet, 72 hours) and hydrated in ultrapure water (500 mL) under magnetic stirring (3 hours); after centrifugation (1500 rpm; 605 RCF; 15 minutes), the supernatant was precipitated in acetone and the solid was filtered and washed successively with ethanol and ultrapure water, and subsequently freeze-dried (batch denoted GG).

*Preparation of carboxymethyl guar gum* - The synthesis of carboxymethyl guar gum was performed as previously reported (Dodi et al., 2011) with slight modifications. Briefly, 1 g of GG was dispersed in 100 mL of ultrapure water and the mixture was stirred for 2 h under

nitrogen atmosphere. The resulting suspension was mixed with 20 mL of NaOH solution (0.1 M) and the mixture was allowed to react for 2 h at room temperature (25°C).

Chloroacetic acid (20 mL; 1.58g/cm<sup>3</sup>; 0.025 mol) was added and the mixture was stirred overnight at 50°C. The reaction mixture was then cooled to ambient temperature, adjusted to pH 7.0 (using 1 M HCl), extracted with acetone and separated by centrifugation (5 000 rpm; 6142 RCF; 10 min). The product was further purified by dialysis against distilled water until neutral pH has been reached (approx. 72 h). The final product (batch denoted CMGG) was then dried by lyophilisation and stored in a desiccator for further analysis.

*Preparation of cross-linked nanoparticles* - Varying amounts of CMGG (concentration ranging from 0.05 to 0.2 % w/v) were added into a 2M NaOH aqueous solution (100 mL; pH=12.0) and were allowed to hydrate for a minimum of 2 h under constant magnetic stirring at room temperature. A STMP aqueous solution (100 mL; concentration varying from 0.2 to 10%, w/v, as described in table VII) was then added at a flow rate of 1 mL/min using a peristaltic pump, and the reaction mixture was then continuously stirred overnight.

The resultant colloidal dispersion was dialyzed against distilled water until neutral pH (approx. 72 h). An aliquot of the sample suspension was kept for particle size measurements, while the remaining product was lyophilized by freeze drying and then stored in a desiccator. Preliminary experiments informed the preparation of 11 formulations, details of which are given in table VII.

**Table VII.** Molecular weight characteristics of GG and CMGG

Sample	M <sub>w</sub> , kDa	PDI
GG	220	1.92
CMGG	261	1.5

### *Characterization*

#### *NMR spectroscopy*

The <sup>1</sup>H and <sup>13</sup>C-NMR spectra were recorded on a Jeol NMR 400 MHz spectrometer at 70°C in D<sub>2</sub>O using sodium trimethylsilyl propionate (TSP) as internal reference.

*FTIR-ATR spectroscopy* - The FTIR spectra were recorded on dried samples using a Nexus FT-IR Diamond HTR instrument (Thermo Scientific) in the range of 400–4000 cm<sup>-1</sup> using a Smart Orbit ATR accessory with diamond crystal and were processed using Omnic 8.0 software.

#### *Gel permeation chromatography (GPC)*

The average molecular mass and the polydispersity index of the guar gum derivatives were determined by gel permeation chromatography (GPC) on a Polymer Laboratories System (PL-GPC 120, Varian) instrument equipped with refractive index detector and three PLaquagel-OH packed columns (8 μm particle size and 20, 40 and 60Å pore type), connected in series. Chromatographic parameters were as follows: eluent (0.2M NaNO<sub>3</sub>; 0.01M NaH<sub>2</sub>PO<sub>4</sub>; pH=7) flow rate 1 mL/min; column temperature 30°C; sample volume 100 μL. Pullulan standards (Type P-82, Lot 01101, Shodex Denko KK, Japan) with sample weights of

$0.6 \times 10^4$ ,  $1 \times 10^4$ ,  $2.17 \times 10^4$ ,  $4.88 \times 10^4$  and  $11.3 \times 10^4$ ,  $21 \times 10^4$ ,  $36.6 \times 10^4$ ,  $80.5 \times 10^4$  g/mol were used as standards.

Samples were prepared by dissolving  $0.1 \pm 0.001$ g of polymer in 10 mL eluent stirred at room temperature overnight, with the subsequent filtration of the solution through a syringe filter with a pore diameter of 0.45  $\mu$ m. All data were recorded and processed using Cirrus GPC software.

#### *Thermal analysis (TG-DTG)*

Thermogravimetric analysis was carried out on a Mettler Toledo TGA-SDTA851 system, in nitrogen atmosphere with a flow rate of 50 mL/min, at a heating rate of 10 K/min in the temperature range of 25–700°C; sample weight range 4–5 mg.

#### *Surface morphology*

The surface morphology of nanoparticles was investigated by scanning electron microscopy using a SEM Jeol JSM-6060LV instrument. Samples were deposited on stubs, dried with nitrogen and coated with golden alloy in an argon atmosphere (current 20 mA, pressure  $10^{-3}$  Pa) using a coater (Quorum, Q 150RES).

#### *Particle size and zeta potential measurements*

The average hydrodynamic diameter of the nanoparticles was determined in water at 25°C by dynamic light scattering measurements using a Malvern Zetasizer ZS90 (Malvern Instruments, Worcester, UK). The same instrument allowed the determination of zeta potential  $\xi$  (mean of three measurements) and polydispersity index (PDI).

In addition, real-time dynamic nanoparticle visualization was performed by nanoparticle tracking analysis (NTA) using a NanoSight LM10 instrument equipped with a sample chamber with a 532-nm laser and a 560-nm long pass filter. The particle size was calculated using the Stokes–Einstein equation.

#### *In vitro experiments*

##### *Cell cultures*

For cytotoxicity tests, normal human dermal fibroblasts (NHDF) cells (from PromoCell) at a passage number lower than 10 were grown in T25 culture flasks with 10 mL of DMEM: F12 medium (from Lonza) supplemented with 10% fetal bovine serum (FBS, Gibco), 1 mM sodium pyruvate (Lonza) and 1 % Penicillin-Streptomycin-Amphotericin B mixture (10K/10K/25  $\mu$ g in 100 mL, Lonza). Cell growing was done at 37 °C and 5 % CO<sub>2</sub> under humidified atmosphere and medium was changed with fresh one every 4 days. NHDF cells were harvested by trypsinization with Trypsin-Versene (EDTA) mixture (Lonza), washed with phosphate buffered saline (PBS, Invitrogen) centrifuged at 200 rpm for 5 min, counted and seeded at a density of  $5 \times 10^3$  cells/well in 96 well plates with 100  $\mu$ L/well of the above specified medium. Cells were incubated and were allowed to adhere in humidified atmosphere at 37°C until the next day.

##### *Cytotoxicity assay (MTS)*

The cytotoxicity induced by CMGG nanoparticles (batch Np11) was investigated by CellTiter 96®AQueousOne Solution Cell Proliferation Assay (MTS) (Promega Corporation,

Madison, Wisconsin, USA). The metabolic cell activity (an indirect measure of cytotoxicity) was measured by quantifying the conversion of MTS to formazan, which can be photometrically detected. The quantity of the formazan product as measured at 490 nm is directly proportional to the number of living cells in a culture. The cells were exposed for 24 and 48 h to different concentrations of nanoparticles (batch Np11) ranging from 0.78 to 100 mg/mL, in 100  $\mu$ L fresh medium. The plates were incubated at 37°C and 5 % CO<sub>2</sub> under humidified atmosphere for 24 or 48 h. Four hours before reading the results, 20  $\mu$ L of CellTiter 96@AqueousOne Solution reagent were pipetted into each well and the plates were returned to the incubator. The absorbance was then recorded with an EnVision Multilabel Plate Reader (PerkinElmer). A total of eight serial dilutions were tested and the experiment was repeated three times.

Data analysis was done with GraphPad Prism version 6.04 for Windows (GraphPad Software, San Diego, CA). To calculate the half maximal inhibitory concentrations (IC<sub>50</sub>), a log (inhibitor) vs. response with variable slope (four parameters) nonlinear regression model was used. At least 3 replicates were included in the analysis.

#### *Optical microscopy*

NHDF cells were seeded at a density of 35x10<sup>3</sup> cells/well in six well plates with 2 mL/well of medium. Cells were allowed to attach in humidified atmosphere at 37°C until the next day. The medium was replaced with serial dilutions of nanoparticles (batch Np11, dispersed in 2 mL fresh medium) and the cells were incubated at 37°C and 5% CO<sub>2</sub> under humidified atmosphere for the next 24 or 48 h. Images were recorded using an inverted microscope Leica DMI 3000 under modulation contrast (MC) at the beginning of experiment, and then 24 and 48 h after incubation with nanoparticles.

#### *RhB loading and release studies*

To determine the actual amount of the entrapped model drug, 100 mg of CMGG nanoparticles (batch Np11 was chosen based on its size distribution) were added in a water-ethanol (1:1) solution of RhB (20 mL; 2 % w) and stirred for 3 h at room temperature. The mixture was adjusted to pH 5.0 using HCl (0.01M) and was left overnight under stirring. The supernatant was separated by centrifugation (13.400 rpm; 12.927 RCF; 20 min) and measured by UV-Vis using a Perkin Elmer Lambda 35 spectrophotometer at 554 nm. The drug entrapment efficiency was calculated from a calibration curve of RhB using the following equation (Vasi et al., 2014):

$$E_e(\%) = \frac{M_i - M_f}{M_i} \times 100, (1)$$

where  $M_i$  is the initial weight of the RhB added and  $M_f$  is the amount of free RhB in the supernatant. The RhB-loaded nanoparticles were washed with ultrapure water in order to remove the unreacted components and then freeze-dried.

The release studies of RhB (Np11\_RhB) were carried out as follows: dehydrated RhB loaded nanoparticles (10 mg) were suspended at 37°C in 5 mL phosphate buffer solutions (0.1 M; pH 2.2 and 7.4, respectively) in an incubated thermostatic shaker (100 rpm). At periodic intervals, a 150  $\mu$ L aliquot was withdrawn and measured by UV-Vis in a 10 mm micro-cell. The amount of the released drug was calculated using a calibration curve.

1.2.2.2 *Results***Silica nanoparticles: Preparation, characterization and in vitro/in vivo biodistribution studies.****SNPs design**

Four types of SNPs were synthesized, as shown in fig. 11 using a derived method with original modifications for the synthesis of spherical and monodisperse silica nanoparticles. First, SNPs bearing OH groups were prepared from aqueous alcohol solutions of silicon alkoxides in the presence of ammonia as a catalyst by hydrolysis with the formation of silanol groups and condensation reaction for the siloxane bridges development (batch AA1).

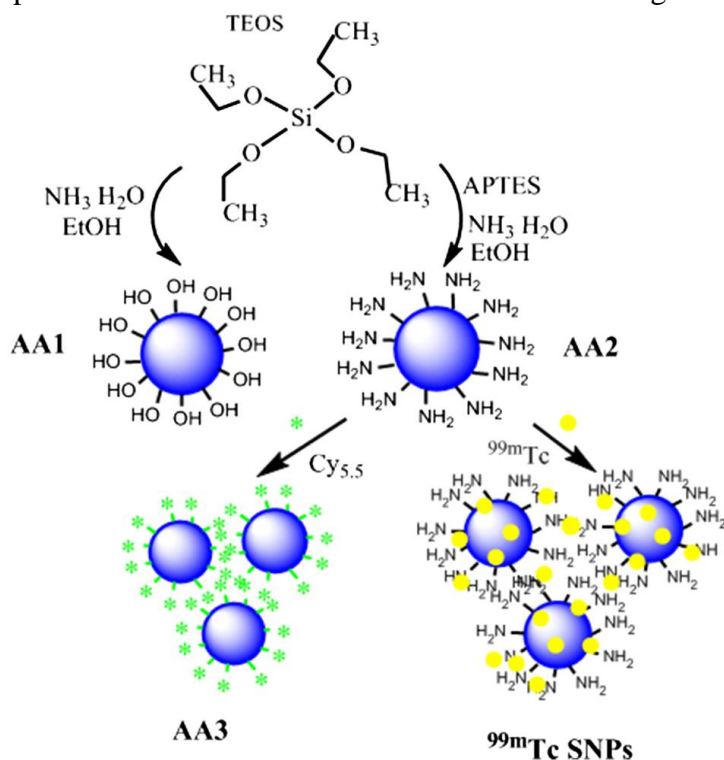


**Fig. 11.** Schematic presentation of SNPs design

Since it is supposed that the binding affinity between the nanocarrier and the radioisotope along with the stability of the obtained radiotracer could be modulated by modifying the surface properties of the silica nanocarrier, functionalization via covalent bonding of organic groups was achieved by co-condensation of TEOS and APTES to obtain amine-functionalized silica nanoparticles with high specific surface area in a one-step reaction (batch AA2). The third type of SNPs involves a contrast agent attachment for biodistribution studies. Cy5.5 is a highly sensitive and bright cyanine dye with superior photostability compared to more commonly used dyes allowing more time for image detection. Cy5.5 is a good candidate for biological applications due to its stability and low non-specific binding. Cy5.5 is commercially available with an N-hydroxysuccinimide (NHS) ester group for binding to amine groups. Thus, SNPs comprising free amino group were used to conjugate Cy5.5 to the particle via active NHS ester.

To monitor their route *in vivo* and obtain an accurate biodistribution profile in each organ,  $\text{NH}_2$ -SNPs were labelled with a gamma emitting radioisotope,  $^{99\text{m}}\text{Tc}$ . Thus, the amino functionalized SNPs (batch AA2), selected for their enhanced

surface reactivity, were first labelled with  $^{99m}\text{Tc}$  radionuclide and then tested in healthy control groups for their visualization and tracking by gamma scintigraphy. The radionuclide.  $^{99m}\text{Tc}$  is commonly used as a radioisotope-tracer for diagnosis in nuclear medicine because it radiates gamma rays and is suitable for labelling different vector molecules.

Physicochemical characterization was performed only on bare, amino and fluorescent SNPs (batches AA1, AA2 and AA3), further studies will be performed regarding the mechanism of labelling between the amino groups and  $^{99m}\text{Tc}$ , their size, surface charge and stability of the formed complex (Sarparanta et al., 2011).

### *Physico-chemical properties of SNPs*

The surface structure and morphology of SNPs were investigated using FE-SEM. Fig. 12 shows SNPs as fairly uniform spherical particles with an average size of 200–300 nm. FE-SEM image of spherical bare SNPs with a mean particle diameter of  $300 \pm 5$  nm (batch AA1) is presented in fig. 12A.

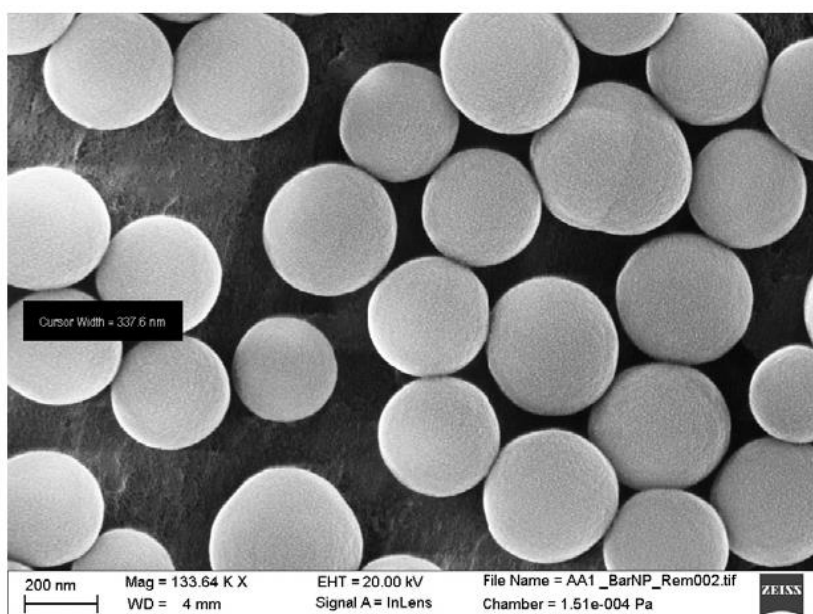


**Fig. 12A.** FE-SEM images of bare SNPs (batch AA1);

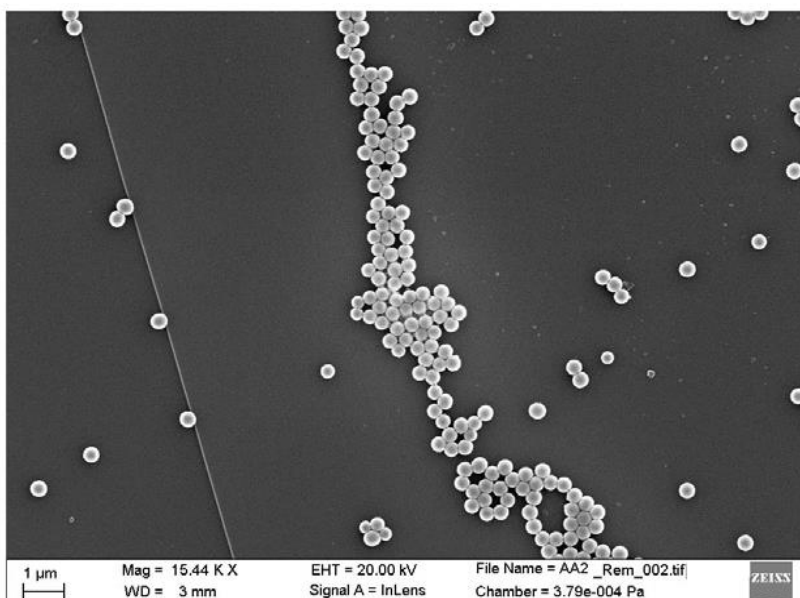


**Fig. 12B.** FE-SEM images of amino SNPs (batch AA2)

Fig. 12B shows the amino-functionalized SNPs (batch AA2) with a narrow particle size distribution of about  $250 \pm 2$  nm. After the Cy5.5 dye attachment on the amino groups, SNPs decreased in size to about  $200 \pm 2$  nm due to the shrinking and partial dissolution of the particle, according to the FE-SEM pictures. The morphology and size distribution of Cy5.5 labelled SNPs (batch AA3) are shown in fig. 12C.

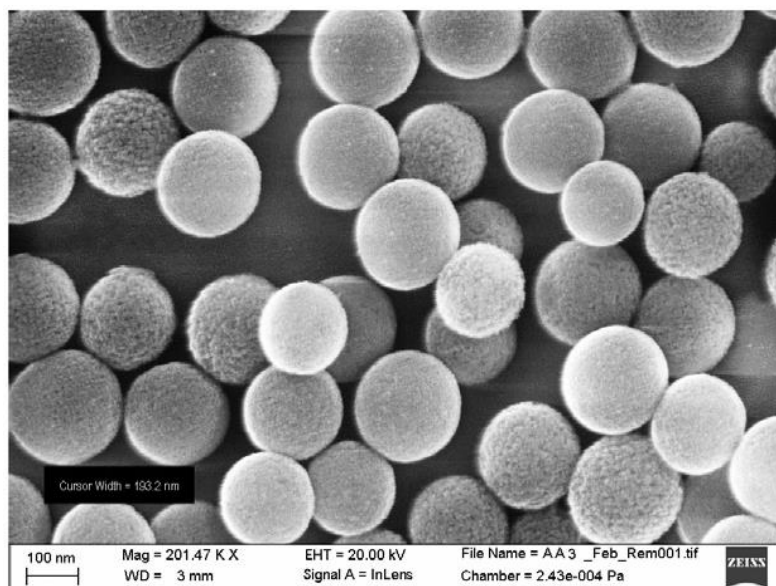


**Fig. 12C.** FE-SEM images of fluorescent SNPs (batch AA3)

In agreement with FE-SEM results, dynamic light scattering measurements evidenced (Table VIII) the increase of the apparent hydrodynamic diameter when dispersed in aqueous solution.

**Table VIII.** Size distribution, zeta potential and PDI data of SNPs derivatives

<i>Batch</i>	<b>Z-average hydrodynamic diameter (nm)</b>	<b>Zeta potential (mV)</b>	<b>PDI</b>
AAA1	$408 \pm 0.91$	$-37.8 \pm 13.8$	0.26
AAA2	$384 \pm 0.72$	$+23.2 \pm 3.6$	0.12
AAA3	$460 \pm 0.89$	$-25.5 \pm 4.91$	0.53

The large diameter (Table VIII) might be explained by the polydispersity of the sample and indirectly confirms the presence of aggregates formed in the presence of water, which modifies the particles' lipophilic character by increasing the hydrophilic balance. To evaluate the surface properties of the produced SNPs, zeta potential measurements were performed. As expected, bare SNPs showed negative zeta potential values ( $-38.7$  mV) due to the silanol groups, which is in agreement with previous studies (Digigow et al., 2014). Upon addition of APTES, the zeta potential increases to a positive value of  $+23.2$  mV, which is attributed to the appearance of the protonated amine ( $-\text{NH}_3^+$ ) groups ( $\text{pK}_a = 9$ ) on the nanoparticle surface.

The zeta potential measurements of samples made with Cy5.5 dye showed a negative value  $320$  ( $-25.5$  mV), which could come from negative charges of the carboxyl groups and the disappearance of the amino moieties. The polydispersity index (PDI) describes the width of the assumed Gaussian distribution of the SNPs. The obtained dimensionless values indicate

that the samples have a broad size distribution since  $PDI > 0.1$ , fact explained by the dispersion of the nanoparticles in water.

Additional stability studies were performed in order to evaluate the strength of the SNPs in biological environment over 240 minutes. The obtained results demonstrate that the bare, amino and fluorescent SNPs tend to form large aggregates when dispersed in water, therefore, the hydrodynamic diameter is increasing over time. Further studies must be conducted to optimize the *in vitro* serum stability of the radiolabeled complexes.

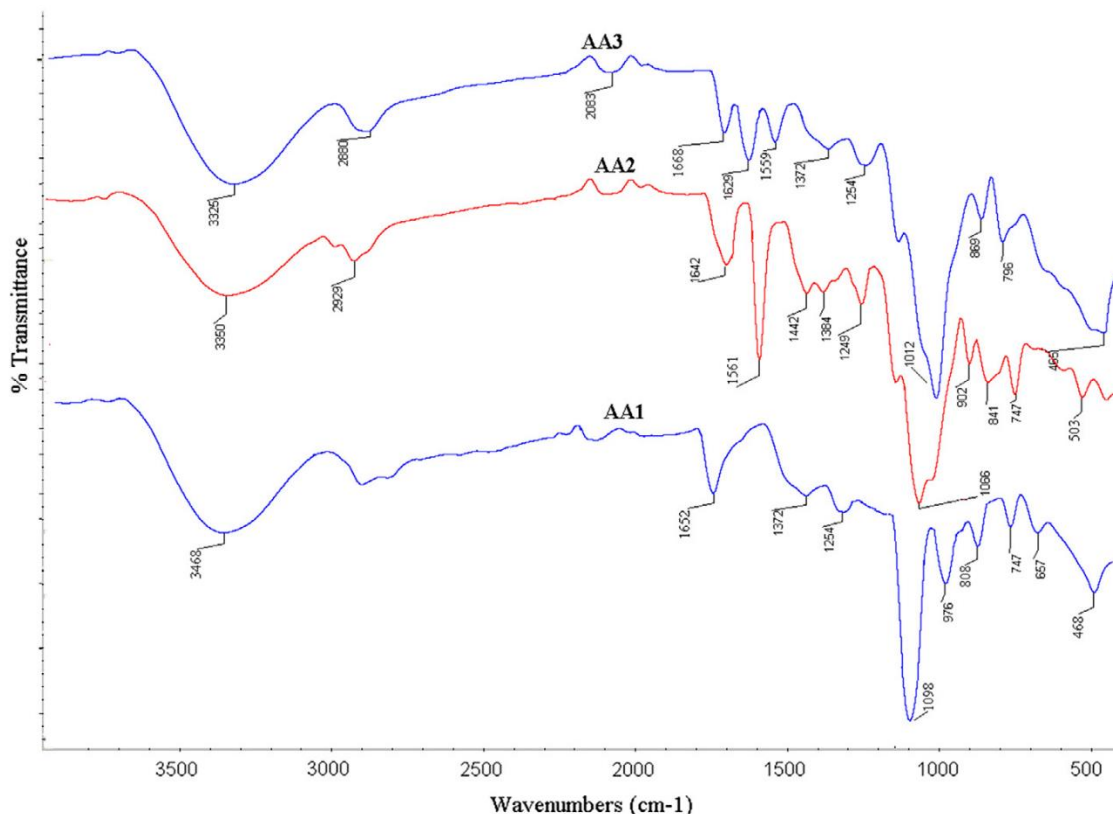


**Fig. 13.** FT-IR of bare SNPs (batch AA1), amino SNPs (batch AA2) and fluorescent SNPs (batch AA3)

FT-IR measurements were performed to identify the structural differences between bare, amino and fluorescent SNPs. Figure 13 illustrates the FT-IR spectra of all samples in the range of  $400\text{--}4000\text{ cm}^{-1}$ . The bare SNPs (batch AA1) exhibited IR peaks at the bands attributed to Si–O–Si bending ( $468\text{ cm}^{-1}$ ), Si–O–Si symmetric stretching ( $808\text{ cm}^{-1}$ ), external Si–OH groups ( $976\text{ cm}^{-1}$ ), Si–O–Si asymmetric stretching ( $1098\text{ cm}^{-1}$ ), water molecules retained by siliceous materials ( $1652\text{ cm}^{-1}$ ), and –OH stretching ( $3468\text{ cm}^{-1}$ ) (Kamarudin et al., 2013).

After modification with APTES, the SNPs still retained its siliceous structure, displaying no major changes in the formation of NH<sub>2</sub>-SNPs (batch AA2). The new absorption band at  $1561\text{ cm}^{-1}$  is attributable to a NH<sub>2</sub> scissor vibration, suggesting the presence of the amino groups of APTES molecules. Also, compared with the bare SNPs, the APTES-modified SNPs show an additional weak band at  $2929\text{ cm}^{-1}$ , which can be assigned to the

alkyl groups  $[-(\text{CH}_2)_n-]$  present in APTES. After cyanine dye attachment, the relative intensity of amine group vibrations became less intense, suggesting that Cy5.5 was successfully loaded onto the surface of SNPs. New bands at  $1668\text{ cm}^{-1}$ , and  $1629\text{ cm}^{-1}$  appeared after the loading process, which might be associated with the aqueous solution of Cy5.5, and N–H group. All these facts suggest that Cy5.5 has been successfully attached to the surface of the  $\text{NH}_2$ -SNPs.

### ***Toxicity evaluation***

In this study, fluorescent SNPs were used for general toxicity assessment. The acute toxicity screening allowed for the identification of the dose of  $100\text{ mg/kg bw}$  as MTD for this study, with no significant changes in animal behavior or weight.

The histological examination (data not shown) of main organ tissue (liver, kidney, heart, stomach and intestine) that followed the five days observation period identified no histological changes from the normal tissues characteristics. The MTD was several times higher than the doses administered in the bioavailability studies, profiling a good safety profile for future therapeutic associations of the SNPs with drugs.

### ***Biodistribution of the fluorescent SNPs by microscopy***

Following the intravenous administration of fluorescent SNPs, batch AA3 (size  $200\text{ nm}$ ), at specific time points (30 minutes and 2 hours) the SNPs did not penetrate the blood brain barrier and were not present in the myocardium. Bladder tissue sample were also negative.

However, SNPs were found in the rest of the investigated organs (liver, kidney, testis, feces and lung, see fig. 14). To validate the obtained results, the organs of the control groups were also evaluated after PBS administration. Fig. 14B represents the comparative control liver examination at 2 hours in the same conditions as the SNPs. The image evidenced the autofluorescence that was taken into consideration for the evaluation of the SNPs biodistribution as an example. The same pattern was observed also for the control images taken for both intravenously and oral administration of the fluorescent SNPs.

The biodistribution studies were performed also after the oral administration at specific time points (1 and 2 hours). The SNPs were present in all the investigated organs (liver, kidney, testis, spleen, and lung) except the brain and heart (fig. 15).

However, we also found that significant amounts of SNPs were distributed at 24 and 48 hours after administration, especially in the liver. After 72 hours, a gradually decrease of SNPs accumulation in liver and spleen was noticed.

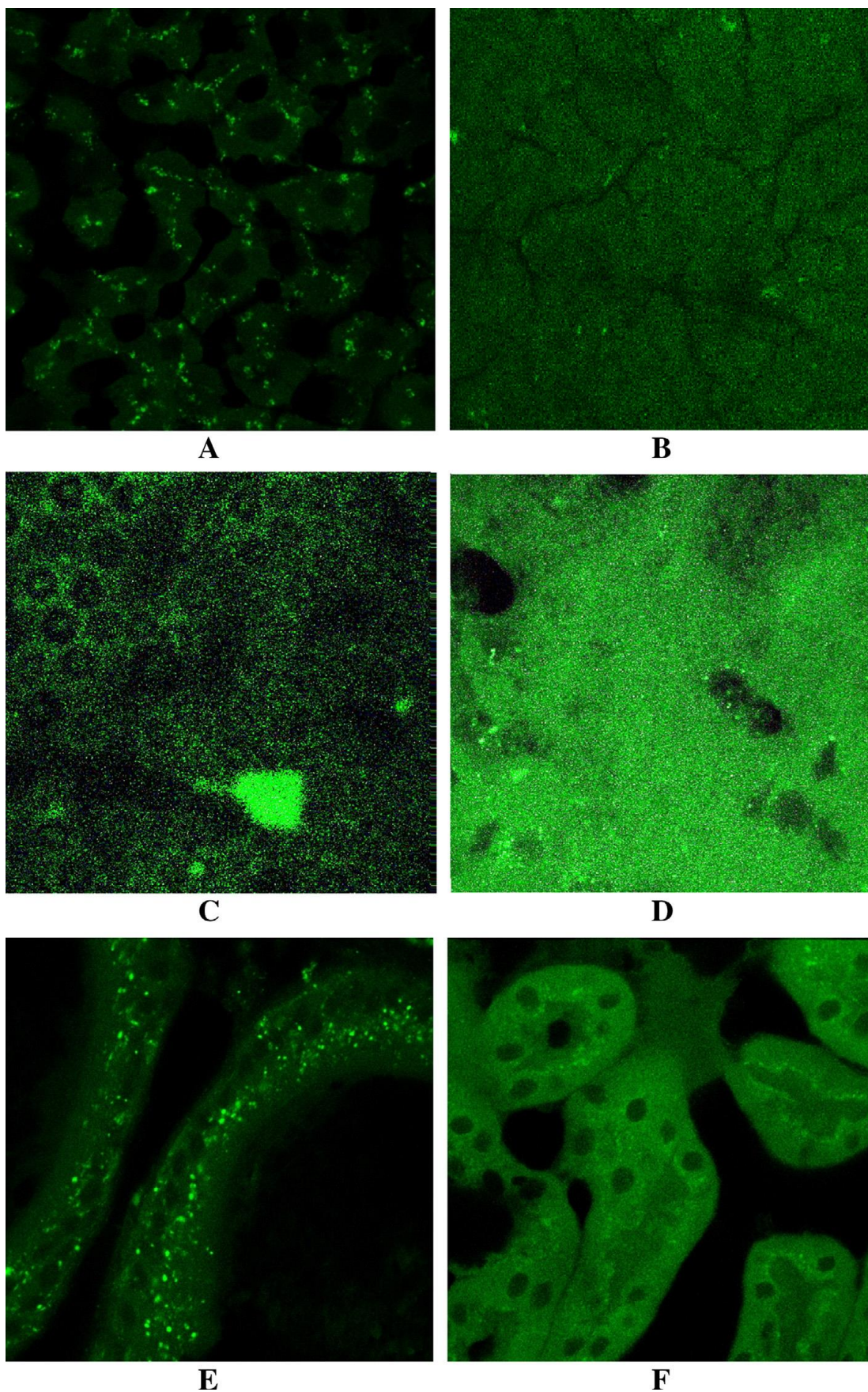


**Fig. 14.** SNPs distribution in A. Liver; B. Liver control; C. Lung; D. Feces; E. Testis and F. Kidney (2 hours after intravenous administration – batch AA3; 630x)

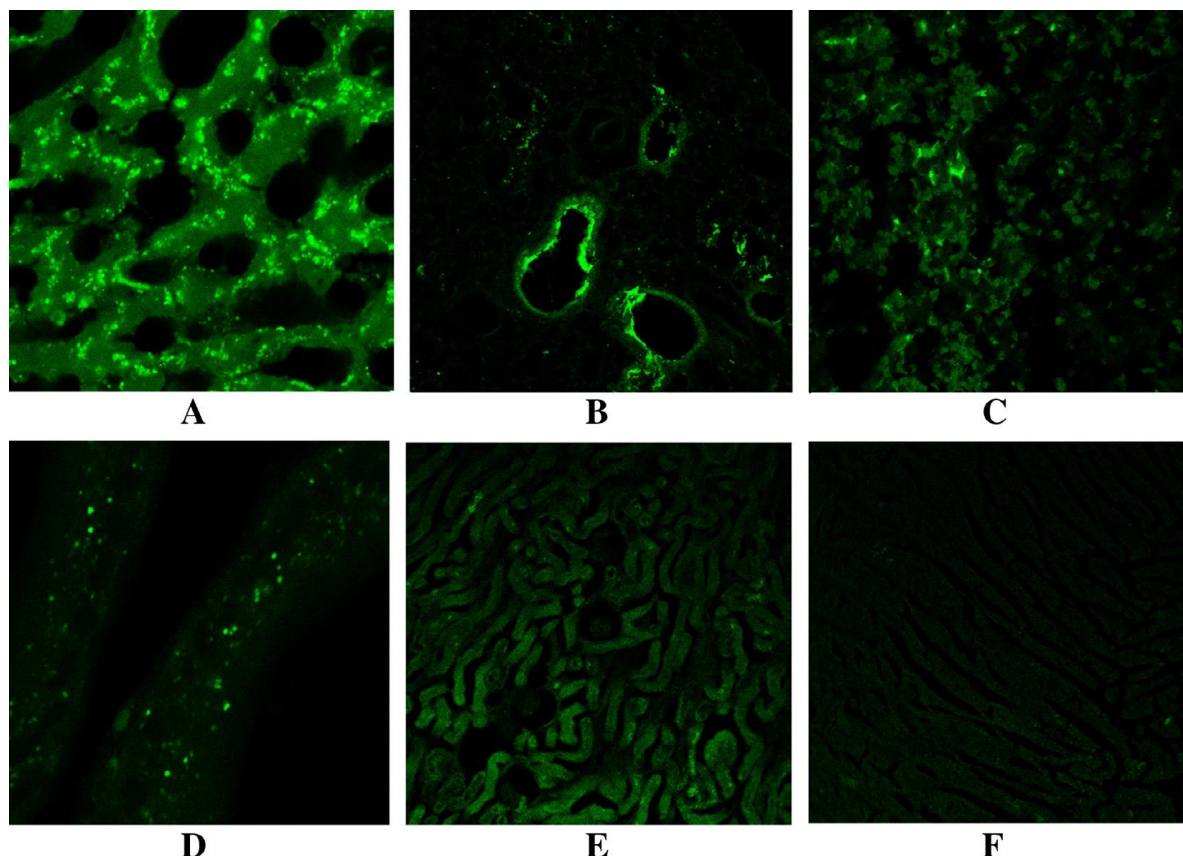


**Fig. 15.** SNPs distribution in A. Liver; B. Lung; C. Spleen; D. Testis; E. Kidney and F. heart (2 hours after oral administration – batch AA3; 630x)

#### ***Biodistribution of the radiolabelled SNPs by scintigraphy***

In our study, the fixation degree of the  $^{99m}\text{Tc}$ -SNPs in different living structures (thyroid, eyeball right and left, salivary glands right and left, heart, stomach, liver, kidney, bowel, gall bladder, urinary bladder and seminal vesicle), at different time intervals was quantitatively evaluated on the scintigraphic images, in comparison with identical dimension background area. The maximum uptake observed was considered 100% (founded to correspond to the stomach region at 4 hours for  $^{99m}\text{Tc}$ -SNPs) and all the other measured uptakes were calculated as percentages in reference to the maximum, per gram organ. Data were graphically represented, making evidence of  $^{99m}\text{Tc}$ -SNPs biodistribution. Same data were obtained on the free  $^{99m}\text{Tc}$  biodistribution images, for the control group. Figure 16 reveals, graphically, the significant difference in biodistribution between  $^{99m}\text{Tc}$  labelled nanoparticles prepared by sodium borohydride method and free  $^{99m}\text{Tc}$ . The  $^{99m}\text{Tc}$ -SNPs exhibited higher uptake in all the investigated organs (27–100% count/gram organ at 4 hours) as compared to free  $^{99m}\text{Tc}$  images (in the range of 18–88% count/gram organ at 4 hours).

In the case of free  $^{99m}\text{Tc}$  (Fig. 16A), a discreet (17–20% count/gram organ) area of fixation corresponding to thyroid was observed always (from 30 to 240 minutes). Also, a high uptake (with diffuse character on the scintigraphic images) was quantified in the upper abdominal region (63–88% count/gram organ). Fixation consistent to the bladder region was also present (16–88% count/gram organ), behavior that can be explained by the fact that the radiotracer was extensively excreted by urine.

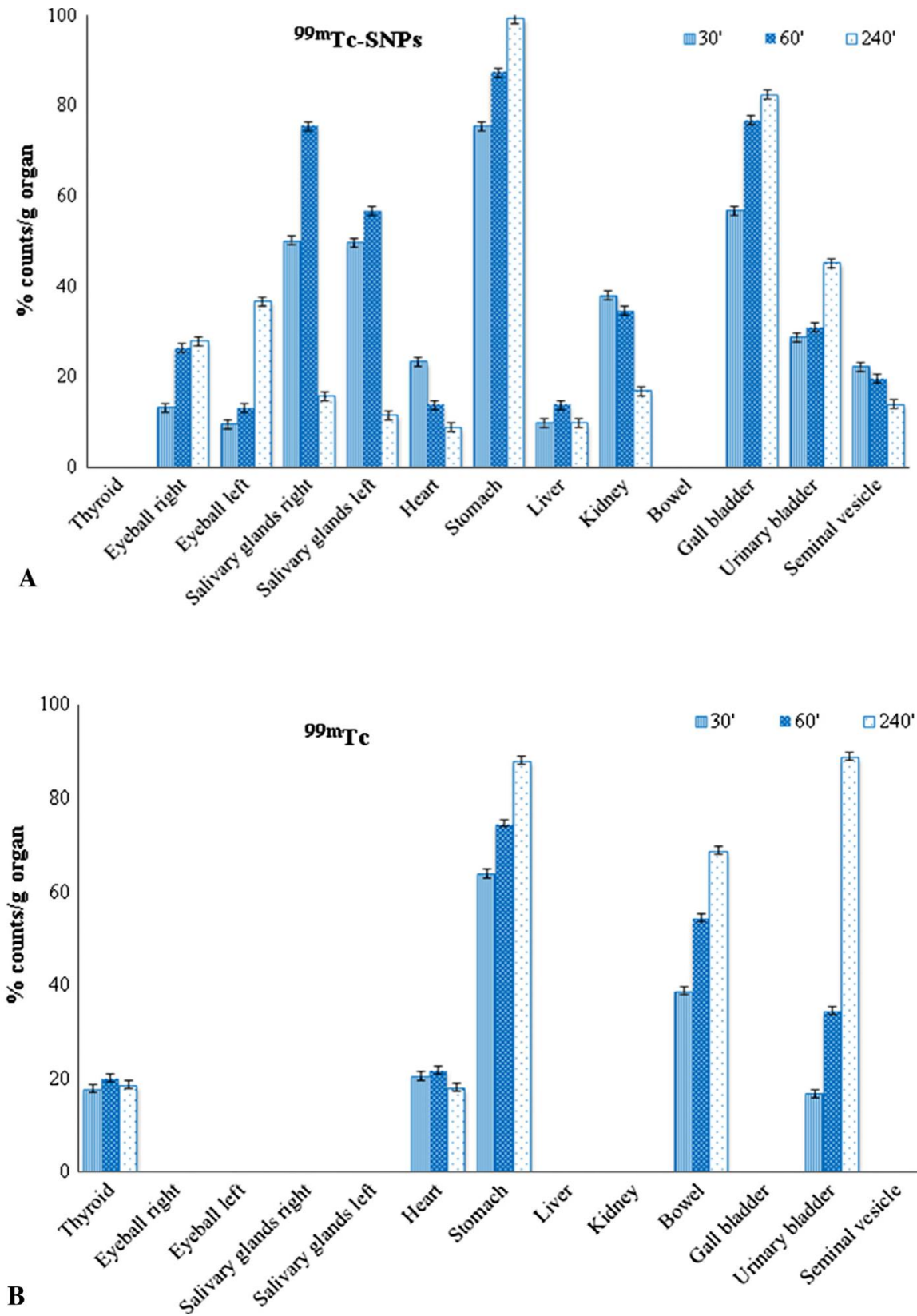


**Fig. 16. A.** Graphic biodistribution profile in different tissues at the times: 30, 60 and 240 minutes of  $^{99m}\text{Tc}$ -SNPs. Values expressed as mean  $\pm$  SD. **B.** Graphic biodistribution profile in different tissues at the times: 30, 60 and 240 minutes of  $^{99m}\text{Tc}$ . Values expressed as mean  $\pm$  SD

The obtained quantified results (fig. 16B) showed that in the case of  $^{99m}\text{Tc}$  labelled nanoparticles, after 30 minutes, reached systemic circulation and were captured mainly in the salivary glands (51% count/gram organ), stomach (75% count/gram organ), and kidney (37% count/gram organ) in addition to a significant accumulation in the bladder region (28% count/gram organ). This behavior was also observed at times of 60 and 240 minutes after injection, as it was expected, due to the nature of the injected compound.

One hour after injection, the  $^{99m}\text{Tc}$ -SNPs were accumulated in all investigated organs and animal tissues, except in the thyroid. We also found that, within 4 hours after injection, silica nanostructures undergo an increasing accumulation in the stomach (100% count/gram organ).

The scintigraphic examination has also evidenced an important percentage (13 and 9% count/gram organ for right and left eyeball, respectively, at 30 minutes) of  $^{99m}\text{Tc}$ -SNPs in the eyeballs with an increasing trend in time (27 and 36% count/gram organ for right and left eyeball, respectively, at 4 hours). After 4 hours, a low percentage of the injected dose could be observed in the liver. This conduct could be explained probably by the fact that SNPs can be metabolized in the body due to the pH-dependent dissolution process that can occurs in aqueous solutions. The fixation corresponding to the urinary bladder also decreases gradually due to the radiotracer's elimination in the urine and also biological and physical half-life of the radioisotope.

These graphical results are validated by studying the gamma scintigraphic images of guinea pigs as shown in fig. 17. The dynamic scintigraphic images showing localization of  $^{99m}\text{Tc}$ -SNPs and free  $^{99m}\text{Tc}$  in different organs, taken in the first 5 minutes (fig. 17A and B) sustained the *in vivo* biodistribution profile observed on the static images and quantified on the graphs.

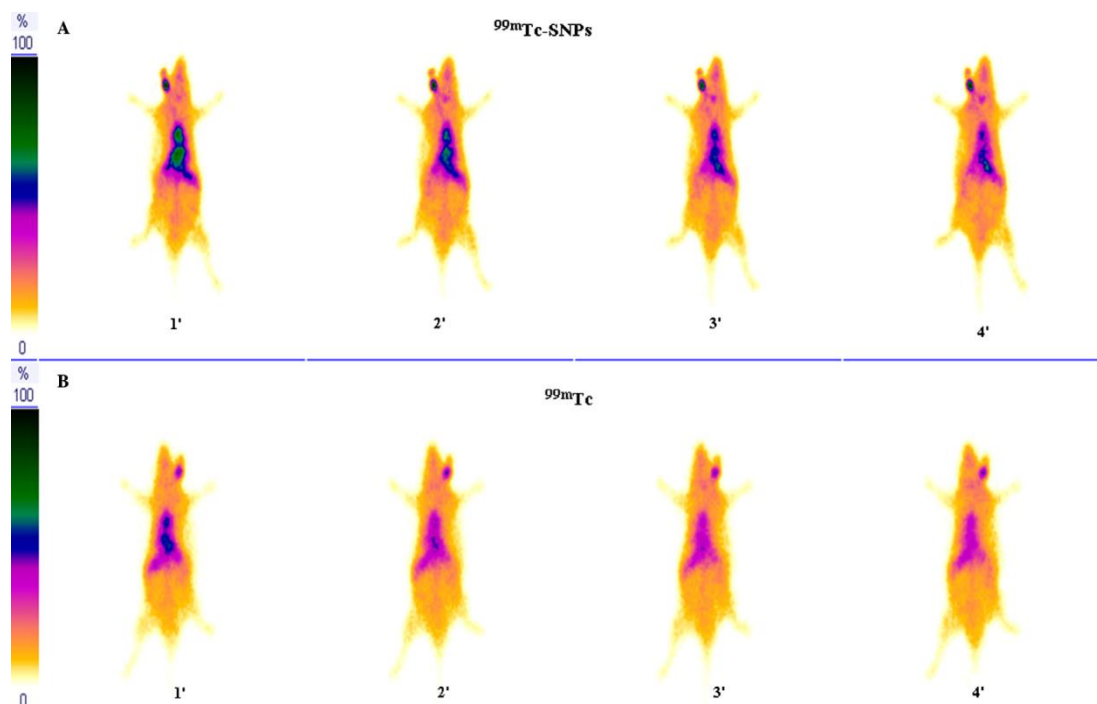


**Fig. 17.** Scintigraphic images after immediately i.v. administration of A.  $^{99m}\text{Tc}$ -SNPs and B. free ( $^{99m}\text{TcO}_4^-$ )

After 30 minutes post-tail injection (Fig. 18), the scintigraphic images showed the rapidly accumulation of  $^{99m}\text{Tc}$ -SNPs in the salivary glands, stomach, kidney and bladder region, which is in accordance with the fluorescent biodistribution study.

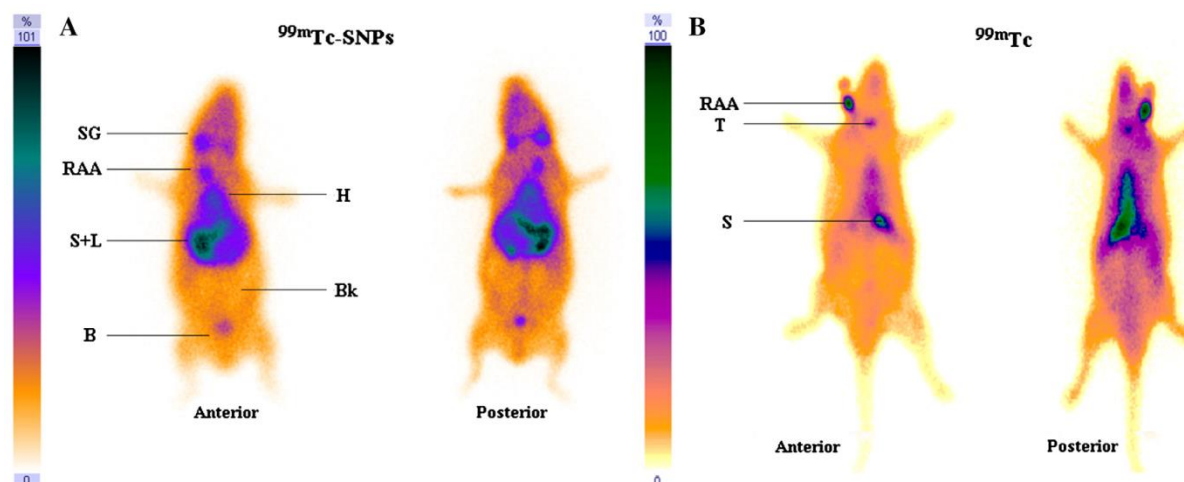


**Fig. 18.** Scintigraphic images at 30 minutes post injection of A.  $^{99m}\text{Tc}$ -SNPs and B. free ( $^{99m}\text{TcO}_4^-$ ). The values explain the image heterogeneity: SG – salivary glands; T – thyroid gland; H – heart; S + L – stomach and liver; B – bladder; RAA – radiotracer administration area; Bk – background.

The most important difference is the presence of the free  $^{99m}\text{Tc}$  fixation area corresponding to thyroid observed always (from 30 to 240 minutes), but not evidenced on the  $^{99m}\text{Tc}$ -SNPs images.

### **Carboxymethyl guar gum nanoparticles for drug delivery applications: Preparation and preliminary in-vitro investigations.**

#### ***CMGG synthesis and characterisation***

Following purification of commercial guar gum by removal of insoluble fractions as well as sugar and protein contaminants, carboxymethylation of the purified guar gum was carried out via a consecutive two-step reaction as previously reported in the literature (Dodi et al., 2011), with minor modifications (fig. 19). The carboxymethylated guar gum obtained following reaction optimization (labelled CMGG) had a degree of substitution of 0.62 %.

The formation of CMGG was confirmed by  $^1\text{H}$  and  $^{13}\text{C}$ -NMR results (Fig. 20), which were in good agreement, with other studies (Manna et al., 2015). The  $^1\text{H}$ -NMR spectrum showed new proton peaks at 3.77, 3.95 and 4.22 ppm, attributed to the methylene protons from the carboxyl group, in addition to the anomeric (4.70 and 5.03 ppm) and sugar protons (3.57 and 4.13 ppm) found in the raw GG.  $^{13}\text{C}$ -NMR spectra of CMGG confirmed the presence of a carbonyl peak at 180 ppm, while the carbon peaks of mannose and galactose appeared in the range 90–110 ppm and the rest of the side chain in the range 60–80 ppm.

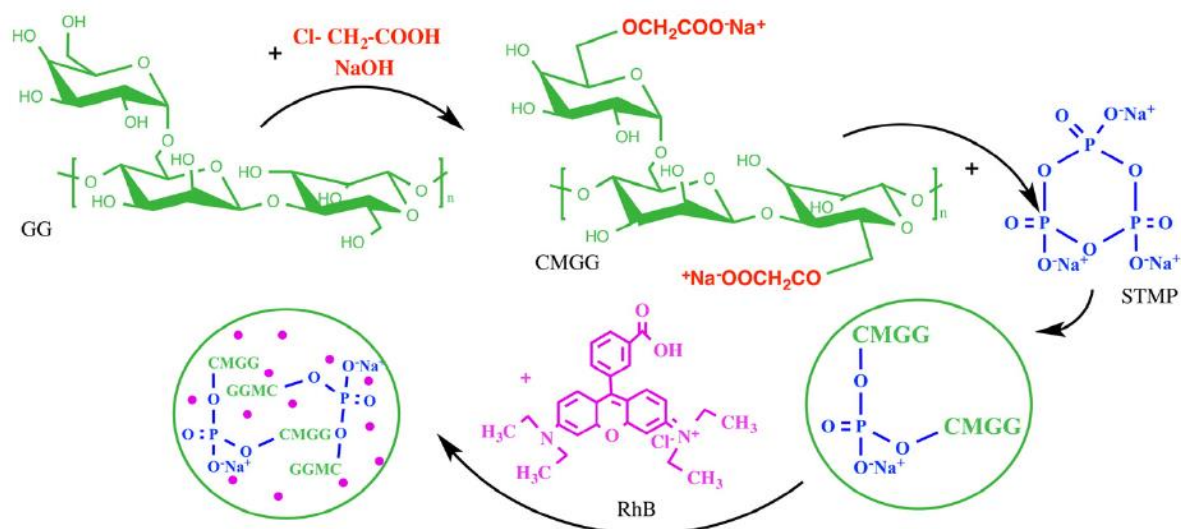


**Fig. 19.** Schematic diagram for carboxymethylation, CMGG nanoparticles formulation and RhB loading

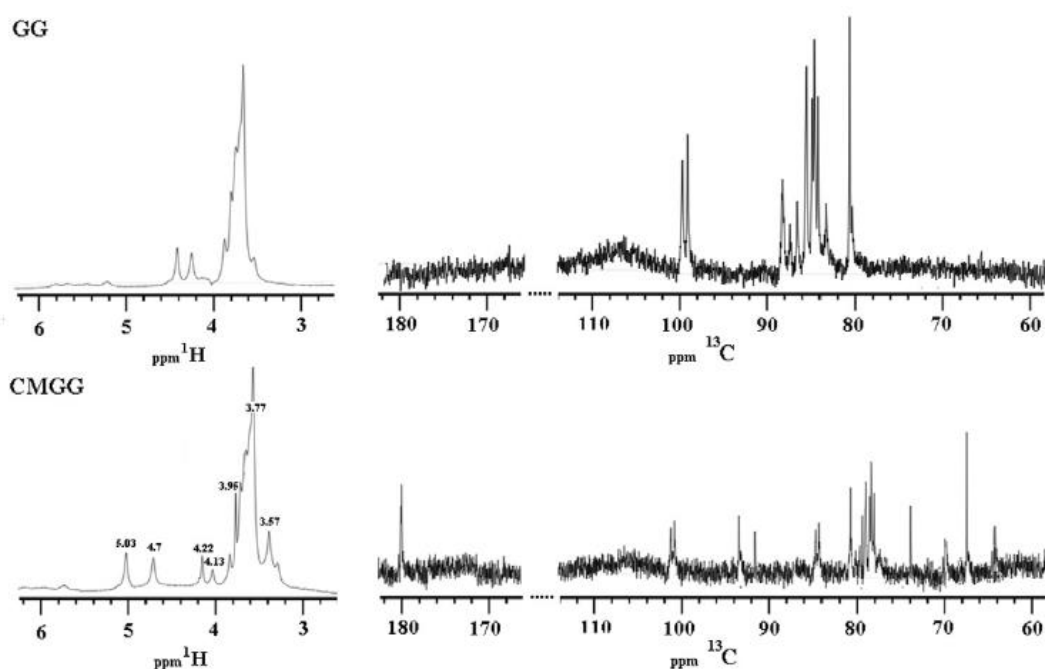


**Fig. 20.**  $^1\text{H}$  and  $^{13}\text{C}$  NMR spectra of GG and CMGG

Successful carboxymethylation was confirmed in the FTIR spectra of CMGG (Fig. 21) by the presence of additional peaks ( $1732$ ,  $1413$  and  $1230\text{ cm}^{-1}$ ) corresponding to the  $\text{COO}^-$  symmetric and asymmetric stretching vibrations; moreover, a shift of the OH stretching band ( $3354\text{ cm}^{-1}$ ) in the GG spectrum to  $3333\text{ cm}^{-1}$  in CMGG, and an increase of the band intensity (both rationalized by an increase in hydrogen bonding interaction consequent to the introduction of a carboxylic group and) were observed.

GPC measurements indicated a higher molecular weight ( $M_w$ ) for CMGG compared to GG, as a direct result of the introduction of carboxymethyl groups onto the polysaccharide backbone. The carboxymethylation step increased considerably the solubility of the modified galactomannan chains compared to GG and also led to an improved polydispersity index.

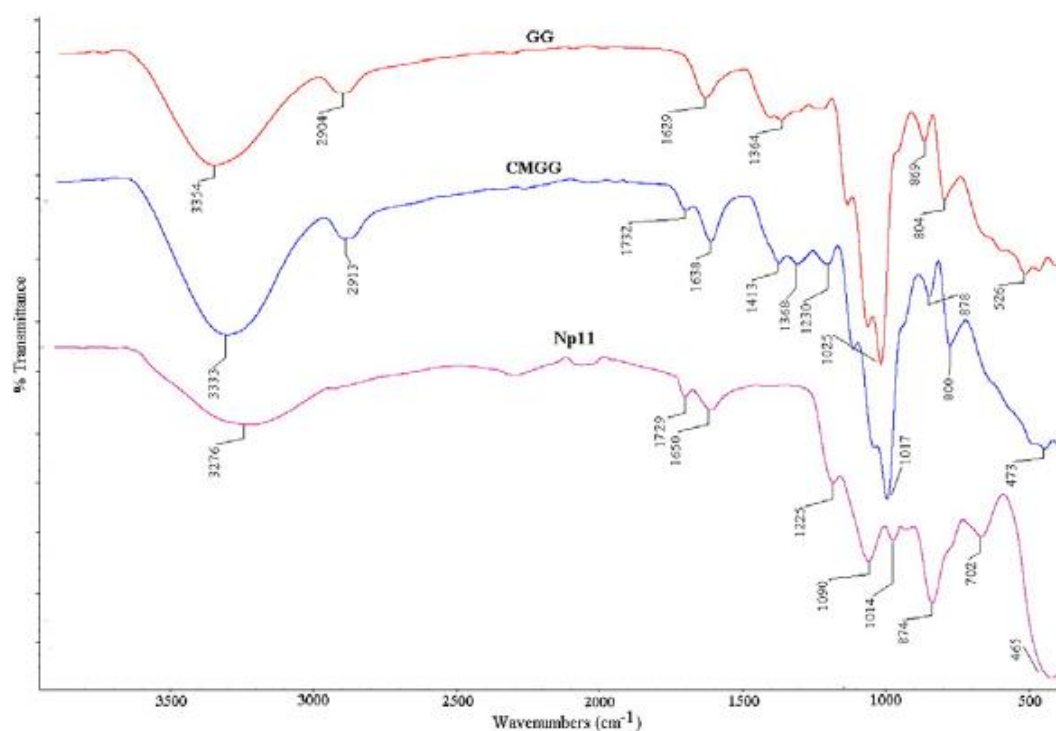


**Fig. 21.** FTIR-ATR spectra of native GG, CMGG sample and CMGG nanoparticles.

#### ***Determination of the nanoparticles optimum reaction conditions***

The synthesized carboxymethyl guar gum was successfully formulated into nanoparticles by using STMP as an ionic gelation agent (Fig. 19). Cross-linking was achieved through the formation of phosphoester linkages between the CMGG chains, in two steps: the opening of the STMP ring by CMGG in the presence of sodium hydroxide was followed by the reaction with another polymer chain and the release of sodium pyrophosphate. The reaction between the carboxylated polysaccharidic chains and STMP under basic conditions resulted overall in nanoparticulate, three-dimensional hydrogel networks. To optimize the conditions for cross-linking in an attempt to yield stable nanoformulations with uniform size distribution, a series of CMGG particles (batches 1–11) were prepared from CMGG by varying the concentration of CMCG and SMTP, as presented in table IX. The crosslinker/polysaccharide ratios were calculated according to the assumption that each mole of STMP reacts with three pairs of hydroxy groups (Gliko-Kabir et al., 2000).

It was found that a larger particle size was obtained as the concentration of both polymer (CMGG) and cross-linker (SMTP) increased. When the concentration of both components was low (e.g. CMGG -0.05% and SMTP 5%), the mean diameter of the nanoparticles was about  $208.8 \pm 0.87$  nm; this could perhaps be attributed to a lower number of macromolecules being linked together as part of the same particle and to better packing (due to stronger inter and intra molecular interactions allowed by the higher flexibility of the lightly cross-linked polymer chains). The PDI values indicate a broad size distribution (Table IX). The negative  $\zeta$ -potential measured for all nanoparticles (expected due to the presence of CMGG terminal carboxylic groups in combination with phosphate groups) contribute to the particle good stability (without any aggregation) observed during storage at room temperature.

According to Akasov et al. (2015) the high negative surface charge of the polysaccharide formulations is a key factor to stabilize colloidal dispersions. Following the optimisation step, the batch labelled Np11 (Table IX) was selected for further investigations.

**Table IX.** Characteristics of different nanoparticle formulations prepared

Batch	CMGG conc., %	STMP conc. %	Size $\pm$ SD nm	$\zeta$ -Potential $\pm$ SD, mV	PDI
<b>Np1</b>	0.1	10	780 $\pm$ 1.4	- 72.6 $\pm$ 1.8	0.5
<b>Np2</b>	0.1	5	460 $\pm$ 1.3	-39.1 $\pm$ 9.5	0.4
<b>Np3</b>	0.1	2.5	360 $\pm$ 16.2	-50.6 $\pm$ 6.3	0.34
<b>Np4</b>	0.2	5	540 $\pm$ 6.6	-39.9 $\pm$ 2.5	0.3
<b>Np5</b>	0.2	2.5	594 $\pm$ 11.5	-37.5 $\pm$ 11.9	0.3
<b>Np6</b>	0.1	1	417.8 $\pm$ 1.9	-27.3 $\pm$ 9.5	0.2
<b>Np7</b>	0.1	0.5	537.4 $\pm$ 8.9	-25.3 $\pm$ 4.3	0.3
<b>Np8</b>	0.1	0.25	450.6 $\pm$ 12.4	-22.5 $\pm$ 8.5	0.31
<b>Np9</b>	0.1	0.2	387.7 $\pm$ 0.6	-29.3 $\pm$ 2.1	0.25
<b>Np10</b>	0.2	0.2	593.4 $\pm$ 1.3	-33.2 $\pm$ 1.4	0.12
<b>Np11</b>	0.05	0.2	208.8 $\pm$ 0.9	39.3 $\pm$ 1.1	0.11

FTIR measurements of the CMGG nanoparticles (batch Np11) showed the appearance of a shoulder of low intensity at 1225  $\text{cm}^{-1}$  that corresponds to P=O stretching (Shalviri et al., 2010), and a shoulder of increased intensity at 1090  $\text{cm}^{-1}$  that was attributed to P–O–C deformation vibrations (Braz et al., 2007). The increased intensity in the 874-1225  $\text{cm}^{-1}$  region is considered therefore a clear indication of the presence of phosphate groups in the prepared nanoparticles.

Figure 22 presents the thermogram (1st derivative) of STMP cross-linked nanoparticles overlaid with those of the guar gum and carboxymethylated guar gum. The results of the thermogravimetric analysis indicate the presence of stronger hydrogen bonding following carboxymethylation of the guar gum, possibly due to an increase in free water content (from 8.54 % in GG to 10.69 % in CMGG, table X).

**Table X.** Thermogravimetric analysis

Sample	Step	T <sub>peak</sub> , °C	Weight loss, %	Residue %
GG	I	51.13	8.54	21.73
	II	262.07	69.73	
CMGG	I	51.04	10.70	23.17
	II	241.98	56.57	
	III	478.51	9.56	
Np11	I	70.05	2.34	26.13
	II	492.91	71.53	

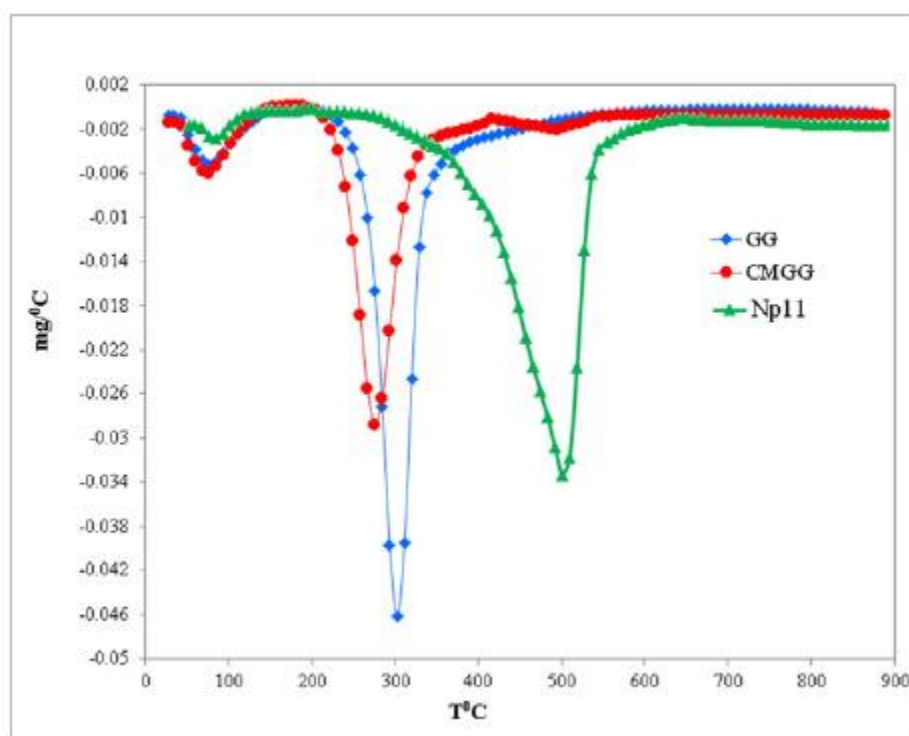


**Fig. 22.** TG curves (1st derivative) of native GG, CMGG sample and CMGG nanoparticle

The thermal stability of CMGG (reflected in the temperature of the peak in the first derivative spectra, corresponding to the main degradation step) appears slightly lower (241°C; 57 % mass loss) than for GG (262 °C; 70 % mass loss), while a second degradation step appears at considerable higher temperatures (478°C; 9.56 % mass loss) due to the carboxymethyl groups that make possible increased inter- and intra-molecular interactions that ultimately impart higher thermal stability (Tripathy et al., 2008). It was interesting however to observe that the nanoparticles (CMGG cross-linked with SMTP) had the major mass loss step at a much higher decomposition temperature than the native guar and CMGG, likely due to the fact that the cross-linking reaction increases the average molecular mass and the intermolecular interactions, which in turn increase considerably the thermal stability of the nanoparticles.

To complement the results of DLS analysis, NTA studies investigated in more detail the particle size distribution of samples in liquid suspension (Fig. 23). The average particle size results were in good agreement with both DLS and SEM data.

The results of SEM analysis confirmed the almost spherical surface morphology of the synthesized CMGG nanoparticles (Fig 24). When in dry state, nanoparticles tend to self-assemble into secondary clusters with grape-like morphology, as a result of the Van der Waals and other inter-particle forces closely correlated with the very high surface area to volume ratio.

### ***In-vitro investigations***

The results of dose-response cytotoxicity tests carried out on NHDF cells using MTS after 24 h incubation with CMGG nanoparticles demonstrated no significant toxic effect at concentrations up to 0.3 mg/mL (Fig. 25). Cell viability was found to decrease substantially

with an increase in nanoparticle concentration up to 25 mg/mL, with a calculated IC50 value of 4.715 mg/mL.

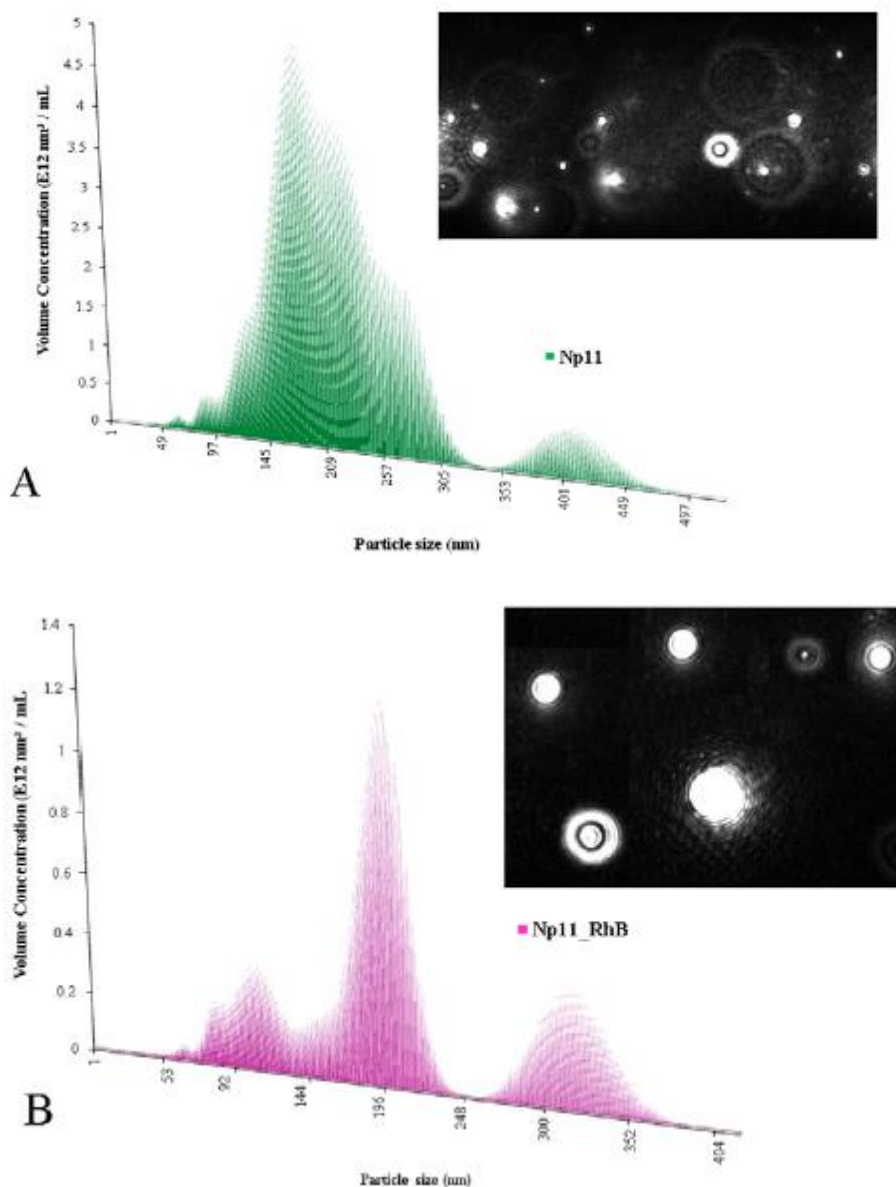


**Fig. 23.** NTA images of typical tracks of particles moving under Brownian and a smoothed 3D plot of size distribution vs. particle concentration for A. CMGG nanoparticles (batch NP11) and B. loaded particles analysed under fluorescent (optically filtered) mode vs. particle concentration (batch Np11\_RhB).

NHDF cell proliferation, distribution and adhesion of the cells following incubation with CMGG nanoparticles were examined at different time points (24 h and 48 h, respectively) and different nanoparticle concentration (1.56 mg/mL and 3.125 mg/mL), fig 26. Even after 48 h, the NHDF cells incubated with nanoparticles at a concentration of 1.56 mg/mL show a good distribution and cover almost the entire substrate, suggesting reasonably good compatibility with the nanoparticles. However, cell proliferation appears to start being affected after 48 h in contact with nanoparticles at concentration reaching 3 mg/mL.

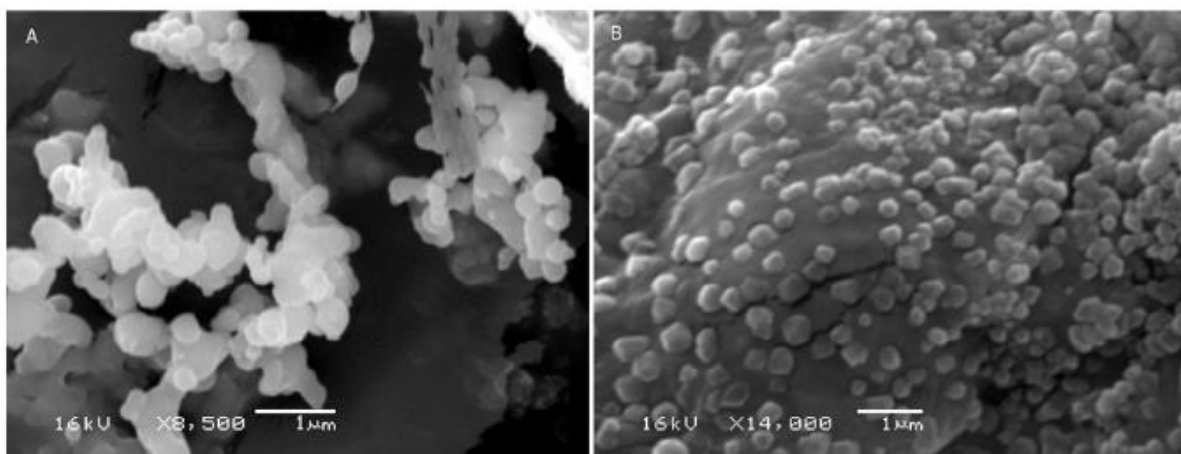


**Fig. 24.** Morphology of A. CMGG nanoparticles (batch Np11) and B. loaded nanoparticles (batch Np11\_RhB)

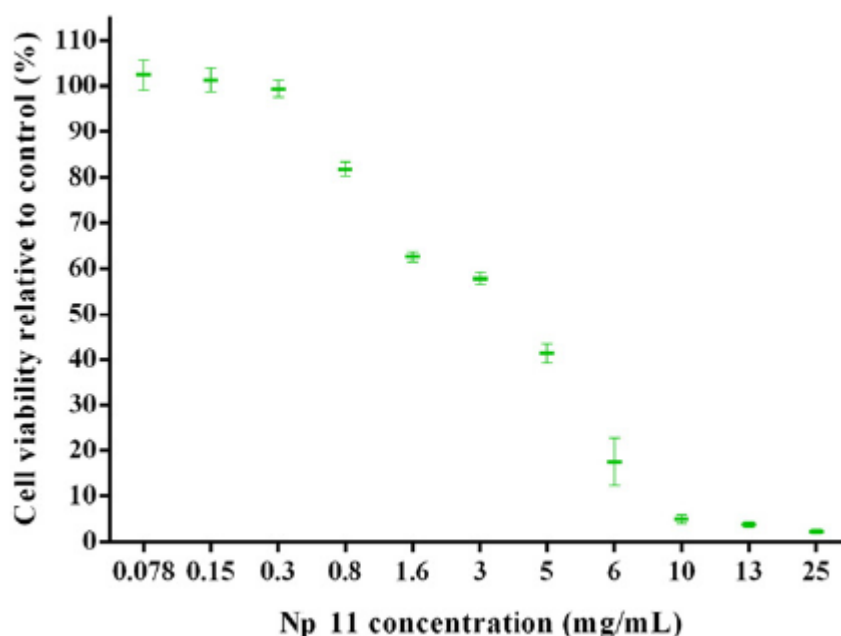


**Fig. 25.** Cellular viability MTS assay on NHDF cells of CMGG nanoparticles

### ***RhB entrapment efficiency and drug release studies***

The lack of toxicity at low concentrations (0.3 mg/mL or less) makes CMGG nanoparticles a good candidate to be considered for drug delivery applications. A hydrophilic fluorescent marker, RhB was chosen as model drug for its lack of toxicity at easily detectable concentrations, strong absorption and emission spectra, and good stability to pH variations (Fig. 19). RhB was successfully entrapped into nanoparticles with high efficiency (of 83.2 %, for batch Np11\_RhB). To optimize the effect of drug concentration on the entrapment efficiency, different concentrations of RhB were tested in the range of 0.25 to 5 mg/mL (Table XI). It was found that high RhB concentrations led to low entrapment efficiency (ranging overall between 33.5 % and 83.2 %), with an optimum found at 0.5 mg/mL RhB.

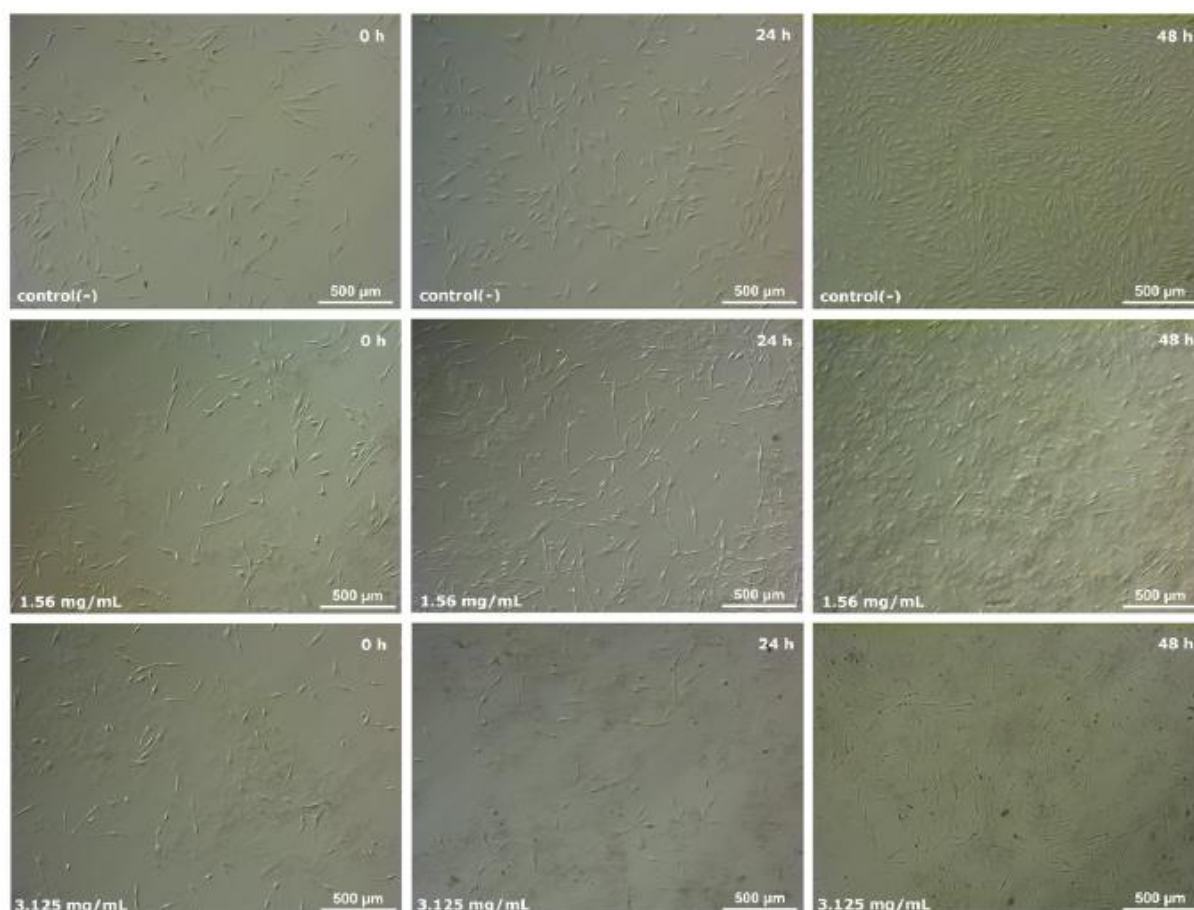


**Fig. 26.** NHDF cell distribution, adhesion and morphology following incubation of CMGG nanoparticles using optical microscopy image

**Table XI.** Entrapment efficiency, size distribution,  $\zeta$ -potential and PDI for RhB loaded CMGG particles (batch NP11)

NP11, mg	RhB, mg/mL	$E_e$ , %	Size $\pm$ SD nm	$\zeta$ -Potential $\pm$ SD mV	PDI
100	5	$33.5 \pm 0.6$	$259.5 \pm 0.49$	$-4.8 \pm 0.5$	0.2
100	1	$57.5 \pm 0.2$	$274.3 \pm 0.74$	$-4.57 \pm 0.27$	0.15
100	0.5	$83.2 \pm 0.6$	$318.4 \pm 0.8$	$-13.4 \pm 0.57$	0.14
100	0.25	$61.4 \pm 0.4$	$321 \pm 1.22$	$-9.54 \pm 1.37$	0.08

A substantial change in size distribution, zeta potential and polydispersity index was observed for the drug loaded nanoparticles compared to the unloaded ones. As expected, the drug loaded nanoparticles had a larger mean diameter and lower negative  $\zeta$ -potential (in absolute values) following the entrapment of RhB, with the colloidal stability not being noticeably affected. The RhB loaded nanoparticles were also analysed using NTA in fluorescence mode (Fig. 24B); while noticeable photo bleaching limited the sensitivity of the measurement, the results confirmed the presence of RhB within the nanoparticles and an increase in the mean diameter compared to unloaded nanoparticles, and were consistent with the of DLS results.

SEM investigations confirmed the size as well increase following loading with RhB, with images showing discrete and near spherical (slightly elongated) nanoparticles, well

separated from one another (Fig. 23B) and with low polydispersity (confirming again DLS results, where measured was 0.08).

Drug release behaviour was investigated in simulated gastric (pH 2.2) and intestinal (pH 7.4) fluids at 37°C as suggested in the literature (Li and Liu, 2008; Chaurasia et al. (2006) and Subrahmanyam (2012)). Figure 27 presents the release profiles for the Np11\_RhB batch.

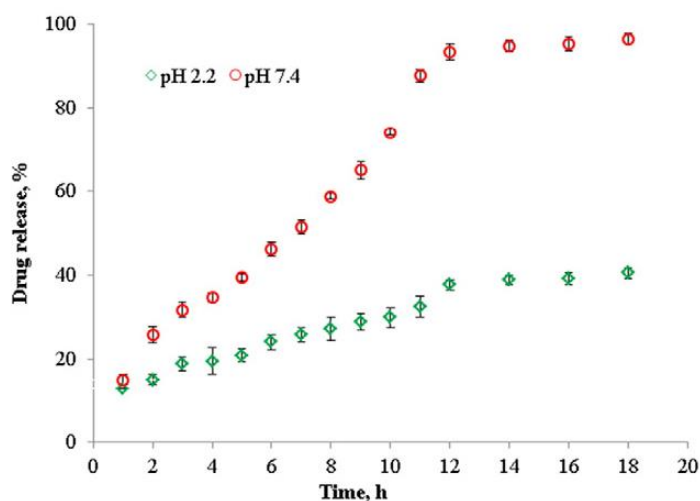


**Fig. 27.** RhB release profiles in simulated gastric and intestinal fluids

A burst release of 13% was observed for both pH values just after the addition of loaded nanoparticles, likely due to a fraction of RhB present on the surface of the nanoparticles being immediately released in contact with the simulated fluids. The RhB released in acidic medium over the total duration of the experiment reached only 37.1 % while in alkaline conditions the model drug was released almost completely (92.7 %), indicating that the release of RhB from the CMGG nanoparticles can be controlled by pH.

To investigate the mechanism of the RhB release, the initial release data was fitted in the Ritger and Peppas equation (Popa et al., 2010; Ritger & Peppas, 1987):

$$\frac{M_t}{M_\infty} = kt^n,$$

where  $M_t/M_\infty$  is the mass ratio of the drug released from nanoparticles at time point  $t$  compared to equilibrium;  $k$  is a characteristic constant related to the structure of the polymeric network; and  $n$  is a diffusion exponent. Constants  $k$  and  $n$  were calculated from the slopes and intercepts of the graph  $\ln M_t/M_\infty$  vs  $\ln t$ . The  $k$  and  $n$  constants are related to a specific transport mechanism, which normally consider the relative rates of drug diffusion, matrix swelling and polymeric network relaxation. Three main models are typically employed to describe the behaviour of the swelling polymeric network that releases the drug in aqueous solutions: Fickian diffusion ( $n = 0.5$ ); non-Fickian, anomalous diffusion ( $0.5 < n < 1$ ); and zero order release ( $n = 1.0$ ) (Mullarney et al., 2006). The values obtained at ( $n = 0.5$ ) suggests an anomalous diffusion mechanism close to the Fickian model for acidic conditions (pH 2.2) and a non-Fickian diffusion release process ( $n = 0.83$ ) in an alkaline environment (pH 7.4).

### 1.2.2.3 *Discussions*

#### **Silica nanoparticles: Preparation, characterization and in vitro/in vivo biodistribution studies.**

In the present investigation, spherical bare, amino functionalized Cy.5.5 fluorescent and  $^{99m}\text{Tc}$  radiolabelled SNPs were successfully synthesised by the hydrolysis reaction of TEOS in ethanol containing water and ammonia. Particle sizes in the range of 200–350 nm, as determined by field emission SEM analysis, as well as the physico-chemical properties made the obtained SNPs potential candidates for in vivo studies. Using confocal microscopy technique, we demonstrated the high uptake of fluorescent SNPs in all the investigated organs (liver, kidney, testis, spleen and lung) for both oral and intravenous administration.

#### ***Toxicity evaluation***

In our study, the MTD was several times higher than the doses administered in the bioavailability studies, profiling a good safety profile for future therapeutic associations of the SNPs with drugs. Nanoparticle toxicity has been shown to occur in a concentration-dependent manner (Lewinski et al., 2008). The determination of the appropriate dose of SNPs to use in a cytotoxicity assay is a key element to understand the toxic effects of the nanoparticles under true physiological conditions (Ansari et al., 2019; Kong et al., 2011). Although, amorphous SNPs are commonly used as an FDA-approved food additive (Barnes et al., 2008) there are still numerous cytotoxicity studies raising concern about their toxic effects for human health: over exposure to amorphous SNPs has been shown to cause cytotoxic damage (as indicated by lactate dehydrogenase release) and a decrease in endothelial cell survival (Napierska et al., 2009).

According to the data obtained by Napierska et al. (2009), the toxicity of the SNP is size dependent, the smaller particles (diameters less than 15 nm), appear to affect the exposed cells faster with cell death, compared with larger ones (diameters of 104 and 335 nm) that showed low toxicity response. Also, the toxic effects depend on the nanoparticle's shape, charge and density, as well as the viscosity and density of the solution, properties that influence the effective dose. As a result, defining the appropriate dose for *in vitro/in vivo* study is still a challenging task.

#### ***Biodistribution of the radiolabelled SNPs by scintigraphy***

Although there are some studies in the literature about the qualitative *in vivo* distribution of SNPs, quantitative distribution data are still lacking. In our study, the fixation degree of the  $^{99m}\text{Tc}$ -SNPs in different living structures (thyroid, eyeball right and left, salivary glands right and left, heart, stomach, liver, kidney, bowel, gall bladder, urinary bladder and seminal vesicle), at different time intervals was quantitatively evaluated on the scintigraphic images, in comparison with identical dimension background area.

After 30 minutes post-tail injection, the scintigraphic images showed the rapid accumulation of  $^{99m}\text{Tc}$ -SNPs in the salivary glands, stomach, kidney and bladder region, which is in accordance with the fluorescent biodistribution study. These results are consistent with data published in the last years (Saroi et al., 2019; Pandey et al., 2014; Simone et al., 2012; Xie et al., 2010) in a previous studies performed on radiolabelled nanoparticles.

The most important difference is the presence of the free  $^{99m}\text{Tc}$  fixation area corresponding to thyroid observed always (from 30 to 240 minutes), but not evidenced on the  $^{99m}\text{Tc}$ -SNPs images. These images can be explained by the known cellular uptake mechanism of the free  $^{99m}\text{Tc}$ : the radioisotope is taken up via sodium iodide symporter system (NIS), a transmembrane transport system that was found to mediate the transport and cellular accumulation of both iodine and  $^{99m}\text{Tc}$  to some tissues including mainly the thyroid, but also stomach, salivary glands, and to some extent the small intestine (Kiratli et al., 2009; Mu et al., 2012). Our SNP carrying amino groups on their surface are also electrically charged. Due to their small size and ionic charge, it is very likely that a passive transport is involved, according to the electrochemical gradient.

In fact, the lack of the thyroid scintigraphic uptake for the SNP sustains the hypothesis of different transmembrane transport mechanisms for the radiotracer. The  $^{99m}\text{Tc}$ -SNPs rapidly appear in the tissues, faster when compared to the  $^{99m}\text{Tc}$ . This could be explained in relation their smaller size which gives them the possibility to a faster transmembrane passage. However, more detailed studies regarding the bioaccumulation of SNPs in the liver, spleen, intestines, kidneys, and bladder is warranted to better clarify the adverse effects arising from such an accumulation.

Considering the results obtained in our study, the SNPs showed *in vivo* similar biodistribution behavior to that demonstrated by other groups on nanostructured systems as silica nanoparticles (obtained by the same method) or chitosan nanoparticle, when the radioactivity was determined by scintigraphy (Banerjee et al., 2005; Xie et al., 2010). Sakai et al. (2012) analyzed the whole-body distribution of  $^{14}\text{C}$ -ADP-labeled silica nanoparticles after intravenous injection into mice and the obtained radioactivity results showed also similar distribution patterns when determined by liquid scintillation counter.

Identifying the specific biodistribution areas (compared with free  $^{99m}\text{Tc}$ ) could be the start point for the use of this nanostructure system as vector molecule for a certain radioisotope, to be used for diagnosis in nuclear medicine imaging (using a classical gamma emitter radioisotope, such as  $^{99m}\text{Tc}$ ) and, respectively, therapy (using a suitable corpuscular emitter radioisotope such as  $^{131}\text{I}$ ) purposes.

### **Carboxymethyl guar gum nanoparticles for drug delivery applications: Preparation and preliminary in-vitro investigations**

Guar gum - a biocompatible, biodegradable, low cost, accessible and versatile polysaccharide of natural origin can be easily converted into carboxymethyl guar gum, which was successfully formulated into nanoparticles by ionic cross-linking complexation with a non-toxic and inexpensive cross-linking agent, trisodium trimetaphosphate. The reaction conditions were optimized through careful investigation of the effects of polymer and cross-linker concentration upon particle size distribution,  $\zeta$ -potential and polydispersity. Following optimization, DLS results revealed a relatively uniform size distribution of CMGG nanoparticles around 208 nm, also confirmed by NTA and SEM analysis.

The results of dose-response cytotoxicity tests carried out on NHDF cells using MTS after 24 h incubation with CMGG nanoparticles demonstrated no significant toxic effect at concentrations up to 0.3 mg/mL. While not application-specific, NHDF cell lines represent a suitable and convenient model for preliminary cytotoxicity assessment. The growth behaviour

of the cells in the presence of CMGG nanoparticles was monitored using optical microscopy, using NHDF cell adhesion as an indicator of viability since the cells detach during apoptosis (furthermore, cell spread can also give an indication of the nature of interactions with nanoparticles present in the media, as an adherent cell which has increased its spreading area is considered to show active proliferation (Rosman et al., 2014).

We attribute the excellent biocompatibility of the samples to the sugars of the polymer backbone, sugars which are suitable for the cell growing. Also, the higher cell compatibility of CMGG nanoparticles could be related to surface charge (Akasov et al., 2015), explained by their ability to interact with the positively charged fibroblast surface. These data indicate that surface modification can be modulated in order to design drug delivery systems with more predictable clinical outcomes.

To investigate the potential of CMGG nanoparticles for drug delivery applications, RhB was employed as a model drug and it was found that the drug initial concentration significantly influenced the entrapment efficiency, which ranged from 33.5 % to 83.2 %. Release studies at 37°C in simulated gastric and intestinal fluids indicated a slow and prolonged release of RhB from CMGG nanoparticles over several hours, and demonstrated that the release process can be controlled by pH.

#### 1.2.2.4 *Conclusions*

The results of radiolabelled biodistribution indicated that  $^{99m}\text{Tc}$ -SNPs accumulated mainly in salivary glands, stomach, kidney and bladder region and retained in these tissues for over 240 minutes. Collectively, the obtained radiolabelled SNPs exhibited high labelling efficiency and stability along with their biodistribution.

Similarly, the results obtained for carboxymethyl guar gum nanoparticles demonstrate the potential of nanoparticles formulated from CMGG via ionic gelation with trisodium trimetaphosphate for the development of sustained and controlled drug delivery systems.

### 1.2.3 **Investigating nanoparticles in the field of pain research**

**Study 1 - In vitro and in vivo behavior of Ketoprofen intercalated into layered double hydroxides.** In this study, we evaluated in vitro and in vivo behavior of Ketoprofen (Ket) intercalated into layered double hydroxides by ion-exchange method using two matrices (MgAILDH and ZnAILDH) under various experimental conditions.

**Study 2 - Antinociceptive effect of morphiceptin loaded poly(butylcyanoacrylate) nanoparticles.** The objective of this study was to determine if a known colloidal carrier, i.e., the poly (butyl cyanoacrylate) nanoparticulate system PBCA-NPs/PS-80, enables the brain delivery of morphiceptin, following systemic administration.

**Study 3 - Local silver nanoparticles administration promotes inflammation and hyperalgesia in rats.** The aim of this study was to assess the potential deleterious effect of local nanosilver administration in an animal model..

### 1.2.3.1 *Material and methods*

#### *Animals*

Animal care was in accordance with the Guide for the Care and Use of Laboratory Animals published by NIH and with the Policies on the Use of Animals and Humans in Research published by the Society for Neuroscience. The International Association for the Study of Pain (IASP) guidelines for the investigation of pain in animals were followed. The design of the experiments was approved by the University of Medicine and Pharmacy Gr. T. Popa ethics committee. All animals were euthanized at the end of the experiment in accordance with the AVMA Euthanasia.

For these studies, the following animals were used:

- Adult Wistar male rats (180-200 g) purchased from the National Institute of Research and Development Victor Babeş, Bucharest. (study 3)
- Adult male Swiss mice with an average weight of  $20 \pm 2$  g (study 1, 2)

The animals were housed individually at  $21 \pm 2^\circ\text{C}$  under a 12-hours light/ dark cycle with ad libitum access to food and water. About 24 hours prior to the beginning of the experiment, each animal was accommodated for 15 minutes to the testing room. In the Ketoprofen study, conducted on Swiss mice, access to food was stopped 16 hours before receiving the drug sample.

#### *Analgesic in vivo tests*

##### *Hot Plate test*

For the hot-plate latency test, a rectangular metal surface was heated to a temperature of  $55 \pm 0.5^\circ\text{C}$ . The antinociceptive response was monitored from the time the mouse was placed on the heated surface until the first overt behavioral sign of nociception (paw withdrawal latency) occurred, such as (i) the mouse licking a hind paw, (ii) the mouse shaking a hind paw, (iii) an escape response. Upon the occurrence of any of these signs, the timer was stopped by a foot-operated pedal and the mouse was immediately removed from the plate. Maximum latency (cut-off time) was set at 60 s to prevent tissue damage to the back paws.

##### *Plantar Test*

The Plantar Test (Hargreaves method) (Alexa et al., 2015) assesses the animal's response latency to a thermal stimulus. The rats are placed into clear acrylic boxes on a Plexiglas floor and a radiant heat source from the Hargreaves unit (Plantar Test-37370 Ugo Basile) is placed under the hind paw. The time until the animal withdraws or moves its paw (thermal paw withdrawal latency - PWL) is automatically recorded due to a chronometer controlled by an infrared sensor connected to the system. Cut-off is set at 30 seconds.

##### *Randall-Selito Method*

The Analgesy-Meter (7200; Ugo Basile, Italy) assesses the animal's response to increasing paw pressure. The force applied progressively increases by 16 g/s; the animal's paw is placed on a small plinth under a cone-shaped pusher with a rounded tip. When the pressure becomes painful for the animal, it withdraws its paw and the time elapsed until that moment is recorded - mechanic PWL (Jeong et al., 2012). Cutoff is set at 250 g (16 s).

##### *Assessing Inflammation*

Colloidal silver's effect on inflammation was assessed with the aid of the Ugo Basile Plethysmometer 7140(©Ugo Basile, Italy). The device is a volume meter that consists of a

water filled cell into which the rat paw is dipped and a transducer that records differences in water level caused by volume displacement (Singh et al., 2005).

#### *Statistical analysis*

Statistical analysis and graphic design was performed with the aid of GraphPad 3.0 software (GraphPad Software, La Jolla, CA). Descriptive statistics and analysis of variance (Mixed ANOVA with Tukey post-hoc test) were performed. Differences between treatment groups were analyzed using ANOVA one-way method for comparison at each time point, followed by Bonferroni post-hoc tests. The experiments were replicated three independent times and the data are presented as  $\pm$ SD (standard deviation). Differences were considered statistically significant when p-value was less than 0.05.

### **In vitro and in vivo behavior of Ketoprofen intercalated into layered double hydroxides.**

#### *Drugs*

All chemicals including  $\text{Zn}(\text{NO}_3)_2 \times 6\text{H}_2\text{O}$ ,  $\text{Al}(\text{NO}_3)_3 \times 9\text{H}_2\text{O}$ ,  $\text{Mg}(\text{NO}_3)_2 \times 6\text{H}_2\text{O}$ , and Ket were reagent grade ([98% purity), purchased from Sigma-Aldrich and were used without further purification. De-ionised water was used for the preparation of aqueous solutions.

#### *Synthesis of precursor hydrotalcites*

The precursor ZnAILDH and MgAILDH were prepared by a pH controlled co-precipitation technique of the corresponding metal nitrate salts at room temperature. In the case of ZnAILDH, a solution containing 0.2 mol of  $\text{Zn}(\text{NO}_3)_2 \times 6\text{H}_2\text{O}$  and 0.1 mol of  $\text{Al}(\text{NO}_3)_3 \times 9\text{H}_2\text{O}$  in 300 ml of distilled water was added drop wise together with 1 M NaOH solution, under vigorous stirring. For MgAILDH preparation, an aqueous solution containing 0.24 mol of  $\text{Mg}(\text{NO}_3)_2 \times 6\text{H}_2\text{O}$  and 0.12 mol of  $\text{Al}(\text{NO}_3)_3 \times 9\text{H}_2\text{O}$  was added drop wise together with 1 M NaOH aqueous solution, under vigorous stirring.

In both processes the solution flow rates are automatically adjusted in order to maintain a constant pH of 8.5 for ZnAILDH and respectively 9.5 for MgAILDH using a TitrLab TIM 854 apparatus. The suspensions were heated for 12 hours at 65°C with vigorous stirring, then the solid precipitate was collected by filtration and washed 3–5 times with 25 ml aliquots of deionized water. The removal of leftover salt in the washing step was verified by conductometric analysis of the supernatant. The material was then dried at 65°C in vacuum.

#### *Preparation of Ket intercalated hydrotalcites*

ZnAILDH\_Ket and MgAILDH\_Ket were prepared using the anionic exchange method. Typically, 1g ZnAILDH or MgAILDH was dispersed in 150 ml H<sub>2</sub>O and placed in a three-neck round bottom flask and degassed with nitrogen for 20 minutes. 1 M NaOH solution was then added until pH reached 8.5 for ZnAILDH and respectively 9.5 for MgAILDH. 150 ml hydro-alcoholic solution (50/50 v/v) containing 1.25 g dissolved Ket was then added to the previous mixture and stirred vigorously at 60°C for 16 hours under nitrogen blanket in order to avoid atmospheric carbonate contamination. The solids were washed 3 to 5 times with 25 ml aliquots of distilled water. The completeness of the washing step was verified by the absence of free Ket in the spectrophotometric analysis. The resulting solids were vacuum-dried and used for subsequent investigation.

### *Determination of intercalated Ket content*

Two methods were used for estimating Ket content of the composite samples: elemental analysis and spectrophotometric technique. For elemental analysis two methods were used: Pregl and Kjeldhal. In the spectrophotometric analysis, a known amount of LDHs\_Ket was dissolved 6 M HCl and diluted successively with phosphate buffer pH 7.2. The absorbance was measured at  $\lambda = 255$  nm (this is the wavelength of maximum absorption for Ket, verified both in distilled water and in the respective buffer solution); the amount of intercalated Ket was calculated using a calibration curve (Fig. 28). For the calibration curve the data were generated using nine aqueous Ket solutions with concentrations in the range of 10 to 90  $\mu\text{g/ml}$ , prepared by diluting a stock solution of Ket (1 mg/ml).

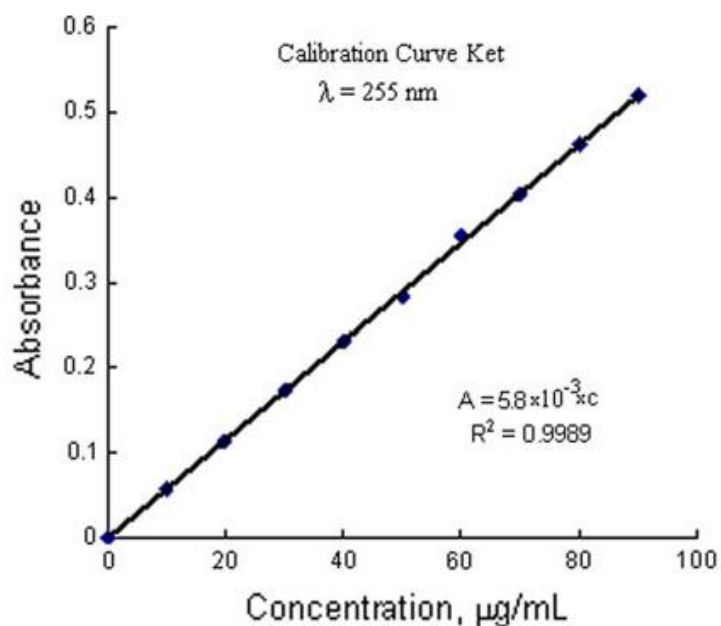


**Fig. 28.** Calibration curve for Ket

Three measurements were averaged for each data point and the equation of the calibration curve obtained by the least-square method was:

$$A = 5.8 \times 10^{-3} \times c$$

### *Characterization techniques*

X-ray powder diffraction (XRD) patterns were recorded on a Bruker AXS D8 diffractometer using monochromatic CuK $\alpha$  radiation ( $\lambda = 0.154$  nm), operating at 40 kV and 50 mA over a 2 hours range from 4 to 70 $^\circ$ . FTIR spectra were recorded on a FT-IR Bomem MB 104 spectrometer under the following experimental conditions: 200 scans in the mid-IR range (400–4000  $\text{cm}^{-1}$ ) using KBr (ratio 5/ 95 wt %) pellets, and a resolution of 4.0  $\text{cm}^{-1}$ .

### *In vitro Ket release study*

The release of Ket from ZnAILDH\_Ket and MgAILDH\_Ket into the media (phosphate buffer solution pH 7.4) was performed using the continuous method described in our previous paper (Jaba et al., 2008). The sample amount was 0.1 g and the buffer solution volume was 100 ml. The study was performed at 37 $^\circ\text{C}$ .

The flow rate was 0.5 ml/min and respectively 1.0 ml/min. The release kinetics of Ket has been followed for 18 hours. The amount of Ket released into the solution was determined

by using UV-visible spectrophotometer analysis at 255 nm wavelength. After the kinetic studies, the recovered solid samples were washed twice, each time using a volume of 100 ml deionized water, then dried and characterized by DRX and FTIR techniques.

#### *In vivo study of gastrointestinal tolerance and analgesic effect*

Two types of *in vivo* pharmacological studies were performed: the gastrointestinal tolerance and the analgesic effect evaluation of the Ket intercalated into LDHs. The choice of animal model consisted in mice models for determining the gastrointestinal tolerance (del Arco et al., 2004; del Hoyo, 2007; Tarnawski et al., 2010; Jaba et al., 2008; Tuo et al., 2010; Krylova et al., 2009; Konturek et al., 1991) and antinociceptive mice models for evaluating the analgesic effect (Jaba et al., 2008; Carstens, 1996; Derbyshire, 2008; Williams, 2008). A total of 68 animals were used in the study.

#### *Pharmacological studies for determining the gastrointestinal tolerance*

The samples (pure Ket, LDHs, ZnAILDH\_Ket and MgAILDH\_Ket) were delivered orally (80 mg active ingredient/kg weight of mouse) to different groups of animals. The compounds, each dispersed in 1 ml saline, were administered per os (p.o.). The ZnAILDH\_Ket and MgAILDH\_Ket composite sample amounts were adjusted to deliver the equivalent Ket dose of 80 mg/kg b.w.

#### *Evaluation of gastrointestinal tolerance*

The total number of animals involved in the gastrointestinal tolerance study was 32. They were divided into 4 groups, 8 animals per group. Each group received one of the following treatments: saline (control group), pure Ket, ZnAILDH\_Ket or MgAILDH\_Ket respectively, in the dose and volume described above. The mice were euthanized 24 hours after the sample administration. The abdominal cavity was surgically cut open, followed by careful extraction of the stomach and of jejunum and ileum fragments. Tissue portions were thoroughly exposed and fixed on a solid support to reveal the lesions. The surface of mucosa was rinsed with saline solution before evaluation.

To quantify the extension of the mucosal lesions, tissue samples were observed with a magnifying glass equipped with an optical zoom of X10. The lesions were quantified according to the following scoring system: 1 = erosion point, 2 = erosion < 1 mm, 3 = erosion of 1–2 mm, 4 = erosion of 2–3 mm, 5 = erosion of 3–4 mm, 6 = erosion > 4 mm. For each studied animal, a score was assigned, calculated by summing up the points given for the diameter of each lesion separately. An average score was calculated for each group.

#### *Antinociceptive testing*

A total number of 36 animals were used in this study. They were divided into 6 groups, containing 6 animals each. Each group received one of the following treatments: saline (control group), pure Ket, ZnAILDH\_Ket, MgAILDH\_Ket, ZnAILDH or MgAILDH respectively. The analgesic effect was measured by nociceptive stimulation through thermo-algesic mechanism (Hot Plate test). Testing was performed prior to sample administration (time 0), and then at intervals of 30, 60, 90, 120, 180 and 210 min after the treatment in the case of the samples administered orally. Samples that produced a significant increase in the latency response in hot plate test were antinociceptive.

## **Antinociceptive effect of morphiceptin loaded poly(butylcyanoacrylate) nanoparticles.**

### *Drugs*

n-Butyl cyanoacrylate (BCA) monomer was kindly supplied by Sichelwerke, Hannover, Germany. Dextran 70 (D, molecular mass 70,000 g/mol) was obtained from Fluka, Switzerland. Tween 80 (Polysorbate 80 - PS 80) and morphiceptin (MF) were purchased from Sigma-Aldrich Chemie GmbH, Germany. All other chemicals used in the study were of analytical grade. Bi-distilled water was used in all experiments.

### *Nanoparticles preparation and drug loading*

The preparation of nanoparticles was performed under sterile conditions, to avoid peptide degradation by bacterial proteases (Vauthier et al., 2003). Two different formulations of MF loaded nanoparticles (NPs) were considered, depending on the moment of drug addition – during (MF-NP, entrapped drug) or after (MF/NP, adsorbed drug) polymerization (Table XII).

#### *A. MF-NP formulation*

1 mL BCA was added in droplet with a syringe to 100 mL hydrochloric solution (pH = 2.2) containing 1.5 w/v % D, under stirring (1100 rpm), at 20°C. 30 min after the onset of the polymerization an appropriate amount of MF was added (15 mg MF in 1.2 mL bi-distilled water, yielding 0.15 mg MF/mL). The reaction mixture was maintained under stirring for 5 h, and then a 0.1 N sodium hydroxide aqueous solution was added for neutralization. The mixture was vigorously stirred for one more hour to complete polymerization. The dispersion was filtered (G3 glass filter, Schott AG, Mainz, Germany), subjected to repeated centrifugation and washing (three cycles at 10,000 x g, for 20 min each, 70 mL washing water), and submitted to size and structure analysis. Solid content was evaluated by centrifugation followed by drying for 3 aliquots of 10 mL from the filtered dispersion. The polymerization yield was approximated relative to total final reaction mixture volume.

#### *B. MF/NP formulation*

1% (v/v) BCA was added in droplet with a syringe to a HCl medium (pH = 2.2) containing 1.5 w/v % D and the reaction mixture was stirred for 6 h with a magnetic stirrer (1100 rpm) to promote polymerization. The reaction was completed by neutralization of the mixture with 0.1 N sodium hydroxide solution and kept under stirring overnight. After filtration through a G3 glass filter, the fine dispersion was subjected to lyophilization with a CHRIST freeze dryer, Alpha 1-4 LSC type. To evaluate the polymerization yield, 100 mg lyophilized NPs were redispersed in bi-distilled water and then were three times submitted to centrifugation – washing cycles (at 17,000 x g, for 10 min with a Hettich® EBA 21 centrifuge, Germany). The total volume of washing water was of 6 mL. The content in free, soluble dextran was found to be of 56 wt%. Two different sets of samples, submitted to different purification procedures, according to earlier (Kreuter et al., 1997) and recent/current protocols, were prepared for administration (Table XII).

For the first set (samples B1-B3), 100 mg lyophilized NPs (containing 44% PBCA NPs) were resuspended by ultrasonication in 4.5 mL isotonic saline. An appropriate amount of morphiceptin solved in 0.5 mL saline was then added, to achieve a final content of 1.2

mg/mL, and the mixture was stirred (700 rpm) for 6 h at 20°C (sample B2). PS-80 was then added to yield a final 1% surfactant solution (relative to the total suspension volume) and the mixture was incubated for 30 min (sample B3).

For the second set of samples (B4-B6), 100 mg lyophilized NP were re-dispersed in 2 mL saline serum and thoroughly purified, to remove residual monomer by threefold centrifugation at 17.000 x g, for 10 min, and washing with isotonic saline after resuspension by ultrasonication. The thoroughly purified PBCA-NPs were redispersed in an appropriate amount of saline serum to reach a final volume of dispersion of 5 mL (sample B4). The before mentioned procedure was then applied to obtain sample B5 (MF loaded NPs) and sample B6 (MF loaded NPs covered with PS-80) with a final dispersion volume of 5 mL and 1.2 mg MF/mL.

### *Characterization*

Aliquots of aqueous dispersions of unloaded nanoparticles (before and after lyophilization), MF loaded nanoparticles, coated or uncoated with PS 80, were subjected to size particle analysis and spectroscopic investigation (<sup>1</sup>H-NMR, FT-IR) after centrifugation and drying, respectively. <sup>1</sup>H-NMR and Fourier transform infrared (FT-IR) spectra were registered with an Avance DRX400 (Bruker) spectrometer working at 400 MHz and with a Vertex 70 (Bruker) spectrophotometer, respectively. DMSO-d<sub>6</sub> or CDCl<sub>3</sub> were used as solvents and TMS as internal standard.

For the drug loaded nanoparticles, aliquots from the prepared dispersions were centrifuged and the supernatant was analyzed by UV-Vis spectroscopy ( $\lambda=275$  nm), SPECORD 200 Analytic Jena instrument, to evaluate the amount of free drug ( $M_1$ ) as compared to the loaded drug percent obtained from 1H-NMR data. The loading efficiency was estimated as the ratio of the amount of bound drug to that of the originally added drug ( $M_0$ ) by the equation  $E = [(M_0 - M_1) / M_0] \times 100\%$ . For MF loaded NPs covered with PS-80 this characterization alternative couldn't be applied due to the superposition of MF and surfactant absorptions.

The particle size analysis ( $D_n$  – mean numerical diameter,  $SD$  – standard deviation) was performed with a Laser Diffraction Particle Size Analyzer Shimadzu-Sald 700. The aqueous nanoparticulate dispersion was added to the sample dispersion unit containing a stirrer, and was stirred to minimize the inter-particle interactions. The analysis was performed trice and the average value was considered. For samples B4-B6, the recovered supernatant and washing water resulted after the centrifugation cycles performed for further purification were subjected to the determination of the unreacted monomer amount by analytical methods (bromometry). An amount as high as 9.5 wt% monomer was found, relative to processed lyophilized NPs.

### ***In vivo testing of MF/NP particles***

#### *Drugs administration*

Different groups of 8 mice each were intraperitoneally injected with one of the following formulations:

- a) saline suspension of empty PBCA-NPs (Table XII, formulations B1, B4, groups 1 and 4);
- b) uncoated MF-loaded NPs (Table XII, formulations B2, B5, groups 2 and 5);

- c) PS-80 coated MF-loaded NPs (Table XII, formulations B3 and B6, groups 3 and 6);
- d) a mixture of MF and PS 80 (group 7);
- e) commercially available MF lyophilized powder solution in saline (group 8) and
- f) equal volume of 0.9% saline for a control/reference group (group 9).

**Table XII.** Characteristics of loaded and unloaded NP-PBCA nanoparticles and in vivo test arrangement

Sample	Polymer yield %	Dn <sup>a</sup> nm	SD <sup>a</sup> nm	Group	MF <sup>b</sup> %	Coating <sup>c</sup>	Dn <sup>d</sup> nm	SD <sup>d</sup> nm	
A	35	59	53	-	0.6	-	-	-	
B	B1	73	19	5	1	-	uc	1318	19
	B2				2	2.8	uc	1000	20
	B3				3	1.2	c	23	6
	B4				4	-	uc	912	38
	B5				5	2.7	uc	345	37
	B6				6	1.1	c	35	5

<sup>a</sup>according to measurements before and after lyophilization and redispersion in deionized water

<sup>b</sup>loaded morphiceptin according to the evaluation results from 1 H-NMR data

<sup>c</sup>coating with PS 80: c-coated, uc-uncoated

<sup>d</sup>according to size analysis data after sample preparation for administration

The nanoparticulate systems were administered in an amount of 200 mg lyophilized NPs/kg, with the before mentioned composition. For the further purified systems, as mentioned before the free dextran was priority removed by repeated centrifugation/saline washing cycles, the remained nanoparticles (88 mg/kg) being carefully recovered and subjected to specific procedures according to the envisaged final formulation. In all cases, the morphiceptin dose was of 12 mg/kg.

The antinociceptive effect of the tested substances was evaluated by hot plate test, a behavioral test that quantifies the thermal nociception. Analgesic measurements were performed before drug administration (base line) and at 15, 30, 60, 90 and 120 minutes after the drug or 0.9 % saline (control group) was administered. Treatments that produced a significant increase in the nociceptive thresholds were considered to be antinociceptive.

### **Local silver nanoparticles administration promotes inflammation and hyperalgesia in rats**

#### *Drugs*

The following drugs were used in the experiment: colloidal solution with 500 parts per million (ppm) silver nanoparticles purchased from US Research Nanomaterials, Inc, Houston, USA (Silver (Ag) Nanopowder /Nanoparticles (Ag, 99.99%, 30-50 nm, w/~0.2 wt% PVP Coated), colloidal silver 20 ppm (©Nano Silver, 30-50 nm, PVP Coated, Vita Crystal, RO),  $\lambda$ -carrageenan 1% diluted in fresh saline (Sigma- Adrich Germany).

Doses were selected according to literature data. In a dermal toxicity study, Korani et al used doses that ranged from 100 ppm to 10000 ppm nanosilver in a subchronic administration regime (Korani et al., 2013). Up to 10 ppm nanosilver were administered daily in pregnant female rats via drinking water in a study to assess the expression of procaspase-3 in newborn rat brain (Ganjuri et al., 2015). Another experiment repeatedly injected 60-2000 ppm nanosilver subcutaneously (intralesional administration) in a mouse model of cutaneous

leishmaniasis (Nilforoushadeh et al., 2012). In the present study, one group received nanosilver 500 ppm and the other treatment group received nanosilver 20 ppm single dose.

#### *Study design*

Rats were divided in three groups (n=6/group) as follows: Group S1 received 10 microliters colloidal silver 500 ppm, group S2 received 10 microliters colloidal silver 20 ppm and group C received an equivalent volume of saline. All drugs were injected subcutaneously (s.c.) in the intraplantar region of right hind paw. Response latencies were assessed by means of the plantar test and the analgesy-meter; inflammation was assessed by means of the plethysmometer. All animals were evaluated at baseline and 3 and 24 hours after colloidal silver/saline administration. After the 24 hours assessment, all animals received an s.c. intraplantar injection of 10 microliters  $\lambda$ -carrageenan 1% into the right hind paw. This lead to a localized inflammatory response (acute inflammation). The above-mentioned assessments were performed 3, 6 and 24 hours after  $\lambda$ -carrageenan administration.

#### 1.2.3.2 **Results**

#### **In vitro and in vivo behavior of Ketoprofen intercalated into layered double hydroxides.**

##### *Elemental analysis and spectrophotometric results*

Both analysis methods used for determining the amount of intercalated Ket yielded the same results (Table XIII). The percentage of intercalated Ket was 46.1% for ZnAILDH\_Ket and 50.1% for MgAILDH\_Ket respectively (by total sample weight), reported as an average value of the two analysis methods.

##### *Powder X-ray diffraction*

The powder X-ray diffraction (XRD) patterns of the precursor ZnAILDH, MgAILDH and its hybrids ZnAILDH\_Ket and MgAILDH\_Ket are shown in figure 29. The diffractograms recorded for LDHs precursors (fig. 29) show typical layered structures. The basal spacing of ZnAILDH and MgAILDH with nitrate as inter lamella anion is 8.74 and 8.50 Å, respectively.

The magnitude of the basal spacing found in hydrotalcite samples increases upon the inclusion of Ket into the LDH lamella. This trend is shown in figure 29, where the basal spacing of ZnAILDH\_Ket and MgAILDH\_Ket is 22.36 and 22.54 Å, respectively. This expanded interlayer separation is due to the molecular size and geometrical arrangement of Ket in the interlayer space.

**Table XIII.** Ket content in LDH\_Ket samples, determined by elemental and spectrophotometric analysis

Sample	Elemental analysis		Spectrophotometric analysis
	C (%)	Ket (%)	Ket (%)
ZnAILDH_Ket	35.4	46.9	45.2
MgAILDH_Ket	37.8	50.0	50.2

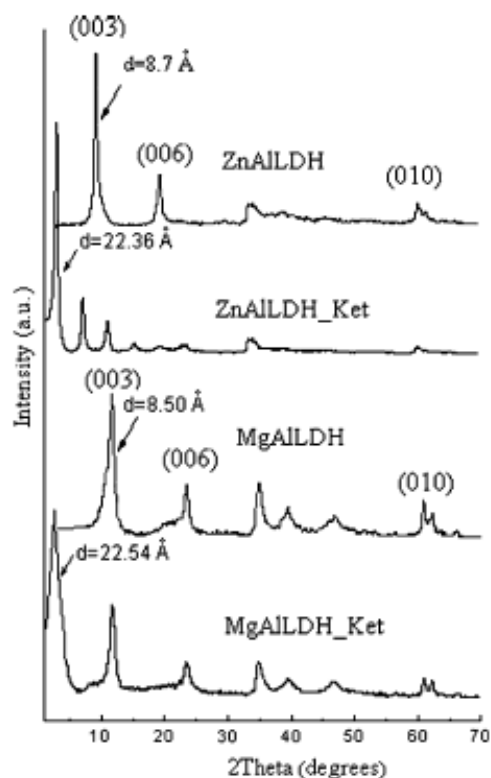


**Fig. 29.** Basal spacing of ZnAILDH, MgAILDH, ZnAILDH\_Ket and MgAILDH\_Ket

#### *FTIR spectroscopy*

FT-IR spectra of Ket, LDHs and LDHs\_Ket samples are presented in figure 30. The results confirm the intercalation of Ket in the MgAILDH and ZnAILDH lamella. The recorded FT-IR spectrum of pure Ket (figure 30), shows characteristic vibration bands associated with its structure (Maestrelli et al., 2008).

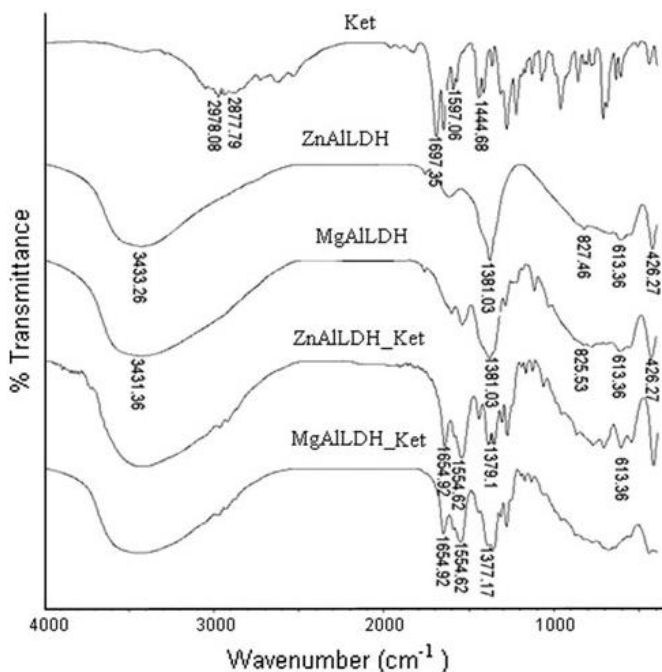


**Fig. 30.** Comparative FTIR spectra for: Ket, ZnAILDH, MgAILDH, ZnAILDH\_Ket and MgAILDH\_Ket

The main peaks correspond to the following frequencies: 2990–2878  $\text{cm}^{-1}$  (methyl m-CH), above 3018  $\text{cm}^{-1}$  (aromatic ring m-CH), 1697  $\text{cm}^{-1}$  (carbonyl  $\nu\text{C}=\text{O}$ ), 1655  $\text{cm}^{-1}$  ( $\nu\text{C}=\text{O}$ , stretching of the ketone) 1597, 1585 and 1445  $\text{cm}^{-1}$  (aromatic ring  $\nu\text{C}=\text{C}$ ) (Vueba et al., 2008). The bands observed in the low-frequency region of the spectrum are associated as the lattice vibration modes and can be attributed to M–O from 850 to 600  $\text{cm}^{-1}$  and M–O–M near 426  $\text{cm}^{-1}$  (M = Al, Zn, Mg) in the LDH sheets (Kanan and Swamy, 1992). The appearance of a strong band at 1381  $\text{cm}^{-1}$  is due to the symmetric vibration of the interlayer nitrate anion from MgAILDH and ZnAILDH (Xu and Zeng, 1999).

All the vibration bands associated with the organic anion are found in the spectra of the samples containing intercalated Ket, together with the absorption bands characteristic for LDHs (figure 30). The band characteristic for the C=O group is located at 1655  $\text{cm}^{-1}$  and the band assigned to the C=C bond in the Ket aromatic ring is located at 1554  $\text{cm}^{-1}$ . The absence of the band at 1381  $\text{cm}^{-1}$  in the spectrum of MgAILDH\_Ket and ZnAILDH\_Ket, confirms the fact that the interlayer nitrate anions have been displaced.

### *Kinetic study*

The *in vitro* release of Ket from LDHs nanohybrid material was investigated under simulated conditions mimicking the gastrointestinal tract environment. The amount of Ket released from the samples was calculated as:

$$m_{\text{Ket}} = c_d V_e + \sum_{i=0}^{n-1} c_i V_i$$

where  $m_{\text{Ket}}$  is the amount of Ket released from the sample at a certain time (mg);  $c_d$  is the concentration of drug in the extracted sample (lg/ml);  $V_e$  is the volume of eluent from the system;  $V_i$  is the volume of extracted sample,  $i$ ; and  $c_i$  is the concentration of Ket in the extracted sample,  $i$ , (lg/ml) determined spectrophotometrically.

Figure 31 shows the release profile of Ket from ZnAILDH\_Ket and MgAILDH\_Ket into the buffer solution pH 7.4 and different flow-rates. Each point represents the calculated average of three measurements. The accumulated Ket released into the aqueous solution increased with contact time and flow-rate when LDHs\_Ket were placed in contact with aqueous solution. When the matrix is relatively stable in the elution medium, it is expected that the drug diffusion is the rate determining step for the release kinetics. Therefore, the empirical equation developed by Ritger and Peppas (Ritger and Peppas, 1987) can be applied to obtain the diffusion parameters from the early stage release data:

$$\frac{M_t}{M_\infty} = kt^n$$

where  $M_t/M_\infty$  represents the fraction of released drug at time  $t$ ,  $k$  is a constant characteristic to the drug-LDH interaction and  $n$  is an empirical parameter characteristic to the release mechanism. When  $\ln(M_t/M_\infty)$  is plotted versus  $\ln(t)$ , the value of the diffusional exponent is obtained.

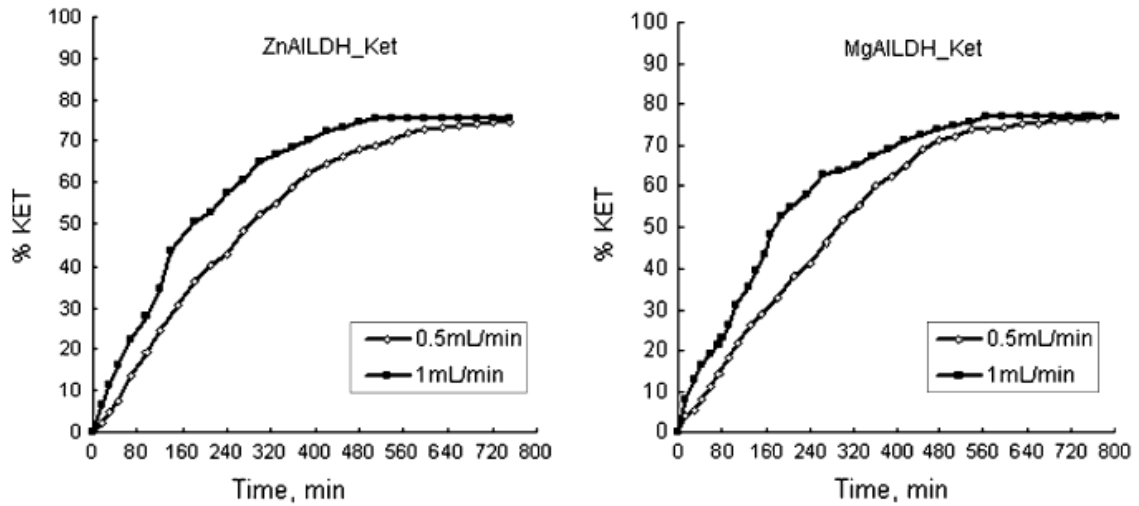


**Fig. 31.** Release profiles of Ket from: ZnAILDH\_Ket and MgAILDH\_Ket into the aqueous solutions at initial Ph 7.4

According to Lee and Jou (2004), the diffusion relative rate and relaxation process cause three different classes of diffusion, characterized by distinct values of the diffusional exponent.

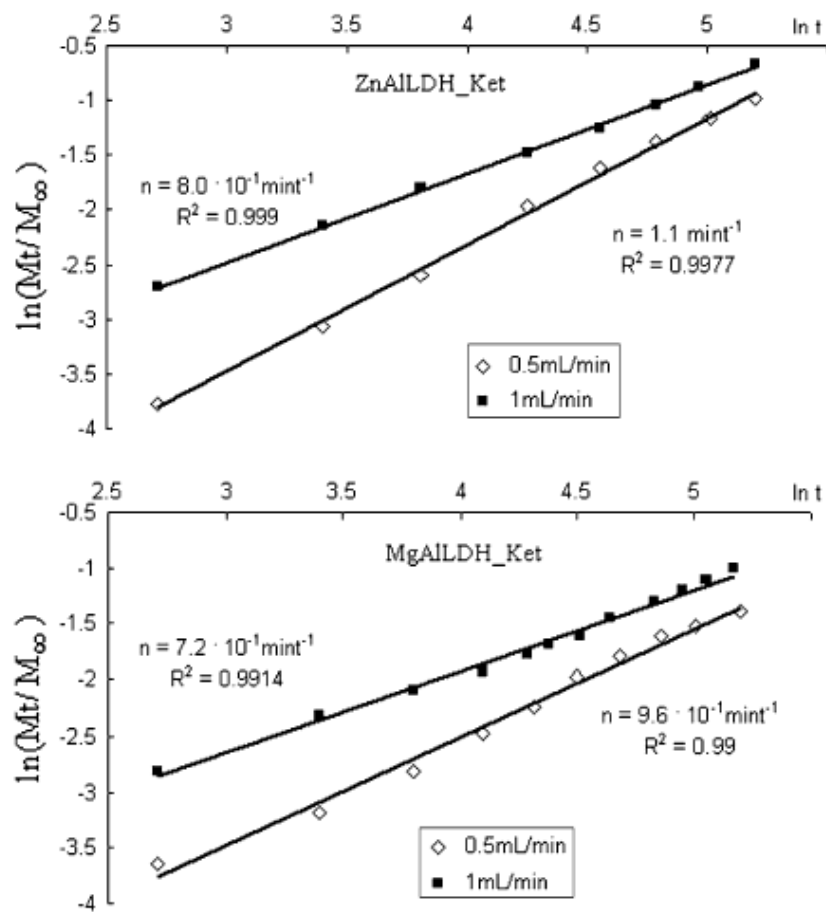


**Fig. 32.** Comparative plots of  $\ln(Mt/M_\infty)$  versus  $\ln(t)$  for: ZnAILDH\_Ket and MgAILDH\_Ket

When  $n = 0.5$  the rate of diffusion is much smaller than the rate of relaxation and the process is called Fickian diffusion.

Secondly, if  $n = 1.0$ , the diffusion process is much faster than the relaxation phenomena. In this case the controlling step is the velocity of the advancing front, which forms the boundary between the swollen outside layer and the glassy core. Thirdly, in non-Fickian diffusion ( $n = 0.5-1.0$ ) the diffusion and relaxation rates are comparable. In this work, the  $n$  parameters were calculated from the plot of  $\ln(M_t/M_\infty)$  versus  $\ln(t)$  (Fig. 32) using the obtained experimental data.

The calculated value of  $n$  parameter is approximately equal to 1 for the two types of layered double hydroxides when the flow-rate is 0.5 ml/min. Under these conditions the release rate is controlled by the ion exchange process between the Ket anion intercalated into LDH and phosphate ions from release environment. At a flow-rate of 1.0 ml/min, the calculations yield  $n = 0.80$  for ZnAILDH\_Ket complex and  $n = 0.72$  for MgAILDH\_Ket complex respectively. In this case the diffusion rate is comparable with the ion exchange reaction rate of the anions involved in the process.

To obtain some information about the release mechanism, we subsequently recovered the residue left in the aqueous solution after the Ket release experiment. The DRX patterns for MgAILDH\_Ket and ZnAILDH\_Ket (residue recovered after release process) are presented in Fig. 33.

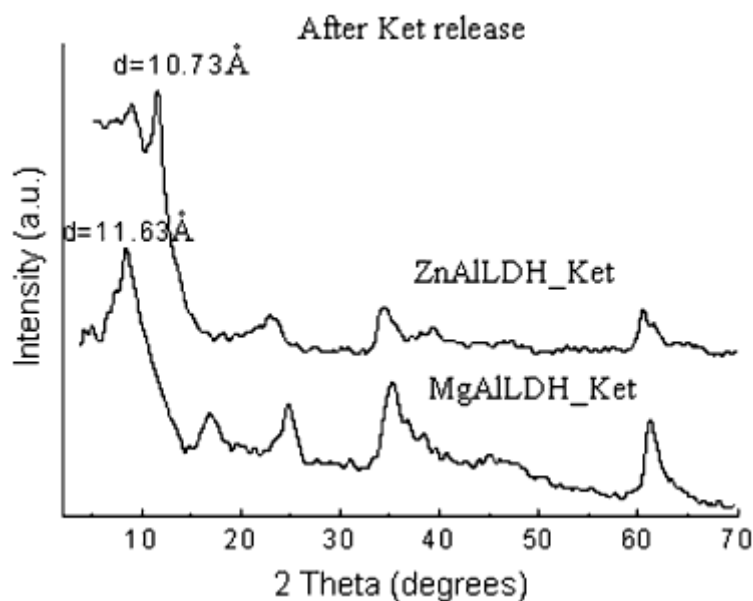


**Fig. 33.** Comparative DRX patterns obtained for solid residue left after the release of Ket from: MgAILDH\_Ket and ZnAILDH\_Ket

The distance between layers of the residue analyzed after release was 11.63 Å for MgAILDH\_Ket and 10.37 Å for ZnAILDH\_Ket. These values are in agreement with expectation for the layered double hydroxides containing phosphate ions intercalated between layers (Costantino et al., 1997). In the FTIR spectra recorded after drug release (residue recovered after release process) at pH 7.4 (Fig. 34), the characteristic bands of Ket disappear, the specific bands of layered double hydroxides are restored and a new band appears at 1050

$\text{cm}^{-1}$  that is characteristic to the presence of phosphate ion. Both DRX and FTIR analysis methods suggest that drug release from hybrids with Ket, is due to the ion exchange process between Ket anions and phosphate ions belonging to the elution medium.

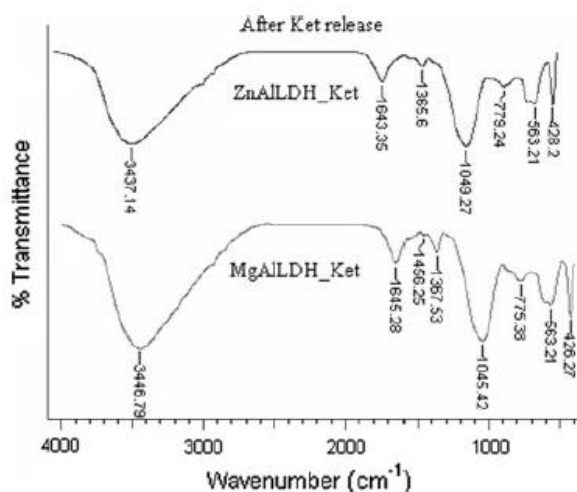


**Fig. 34.** Comparative FTIR spectra obtained for solid residue left after the release of Ket from: MgAlLDH\_Ket and ZnAlLDH\_Ket

#### *Evaluation of gastrointestinal tolerance*

The administration of a single dose of 80 mg/kg p.o Ket in mice caused significant gastric irritation effects. The gastric mucosa has an edematous aspect, with areas of microhemorrhages and erosion points. The lesions are present both in the stomach, jejunum and in the ileum.

Administration of Ket intercalated with the chosen versions of hybrid materials, LDHs\_Ket, causes an irritation syndrome significantly lower when compared with the group that received matrix free Ket. Although the incorporation in the matrix significantly reduced the lesions in number and size when compared to the group that received raw Ket, certain micro erosions were still found in all three types of gastrointestinal tissue segments (stomach, jejunum and ileum) following the administration of ZnAlLDH\_Ket.

Errosions are missing or barely visible in stomachs of mice that received MgAlLDH\_Ket (Fig. 35). These results are in accordance with the phenomena observed in the preliminary studies with these materials (Jaba et al., 2008).

Compared to the ZnAlLDH, the inclusion of Ket in MgAlLDH provides better protection, with normal appearance of the digestive mucosa, even when the high Ket doses were used. Therefore, the results obtained on the two newly synthesized versions of LDHs showed good local gastric tolerance, revealed by the normal aspect of the macroscopically analyzed gastric mucosa (Fig. 36). Erosion or hemorrhagic points are marked by arrows and very pronounced on Ket images, barely visible on ZnAlLDH\_Ket and missing on MgAlLDH\_Ket, reinforcing the information provided by the scores reported in figure 35.

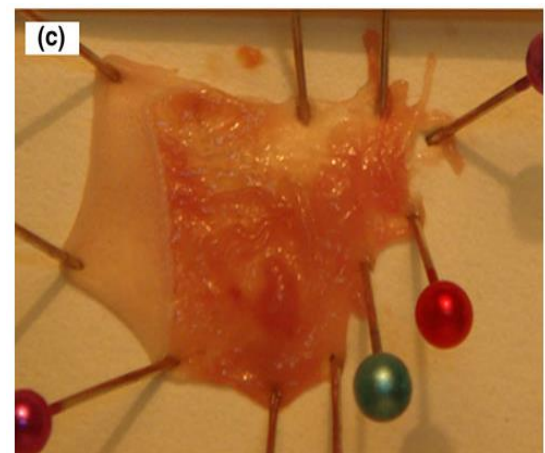
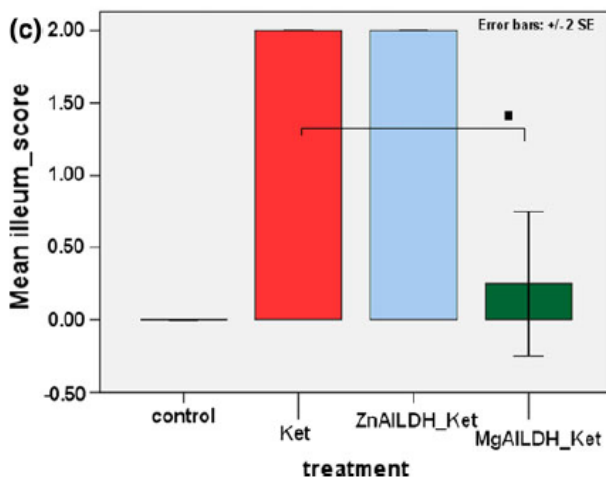
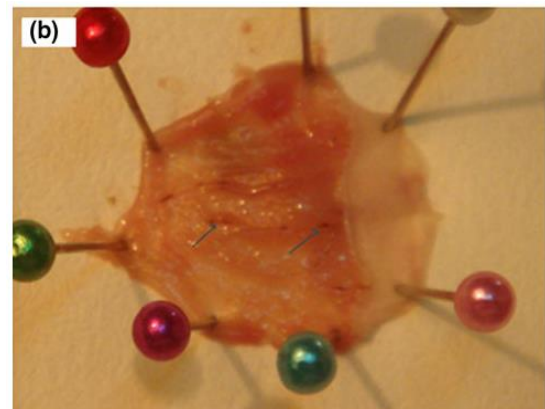
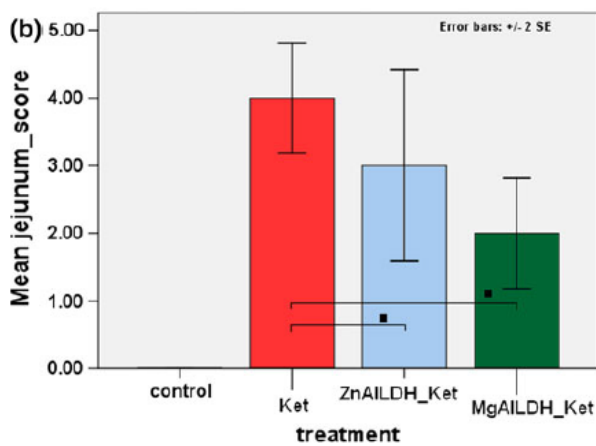
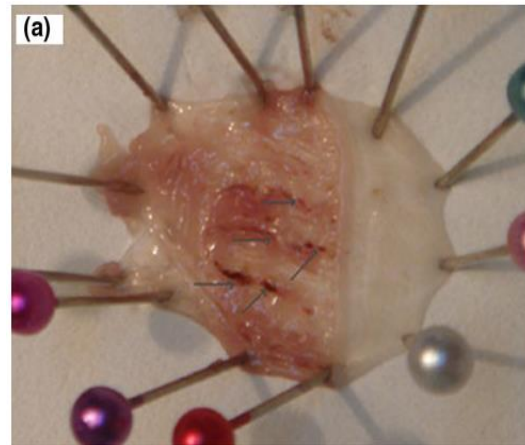
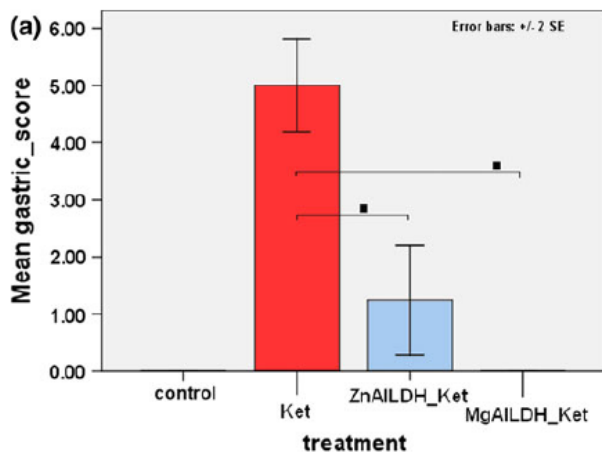


**Fig. 35.** Evaluation of gastrointestinal tolerance. The quantified score: gastric score (a), jejunum score (b), ileum score(c) (n = 8 for each treatment group)

**Fig. 36.** Photographs of extracted stomachs after treatment with: Ket (a), ZnAILDH\_Ket (b), MgAILDH\_Ket (c); arrows indicate erosion/hemorrhagic points

*Antinociceptive testing*

The oral administration of raw LDH did not significantly influence the response latency to thermal nociceptive stimuli. Orally administered doses of 80 mg/kg Ket significantly increased the response latency (Fig. 37). The observed antinociceptive effect of

both versions of intercalated Ket into LDHs is significant when compared to both the records obtained before the administration of samples and records measured in the control group.

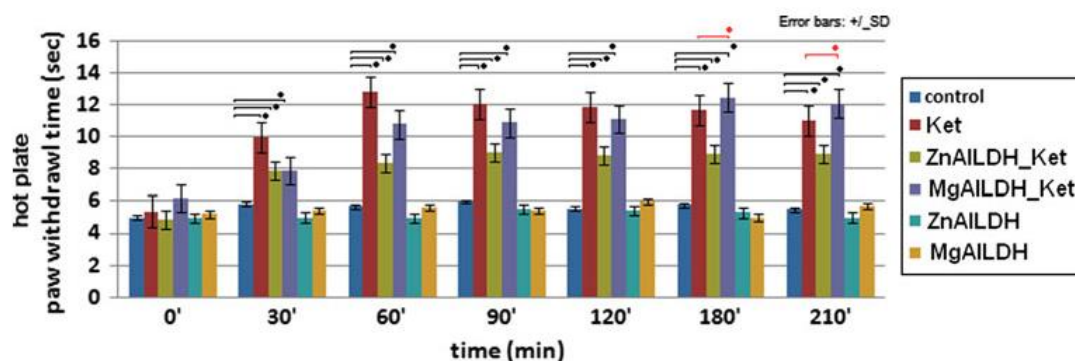


**Fig. 37.** Quantification of analgesic activity by thermoalgesic nociception test (hot plate) at i.p injection of Ket, ZnAILDH\_Ket, MgAILDH\_Ket, ZnAILDH, MgAILDH (n = 6 for each treatment group)

Both combinations of Ket with LDH induced an analgesic effect comparable in intensity and duration with the matrix-free Ket group. The antinociceptive effect of the MgAILDH\_Ket retains a significant value of analgesia for a longer period of time compared to the ZnAILDH\_Ket compound.

The MgAILDH\_Ket formulation shows a tendency towards a stronger antinociceptive effect than the ZnAILDH\_Ket counterpart during the 210-min recorded period.

#### **Antinociceptive effect of morphiceptin loaded poly(butylcyanoacrylate) nanoparticles.**

After preliminary polymerization experiments, the preparation of PBCA-NPs was performed by adding 1% (v/v) butyl cyanoacrylate monomer to a 1.5% w/v solution of dextran 70 in 0.01 N hydrochloric acid (stirring rate: 1100 rpm, 20°C) – a recipe yielding nanoparticles with a mean diameter as low as 19 nm and a narrow size distribution with a SD = 5.5 nm (Fig. 38).

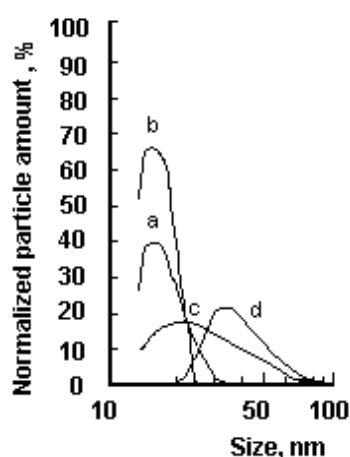


**Fig. 38.** PBCA-NPs size distribution. Empty nanoparticles (a) before lyophilization and (b) 6 months after lyophilization and PS-80 coated MF/PBCA-NPs (c) sample B3 and (d) sample B6.

According to  $^1\text{H-NMR}$  data, the inclusion of MF in PBCA-NPs during the polymerization process gave rise to drug structure modification, most probably by covalent bonding of the peptide on the polymeric support, the resulted MF-NP product being not recommended for injectible administration. Low values were obtained for the polymerization

yield, as well as for the amount of the loaded drug into the NPs. The nanoparticles size distribution was large in this case.

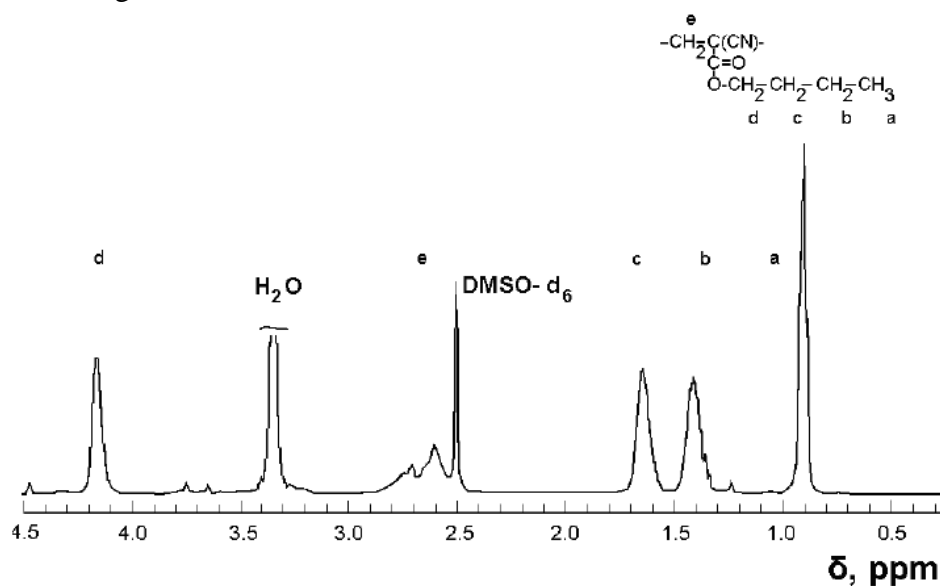


**Fig. 39.**  $^1\text{H}$ - NMR spectrum of PBCA nanoparticles – sample B4 (DMSO- $d_6$ ).

The adsorption of MF on presynthesize PBCA-NPs gave better results. The nanoparticles stored at  $-20^\circ\text{C}$  maintained their characteristics as long as six months after lyophilization (Fig. 38, plots a, b). However, during the preparation of drug loaded nanoparticles at the concentration imposed by the adopted formulation, an agglomeration tendency was observed before or after drug loading.

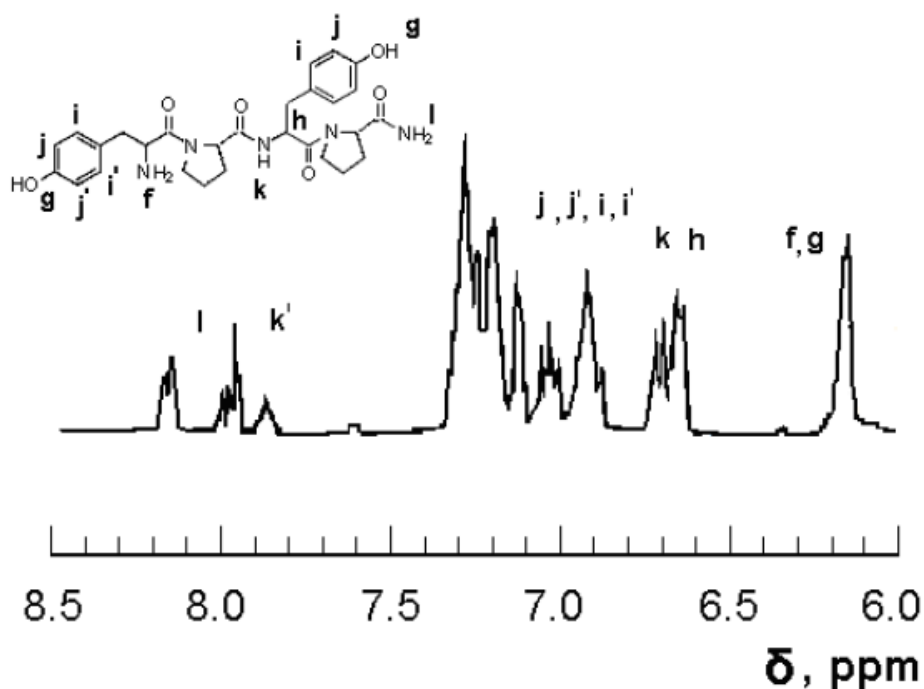


**Fig. 40.**  $^1\text{H}$ - NMR spectrum and signals attribution for morphiceptin loaded PBCA nanoparticles (detail) – sample B3. Solvent: DMSO- $d_6$

This instability problem was solved by surfactant addition, the colloidal system generally regaining the initial characteristics (Fig. 38). One should note that even after further

purification, the PBCA-NPs retained about 6 wt% dextran, this suggesting a core-shell structure.

The amount of loaded drug was evaluated by comparing the areas of specific NMR signals appearing in the 6 to 9 ppm range, attributed to MF, with those of the signals situated in the 1 to 4 ppm domain ranging, mainly ascertained to PBCA (Fig. 39 and 40).

The calculations indicate a MF loading on dextran-PBCA-NPs of about 2.8 wt/wt % before surfactant addition (20.4 % loading efficiency), and of only 1.2 % after surfactant coating. Apparently, the loading process is not influenced by the presence or absence of free dextran or residual monomer in the final system.

The results of antinociceptive testing following intraperitoneal injection show different effects, depending on the applied formulation and on the purity of the polymeric carrier (Table XIV).

**Table XIV.** Antinociceptive effect in mice (mean and standard error of latency) following intraperitoneal injection (n=8)

Group	0 min	15 min	30 min	60 min	90 min	120 min
1	9.516±0.649	10.066±0.750	10.75±0.954	10.9±1.021	12.316±1.034*	11.9±0.909*
2	9.25±0.463	10.15±0.887	11.2±1.261	11.316±1.182**	12.866±0.781*	12.333±0.527*
3	9.233± 0.708	11.133±1.040**	12.1±0.456*	11.95±0.361**	12.883±0.923*	12.55±0.671*
4	9.783±0.462	10.85±0.450	11.716±0.796**	11.933±0.539**	11.266±1.102	10.266±0.524
5	10.066±0.546	13.683±0.343*	14.45±0.472*	14.166±0.344*	11.233±0.877	10.15±0.983
6	9.316±0.453	13.633±0.445*	14.433±0.496*	14.183±0.699*	12.15±2.448*	10.816±1.396**
7	9.85±0.450	10.85±1.052	11.133±1.121	11.5±1.031	11±0.712	10.616±0.556
8	9.233± 0.417	8.083±0.685	8.383±0.617	9.016±0.402	8.516±0.567	8.683±0.397
9	8.733±0.697	8.45±0.700	9.166±2.154	8.716±1.108	9.0167±0.793	8.933±0.768

\* The mean difference is significant at the 0.01 level when compared to control

\*\* The mean difference is significant at the 0.05 level when compared to control

The nociceptive response latencies to the applied thermal nociceptive stimulus clearly demonstrate that free MF does not penetrate the brain in amounts able to induce an antinociceptive effect. The analgesic effect of this treatment (group 8) is not different from that induced by the control sample (group 9), when systemically administered. The simple mixing of MF with pure PS 80 is not sufficient to ensure the transport of drug through the BBB barrier, as shown by the lack of antinociceptive effect (Fig. 41).

Empty nanoparticles (groups 1 and 3) were also not able to evoke a prominent analgesic activity. There is also no significant difference in the analgesic effect between the empty nanoparticles (groups 1 and 3) submitted to different purification procedures, this suggesting that monomer traces are not involved in a decisive manner in system's behavior. However, MF-PS 80 solutions and empty PBCA-NPs suspensions cause a slight BBB disturbance as compared to control saline solution, which may be considered as a minimum response to a polymeric chemical agent administration/BBB penetration.

Both formulations with MF adsorbed on the surfactant-coated or uncoated PBCA-NPs could induce analgesia after ~30 min from the administration moment (Fig. 42 and 43). A further purification of the particles increases the analgesic effect (see the specific behavior of groups 2 and 3 as compared to 5 and 6).

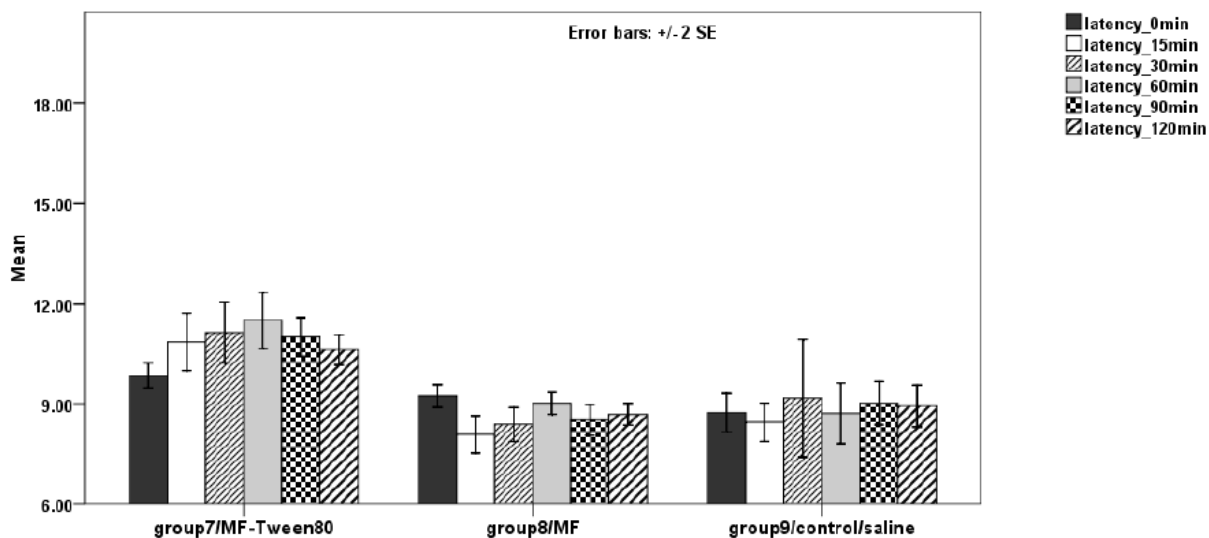


**Fig. 41.** Hot plate test. Antinociceptive effect in mice (latency in seconds) after intraperitoneal injection of MF-PS 80 mixture (group 7), MF solution (group 8) and isotonic saline (group 9). (\*p < 0.01 when compared to saline control)

For groups 2 and 3, the latency increased slower as compared to groups 5 and 6, but showed a prolonged duration of the analgesic effect. As for the targeting efficiency, even if apparently the difference between the PS 80 coated and uncoated particles is a minimum one, it is to note that the amount of the adsorbed  $\mu$ -peptide opioid is nearly half on the PBCA-NPs carrier in the surfactant-containing system.

The efficiency was not so remarkable mainly due to the low drug loading capacity of PBCA-NPs (~20 %). Thus, although plenty of nanoparticles might have entered the central nervous system, according to the mentioned effect of empty particles administration, only a limited amount of peptide is transported across the BBB, and the administered drug dose is known to be important.

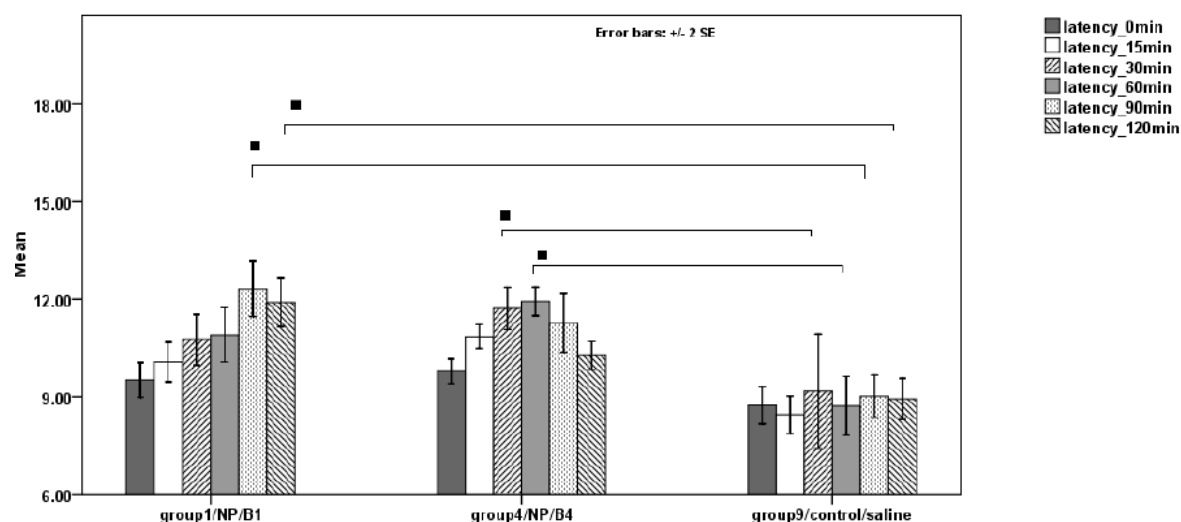


**Fig. 42.** Hot plate test. Antinociceptive effect in mice (latency in seconds) after intraperitoneal injection of empty NPs prepared according the two procedures: samples B1 and B4 as compared to isotonic saline as reference (\*p < 0.01)

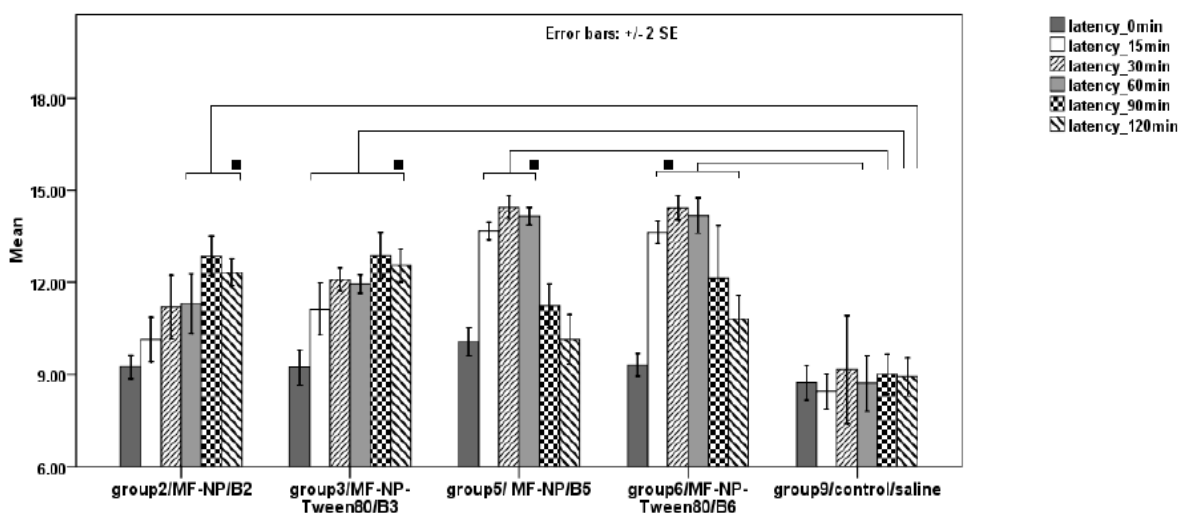


**Fig. 43.** Hot plate test. Antinociceptive effect in mice (latency in seconds) after intraperitoneal injection of morphiceptin loaded PBCA nanoparticles uncoated (groups 2 and 4) or coated with PS 80 (groups 3 and 6) as compared to isotonic saline (group 9) (\*p < 0.01)

### Local silver nanoparticles administration promotes inflammation and hyperalgesia in rats

#### Plantar test

There were no significant differences between groups at baseline and three hours after treatment. Twenty-four hours after colloidal silver administration, group averages were  $14.73 \pm 1.17$  for group S1,  $16.68 \pm 1.3$  s for group S2 and  $16.08 \pm 1.9$  s for group C. However, this difference did not reach statistical significance. After  $\lambda$ -carrageenan (CG) was injected, there was an important decrease in thermal PWLs in all groups, with an average of  $3.5 \pm 0.4$  s in the S1 group,  $6.50 \pm 1.1$  s in the S2 group and  $6.2 \pm 1.3$  s in the Cgroup 3 hours after CG. Twenty-four hours after CG, mean PWLs were significantly lower in the S1 group when compared to both S2 and control groups ( $p < 0.0001$ ). At this time point, average values were  $6.61 \pm 0.6$  s in the S1 group,  $15.10 \pm 1.0$  s in the S2 group and  $15.46 \pm 1.1$  s in the C group (Fig. 44).

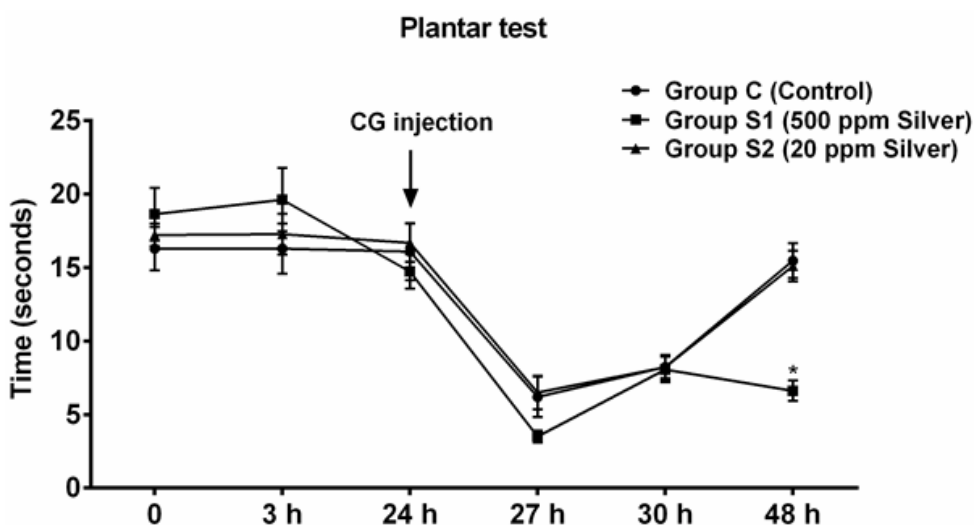


**Fig. 44.** Average thermal PWLs throughout the experiment. \* =  $p < 0.05$  (Tukey post-hoc) Randall-Selitto test

There were no significant differences between groups at baseline and three hours after treatment. However, 24 hours after colloidal silver administration both treatment groups had a significantly higher sensibility to mechanical stimuli, with averages of  $4.16 \pm 0.2$  s for group S1,  $4.75 \pm 0.2$  s for group S2 and  $5.63 \pm 0.4$  s for group C ( $p=0.02$  for S1 vs. C and  $p=0.03$  for S2 vs. C). After CG injection, in all three groups a decrease in mechanical PWLs was recorded- (1 s latency for all rats three hours after CG). Twenty-four hours after CG, control averages increased to 2 s, whereas averages in the treatment groups were  $1.60 \pm 0.2$  s (S1) and  $2.25 \pm 0.3$  s (S2). After CG administration, there were no statistically significant differences between groups (Fig. 45).

### Plethysmometry

There were no significant differences between groups at baseline. Three hours after colloidal silver injection, paw volume was  $1.31 \pm 0.03$  in group S1,  $1.27 \pm 0.03$  in group S2 and  $0.91 \pm 0.03$  in group C. This difference was statistically significant, with  $p < 0.0001$  for S1 vs. C and  $p = 0.0002$  for S2 vs. C (Fig. 46).

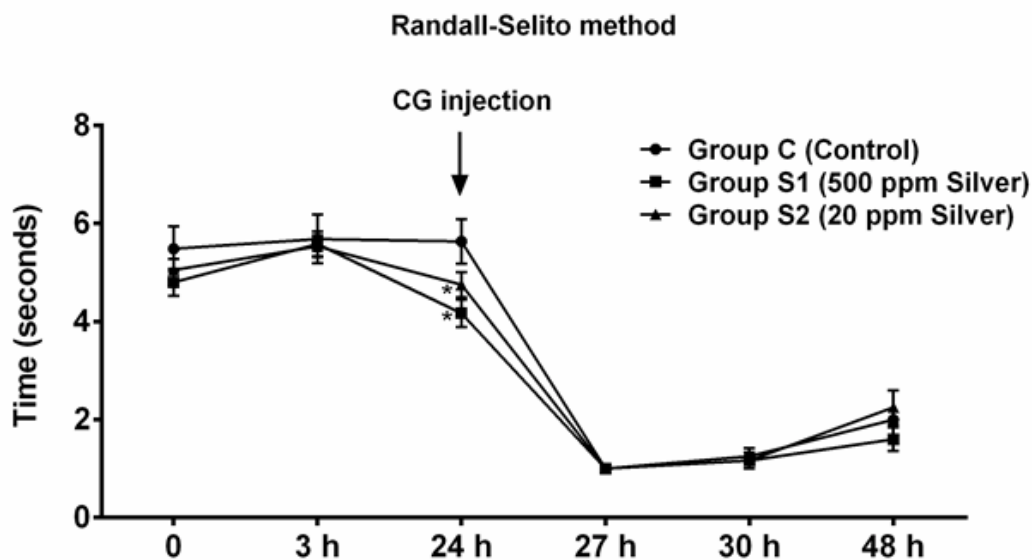


Fig. 45. Average mechanical PWLs throughout the experiment  $*=p<0.05$  (Tukey post-hoc)

Colloidal silver's effect was persistent – 24 h after treatment S1 and S2 groups had an increased paw volume when compared with C group, with  $p = 0.02$  for both S1 vs. C and S2 vs. C. Three hours after CG injection, an increase in paw volume was noted for all groups. However, paw edema was more pronounced in the silvertreated groups, with an average of  $2.19 \pm 0.1$  in group S1,  $2.15 \pm 0.07$  in group S2 and  $1.92 \pm 0.09$  in group C ( $p < 0.006$  for S1 vs. C and  $p = 0.004$  for S2 vs. C) (Fig. 46).

In the control group, paw edema reached a maximum 6 h after CG injection (mean of  $2.24 \pm 0.06$ ); now, no statistically significant differences were noted between groups. Paw edema began to decrease afterwards and 24 hours after CG injection averages were  $1.76 \pm 0.03$  in group S1,  $1.54 \pm 0.09$  in group S2 and  $1.56 \pm 0.08$  in group C. Paw volume of group S1 rats was significantly larger than paw volume in group C ( $p=0.01$ ).

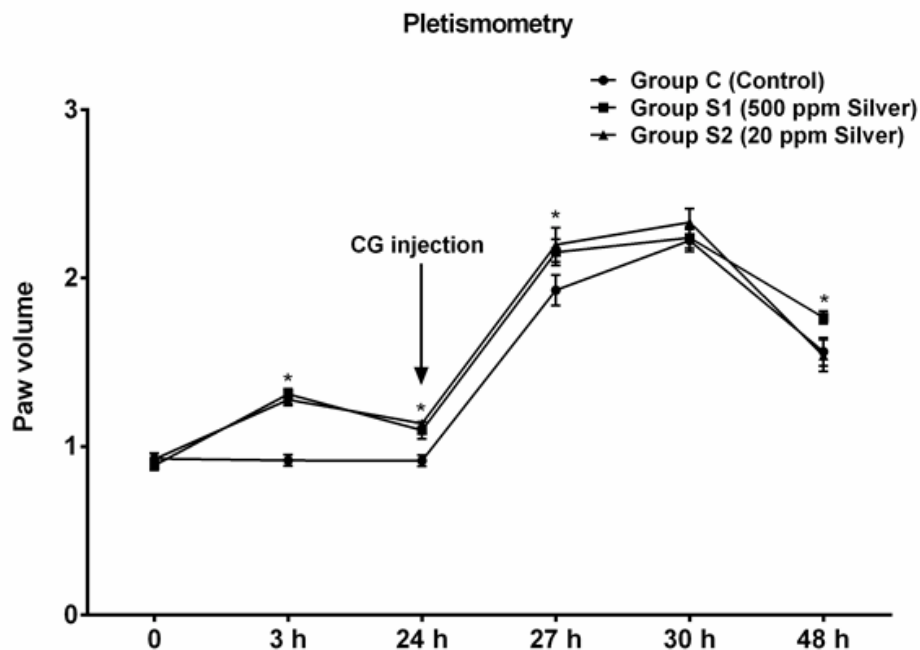


Fig. 46. Paw volume throughout the experiment  $*=p<0.05$  (Tukey post-hoc)

### 1.2.3.3 Discussions

#### **In vitro and in vivo behavior of Ketoprofen intercalated into layered double hydroxides.**

Both analysis methods used for determining the amount of intercalated Ket yielded the same results. The diffractograms recorded for LDHs precursors show typical layered structures like those reported in the literature for this type of materials (Olanrewaju et al., 2000; Xu and Zeng, 2001). The basal spacing of ZnAlLDH and MgAlLDH with nitrate as inter lamella anion is 8.74 and 8.50 Å, respectively. These values correspond to the expected basal spacing of nitrate anion incorporated in hydroxide layer (Xu and Zeng, 2001).

The basal spacing of ZnAlLDH\_Ket and MgAlLDH\_Ket was 22.36 and 22.54 Å, respectively. These results are in good agreement with those reported in the literature regarding intercalation of organic anions of similar size to Ket. For example, upon intercalation of diclofenac, 4-biphenylacetic acid, mefenamic acid, meclofenamic acid and ibuprofen anions the expanded interlayer spacing was in the range of 20.4 to 23.2 Å (del Arco et al., 2004, 2007; Frunza et al., 2008; Silion et al., 2008).

Regarding FTIR spectroscopy for ZnAlLDH and MgAlLDH, the broad and strong band located in the frequency range of 3600–3200  $\text{cm}^{-1}$  and centered at 3431  $\text{cm}^{-1}$ , is a common feature for all the hydrotalcite-type materials corresponding to the OH stretching vibration due to the presence of water molecules (Cavani et al., 1991).

The most significant downside of chronic clinical use of NSAIDs is the irritation syndrome at the level of gastrointestinal mucosa, where erosions and hemorrhagic lesions have been frequently described. The in vivo gastric tolerance study was aimed at evaluating LDH's capacity of protecting against this side effect of NSAIDs.

The *in vitro* release of Ket from LDHs nanohybrid material was investigated under simulated conditions mimicking the gastrointestinal tract environment and our results are in agreement with previous studies (Aelenei et al., 2009; Dashevsky et al., 2006; Mastiholimath

et al., 2007; Rokhade et al., 2007; Serra et al., 2006). Subsequently we assessed the in vivo gastrointestinal tolerance of Ket and we noted that the administration of a single dose of 80 mg/kg p.o Ket in mice caused significant gastric irritation effects, whereas LDH incorporated Ket causes an irritation syndrome significantly lower when compared with the group that received matrix free Ket. The significant difference observed between the raw Ket and the LDH incorporated Ket is since the hydrotalcites not only have the capability to neutralize acids, but also are known to inhibit pepsin action at Ph values at which its activity is still high (Playle et al., 1974; Pawlaczuk et al., 1985; Dreyer et al., 1991). Other studies have also shown that hydrotalcites are responsible for an activation mechanism that takes place in the gastric mucosa and is related to genes encoding for the epidermal growth factor and its receptor. This observation might provide a physiological basis for an ulcer healing action (Tarnawski et al., 2000).

#### **Antinociceptive effect of morphiceptin loaded poly(butylcyanoacrylate) nanoparticles.**

Generally, BCA can be polymerized by two techniques, the dispersion polymerization (DP) and emulsion polymerization (EP), both involving the basic mechanism of anionic polymerization (Liu et al., 2006; Vauthier et al., 2003; Kreuter et al., 1997). Nanoparticles with an average particle size of about 300 nm and a broad particle size distribution are generally yielded by dispersion polymerization, while EP nanoparticles show an average particle size of up to 200 nm with a narrow particle size distribution. The characteristics of the resulting particles can be controlled adjusting the polymerization mixture recipe, the pH and the stirring rate. Our choice was dispersion polymerization, using dextran as a stabilizer and cryoprotector, the dextran shell favoring drug adsorption (Verdun et al., 1986; Vauthier et al., 2003; Sommerfeld et al., 1998; Abdelwahed et al., 2006).

The dependence of BBB permeation efficacy on PBCA-NPs size was recently clearly demonstrated (Gao and Jiang, 2006). The data agree with the hypothesis considering that the mechanism for surface-coating of the nanoparticles to overcome the BBB supposes that the coated NPs mimic LDL (low density lipoprotein) following the intravenous administration, PS 80 playing a special role as an anchor between NPs and the apolipoprotein, especially ApoE. NPs combined with the apolipoprotein are considered as LDL and LDL receptor-mediated transcytosis transports drug-loaded nanoparticles across the BBB. It seems that therefore nanoparticles of sizes like LDL are more efficient than any other types. The size range of LDL was reported to be from 20 to 25 nm (Chen, 1999).

The results of antinociceptive testing following intraperitoneal injection show different effects, depending on the applied formulation and on the purity of the polymeric carrier. The simple mixing of MF with pure PS 80 is not sufficient to ensure the transport of drug through the BBB barrier, as shown by the lack of antinociceptive effect. The number of nanoparticles injected in the present study is without apparent toxic effect in the intact animal and is below the suggested LD50 of 230 mg/kg (Kante et al., 1982).

For groups 2 and 3, the latency increased slower as compared to groups 5 and 6, but showed a prolonged duration of the analgesic effect. Considering the high D content of the administered formulations for groups 1-3 (free D included), one possible reason for the specific behavior may be considered the free diffusion of most injected formulations, allowed as effect of the disruption of the BBB by infusion of hyperosmotic solutions, resulting in tight junctions opening. The slow onset of the analgesic effect after MF binding to nanoparticles

and the administration of this formulation intravenously is consistent with a direct interaction of nanoparticles with and subsequent uptake by the brain blood capillary endothelial cells.

As for the targeting efficiency, surface chemistry is of highest importance (Garcia-Garcia et al., 2005). Even if apparently the difference between the PS 80 coated and uncoated particles is a minimum one, it is to note that the amount of the adsorbed  $\mu$ -peptide opioid is nearly half on the PBCA-NPs carrier in the surfactant-containing system, most probably its micellar trapping reducing the free drug concentration available for transcellular flux. Micellar trapping effects were observed for high surfactant concentrations in formulations based on polymeric micelles as drug delivery systems (Garcia-Garcia et al., 2005). Similar drug loading lowering effect by surfactant coating of NPs carriers was reported by J. C. Olivier (1999).

The efficiency was not so remarkable mainly due to the low drug loading capacity of PBCA-NPs (~20 %). Thus, although plenty of nanoparticles might have entered the central nervous system, according to the mentioned effect of empty particles administration, only a limited amount of peptide is transported across the BBB, and the administered drug dose is known to be important.

These results support previous studies that have demonstrated the delivery of several drugs to the CNS using Tween 80 coated PBCA nanoparticles as a delivery system.

The delivery mechanism remains unclear. Due to the diameter of the nanoparticles, approximately 20 nm, the movement of the MF/NP/PS 80 complex is expected to be the result of a process different from the simple tight junction disruption or modification followed by diffusion.

Earlier studies have shown internalization of PS 80-coated PBCA-NPs by cerebral endothelial cells in vitro, which may be a critical step in the delivery of adsorbed drug to the brain (Kreuter et al., 2003; Schröder and Sabel, 1996). Some investigations indicated that the PS 80-coated PBCA-NPs are inducing changes at cell membranes level, not detected to the same degree for uncoated PBCA nanoparticles (Kreuter et al., 2003; Kreuter et al., 2002; Kreuter and Alyautdin, 2000; Kreuter, 2004; Kreuter and Alyautdin, 1995). According to other authors, PBCA-NPs can increase brain uptake of drugs simply by nonspecifically opening the tight junctions between the brain endothelial cells through a generalized toxic effect as a result of breakdown products of the polymer nanoparticle. However, most authors consider that PBCA nanoparticles exert no generalized toxic effect on BBB cells (Kreuter et al., 2002; Kreuter and Alyautdin, 2000; Kreuter, 2004; Kreuter and Alyautdin, 1995; Alyautdin et al., 2001).

Here, the improved action of MF/NP/PS 80 system as compared to uncoated nanoparticles points on the importance of surface properties modification by surfactant presence and its effect on drug delivery mechanism, and supports the hypothesis that if there are indeed modifications induced at the level of the BBB cells, these changes are mainly due to the used emulsifier (PS 80) and less likely to NPs chemical nature.

However, knowing that different delivery pathways may occur depending on drug, carrier and surfactant nature and ratio, further studies are required to elucidate the BBB permeation mechanism for the studied system.

## **Local silver nanoparticles administration promotes inflammation and hyperalgesia in rats**

Despite the many advantages of nanotechnology, the use of metals at such a small scale comes with some changes in an element's properties. Certain nanomaterials may exhibit significant toxicity to mammalian cells even if they are biochemically inert and biocompatible in bulk size (Shvedova et al., 2005). Upon reaching nanoscale, like other nanomaterials, silver particles exhibit remarkably unusual physicochemical properties and biological activities, which may lead to unpredictable effects and interactions.

*In vitro*, silver nanoparticles are cytotoxic for macrophages and generate free radicals (Yu, 2019; Schins and Knaapen, 2007); also, a recent review emphasizes nanosilver's effect on cells pointing out that accumulation of nanoparticles of silver within the cell leads to oxidizing stress, genotoxicity, and cytotoxicity through apoptosis (Fontenoy and Kamel, 2011). Carlson et al further underlined that the smallest particles have the most toxic effects. In rats, chronic ingestion of silver nanoparticles induced heart and liver dysfunction and promoted systemic oxidation and inflammation (Ebabe Elle et al., 2013). However, scientific papers in the field mainly focus on the effects of inhalation, ingestion or topical use of silver nanoparticles; only few studies explore the effect of direct contact between internal organs/structures and silver nanoparticles and its consequences on local pain and inflammation. In one study performed by Sarhan and Hussein (2014) that explored the effects of intraperitoneal (i.p.) silver nanoparticles administration, results indicated marked citopathological changes in both renal and hepatic tissues, with increased white blood cell count. In our study, nanosilver induced hyperalgesia, but only in an inflammatory setting. There were no differences in pain behavior throughout the 24-h assessments performed after nanosilver administration. After CG administration, however, tissues previously treated with nanosilver exhibited a more pronounced pain-related behavior and more important inflammation. One study indicated that s.c. administration of silver nanoparticles increased infiltration of endothelial cells, VEGF and NO concentration (Kang et al., 2011). Samberg et al. found that human epidermal cells exposed to silver nanoparticles produced an increase in inflammatory cytokines such as IL-1 $\beta$ , IL-6, IL-8 and TNF- $\alpha$  (Samberg, 2010). These findings are in accordance with our results, because both endothelial cell infiltration and increased NO release are associated with both mechanical and thermal sensibility for stimuli in nanosilver infiltrated tissues. As such, potential explanations for our results derive from silver's interaction with local cellular environment, nervous system and inflammation.

One other possible explanation for colloidal silver's hyperalgesic effect is the induction of reactive oxygen species (ROS) - a side-effect of nanosilver reported by *in vitro* studies (Arora et al., 2008). ROS have been more and more implicated in the enhancement of excitatory synaptic transmission (Nishio et al., 2013) and sensitization of dorsal horn neurons (Lee et al., 2012); they are considered to be proalgesic mediators that produce elicit pain by stimulating transient receptor potential channels (Hackel et al., 2013). Also, silver nanoparticles may induce hyperalgesia through cell apoptosis and necrosis (Foldbjerg et al., 2009); this hypothesis is extremely probable, especially since in the present study nanosilver's hyperalgesic effects were noted 24-48 h after s.c. injection. Some studies have also suggested that nanosilver has neurotoxic effects. Due to their small size, nanoparticles are highly mobile in the human body and systemic distribution can occur after inhalation or oral uptake.

Nanoparticles cross the blood-brain barrier, reaching the olfactory bulb and the cerebellum (Borm and Kreyling, 2004) and may have a direct effect on the central nervous system. A study performed by Ganjuri et al recently proved that developmental exposure to nanosilver induces neurotoxicity and apoptosis. Neuronal damage, both in the peripheral and in the central setting, could be another possible explanation for silver nanoparticles' hyperalgesic effect. It is also possible that the pain-related behavior observed after nanosilver administration to be a response to silver's toxicity. Indeed, there have been reports of dermal toxicity after topical application and preferential uptake of nanosilver by several organs and tissues, including the musculo-skeletal system. However, we believe this is not applicable to our results because, on the one hand, in our study nanosilver was administered in an acute setting (single dose) and, on the other hand, because the doses used in our study are significantly smaller than the ones used in toxicity studies. CG administration produced a local edema that persisted until the end of the experiment. Sensibility to thermal and mechanical stimuli increased in all groups shortly after CG injection due to the localized inflammatory response; all groups had similar PWLs 3 and 6 h after CG administration, probably due to the tests' inability to detect differences in pain behavior beneath a certain threshold. However, 24 h after CG injection, thermal sensibility was significantly decreased in the S1 group that had received highconcentration SNPs. In the Randall-Selitto test, the rats still had an increased sensitivity for mechanical stimuli and the Analgesy-Meter was probably still unable to detect fine differences.

The present study indicates that silver nanoparticles had a pronounced pro-inflammatory effect that started 3 hours after silver nanoparticle injection and persisted throughout the experiment, with 20-40% increase in paw edema in the silver nanoparticle groups when compared with control (as assessed by plethysmometry). This difference remained significant even after CG injection. Other nanotechnologies have been associated with increased inflammatory response as well - a study performed by Shvedova et al in mice indicated that pharyngeal aspiration of single-walled carbon nanotubes induced a robust inflammatory response with early onset, progressive fibrosis and granulomas. Reference materials also tested -ultrafine carbon black, SiO<sub>2</sub> or PBS- did not cause thickening of alveolar walls, did not induce formation of granulomas, and resulted in a significantly lower magnitude of inflammatory responses. However, other studies suggest that silver nanoparticles have anti-inflammatory effects and can attenuate allergic airway inflammation and hyperresponsiveness (Park et al., 2010) or decrease inflammation in a postoperative peritoneal adhesion animal model (Wong et al., 2009). A study performed by Wright et al. indicated that nanocrystalline silver-coated dressings lead to diminished production of matrix metalloproteinase, decreased inflammation and more rapid wound healing (Wright et al., 2002). One other study suggested that nanocrystalline silver's topical effect is so strong it may have therapeutic potential for treatment of several inflammatory skin diseases (Bhol et al., 2004). Contrary to the above-mentioned studies, our research indicates that nanosilver has a proinflammatory effect. This can be partly explained by the route of administration used in our study (local subcutaneous administration), that is different from topical dermal application in terms of concentration and kinetics. Also, most studies involving nanosilver and the cellular microenvironment have contradicting results, most likely because toxicity of nanoparticles depends on many factors including size, shape, chemical composition, surface

area and surface charge (Park et al., 2010), which may vary greatly across study and/or geographic region.

This study has a couple of **limitations**. First, the number of tests performed is limited: analgesia and inflammation were evaluated by means of behavioral assessment and plethysmometry. Second, administration of nanosilver was local and not systemic, so we could only assess the activation of local mechanisms and processes. The exact mechanisms by which SNPs induce hyperalgesia and inflammation are not entirely explored and assessed. This study should be followed by another one with similar design, but with systemic nanosilver administration, to see if the hyperalgesic and pro-inflammatory effect persist in this setting.

#### 1.2.3.4 *Conclusions*

- *In vivo* experiments with mice have demonstrated that the analgesic effect of morphiceptin delivered via systemic administration can be obtained only when the morphiceptin drug is preadsorbed onto PBCA-NPs, the effect being enhanced by their coating with polysorbate 80. When formulated according to the described procedure, this  $\mu$ -peptide opioid is delivered to the brain following intravenous administration and exerts a biologic effect which is comparable to direct CNS injection. The presence of free osmotic agents – like dextran – in the administered formulation may influence the delivery efficiency by affecting, most probably, the BBB crossing mechanism.
- Our *in vivo* studies over the analgesic efficacy of the new Ket intercalated into LDHs formulations demonstrated a slightly higher antinociceptive effect, maintained for longer periods of time when compared with Ket alone. Among the two proposed formulations, MgAILDH\_Ket showed a stronger antinociceptive effect that was sustained for a longer period than the ZnAILDH\_Ket.
- Local subcutaneous silver nanoparticle administration leads to an increased inflammatory response and to hyperalgesia. The current results are insufficient for drawing a definitive conclusion regarding nanosilver's local and systemic toxicity. However, the authors believe that, considering the constant increase in silver nanoparticles' biomedical use, the current paper sends a clear warning for the need of urgent more in-depth research on the matter.



## SECTION II – PAST, PRESENT AND FUTURE

### 2.1 CAREER OVERVIEW

Currently, my assignments involve being the Director of the Advanced Research and Development Center for Experimental Medicine (CEMEX) and acting as Senior Scientific Researcher grade I in Pharmacology at the University of Medicine and Pharmacy “Grigore T. Popa” Iasi, Romania. In the following paragraphs, some of the milestones that have contributed to my career development will be presented:

- 2004 - graduate of Medical School in Iasi
- 2010 - board certification in Clinical Pharmacology and PhD in Medicine.
- 2006 - “Outstanding leadership award” from People to People International
- 2008 - EACPT bursary for the Summer School in 2008 and receiver of EACPT Young Investigator Bursary in 2009 (European Association of Clinical Pharmacology and Toxicology).
- 2010 - IASP scholar for the 13th World Congress on Pain, Montreal, Canada
- 2011 - accredited trainer CNFPA, graduate of the training program for occupation by trainer
- 2011 - assistant in Public Relations accredited by CNFPA, graduate of the training program for Public Relations Assistant
- 2011 - graduate of the Human Resource Management in Health course organized by the University of Medicine and Pharmacy “Grigore T. Popa” Iasi
- 2014 and 2015 - President of the Organizing Committee of the Romanian National Pain Congresses
- 2016 - Senior Researcher position at the Centre for the Study and Therapy of Pain, Iasi
- 2016 - Clinical Pharmacologist at Grunenthal (2016).

My research experience has been significantly improved through leading or participating in 16 research projects (7 of which were international grants) totaling over €8 mil. Of these projects, the one that has led to the founding of CEMEX, financed by the Romanian government and the EU, totaling over EUR 6 mil. for 24 months, is the most important accomplishment.

My interest in pharmacology/algesciology and education spans over 12 years of teaching (graduate and post graduate), educational grants and initiatives and publications. Throughout this period, I have contributed to the creation of 8 books and/or book chapters and over 80 published papers, with 178 citations (h-index 9, ISI Thompson). The main research areas on which I plan to maintain my focus are clinical pharmacology, drug development, nanotechnologies, pain, and inflammation.

- Other distinctions during my career include:

- Member of the EACPT, International Association for the Study of Pain (IASP), American College of Clinical Pharmacology (ACCP), Romanian Society of Clinical Pharmacology, Therapeutics and Toxicology; and Treasurer of the Algesiology Association of Romania (AAR).
- Scientific adviser for ISI rated journals: The American Journal of Geriatric Pharmacotherapy, Gender Medicine, Clinical Therapeutics, and Current Therapeutics Research.
- Member of the editorial committee for the International Journal of Anesthesiology Research
- Member of the Editorial Committee for EC Pharmaceutical Science (ECPS) journal.
- Reviewer for the Internal Grants Competition within the University of Medicine and Pharmacy "Grigore T. Popa" Iasi.
- Co-founder & Managing Director of bioROne – the first biotech cluster in Romania.

## **2.2 FUTURE PROJECTS IN THE ACADEMIC AND PROFESSIONAL FIELD**

### **2.2.1 Improvements in the academic and educational areas**

Since 2005, I have been continuously involved in the educational process, either as a researcher or as a teaching assistant then associate professor in the Department of Pharmacology and Algesiology of the "Grigore T. Popa" University of Medicine and Pharmacy, Iasi.

One goal for my career future is developing and improving the research projects initiated in collaboration with young scientists/PhD students/Post-Docs as well as continuing to participate in dissemination activities/congresses dedicated to them as coordinator of scientific papers and moderator of sessions.

As far as of laboratory activities are concerned, CEMEX will actively pursue attracting students to the area of fundamental and applicative research. The ability to plan and execute a real-time, hands-on, data processing and interpretation experiment will be stimulated for as many young doctors as possible.

Also, because many of my former students have later become interested in an academic career and are currently teaching or doing research both in Romania and abroad, I will work on creating and fostering networks of like-minded individuals that will help CEMEX team have access to state of the art laboratories and the latest available techniques for their own research.

One other goal of my future academic and educational development is improving the general level of knowledge of the medical professionals in the field of chronic pain, especially in Romania, where treating this condition is hindered because of several socio-economic regional characteristics, such as:

- thousands of the old, more experienced physicians have left the country for better paid jobs across Europe, leaving the health system with insufficient, novice and poorly trained personnel;
- remaining medical personnel continue to resist and have prejudice regarding the use of opioids for their patients with chronic pain;
- physicians mistakenly overestimate the risk of addiction, are afraid of the regulatory oversight, of the side effects;
- lack or improper medical training programs for the nurses addressing the patient with chronic pain;
- the new opioid law, approved back in 2005, is unknown to most general practitioners working with chronic pain patients.

All these aspects lead to an inadequate pain treatment, making us believe that better education is one part of the solution to this critical health problem.

### 2.2.2 Additional professional development

Although the academic field has always played a crucial role in my future development plans, I believe no professor should limit himself to academic development only. As such, I intend to develop interactions with opinion leaders in the field, in order to include in the international excellence network the pain and nanotechnology research activities within the laboratory where I work. Also, participation in conferences, symposiums, congresses, both European and international will be a constant of my professional activity. Workshop events, training, experience exchanges with prestigious partners will provide the basis for my continuous individual training. These activities will give me the opportunity to access information of immediate interest and with potential for future rapid development, which I will be able to integrate in new research projects and themes.

I will organize, together with experts and opinion leaders in advanced research, new editions of the National Pain Congress (CND by AAR), which will become the reference platform in Romania for the interaction of the four main actors in translational research: fundamental research (academia, research institutes); clinical research (hospitals); education (academia, NGOs, decision-makers); business (SMEs, large pharmaceutical companies).

## 2.3 PERSPECTIVES FOR FUTURE RESEARCH

After finishing my PhD, my research interest was constantly fueled by applying and developing certain techniques that myself and my team learned both in Romania and abroad. As such, one of my main focuses in research was assessing the influence of trace elements on analgesic drugs and pain, either as analgesics or co-analgesics. Over the years, a second area of interest has become more and more prominent – the potential uses of nanotechnology in pain therapy and, together with that, a general interest for innovative drug delivery systems. After receiving funding for upgrading the university's research facilities (2013-2016: POSCCE – A2-02.2.1-2013-1 ID 1896, cod SMIS-CSNR 48880: Advanced Research and Development Center for Experimental Medicine (CEMEX), budget: 30.883.856 lei, Project

Manager: Daniela Drugus, *Expert researcher: Bogdan Ionel Tamba*), my focus began to align with the center's thematic *areas of research*, which are:

Since 2005, I have been continuously involved in the educational process, either as a researcher or as a teaching assistant then associate professor in the Department of Pharmacology and Algesiology of the "Grigore T. Popa" University of Medicine and Pharmacy, Iasi.

One goal for my career future is developing and improving the research projects initiated in collaboration with young scientists/PhD students/Post-Docs as well as continuing to participate in dissemination activities/congresses dedicated to them as coordinator of scientific papers and moderator of sessions.

As far as of laboratory activities are concerned, CEMEX will actively pursue attracting students to the area of fundamental and applicative research. The ability to plan and execute a real-time, hands-on, data processing and interpretation experiment will be stimulated for as many young doctors as possible.

Also, because many of my former students have later become interested in an academic career and are currently teaching or doing research both in Romania and abroad, I will work on creating and fostering networks of like-minded individuals that will help CEMEX team have access to state of the art laboratories and the latest available techniques for their own research.

One other goal of my future academic and educational development is improving the general level of knowledge of the medical professionals in the field of chronic pain, especially in Romania, where treating this condition is hindered because of several socio-economic regional characteristics, such as:

- thousands of the old, more experienced physicians have left the country for better paid jobs across Europe, leaving the health system with insufficient, novice and poorly trained personnel;
- remaining medical personnel continue to resist and have prejudice regarding the use of opioids for their patients with chronic pain;
- physicians mistakenly overestimate the risk of addiction, are afraid of the regulatory oversight, of the side effects;
- lack or improper medical training programs for the nurses addressing the patient with chronic pain;
- the new opioid law, approved back in 2005, is unknown to most general practitioners working with chronic pain patients.

All these aspects lead to an inadequate pain treatment, making us believe that better education is one part of the solution to this critical health problem.

Since 2005, I have been continuously involved in the educational process, either as a researcher or as a teaching assistant then associate professor in the Department of Pharmacology and Algesiology of the "Grigore T. Popa" University of Medicine and Pharmacy, Iasi.

One goal for my career future is developing and improving the research projects initiated in collaboration with young scientists/PhD students/Post-Docs as well as continuing to participate in dissemination activities/congresses dedicated to them as coordinator of scientific papers and moderator of sessions.

As far as of laboratory activities are concerned, CEMEX will actively pursue attracting students to the area of fundamental and applicative research. The ability to plan and execute a real-time, hands-on, data processing and interpretation experiment will be stimulated for as many young doctors as possible.

Also, because many of my former students have later become interested in an academic career and are currently teaching or doing research both in Romania and abroad, I will work on creating and fostering networks of like-minded individuals that will help CEMEX team have access to state of the art laboratories and the latest available techniques for their own research.

One other goal of my future academic and educational development is improving the general level of knowledge of the medical professionals in the field of chronic pain, especially in Romania, where treating this condition is hindered because of several socio-economic regional characteristics, such as:

- thousands of the old, more experienced physicians have left the country for better paid jobs across Europe, leaving the health system with insufficient, novice and poorly trained personnel;
- remaining medical personnel continue to resist and have prejudice regarding the use of opioids for their patients with chronic pain;
- physicians mistakenly overestimate the risk of addiction, are afraid of the regulatory oversight, of the side effects;
- lack or improper medical training programs for the nurses addressing the patient with chronic pain;
- the new opioid law, approved back in 2005, is unknown to most general practitioners working with chronic pain patients.

All these aspects lead to an inadequate pain treatment, making us believe that better education is one part of the solution to this critical health problem.

Since 2005, I have been continuously involved in the educational process, either as a researcher or as a teaching assistant then associate professor in the Department of Pharmacology and Algesiology of the "Grigore T. Popa" University of Medicine and Pharmacy, Iasi.

One goal for my career future is developing and improving the research projects initiated in collaboration with young scientists/PhD students/Post-Docs as well as continuing to participate in dissemination activities/congresses dedicated to them as coordinator of scientific papers and moderator of sessions.

As far as of laboratory activities are concerned, CEMEX will actively pursue attracting students to the area of fundamental and applicative research. The ability to plan and execute a real-time, hands-on, data processing and interpretation experiment will be stimulated for as many young doctors as possible.

Also, because many of my former students have later become interested in an academic career and are currently teaching or doing research both in Romania and abroad, I will work on creating and fostering networks of like-minded individuals that will help CEMEX team have access to state of the art laboratories and the latest available techniques for their own research.

One other goal of my future academic and educational development is improving the general level of knowledge of the medical professionals in the field of chronic pain, especially in Romania, where treating this condition is hindered because of several socio-economic regional characteristics, such as:



- thousands of the old, more experienced physicians have left the country for better paid jobs across Europe, leaving the health system with insufficient, novice and poorly trained personnel;
- remaining medical personnel continue to resist and have prejudice regarding the use of opioids for their patients with chronic pain;
- physicians mistakenly overestimate the risk of addiction, are afraid of the regulatory oversight, of the side effects;
- lack or improper medical training programs for the nurses addressing the patient with chronic pain;
- the new opioid law, approved back in 2005, is unknown to most general practitioners working with chronic pain patients.

All these aspects lead to an inadequate pain treatment, making us believe that better education is one part of the solution to this critical health problem.

- Fundamental Research Area of the drug: Study areas from the discovery of new target molecules up to the assessment use of a drug at experimental animal level;
- Preclinical research of pharmacological agents;
- Advanced Medical Imaging Area: use of medical imaging techniques for exploring physiological or pathological processes, pharmacogenetic exploration or mechanisms of action of new molecules; development of new products (contrast agents, radiomarkers, and immunomarkers) to be transferred to industry.

In the following subsections I will present the three main research directions that have evolved from my work so far and that will be the focus of the next grant applications I will submit.

### 2.3.1 Translating basic research to pain management practice

While being a PhD student, my research was focused on investigating the influence of some trace elements and drug associations on behavior and pain. Trace elements' pathology is often overlooked in research and current data is at best insufficient and often controversial. This is even more obvious when one takes into consideration the possible relations between trace elements and neural signal transmission or pain modulation. Recent data indicate that there are some intra and extra cellular changes of the trace elements' transport during general or local anesthesia or during presurgery analgesia (as it's the case for zinc and selenium). As such, investigating the relationship between trace elements, analgesics and pain has been a constant source of interest for me. My publications and grants so far have been focused on up-to-date information about trace elements, with emphasis on their relationship with nociception and the main data on physicochemical properties, absorption, transport, metabolism, deficiency, toxicity and the biological role of each of the main trace elements (zinc, magnesium, manganese, cobalt, copper, cadmium, nickel and molybdenum). Special attention

was given to the relationship between each trace element and the nociceptive process, trying to present complex data and all the current theories. In our research laboratory, we have used different strains of mice or rats in order to investigate the effects on the pain modulation, transmission and perception, of various trace elements salts and drugs (Zinc sulphate, Zinc citrate, Magnesium chloride, Manganese chloride, Cobalt chloride, Copper chloride, Copper sulphate, Cadmium chloride, Nickel chloride, Sodium molybdate, Acetaminophen). We have assessed both peripheral pain (writhing test) and central pain (hot plate tail flick) together with the effect of trace elements on spontaneous behavior.

Analyzing the results obtained in the analgesic tests (thermoalgesic and chemoalgesic) for the eight trace elements studied has led to the following conclusions:

1. *Magnesium* has an antinociceptive effect in analgesic testing, with increased values for the writhing test, as well a mild sedative and anxiolytic effect.
2. *Acetaminophen and magnesium* drug association does not produce an overall superior effect when compared to acetaminophen alone. Sedation levels are similar.
3. *Zinc* has a moderate antinociceptive effect, more visible in the writhing test, and is not associated with significant behavior changes.
4. *Manganese* has an antinociceptive action, with important changes in hot plate and writhing test, but no significant effect on the animal's mobility.
5. *Cobalt* has an antinociceptive activity with moderate values in thermoalgesic testing, and increased effect on the writhing test. Behavioral testing showed sedative and anxiolytic actions.
6. *Molybdenum* has a significant antinociceptive activity in the writhing test and a mild sedative effect.
7. *Nickel* displays a moderate antinociceptive action in thermoalgesic testing with a dual effect on the writhing test: a short antinociceptive activity followed by a prolonged, hyperalgesic effect, possible due to the variable modulation of various calcium channel subtypes. No behaviors changes were noticed.
8. *Cadmium* has a moderate antinociceptive effect in thermoalgesic testing and a significant analgesic effect in the writhing test. An anxiolytic action was observed.
9. *Copper* has a dose-dependent antinociceptive effect in tail flick and hot plate testing, as well as an anxiolytic effect.
10. *All the trace elements* tested displayed in acute testing various degrees and durations of antinociceptive actions, as seen in the thermic and chemical pain testing.

These findings have received significant interest in the international research community as indicated by the high-impact factor journals in which we have published our results. The next logical step for this research interest is translating what we have seen in rodents to clinical practice. This objective can be easily accomplished because adding supplements to the analgesic treatment does not put the test subject at significant risk. In order to pursue this objective, I have started a collaboration with the Palliative Care department of the Regional Institute of Oncology Iasi and have begun creating a clinical research protocol. The aim of our clinical study is to assess if adding a magnesium supplement to the standard

analgesic treatment of pain in cancer patients can lead to decreasing analgesic requirement or increasing analgesic efficacy.

The study objectives are:

1. to assess the incidence of refractory pain in cancer patients admitted to the Palliative Care department of the Regional Institute of Oncology Iasi
2. to evaluate potential benefits of adding a Magnesium supplement to the standard analgesic therapy that cancer patients with refractory pain receive.

The study will have a prospective design and pain will be assessed by means of questionnaires (BPI) and the visual analogue scale before and after intervention. The design of the study requires the creation of two patient groups – a control group that will receive analgesic medication only and the intervention group that will receive analgesic medication and Magnesium supplementation. Currently, we have written a clinical research protocol and we intend to submit this project for ethical approval in March 2019.

Algesiology (the study and therapy of pain) is an interdisciplinary science. The present tendencies of pain research are to use a dual approach, both from a physiologic and a pharmacologic point of view. The physiological approach in identifying new analgesic agents has a special significance. In this respect, using pharmacological doses of substances involved in physiological circuits of pain modulation could be useful for pain treatment. Identifying such agents could lead to reduced side effects when compared to classical analgesics. Apart from the clinical project I have presented above, I intend to continue identifying novel analgesics or innovative drug combinations through basic research and, as soon as possible, ensuring the transition of positive results from bench to bedside.

### 2.3.2 Advanced drug delivery systems and nanotechnology

The pharmaceutical industry impacts countless lives around the world by researching and developing lifesaving and life-enhancing products. Operating sustainably is reflected in a commitment to supply high-quality and safe products, while developing new and improved therapies to address unmet medical needs.

Nanomedicine is the controlled application of nanotechnology to achieve breakthrough innovations in healthcare. Physical properties of materials change at the nanometer scale and nanomedicine exploits these specific properties to change healthcare treatment paradigms. Nanoparticles can already be used as innovative contrast agents to improve the performances of imaging techniques as Magnetic Resonance Imaging (MRI), Computed Tomography (CT) scan, and fluorescence imaging.

Nanoparticles can also be used to enhance the signal and better detect cancer biomarkers. These are molecules indicative of the presence of cancer in the body, whether produced by the tumour itself or by the body as a specific response to the presence of the tumour. Last, but certainly not least, nanomedicine products can improve the efficiency of chemical and biological based treatments, e.g., nano-carriers can encapsulate drugs to enable them to reach their target with higher accuracy, thus simultaneously improving treatment efficiency and reducing drug-related toxicity.

In 2016, the nanomedicine market was estimated to be between \$90 and \$120 billion and was projected to steadily increase. 230 nanomedicine products were identified on the

market or under clinical development for different therapeutic areas including cancer, diabetes, cardiovascular, neurodegenerative, osteo-articular, infectious diseases, etc.

Nanotherapeutics exhibit major benefits with respect to unmodified drugs, including improved half-life, more efficient targeting, and reduced side effects. However, only a few nanotherapeutics have reached the commercial level, most still being in the investigational phase. Due to my research interest in nanotechnologies, I intend to continue working in this area and to apply for funding together with my partners. In order to achieve this goal, I plan to be more involved in the bioROne cluster I helped establish in 2012.



*bioROne* is the first joint biotech initiative in North-East (NE) Romania, founded in 2012, connecting a striving academic and research community, industry and government.

BioROne was founded by a selected group of 12 members, which includes individuals from top universities and research centres, key national or regional industry players, development agencies, as well as high profile international advisors and strategic partners.

*bioROne* aims to act as a network and common platform to help maximise the innovation potential of NE Romania, and shorten the process from an original idea to a product.

*Key objectives:* shift the innovation culture from education to economy; explore and develop the highly-trained human resource pool that exists in the region; support successful collaborations between members of the cluster, as well as between the cluster and external partners (e.g. investors); move from small single-entity projects, to fewer large multi-partner projects, with higher eligibility for funding; help with advice on finance opportunities and funding programs; support entrepreneurial initiatives in the biotech space; represent the region's innovation hub at the international level; attract new partners and investments to the region.

*Research areas:* applications of bioinformatics; drug production; pharmacogenomics; gene therapy, genetic testing; nanotechnologies, bioengineering; health services, and human diagnosis; biopharmaceuticals and equipment manufacturers.

Together with these partners, I will focus on three main projects reflecting different areas of nanotechnology and advanced drug delivery – cancer research, combating counterfeit drugs and new analgesic formulations.

#### **a. cancer research**

Effective retention of nano-theranostics in diseased tissues, especially neoplastic ones, is one of the essential prerequisite for their successful applications, along with non-toxic, bio-compatible and stealth properties. Customised active retention and accumulation of nano-assemblies in the tumors to obtain a specific therapeutic concentration diminishes the risks of secondary effects on healthy organs.

A combined methodology is foreseen to achieve active nano-assembly's retention, by conferring them a selective high affinity by binding to altered neoplastic cells, i.e. coupling

with tumor antigen specific ligands - like monoclonal antibodies, and due to passive accumulation via EPR effect.

The main research purpose will be to design and develop several classes of bio-compatible – targets and thermo-activable - nano-therapeutics, for the improved treatment of deadly human primary and secondary tumors, by means of development of nano-magnetic carrier particles, coupled with monoclonal antibodies to inflamed endothelial (P-selectin) and/or sub- endothelial (collagen IV, I) antigens.

We have obtained some promising data in the field during our research performed on hepatic tumors (2012-2014 - ERA-Net EuroNanoMed JTC – Chemohyperthermal delivery – Combined chemo-hyperthermal delivery of hepatic tumors, based on microwave-activated subendothelial-targeted magnetic nano-assemblies), which is a strong argument for additional funding. Also, due to the new and improved equipment acquired through CEMEX, we are now better capable of performing complex imaging studies to assess biodistribution and effectiveness of these novel nanoparticles.

#### **b. combating counterfeit drugs**

Medicine counterfeiting has become a global threat since 1985, involving networks of manufacture and distribution. Counterfeiting, according to the World Health Organization (WHO) definition is the deliberate or intentional (fraudulently) nature of the mislabelling or adulteration of a drug.

Counterfeit products can be found in any country and often look identical to authentic versions, making them difficult to detect, particularly for patients. Counterfeiting can apply to both branded and generic products. A counterfeit drug can contain the correct, insufficient or a higher amount of active ingredient, the wrong ingredients, or without active ingredients or with fake packaging.

Despite the potentially devastating health repercussions involved, legal sanctions are often inappropriate or simply not applied. In this context, international cooperation is needed to prevent the spread of counterfeiting. Moreover effort is urgently required on the legal, enforcement and scientific levels.

Up to now, a wide variety of nanomaterials: carbon dots, quantum dots, anisotropic nanoparticles, gold nanorods, plasmonic nanoparticles, one-dimensional photonic crystals based on alumina, magnetic nanoparticles, nanocomposites based on nanosized cellulose fibrils and up-converting nanoparticles, have been used for anti-counterfeiting of various products. In spite of this effort, a wide-ranging nanomaterials-based authentication method is not yet available in the pharmaceutical field.

In this context, we are currently working on a project that aims to design anti-counterfeit sustainable strategies based on nanotechnology, to combat this global threat to public health and help ensure the integrity of original products.

The project aims to develop a range of nanometric based polymer neutral powders for the invisible marking of drug products. This technology will be designed to counter the problem of counterfeiting. The obtained markers aim to emit colour when illuminated with a specific type of ultraviolet light. This marking process is guaranteed indelible, difficult to copy or alter and has no effects in any way.

### c. new analgesic formulations

Chronic pain is a very important public health problem, with more and more individual suffering from different types of painful conditions. Advances in this area can mostly be achieved through identifying novel drug classes that better target processes involved in pain perception and transmission or through improving drug delivery systems as to minimize side effects and maximize efficacy.

In this field, my research interest focuses on employing nanotechnologies for new drug formulations in topical administration. So far, our team has successfully obtained a patent for a novel beta-cyclodextrine-based topical lidocaine formulation. Currently, we are working on a research proposal to further refine our patent and translate our findings in clinical practice.

#### 2.3.3 Networks for advanced preclinical and clinical imaging studies

Thanks to the developments in Medical Imaging, diagnosis is earlier than ever. Physicians have more information and insight. Care is less invasive and less painful for patients. Access to tests and treatments is easier as imaging procedures are available in convenient settings, such as independent imaging centers. In addition, patient outcomes—from fewer complications to saved lives—are dramatically improved. And we are not at the end of our journey, yet! The “Next Generation” of Medical Imaging is just here out of the integration and cross-disciplinary use of NanoMedicine, Pharmacological breakthroughs, Biotechnologies for healthcare and ICT combined with standard Medical Imaging evolution.

Unfortunately, the healthcare sector is quite diverse and collaboration has been difficult as a result, so the challenge is to build expertise in the development of integrated systems that address unmet clinical needs while providing a solid and consistent network of research and development groups.

The North-East Innovative Regional Cluster for Structural and Molecular Imaging (IMAGO-MOL), was established like a nongovernmental, non-profit organization that aims to support the growth of scientific competitiveness of its members and the competitiveness of the North East Region in the field of Medical Imaging by developing a framework of cooperation based on diversification and optimization of services in this area.

The cluster was established on 2012, as a result of the project AMI4Europe, by joint decision and contribution of its founding members - University of Medicine and Pharmacy Iasi „Grigore T. Popa”, North East Regional Development Agency, Sf. Spiridon Emergency Clinical Hospital of Iasi, Regional Oncological Institute and Romsoft SRL Iași, in order to develop a better collaboration in the use of innovative medical imaging and implementing better health care services by establishing a framework to improve efficiency, quality, productivity and visibility of these members. Subsequently, joined the cluster as associated members: Iași County Council, Scientific and Technological Park TEHNOPOLIS, Technical University “Gheorghe Asachi” Iași, Al. I. Cuza University Iași, Emergency Clinical Hospital “Prof. Dr. N. Oblu” and 10 SMEs from the IT and health sector (Phoenix Diagnostic Clinic, Micromedica Medical Center SRL Piatra Neamț, Scan Expert Roman, X Med Center Iași,



Unmet clinical needs while providing a solid and consistent network of research and development groups.

Optim Diagnostic Botoșani, Tissuegnostics Romania Iași, Centrul Medical Sapientek Buzău, Coramed Suceava, Serv Sistem Iași, Shopfit Online Iași). With the aid of this cluster, combined with the performant imaging capabilities of CEMEX, I intend to initiate and develop medical studies in vivo and in vitro, fundamental and applied. The studies will track the physiological and pathological medical aspects through molecular imaging methods, functional (eg. scintigraphy) and structural proper resolution (CT, MRI, ultrasound etc.). Also, I will develop a platform for molecular and structural medical imaging competitive in the context of medical imaging on national and international level.

## BIBLIOGRAPHIC REFERENCES

1. Aelenei N, Popa MI, Novac O et al. Tannic acid incorporation in chitosan-based microparticles and in vitro controlled release. *J Mater Sci Mater Med* 2009; 20:1095–102.
2. Abbott NJ, Romero IA. Transporting therapeutics across the blood-brain barrier. *Mol. Med. Today* 1996; 2:106-113.
3. Abdelwahed W, Degobert G, Stainmesse S et al. Freeze-drying of nanoparticles: formulation, process and storage considerations. *Adv. Drug Deliv. Rev* 2006; 58(15):1688-713.
4. Akasov R, Borodina T, Zaytseva E et al. Ultrasonically Assisted Polysaccharide Microcontainers for Delivery of Lipophilic Antitumor Drugs: Preparation and in Vitro Evaluation. *Applied Materials & Interfaces* 2015; 7:16581–16589.
5. Allen GV, Pronych SP. Trigeminal autonomic pathways involved in nociception-induced reflex cardio-vascular responses. *Brain Res* 1997; 754:269-278.
6. Alyautdin RN, Reichel A, Löbenberg R et al. Interaction of poly(butylcyanoacrylate) nanoparticles with the blood-brain barrier in vivo and in vitro. *J. Drug Target* 2001; 9:209-221.
7. Alyautdin RN, Tezikov EB, Range P et al. Significant entry of tubocurarine into the brain of rats by adsorption to polysorbate study. *J Microencapsul* 1998; 15:67–74.
8. Angstadt JD, Friesen WO. Synchronized oscillatory activity in leech neurons induced by calcium channel blockers. *J. Neurophysiology* 1991; 66(6):1858-73.
9. Ansari AA, Khan A, Labis JP, Alam M, Aslam Manthrammel M, Ahamed M, Akhtar MJ, Aldalbahi A, Ghaithan H. Mesoporous multi-silica layer-coated Y2O3:Eu core-shell nanoparticles: Synthesis, luminescent properties and cytotoxicity evaluation. *Mater Sci Eng C Mater Biol Appl.* 2019; 96:365-373.
10. Argyo C, Weiss V, Bräuchle C et al. Multifunctional mesoporous silica nanoparticles as a universal platform for drug delivery. *Chem. Mater* 2014; 26:435–451.
11. Babazadeh M. Synthesis and study of controlled release of ibuprofen from the new acrylic type polymers. *Int J Pharm* 2006; 316:68–73.
12. Balan V, Verestiuc L. Strategies to improve chitosan hemocompatibility: A review, *European Polymer Journal* 2014; 53:171–188.
13. Banerjee T, Singh AK, Sharma RK et al. Labeling efficiency and biodistribution of Technetium-99m labeled nanoparticles: interference by colloidal tin oxide particles. *Int. J. Pharm* 2005; 289:189–195.
14. Barbee NC, Ganio K, Swearer SE. Integrating multiple bioassays to detect and assess impacts of sublethal exposure to metal mixtures in an estuarine fish. *Aquat Toxicol* 2014; 152:244–25.
15. Barnes CA, Elsaesser A, Arkusz J et al. Reproducible comet assay of amorphous silica nanoparticles detects no genotoxicity. *Nano Lett.* 2008; 8:3069– 3074.

16. Barritt GJ. Receptor-activated  $\text{Ca}^{2+}$  inflow in animal cells: a variety of pathways tailored to meet different intracellular  $\text{Ca}^{2+}$  signalling requirements. *Biochem. J.* 2009; 337(2):153–169.
17. Battaglia V, Compagnone A, Bandino A et al. Cobalt induces oxidative stress in isolated liver mitochondria responsible for permeability transition and intrinsic apoptosis in hepatocyte primary cultures. *The International Journal of Biochemistry & Cell Biology* 2009; 41:586–594.
18. Begon S, Pickering G, Eschalier A et al. Magnesium increases morphine analgesic effect in different experimental models of pain. *Anesthesiology* 2002; 96:627–632.
19. Beldie C, Dumitriu S, Aelenei N et al. Polymers LX. Kinetics of delayed release neomycin-xanthan complex. *Biomaterials* 1989; 10:622–4.
20. Bertholon I, Vauthier C, Labarre D. Complement activation by core-shell poly (isobutylcyanoacrylate)-polysaccharide nanoparticles: influences of surface morphology, length, and type of polysaccharide. *Pharm. Res* 2006; 23:1313-1323.
21. Biernat P, Musiał W, Gosławska D. The impact of selected preparations of trace elements - magnesium, potassium, calcium, and zinc on the release of diclofenac sodium from enteric coated tablets and from sustained release capsules. *Advances in Clinical and Experimental Medicine* 2014; 23(2):205-213.
22. Bird ED, Anton AH, Bullock B. The effect of manganese inhalation on basal ganglia dopamine concentrations in rhesus monkey. *Neurotoxicology* 1984; 5(1):59–65.
23. Bonina FP, Puglia C, Barbuzzi T et al. In vitro and in vivo evaluation of polyoxyethylene esters as dermal prodrugs of Ketoprofen, naproxen and diclofenac. *Eur J Pharm Sci* 2001; 14:123–34.
24. Bosio VE, Basu S, Abdulla F et al. Encapsulation of Congo Red in carboxymethyl guar gum–alginate gel microspheres, *Reactive & Functional Polymers* 2014; 82:103–110.
25. Braz R, Hechenleitner AA, Cavalcanti OA. Extraction, structural modification and characterization of Lotus Roots polysaccharides (*Nelumbo nucifera* Gaertn) excipient with potential application in modified drug delivery systems. *Latin American Journal of Pharmacy* 2007; 26:706-10.
26. Bresink I, Ebert B, Parsons CG et al. Zinc changes AMPA receptor properties, results of binding studies and patch clamp recordings. *Neuropharmacology* 1996; 35:503–509.
27. Brill S, Sadgwick PM, Hamann W et al. Efficacy of intravenous magnesium in neuropathic pain. *Br J Anaesth* 2002; 89:711–714.
28. Carlino S. The intercalation of carboxylic acids into layered double hydroxides: a critical evaluation and review of the different methods. *Solid State Ionics* 1997; 98:73–84.
29. Carstens E. Quantitative experimental assessment of pain and hyperalgesia in animals and underlying neural mechanisms. In: Carli G, Zimmermann M, editors. *Brain Research* 1996; 17–31.
30. Cavani F, Trifiro F, Vaccari A. Hydrotalcite-type anionic clays: preparation, properties and application. *Catal Today* 1991; 11:173–301.

31. Cavun S, Goktalay G, Millington WR. The hypotension evoked by visceral nociception is mediated by delta opioid receptors in the periaqueductal gray. *Brain Res.* 2004; 101(9):237–45.
32. Cazanga V, Hernandez A, Morales B, Pelissier T, Constandil L. Antinociception Induced by Copper Salt Revisited: Interaction with Ketamine in Formalin-Induced Intraplantar and Orofacial Pain in Mice. *J Oral Facial Pain Headache.* 2018;32(3):247–257.
33. Chaurasia M, Chourasia MK, Jain NK et al. Cross-Linked Guar Gum Microspheres: a viable approach for improved delivery of anticancer drugs for the treatment of colorectal cancer. *Journal of American Association of Pharmaceutical Science Technology* 2006; 7:143-151.
34. Chen CC, Zimmer A, Sun WH et al. A role for ASIC3 in the modulation of high-intensity pain stimuli. *Proc Natl Acad Sci USA* 2002; 99:8992–8997.
35. Chen JZ. Chemistry and metabolism of lipids. In: Q. H Chen (Ed.), *Biochemistry.* People’s Health Publishing House 1999; 256-260.
36. Cho GS, Han MW, Lee B. Zinc deficiency may be a cause of burning mouth syndrome as zinc replacement therapy has therapeutic effects. *Journal of oral pathology & medicine* 2010; 39(9):722–7.
37. Costantino U, Ambrogi V, Nocchetti M et al. Hydrotalcitelike compounds: versatile layered hosts of molecular anions with biological activity. *Microporous Mesoporous Mater* 2008; 107:16–149.
38. Costantino U, Casciola M, Massinelli L et al. Intercalation and grafting of hydrogen phosphates and phosphonates into synthetic hydrotalcites and a.c.-conductivity of the compounds thereby obtained. *Solid States Ionics* 1997; 97:203–12.
39. Couvreur P, Kante B, Roland M et al. Polycyanoacrylate nanocapsules as potential lysosomotropic carriers: preparation, morphological and sorptive properties. *J. Pharm. Pharmacol.* 1979; 31:331-332.
40. Cunha MP, Machado DG, Bettio LE et al. Interaction of zinc with antidepressants in the tail suspension test. *Progress in Neuro-Psychopharmacology & Biological Psychiatry*, 2008; 32(8):1913–20.
41. Cunha PL, Paula RC, Feitosa JP. Purification of guar gum for biological applications, *International Journal of Biological Macromolecules* 2007; 41:324–331.
42. Dacey MJ. Hypomagnesemic disorders. *Critical Care Clinics* 2001; 17(1):155–73.
43. Dashevsky A, Mohamad A. Development of pulsatile multiparticulate drug delivery system coated with aqueous dispersion Aquacoat ECD. *Int J Pharm* 2006; 318:124–31.
44. De Oliveira GS, Castro-Alves LJ, Khan JH, et al. Perioperative systemic magnesium to minimize postoperative pain: a meta-analysis of randomized controlled trials. *Anesthesiology* 2013; 119(1):178–90.
45. del Arco M, Cebadera E, Gutierrez S et al. Mg, Al layered double hydroxides with intercalated indomethacin: synthesis, characterisation and pharmacological study. *J Pharm Sci* 2004; 93:1649–58.

46. del Arco M, Fernandez A, Martín C et al. Intercalation of mefenamic and meclofenamic acid anions in hydrotalcite-like matrices. *Appl Clay Sci* 2007; 36:133–40.
47. del Arco M, Fernandez A, Martín C et al. Release studies of different NSAIDs encapsulated in Mg, Al, Fe-hydrotalcites. *Appl Clay Sci* 2009; 42:538–44.
48. del Arco M, Gutierrez S, Martín C et al. Synthesis and characterisation of layered double hydroxides (LDH) intercalated with non-steroidal anti-inflammatory (NSAID) drugs. *J. Solid State Chem* 2004; 177:3954–62.
49. Del Gobbo LC, Imamura F, Wu JH et al. Circulating and dietary magnesium and risk of cardiovascular disease: a systematic review and meta-analysis of prospective studies. *The American Journal of Clinical Nutrition* 2013; 98(1):160–73.
50. del Hoyo C. Layered double hydroxides and human health: an overview. *Appl Clay Sci* 2007; 36:103–21.
51. Derbyshire SWG. Assessing pain in animals. In: Basbaum AI, Kaneko A, Shepherd GM, Westheimer G, Albright TD, Masland RH, Dallos P, Oertel D, Firestein S, Beauchamp GK, Bushnell MC, Kaas JH, Gardner Esther, editors. *The senses: a comprehensive reference*. Oxford: Elsevier Inc 2008; 969–74.
52. Dhillon S. Tramadol/paracetamol fixed-dose combination: a review of its use in the management of moderate to severe pain. *Clinical Drug Investigation* 2010; 30(10):711–38.
53. Digigow RG, Dechézelles JF, Dietsch H et al. Preparation and characterization of functional silica hybrid magnetic nanoparticles. *J. Magn. Magn. Mater* 2014; 362, 72–79.
54. Dodi G, Hritcu D, Popa MI. 2011. Carboxymethylation of guar gum: synthesis and characterization. *Cellulose Chemistry and Technology* 2011; 45, 171-176.
55. Dreyer M, Marwinski D, Wolf N et al. Acid suppression profile of hydrotalcite in man. *Arzneim-Forsch* 2011; 41:738–41.
56. Dubé L, Granry JC. The therapeutic use of magnesium in anesthesiology, intensive care and emergency medicine: a review. *Canadian Journal of Anaesthesia* 2003; 50(7):732–46.
57. Dulong V, Lack S, Le Cerf D et al. Hyaluronan-based hydrogels particles prepared by crosslinking with trisodium trimetaphosphate. *Synthesis and characterization, Carbohydrate Polymers* 2004; 57:1–6.
58. Durlach J, Bac P, Bara M et al. Physiopathology of symptomatic and latent forms of central nervous hyperexcitability due to magnesium deficiency, a current general scheme. *Magnesium Res* 2000; 13:293–302.
59. Eisenberg DM, Davis RB, Ettner SL et al. Trends in alternative medicine use in the United States, 1990–1997: results of a follow-up national survey. *JAMA* 1998; 280:1569–1575.
60. Engelman HS, Allen TB, Macdermott AB. The distribution of neurons expressing calcium-permeable AMPA receptors in the superficial laminae of the spinal cord dorsal horn. *J Neurosci* 1999; 19(6):2081-9.
61. Fawcett WJ, Haxby EJ, Male DA. Magnesium, physiology and pharmacology. *Br J Anaesth* 1999; 83:302–320.

62. Felsby S, Nielsen J, Arendt-Nielsen L et al. NMDA receptor blockade in chronic neuropathic pain, a comparison of ketamine and magnesium chloride. *Pain* 1995; 64:283–291.
63. Fisher JL, Macdonald RL. The role of an  $\alpha$  subtype  $M_2$ - $M_3$  his in regulating inhibition of GABAA receptor current by Zinc and other divalent cations. *J. Neurosci* 1998; 18:2944.
64. Friese A, Seiller E, Quack G et al. Increase of the duration of the anticonvulsive activity of a novel NMDA receptor agonist using poly (butylcyanoacrylate) nanoparticles as a parenteral controlled release system. *Eur. J. Pharm. Biopharm.* 2000; 49:103-109.
65. Frunza M, Hritcu D, Popa MI. Intercalation of salicylic acid into ZnAl layered double hydroxides by ion-exchange and coprecipitation method. *J Optoelectron Adv Mater* 2009; 11:528–34.
66. Frunza M, Lisa G, Zonda R, Popa MI. Intercalation of Ketoprofen into Mg-Al hydrotalcites. Synthesis and characterization. *Rev Chim* 2008; 59:409–12.
67. Frunza M, Popa MI, Hulea V. Controlled release of salicylate from the lamella Zn-Al layered double hydroxide nanocomposite. *J Optoelectron Adv Mater* 2007; 9:3376–8.
68. Gao K, Jiang MX. Influence of particle size on transport of methotrexate across blood brain barrier by polysorbate 80-coated polybutylcyanoacrylate nanoparticles. *Int J Pharm* 2006; 310, 213-219.
69. Garcia-Garcia E, Andrieux K, Gilb S et al. Colloidal carriers and blood-brain barrier (BBB) translocation: a way to deliver drugs to the brain? *Int. J. Pharm* 2006; 298, 274-292.
70. Garg M, Garg BR, Jain S et al. Radiolabeling, pharmacoscintigraphic evaluation and antiretroviral efficacy of stavudine loaded  $^{99m}\text{Tc}$  labeled galactosylated liposomes. *Eur. J.Pharm. Sci.* 2008; 33, 271–281.
71. Gliko-Kabir I, Yagen B, Penhasi A et al. Phosphated crosslinked guar for colonspecific drug delivery: I. Preparation and physicochemical characterization, *Journal of Controlled Release* 2008; 63, 121–127.
72. Gong H, Liu M, Chen J et al. Synthesis and characterization of carboxymethyl guar gum and rheological properties of its solutions, *Carbohydrate Polymers* 2010; 88, 1015–1022.
73. Gonzales-Guerrero M, Arguello JM.. Mechanism of Cu transporting ATP-ases, soluble CuI chaperones directly transfer CuI to transmembrane transport sites. *Proc Natl Acad Sci USA* 2008; 195:5992–5997.
74. Gromiec JP, Kupczewska-Dobecka M, Jankowska A, et al. Predictive models for the assessment of occupational exposure to chemicals: A new challenge for employers. *Med Pr* 2013; 64(5):699–716.
75. Grond S, Sablotzki A. Clinical pharmacology of tramadol. *Clinical Pharmacokinetics* 2004; 43(13):879–923.
76. Guilarte TR, Chen MK. Manganese inhibits NMDA receptor channel function, implications to psychiatric and cognitive effects. *Neurotoxicology* 2007; 28:1147–1152.

77. Gulyaev AE, Gelperina SE, Skidan IN et al. Significant transport of doxorubicin into the brain with polysorbate 80-coated nanoparticles. *Pharm. Res.* 1999; 16:1564-1569.
78. Gumilar F, Agotegaray M, Bras C et al. Anti-nociceptive activity and toxicity evaluation of Cu(II)-fenoprofenate complexes in mice. *Eur J Pharmacol* 2015; 675:32–39.
79. Gunter TE, Gavin CE, Aschner M et al. Speciation of manganese in cells and mitochondria: a search for the proximal cause of manganese neurotoxicity. *Neurotoxicology* 2006; 27(5):765–76.
80. Guo D, Ling J, Wang MH et al. Physical interaction and functional coupling between ACDP4 and the intracellular ion chaperone COX11, an implication of the role of ACDP4 in essential metal ion transport and homeostasis. *Mol. Pain.* 2005; 1:15.
81. Gupta AP, Verma DK. Preparation and characterization of carboxymethyl guar gum nanoparticles, *International Journal of Biological Macromolecules* 2004; 68:247–250.
82. Hamann SR, Holtman JR, Martin WR. Analgesic actions of local anesthetics and cobalt chloride in the rat brain stem. *Pharmacol. Biochem.* 1992; 43:925-927.
83. Hasanein P, Parviz M, Keshavarz M et al. Oral magnesium administration prevents thermal hyperalgesia induced by diabetes in rats. *Diabetes Res Clin Pract* 2006; 75:17–22.
84. Hazell AS. Astrocytes and manganese neurotoxicity. *Neurochemistry International* 2002; 41(4):271–277.
85. He LS, Jiang B, Wang K. Determination of the degree of the substitution of hydroxyethyl guar gum. *Carbohydrate Polymers* 2008; 72, 557–560.
86. Heyneman CA, Lawless-Liday C, Wall GC. Oral versus topical NSAIDs in rheumatic disease: a comparison. *Drugs* 2006; 60:555–74.
87. Holzinger S, Anke M, Röhrig B et al. Rates of intestinal absorption of molybdenum in humans. *Analyst* 1998; 123:447.
88. Hong H, Zhang Y, Sun J et al. Molecular imaging and therapy of cancer with radiolabeled nanoparticles. *Nano Today* 2009; 4, 399–413.
89. Honkanen V, Konttinen YT, Sorsa T et al. Serum zinc, copper and selenium in rheumatoid arthritis. *J Trace Elem Electrolytes Health Dis* 1999; 5:261–263.
90. Hsiao B, Mihalak KB, Maglebyet KL al., 2008. Zinc potentiates neuronal nicotinic receptors by increasing burst duration. *Journal of Neurophysiology* 2008; 99(2):999–1007.
91. Huk OL, Catelas I, Mwale F et al. Induction of apoptosis and necrosis by metal ions in vitro. *J. Arthroplasty* 2004; 19-84.
92. Hunskar S, Hole K. The formalin test in mice: dissociation between inflammatory and non-inflammatory pain. *Pain* 1987; 30:103–14.
93. Iannello S, Belfiore F. Hypomagnesemia. A review of pathophysiological, clinical and therapeutical aspects. *Panminerva Medica* 2001; 43(3):177–209.
94. Ilouz R, Kaidanovich O, Gurwitz D et al. Inhibition of glycogen synthase kinase-3 by bivalent zinc ions: insight into the insulin-mimetic action of zinc. *Biochemical and Biophysical Research Communications* 2002; 295(1):102–106.
95. Jaba IM, Ionescu D, Popa MI. The analgesic effect and local tolerance of new anorganic nanohybrid systems with ketoprofen. *InfoMedica* 2008; 3:10–3.

96. Jacka T, Bernard CC, Singer G. Copper salicylate as an anti-inflammatory and analgesic agent in arthritic rats. *Life Sci* 1983; 32:1023.
97. Jia C, Roman C, Hegg CC. Nickel sulfate induces location-dependent atrophy of mouse olfactory epithelium: protective and proliferative role of purinergic receptor activation. *Toxicol. Sci.* 2010; 115(2):547-56.
98. Jomova K, Valko M. Advances in metal-induced oxidative stress and human disease. *Toxicology* 2011; 283(2-3):65-87.
99. Jones CE, Endergood CK, Coulson EJ et al. Copper induced oxidation of serotonin, analysis of products and toxicity. *J Neurochem* 2007; 10:1035–1043.
100. Kamarudin NHN, Jalil AA, Triwahyono S et al. Role of 3-aminopropyltriethoxysilane in the preparation of mesoporous silica nanoparticles for ibuprofen delivery: effect on physicochemical properties. *Micropor. Mesopor. Mater.* 2013; 180, 235–241.
101. Kanan S, Swamy CS. Synthesis and physicochemical characterization of cobalt aluminium hydrotalcite. *J Mater Sci Lett.* 1992; 11:1585–7.
102. Kang HW, Moon HJ, Joo SH, Lee JH. Histidine residues in the IS3-IS4 loop are critical for nickel-sensitive inhibition of the Cav2.3 calcium channel. *FEBS Lett* 2007; 581(30):5774-80.
103. Kang HW, Park JY, Jeong SW et al. A molecular determinant of Nickel inhibition in cav3.2 T-type Calcium channels. *J. Biol. Chem.* 2006; 281:4823.
104. Kante B, Couvreur G, Dubois-Krack C et al. Toxicity of Polyalkylcyanoacrylate Nanoparticles I: Free Nanoparticles. *J. Pharm. Sci.* 1982; 71:786-790.
105. Kantor TG. Ketoprofen: a review of its pharmacologic and clinical properties. *Pharmacotherapy* 1986; 6:93–103.
106. Karson A, Demirta T, Bayramgürler D et al. Depressive symptoms are associated with tumor necrosis factor alpha in systemic lupus erythematosus. *Basic Clin. Pharmacol. Toxicol* 2013; 112:335.
107. Kay AR, Toth K. Is zinc a neuromodulator? *Sci Signaling* 2008; 1:3.
108. Keay K, Crowfoot LJ, Floyd NS et al. Cardiovascular effects of microinjections of opioid agonists into the ‘Depressor Region’ of the ventrolateral periaqueductal gray region. *Brain Res* 1997; 762:61-71.
109. Ketterman JK, Li YV. Presynaptic evidence for zinc release at the mossy fiber synapse of rat hippocampus. *J Neurosci Res* 2008; 86:422–434.
110. Khandave SS, Sawant SS, Joshi SS et al. Comparative bioequivalence studies of tramadol hydrochloride sustained-release 200 mg tablets. *Drug Design, Development and Therapy* 2010; 4:367–74.
111. Kharkevich A, Kreuter J. Delivery of Loperamide across the blood-brain barrier with polysorbate 80-coated polybutylcyanoacrylate nanoparticle. *Pharm. Res.* 1997; 14: 325-328.
112. Kim BE, Nevitt T, Thiele DJ. Mechanism for copper acquisition, distribution and regulation. *Nat Chem Biol* 2008; 4:176–185.
113. Kim MH, Hwang JW, Jeon YT et al. Effects of valproic acid and magnesium sulphate on rocuronium requirement in patients undergoing craniotomy for cerebrovascular surgery. *British Journal of Anaesthesia* 2012; 109(3):407–12.

114. Kiratli PO, Aksoy T, Bozkurt MF et al. Detection of ectopic gastric mucosa using  $^{99m}\text{Tc}$  pertechnetate: review of the literature. *Ann. Nucl. Med.* 2010; 23:97–105.
115. Knyazeva SI, Loginova NA, Loseva EV. Anxiety level and body weight changes in rats living in overpopulated cages. *Bull. Exp. Biol. Med.* 2012; 154, p. 3.
116. Ko JA, Park HJ, Hwang SJ et al. Preparation and characterization of chitosan microparticles intended for controlled drug delivery. *Int J Pharm.* 2002; 249:65–74.
117. Komeda H, Kobayashi M, Shimizu S. Characterization of the gene cluster of high-molecular-mass nitrile hydratase (H-NHase) induced by its reaction product in *Rhodococcus rhodochrous* J1. *Proc Natl Acad Sci USA* 1997; 93:4267–4272.
118. Kondakis XG, Makris N, Leotsinidis M et al. Possible health effects of high manganese concentration in drinking water. *Archives of Environmental Health* 1989; 44(3):175–8.
119. Kong B, Seog JH, Graham LM et al. Experimental considerations on the cytotoxicity of nanoparticles. *Nanomedicine* 2011; 6:929–941.
120. Konig H, Wallner T, Marhofer P et al. Magnesium sulfate reduces intra- and postoperative analgesic requirements. *Anesth Analg* 1998; 87:206–210.
121. Kono H, Hara H, Hashimoto H et al. Nonionic gelation agents prepared from hydroxypropyl guar gum. *Carbohydrate Polymers* 2015; 117:636–643.
122. Kontargiris E, Vadalouka A, Ragos V et al. Zinc inhibits apoptosis and maintains NEP downregulation, induced by ropivacaine, in HaCaT cells. *Biological Trace Element Research* 2012; 150(1-3):460–6.
123. Konturek SJ, Brzozowski T, Garlicki J et al. Intragastric pH in the gastroprotective and ulcer-healing activity of aluminum-containing antacids. *Digestion* 1991; 49:140–50.
124. Kreuter J, Alyautdin RN, Kharkevich DA et al. Passage of peptides through the blood-brain barrier with colloidal polymer particles (nanoparticles). *Brain Res.* 1995; 674:171-174.
125. Kreuter J, Alyautdin RN. Using nanoparticles to target drugs to the central nervous system, in: “The Blood–Brain Barrier and Drug Delivery to the CNS”, Marcel Dekker, D. J. Begley, M. W. Bradbury, and J. Kreuter 1995; 205-223.
126. Kreuter J. Influence of the surface properties on nanoparticle-mediated transport of drugs to the brain. *J Nanosci Nanotechnol.* 2004; 4(5):484-8.
127. Kreuter J, Petrov VE, Kharkevich DA et al. Influence of the type of surfactant on the analgesic effects induced by the peptide dalargin after its delivery across the blood-brain barrier using surfactant-coated nanoparticles. *J. Contr. Release* 1997; 49, 81-87.
128. Kreuter J, Range P, Petrov V et al. Direct evidence that polysorbate-80-coated poly(butylcyanoacrylate) nanoparticles deliver drugs to the CNS via specific mechanisms requiring prior binding of drug to the nanoparticles. *Pharm. Res.* 2003; 20:409-416.
129. Kreuter J, Shamenkov D, Petrov V et al. Apolipoprotein-mediated transport of nanoparticle-bound drugs across blood-brain barrier *J. Drug Target* 2002; 10:317-325.
130. Krocicka B, Branski P, Palucha A et al. Antidepressant-like properties of zinc in rodent forced swim test. *Brain Res Bull* 2001; 55:297–300.

131. Krylova SG, Fomina TI, Efimova LA et al. Antiulcer effect of calcium pectate on model of chronic gastric ulcer in rats. *Eksp Klin Farmakol* 2001; 72:35–8.
132. Kugelmas M. Preliminary observation: oral zinc sulfate replacement is effective in treating muscle cramps in cirrhotic patients. *J Am Coll Nutr* 2000; 19:13–15.
133. Kumari A, Yadav SK, Yadav SC. Biodegradable polymeric nanoparticles based drug delivery systems. *Colloids and Surfaces B: Biointerfaces* 2010; 75:1-18.
134. Laires MJ, Monteiro CP, Bicho M. Role of cellular magnesium in health and human disease. *Frontiers in Bioscience: A Journal and Virtual Library* 2004; 9:262–76.
135. Lansdown AB. Zinc in the healing wound. *Lancet* 1996; 347:706.
136. Larson AA, Giovengo SL, Shi Q. Zinc in the extracellular area of the central nervous system is necessary for the development of kainic acid-induced persistent hyperalgesia in mice. *Pain* 2000; 86:177–184.
137. Larson AA, Kitto KF. Manipulations of zinc in the spinal cord, by intrathecal injection of zinc chloride, disodium-calcium-EDTA, or dipicolinic acid, alter nociceptive activity in mice. *J. Pharmacol. Exp. Ther.* 1997; 282(3):1319-25.
138. Lee AR, Yi HW, Chung IS et al. Magnesium added to bupivacaine prolongs the duration of analgesia after interscalene nerve block. *Can J Anaesth* 2012; 59:21–27.
139. Lee C, Song YK, Jeong HM et al. The effects of magnesium sulfate infiltration on perioperative opioid consumption and opioid-induced hyperalgesia in patients undergoing robot-assisted laparoscopic prostatectomy with remifentanyl-based anesthesia. *Kor J Anesthesiol* 2011; 61:244–250.
140. Lee WF, Jou LL. Effect of the intercalation agent content of montmorillonite on the swelling behavior and drug release behavior of nanocomposite hydrogels. *J Appl Polym Sci.* 2004; 94:74–82.
141. Leffler CT, Philippi AF, Leffler SG et al. Glucosamine, chondroitin, and manganese ascorbate for degenerative joint disease of the knee or low back: a randomized, double-blind, placebo-controlled pilot study. *Military Medicine* 1999; 164(2):85–91.
142. Legrand S, Catheline A, Kind L et al. Controlling silica nanoparticle properties for biomedical applications through surface modification. *New J. Chem.* 2008; 32:588–593.
143. Lewinski N, Colvin V, Drezek R. Cytotoxicity of nanoparticles. *Small* 2008; 4:26–49.
144. Li B, He J, Evans DG et al. Inorganic layered double hydroxides as a drug delivery systems intercalation and in vitro release of fenbufen. *Appl Clay Sci.* 2004; 27:199–207.
145. Li S, Liu X. Synthesis, characterization and evaluation of semi-IPN hydrogels consisted of poly (methacrylic acid) and guar gum for colon-specific drug delivery. *Polymer Advanced Technology* 2008; 19:371–376.
146. Li X, Clark JD. The role of heme oxygenase in neuropathic and incisional pain. *Anesth Analg* 2000; 90:677–682.
147. Li Y, Che J, Bao F. Effects of kuo-guan granule on plasma zinc, copper and erythrocyte GSH-Px (glutathione peroxidase) in patients with angina pectoris. *Zhong Xi Yi Jie He Za Zhi* 1990; 10:348–350.

148. Liu M, Liu XF, Yao J et al. Mechanism of the cardioprotection of rhEPO pretreatment on suppressing the inflammatory response in ischemia-reperfusion. *Pharmacol. Exp. Therap.* 2006; 310:308-316.
149. Liu T, Walker JS, Tracey DJ. Zinc alleviates thermal hyperalgesia due to partial nerve injury. *Neuroreport* 1999; 10,1619–1623.
150. Liu Z, Jiao Y, Wang Y et al. Polysaccharides-based nanoparticles as drug delivery systems. *Adv Drug Deliv Rev.* 2008; 60:1650–62.
151. Loudos G, Kagadis GC, Psimadas D. Current status and future perspectives of in vivo small animal imaging using radiolabeled nanoparticles. *Eur. J. Radiol.* 2011; 78:287–295.
152. Lowe NM, Dykes FC, Skinner AL et al. EURRECA-Estimating zinc requirements for deriving dietary reference values. *Critical Reviews in Food Science and Nutrition* 2013; 53(10):1110–23.
153. Lu J, Liong M, Zink JI et al. Mesoporous silica nanoparticles as a delivery system for hydrophobic anticancer drugs. *Small* 2007; 3:1341–1346.
154. Luebbert M, Radtke D, Wodarski R. Direct activation of transient receptor potential V1 by nickel ions. *Pflugers Arch.* 2010; 459:737–750.
155. Luo J, Bavencoffe A, Yang P, Feng J, Yin S, Qian A, Yu W, Liu S, Gong X, Cai T, Walters ET, Dessauer CW, Hu H. Zinc Inhibits TRPV1 to Alleviate Chemotherapy-Induced Neuropathic Pain. *J Neurosci.* 2018;38(2):474-483.
156. Ma Z, Wong KY, Horrigan FT. An extracellular Cu<sup>2+</sup> binding site in the voltage sensor of BK and Shaker potassium channels. *J Gen Physiol* 2008; 131:483–502.
157. Maestrelli F, Zerrouk N, Cirri M. Microspheres for colonic delivery of ketoprofen-hydroxypropyl-bcyclodextrin complex. *Eur J Pharm Sci.* 2008; 34:1–11.
158. Mamaeva V, Sahlgren C, Lindén M. Mesoporous silica nanoparticles in medicine – Recent advances. *Adv. Drug Deliv. Rev.* 2013; 65:689–702.
159. Manna PJ, Mitra T, Pramanik N. Potential use of curcumin loaded carboxymethylated guar gum grafted gelatin film for biomedical applications, *International Journal of Biological Macromolecules* 2015; 75:437-446.
160. Marcellini F, Giuli C, Papa R et al. Zinc status, psychological and nutritional assessment in old people recruited in five European countries: Zincage study. *Biogerontology* 2006; 7(5-6):339–45.
161. Marie RG. Nonsteroidal anti-inflammatory drugs: practical and theoretical considerations in their selection. *Am J Med* 1996; 100:31S.
162. Marie RG. Epidemiology of nonsteroidal anti-inflammatory drug-associated gastrointestinal injury. *Am J Med.* 1998; 104:23S.
163. Martinez-Finley EJ, Gavin CE, Aschner M et al. Manganese neurotoxicity and the role of reactive oxygen species. *Free Radical Biology & Medicine* 2013; 62:65–75.
164. Maserejian NN, Hall SA, McKinlay JB. Low dietary or supplemental zinc is associated with depression symptoms among women, but not men, in a population-based epidemiological survey. *Journal of Affective Disorders* 2012; 136(3):781–8.
165. Mastiholmath VS, Dandagi PM, Jain SS et al. Time and pH dependent colon specific, pulsatile delivery of theophylline for nocturnal asthma. *Int J Pharm.* 2007; 28:49–56.

166. Matsunami M, Kirishi S, Okui T et al. Chelating luminal zinc mimics hydrogen sulfide-evoked colonic pain in mice, possible involvement of T-type calcium channels. *Neuroscience* 2011; 181:257–264.
167. Mauskop A, Altura BT, Cracco RQ et al. Chronic daily headache—one disease or two? Diagnostic role of serum ionized magnesium. *Int J Headache* 1994; 14:24–28.
168. Mayer ML, Vyklicky L Jr. The action of zinc on synaptic transmission and neuronal excitability in cultures of mouse hippocampus. *J Physiol* 1989; 415:351–365.
169. Md S, Khan RA, Mustafa G et al. Bromocriptine loaded chitosan nanoparticles intended for direct nose to brain delivery: pharmacodynamic, pharmacokinetic and scintigraphy study in mice 600 model. *Eur. J. Pharm. Sci.* 2013; 48, 393–405.
170. Meyer MD. Neuronal nicotinic acetylcholine receptors as a target for the treatment of neuropathic pain. *Drug Dev Res* 2006; 67:355–359.
171. Miyano K, Morioka N, Sugimoto T et al. Activation of the neurokinin-1 receptor in rat spinal astrocytes induces  $Ca^{2+}$  release from IP<sub>3</sub>-sensitive  $Ca^{2+}$  stores and extracellular  $Ca^{2+}$  influx through TRPC3. *Neurochemistry International* 2010; 57(8):923–34.
172. Mocanu G, Mihai D, Le Cerf D et al. Synthesis of new associative gel microspheres from carboxymethyl pullulan and their interactions with lysozyme. *European Polymer Journal* 2004; 40:283–289.
173. Morales-Avila E, Ferro-Flores G, Ocampo-García BE et al. Radiolabeled nanoparticles for molecular imaging. In: Schaller, Bernhard (Ed.) *Molecular Imaging*. 2012; 15–38.
174. Moss M. Effects of Molybdenum on pain and general health: a pilot study. *J Nutr Environ Med* 1995; 5: 55-61.
175. Mu Q, Hondow NS, Krzeminski L et al. Mechanism of cellular uptake of genotoxic silica nanoparticles. *Part Fibre Toxicol* 2010; 9–29.
176. Mullarney MP, Seery TA, Weiss RA. Drug diffusion in hydrophobically modified N, N-dimethylacrylamide hydrogels. *Polymer* 2006; 47, 3845–3855.
177. Mungiu OC, Ionescu DG, Jaba IM. Zinc and nociception, a pharmacological approach. *Rev Med Chir Soc Med Nat* 2002; 106:10–13.
178. Murphy JD, Paskaradevan J, Eisler LL et al. Analgesic efficacy of continuous intravenous magnesium infusion as an adjuvant to morphine for postoperative analgesia: a systematic review and meta-analysis. *Middle East Journal of Anesthesiology* 2013; 22(1):11–20.
179. Napierska D, Thomassen LC, Rabolli V et al. Size-dependent cytotoxicity of monodisperse silica nanoparticles in human endothelial cells. *Small* 2009; 5:846–853.
180. Narasimha MS, Hiremath SR, Paranjothy KL. Evaluation of carboxymethyl guar films for the formulation of transdermal therapeutic systems. *International Journal of Pharmaceutics* 2004; 272, 11–18.
181. Nelson MT, Woo J, Kang HW et al. Reducing agents sensitize C-type nociceptors by relieving high-affinity zinc inhibition of T-type calcium channels. *J. Neurosci.* 2007; 27:8250.
182. Newman SP, Hirst PH, Wilding I. New developments in radionuclide imaging for assessing drug delivery in man. *Eur. J. Pharm. Sci.* 2003; 18:19–22.

183. Nicholas RS, Winter J, Wren P et al. Pheripheral inflammation increases the capsaicin sensitivity of dorsal root ganglion neurons in a nerve growth factor-dependent manner. *Neuroscience* 1999; 911:425.
184. Nieto-Fernandez FE, Ruiz A, Ntukogu N et al. Short term lead exposure induces a stress-like response in adult mice. *Med. Sci. Monit.* 2006; 12, no. 10, p. BR325.
185. Nikolaev MV, Magazanik LG, Tikhonov DB. Influence of external magnesium ions on the NMDA receptor channel block by different types of organic cations. *Neuropharmacology* 2012; 62:2078–2085.
186. Niu S, Wang J, Zhao B et al. Regioselective synthesis and antioxidant activities of phosphorylated guar gum, *International Journal of Biological Macromolecules* 2013; 62:741– 747.
187. Nolen RS. AVMA board approves Panel on Euthanasia report: updated guidelines cover more species and methods. *J. Am. Vet. Med. Assoc.* 2011; 239:1269.
188. Nozaki C, Vergnano AM, Filliol D et al. Zinc alleviates pain through high-affinity binding to the NMDA receptor NR2A subunit. *Nature Neuroscience* 2011a; 14(8):1017–22.
189. Okuyama S, Hashimoto S, Aihara H et al. Copper complexes of non-steroidal antiinflammatory algesic activity and possible opioid receptor activation. *Agents Actions* 1997; 21:130–144.
190. Olanrewaju J, Newalkar BL, Mancino C et al. Simplified synthesis of nitrate form of layered double hydroxide. *Mater Lett.* 2009; 45:307–10.
191. Olivier JC, Fenart L, Chauvet R et al. Indirect evidence that drug brain targeting using polysorbate 80-coated polybutylcyanoacrylate nanoparticles is related to toxicity. *Pharm. Res.* 1999; 16 :1836-1842.
192. Pan E, Zhang XA, Huang Z et al. Vesicular zinc promotes presynaptic and inhibits postsynaptic long-term potentiation of mossy fiber-CA3 synapse. *Neuron* 2011; 71:1116–1126.
193. Pandey U, Kameswaran M, Dev Sarma H et al. <sup>99m</sup>Tc carbonyl DTPA– Rituximab: preparation and preliminary bioevaluation. *Appl. Radiat. Isotopes.* 2014; 86:52–56.
194. Parveen S, Ranjita M, Sahoo SK. Nanoparticles: A Boon to Drug Delivery, Therapeutics, Diagnostics and Imaging, *Nanomedicine: Nanotechnology. Biology and Medicine* 2012; 8, 147-166.
195. Patel JJ, Karve M, Pate NK. Guar gum: a versatile material for pharmaceutical industries. *International Journal of Pharmacy and Pharmaceutical Sciences* 2014; 6:13-19.
196. Pawlaczyk J, Kokot Z, Rafinska A. In vitro study of the antipeptic activity of antacid preparations. *Acta Pol Pharm.* 1985; 42:153–8.
197. Peer D, Karp JM, Hong S et al. Nanocarriers as an emerging platform for cancer therapy. *Nat. Nanotechnol.* 2007; 2:751–760.
198. Petri B, Bootz A, Khalansky A et al. Chemotherapy of brain tumour using doxorubicin bound to surfactant-coated poly(butyl cyanoacrylate) nanoparticles: Revisiting the role of surfactants. *J. Contr. Release* 2007; 11:51-58.

199. Phadke KV, Manjeshwar LS, Aminabhavi TM. Biodegradable polymeric microspheres of gelatin and carboxymethyl guar gum for controlled release of theophylline. *Polymer Bulletin* 2014; 71:1625–1643.
200. Playle AC, Gunning SR, Llewellyn AF. The in vitro antacid and anti pepsin activity of hydrotalcite. *Pharm Acta Helv.* 1974; 49:298–302.
201. Poleszak E, Wlaz P, Wrobel A et al. NMDA/glutamate mechanism of magnesium-induced anxiolytic-like behavior in mice. *Pharmacol Rep* 2007; 60:655–663.
202. Popa M, Lerche H. Cu<sub>2</sub>(1,10 phenantroline)<sub>3</sub> is an open-channel blocker of the human skeletal muscle sodium channel. *Br J Pharmacol* 2010; 14:808–814.
203. Popa N, Novac O, Profire L et al. Hydrogels based on chitosan–xanthan for controlled release of theophylline. *Journal of Materials Science: Materials in Medicine* 2010; 21, 1241–1248.
204. Prabakaran M. Prospective of guar gum and its derivatives as controlled drug delivery systems: Review, *International Journal of Biological Macromolecules* 2011; 49:117–124.
205. Prado WA. Involvement of calcium in pain and antinociception. *Braz. J. Med. Biol. Res.* 2001; 34, p. 449.
206. Rana V, Rai P, Tiwary AK et al. Modified Gums: Approaches and applications in drug delivery. *Carbohydrate Polymers* 2011; 83:1031-1047.
207. Reddi B. Why is saline so acidic (and does it really matter.)? *Int J Med Sci.* 2013; 10:747–50
208. Ringe K, Walz CM, Sabel BA. *Encyclopedia Nanosci. Nanotech* 2004; 7:91-104.
209. Risica D, Dentini M, Crescenzi V. Guar gum methyl ethers. Part I. Synthesis and macromolecular characterization, *Polymer* 2005; 46:12247–12255.
210. Ritger PL, Peppas NA. A simple equation for description of solid release. II. Fickian and anomalous release from swellable devices. *J Control Release* 1987; 5:37–42.
211. Ritger PL, Peppas NA. A simple equation for description of solute release I. Fickian and nonfickian release from non-swellable devices in the form of slabs, spheres, cylinders or discs. *Journal of Controlled Release* 1987; 5:23-36.
212. Rodriguez-Munoz M, de la Torre-Madrid E, Sanchez-Blazquez P et al. NO-released zinc supports the simultaneous binding of Raf-1 and PKC gamma cysteine-rich domains to HINT1 protein at the mu-opioid receptor. *Antiox Redox Signal* 2011; 14:2413–2425.
213. Rokhade AP, Shelke NB, Patil SA et al. Novel interpenetrating polymer microspheres of chitosan and methylcellulose for controlled release of theophylline. *Carbohydr Polym.* 2014; 69:678–87.
214. Rosa AO, Egea J, Lorrio S et al. Nrf2-mediated haeme oxygenase-1 up-regulation induced by cobalt protoporphyrin has antinociceptive effects against inflammatory pain in the formalin test in mice. *Pain* 2008; 137(2):332-9.
215. Rosman C, Pierrat S, Tarantola M et al. Mammalian cell growth on gold nanoparticle-decorated substrates is influenced by the nanoparticle coating, *Beilstein Journal of Nanotechnology* 2014; 5, 2479–2488.
216. Rowley TJ, Payappily J, Lu J et al. The antinociceptive response to nicotinic agonists in a mouse model of postoperative pain. *Anesth Analg* 2008; 107:1952–1957.

217. Sakai N, Takakura M, Imamura H et al. Whole-body distribution of <sup>14</sup>C-labeled silica nanoparticles and submicron particles after intravenous injection into mice. *J. Nanopart. Res.* 2008; 14:849–859.
218. Saroj S, Rajput SJ. Etoposide encased folic acid adorned mesoporous silica nanoparticles as potent nanovehicles for enhanced prostate cancer therapy: synthesis, characterization, cellular uptake and biodistribution. *Artif Cells Nanomed Biotechnol.* 2019:1-16.
219. Sarparanta M, Mäkilä E, Heikkilä T et al. <sup>18</sup>F-labeled modified porous silicon particles for investigation of drug delivery carrier distribution in vivo with positron emission tomography. *Mol. Pharm.* 2011; 8 (5):1799–1806.
220. Savage RL, Moller PW, Ballantyne CL et al. Variation in the risk of peptic ulcer complications with nonsteroidal anti-inflammatory drug therapy. *Arthritis Rheum.* 1993; 36:84–90.
221. Schaumlöffel D. Nickel species: Analysis and toxic effects. *J. Trace Elem. Med. Biol.* 2012; 26:1-6.
222. Schröder U, Sabel BA. Nanoparticles, a drug carrier system to pass the blood-brain barrier, permit central analgesis effects of iv dalargin injection. *Brain Res.* 1996; 710:121-124.
223. Schröder U, Sommerfeld P, Sabel BA. Nanoparticle technology for delivery of drugs across the blood brain barrier. *Peptides* 1998; 19:777-780.
224. Sedighinejad A, Haghighi M, Nabi BN et al. Magnesium sulfate and sufentanil for patient-controlled analgesia in orthopedic surgery. *Anesthesiology and Pain Medicine* 2014; 4(1): e11334.
225. Serra L, Domenech J, Peppas NA. Drug transport mechanisms and release kinetics from molecularly designed poly (acrylic acid-ethylene glycol) hydrogels. *Biomaterials* 2006; 27:5440–51.
226. Shalviri A, Liu Q, Abdekhodaie MJ et al. Novel modified starch-xanthan gum hydrogels for controlled drug delivery: Synthesis and characterization, *Carbohydrate Polymers* 2010; 79:898–907.
227. Shukla D, Verma A, Agarwal A et al. Comparative study of intrathecal dexmedetomidine with intrathecal magnesium sulfate used as adjuvants to bupivacaine. *Journal of Anaesthesiology, Clinical Pharmacology* 2011; 27(4): 495–499.
228. Silion M, Popa MI, Lisa G et al. New hybrid compounds containing intercalated ciprofloxacin into layered double hydroxides: synthesis and characterization. *Rev Roum Chim.* 2008; 53:827–31.
229. Silion M, Popa MI. Preparation and characterization of ketoprofen-layered double hydroxide compounds. *J Optoelectron Adv Mater* 2010; 23:345-350.
230. Silva GA. Nanotechnology approaches for the regeneration and neuroprotection of the central nervous system. *Surg. Neur.* 2007; 67:113-116.
231. Simone EA, Zern BJ, Chacko AM et al. Endothelial targeting of polymeric nanoparticles stably labeled with the PET imaging radioisotope iodine-124. *Biomaterials* 2012; 33:5406–5413.

232. Siwek M, Dudek D, Schlegel-Zawadzka M et al. Serum zinc level in depressed patients during zinc supplementation of imipramine treatment. *Journal of Affective Disorders* 2010; 126(3):447–52.
233. Siwek M, Dudek D, Zieba A et al. Zinc supplementation augments efficacy of imipramine in treatment resistant patients: a double blind, placebo-controlled study. *Journal of Affective Disorders* 2009, 118(1-3):187–95.
234. Slowing II, Trewyn BG, Giri S et al. Mesoporous silica nanoparticles for drug delivery and biosensing applications. *Adv. Funct. Mater.* 2007; 17:1225–1236.
235. Smart TG, Hosie AM, Miller PS. Zn<sup>2+</sup> ions: modulators of excitatory and inhibitory synaptic activity. *The Neuroscientist: A Review Journal Bringing Neurobiology, Neurology and Psychiatry* 2004; 10(5):432–42.
236. Sommerfeld P, Schröder U, Sabel BA. Long-term stability of PBCA nanoparticle suspensions suggest clinical usefulness. *Int. J. Pharm.* 1997; 155:201-207.
237. Sommerfeld P, Schröder U, Sabel BA. Sterilization of unloaded polybutylcyanoacrylate nanoparticles. *Int. J. Pharm.* 1998; 164:113-118.
238. Soni MG, Thurmond TS, Miller ER 3rd et al. Safety of vitamins and minerals: controversies and perspective. *Toxicological Sciences: An Official Journal of the Society of Toxicology* 2010; 118(2):348–55.
239. Srebro DP, Vučković SM, Dožić IS, Dožić BS, Savić Vujović KR, Milovanović AP, Karadžić BV, Prostran MŠ. Magnesium sulfate reduces formalin-induced orofacial pain in rats with normal magnesium serum levels. *Pharmacol Rep.* 2018;70(1):81-86.
240. Stangl GI, Kirchgessner M. Nickel deficiency alters liver lipid metabolism in rats. *The Journal of Nutrition* 1996; 126:2466-2473.
241. Staruschenko A, Dorofeeva NA, Bolshakov KV et al. Acid-sensing ion channels in pain and disease. *Dev. Neurobiol.* 2007; 67:97.
242. Stober W, Fink A, Bohn E. Controlled growth of monodisperse silica spheres in the micron size range. *J. Colloid Interface Sci.* 2000; 26:62–69.
243. Su R, Mei X, Wang Y et al. Regulation of zinc transporter 1 expression in dorsal horn of spinal cord after acute spinal cord injury of rats by dietary zinc. *Biological Trace Element Research* 2012; 149(2):219–26.
244. Subrahmanyam PJ. Design and development of guar gum and borax cross-linked guar gum matrix tablets of theophylline for colon specific drug. *Journal of Chemical Pharmaceutical Research* 2012; 4:1052-1060.
245. Sullad AG, Manjeshwar LS, Aminabhavi TM. Microspheres of Carboxymethyl Guar Gum for In Vitro Release of Abacavir Sulfate: Preparation and Characterization, *Journal of Applied Polymer Science* 2011; 122:452–460.
246. Surprenant A, Shen ZK, North RA et al. Inhibition of calcium currents by noradrenaline, somatostatin and opioids in guinea-pig submucosal neurones. *The Journal of Physiology* 1990; 431:585–608.
247. Takano Y, Soto E, Kaneko T, Sato I. Antihyperalgesic effects of intrathecally administered magnesium sulfate in rats. *Pain* 2002; 84:175–179.
248. Takeda A, Minumi A, Seki Y et al. Differential effects of zinc on glutamatergic and GABA-ergic neurotransmitter systems in the hippocampus. *J Neurosci Res* 2003; 75:225–229.

249. Taly A, Corringier PJ, Guedin D et al. Nicotinic receptors: allosteric transitions and therapeutic targets in the nervous system. *Nature Reviews-Drug Discovery* 2009; 8(9):733–50.
250. Tamba BI, Jaba IM, Serban DN et al. The influence of systematically administered divalent trace elements on the nociceptive process—new experimental data. *J Clin Pharmacol* 2009; 48:1135.
251. Tamba BI, Leon MM, Petreus T. Common trace elements alleviate pain in an experimental mouse model. *Journal of Neuroscience Research* 2013; 91(4):554–61.
252. Tarnawski AS, Ahluwalia A, Gandhi V et al. Hydrotalcite protects aging gastric mucosa against NSAID- and ethanol-induced injury by preserving endothelial and progenitor cells. Underlying molecular mechanisms include activation of survivin and VEGF. *Gastroenterology* 2010; 138: S-721.
253. Tarnawski AS, Tomikawa M, Ohta M et al. Antacid talc activates in gastric mucosa genes encoding for EGF and its receptor. The molecular basis for its ulcer healing action. *J Physiol Paris* 2000; 94:93–8.
254. Tartau L, Jaba I, Tamba BI et al. Experimental data regarding the antinociceptive effect of systemically administered manganese. *Therapeutics, Pharmacology and Clinical Toxicology* 2006; 10(1):72–77.
255. Thimma RT, Tammishetti S. Barium chloride crosslinked carboxymethyl guar gum beads for gastrointestinal drug delivery, *Journal of Applied Polymer Science* 2001; 82: 3084–3090.
256. Tjalkens RB, Zoran MJ, Mohl B et al. Manganese suppresses ATP-dependent intercellular calcium waves in astrocyte networks through alteration of mitochondrial and endoplasmic reticulum calcium dynamics. *Brain Research* 2006; 1113(1):210–9.
257. Tong CK, Macdermott AB. Ionotropic glutamate receptors in spinal nociceptive processing. *J. Physiol.* 2006; 260–288.
258. Tripathy J, Mishra DK, Srivastava A et al. Synthesis of partially carboxymethylated guar gum-g-4-vinyl pyridine and study of its water swelling, metal ion sorption and flocculation behavior. *Carbohydrate Polymers* 2008; 72:462–472.
259. Tugrul S, Degirmenci N, Eren SB et al. Analgesic effect of magnesium in post-tonsillectomy patients: a prospective randomised clinical trial. *European Archives of Oto-Rhino-Laryngology* 2014; 9:2483–2487.
260. Tuo B, Wen G, Wang X et al. Estrogen potentiates prostaglandin E2-stimulated duodenal mucosal bicarbonate secretion in mice. *Gastroenterology* 2010; 138:S-721.
261. Turner PV, Brabb T, Pekowet C et al. Administration of substances to laboratory animals: routes of administration and factors to consider. *JAALAS* 2009; 50(5):600–13.
262. Van Hecke O, Torrance N, Smith BH. Chronic pain epidemiology and its clinical relevance. *British Journal of Anaesthesia* 2011; 111(1):13–8.
263. Vasi AM, Popa MI, Tanase EC et al. Poly (acrylic acid)– poly (ethylene glycol) nanoparticles designed for ophthalmic drug delivery. *Journal of Pharmaceutical Sciences* 2014; 103:676–686.
264. Vauthier C, Dubernet C, Fattal E et al. Drug delivery to resistant tumors: the potential of poly (alkyl cyanoacrylate) nanoparticles. *Adv. Drug Deliv. Rev.* 2003; 55:519-548.

265. Verdun C, Couvreur P, Vranckx H et al. Development of a nanoparticle controlled-release formulation for human use. *J. Contr. Release* 1986; 3:206-210.
266. Voiley N. Acid-sensing ion channels (ASICs): new targets for the analgesic effects of non-steroid anti-inflammatory drugs (NSAIDs). *Curr. Drug Targets Inflamm Allergy* 2004; 3:71-79.
267. Vueba ML, Pina ME, Veiga F et al. Conformational study of ketoprofen by combined DFT calculations and Raman spectroscopy. *Int J Pharm.* 2006; 307:56-65.
268. Wang C, Bhattacharyya MH. Effect of cadmium on bone calcium and  $^{45}\text{Ca}$  in mouse dams on a calcium-deficient diet: evidence of Itai-Itai-like syndrome. *Toxicol Appl Pharmacol* 1994; 127:320-330.
269. Wang J, Niu S, Zhao B et al. Regioselective synthesis of sulfated guar gum: Comparative studies of structure and antioxidant activities, *International Journal of Biological Macromolecules* 2013; 62:734-740.
270. Wang Y, Me X, Zhang L et al. Supplement moderate zinc as an effective treatment for spinal cord injury. *Medical Hypotheses* 2011; 77(4):589-590.
271. Williams M. Use of animal models for drug discovery. In: Enna SJ, Bylund DB, editors. *x Pharm: the comprehensive pharmacology reference*. New York: Elsevier. 2008; 1-7.
272. Wong MH, Armour MA, Naidu R et al. Persistent toxic substances: sources, fates and effects. *Rev Environ Health* 2012; 27:207-213.
273. Wu HE, Han-Sen S, Moses D et al. Dynorphinergic mechanism mediating endomorphin-2-induced antianalgesia in the mouse spinal cord. *The Journal of Pharmacology and Experimental Therapeutics* 2003; 307(3):1135-41.
274. Wu T, Tian-Shan W, Fang-Zhou Y et al. Analgesic and anti-inflammatory properties of brucine and brucine-N-oxide extracted from seeds of *Strychnos nuxvomica*. *J Ethnopharmacol* 2003, 88:205-214.
275. Wu X, Wu M, Xiaojun Zhao J. Recent development of silica nanoparticles as delivery vectors for cancer imaging and therapy, a review. *Nanomed. Nanotech. Biol. Med.* 2014; 10:297-312.
276. Xiao WH, Bennett GJ. Magnesium suppresses neuropathic pain responses in rats via a spinal site of action. *Brain Res* 1994; 666:168-172.
277. Xie G, Sun J, Zhong G et al. Biodistribution and toxicity of intravenously administered silica nanoparticles in mice. *Arch. Toxicol.* 2003; 84:183-190.
278. Xu ZP, Zeng HC. Interconversion of brucite-like and hydrotalcite-like phases in cobalt hydroxide compounds. *Chem Mater.* 1999; 11:67-74.
279. Xu ZP, Zeng HC. Abrupt structural transformation in hydrotalcite-like compounds  $\text{Mg}_{1-x}\text{Al}_x(\text{OH})_2(\text{NO}_3)_x\text{nH}_2\text{O}$  as a continuous function of nitrate anions. *J Phys Chem B.* 2001; 105:1743-9.
280. Xu ZP, Zeng HC. Sulfate-functionized carbon/metal-oxide nanocomposites from hydrotalcite-like compounds. *Nano Lett.* 2001; 1:703-6.
281. Yadav M, Mishra DK, Behari K. Synthesis of partially hydrolyzed graft copolymer (Hpartially carboxymethylated guar gum-g-methacrylic acid): A superabsorbing material, *Carbohydrate Polymers* 2011; 85:29-36.

282. Yin W, Wang TS, Yin FZ et al. Analgesic and antiinflammatory properties of brucine and brucine N-oxide extracted from seeds of *Strychnos nux-vomica* J. Ethnopharmacol. 2003; 88:205–214.
283. Yu BP, Sun J, Li MQ et al. Preventive effect of hydrotalcite on gastric mucosal injury in rats induced by taurocholate. *World J Gastroenterol*. 2003; 9:1427–30.
284. Yu F, Kamada H, Niizuma K et al. Induction of mmp-9 expression and endothelial injury by oxidative stress after spinal cord injury. *J Neurotrauma* 2009; 25:184–195.
285. Yu WR, Jiang H, Wang J et al. Copper (Cu21) induces degeneration of dopaminergic neurons in the nigrostriatal system of rats. *Neurosci Bull* 2008; 24:73–78.
286. Yu Z, Wang W, Kong F, Lin M, Mustapha A. Cellulose nanofibril/silver nanoparticle composite as an active food packaging system and its toxicity to human colon cells. *Int J Biol Macromol*. 2019. doi: 10.1016/j.ijbiomac.2019.02.084.
287. Zwingmann C, Leibfritz D, Hazell AS. Energy metabolism in astrocytes and neurons treated with manganese: relation among cell-specific energy failure, glucose metabolism, and intercellular trafficking using multinuclear NMR-spectroscopic analysis. *Journal of Cerebral Blood Flow and Metabolism* 2003a; 23(6):756–71.